Investigating the mechanisms of renal fibrosis following ischaemia and reperfusion injury

Rishab Kapoor

Thesis submitted in partial fulfilment of the requirements of the regulations for the degree of Doctor of Philosophy

Applied Immunobiology and Transplantation Group
Institute of Cellular Medicine
Newcastle University, UK

January 2018

Abstract

Ischaemia-reperfusion injury (IRI) is the major cause of acute kidney injury (AKI) and predisposes to the development of chronic kidney disease (CKD). The role of TGF-β in extracellular matrix deposition and renal fibrosis has been well established. This study was designed to establish an *in vitro* model of renal tubular IRI, evaluate the role of TGF-β in IRI in human proximal tubular epithelial cells (HKC8 and HK2 cells) and further determine the role of αvβ6 integrin in IRI. Initially an *in vitro* model of hypoxia and free radical stress by treating HKC8, HK2 and fibroblasts (MRC-5 cells) with $CoCl_2$ and H_2O_2 respectively was established. These treatments led to pro-fibrotic changes characterised by increased expression of fibrotic marker α-SMA and reduced expression of epithelial cell marker E-Cadherin at mRNA and protein level. Binding of TGF-β to its receptor leads to activation of the kinase ALK5. ALK5 inhibition prevented the changes induced by H_2O_2 or $CoCl_2$ suggesting the involvement of TGF-β to the cellular response to IRI. To confirm that TGF-β is released after treatment of cells to mimic IRI, media transfer and co-culture studies were performed. These experiments confirmed that bioactive TGF-β was being released. Lastly, the role of αvβ6 integrin was studied post H_2O_2 or $CoCl_2$ treatment. Expression of αvβ6 integrin was elevated in conditions mimicking IRI *in vitro* and in biopsy samples acquired from patients with acute tubular necrosis and in mouse kidney following IRI. Knockdown of αvβ6 integrin in HKC8 cells decreased the bioavailability of active TGF-β following $CoCl_2$ or H_2O_2 treatment and therefore the pro-fibrotic changes that were seen. This study confirms that bioactive TGF-β is produced following IRI and αvβ6 plays an important role in its release.

Acknowledgements

“Loyal and efficient work in a great cause, even though it may not be immediately recognised, ultimately bears fruit.”

-Jawaharlal Nehru (1st PM of independent India)

I would like to express my special appreciation and sincere gratitude to my supervisors, Prof Neil Sheerin and Prof John Kirby. Thank you for being tremendous mentors for me, for insightful comments and encouragement, guiding me at all times of research and writing of this thesis. I would also like to thank Newcastle University would for providing me Overseas Research Scholarship for this project and supporting me throughout this PhD programme. I am especially grateful to my assessors Dr Alison Tyson and Dr John Sayer for their support and feedback during my PhD.

My sincere thanks to Dr Ian Logan for providing cell lines and helping with transfection. For assistance in tissue staining, I would like to thank Barbara Innes and Ana moles. I thank my fellow lab mates Victoria Shuttleworth, Lotfia and Aldi Situmorang for the stimulating discussions and for all the fun we have had in the last four years. My gratitude is due to all other faculty members for their help, inspiration and moral support, during my study.

Many thanks to Shameem Ladak for supporting me for everything, and especially I can’t thank you enough for encouraging me throughout this experience. A special thanks to my family for their financial support and motivation. Words cannot express how grateful I am to my care-taker. Your prayer for me was what sustained me this far.

List of Abbreviations

AKI	Acute kidney injury
ATN	Acute tubular necrosis
ATP	Adenosine tri phosphate
CKD	Chronic Kidney Disease
ESRD	End Stage Renal Disease
TGF	Transforming Growth Factor
RRT	Renal replacement therapy
ACE	Angiotensin converting-enzyme
NO	Nitric oxide
iNOS	Nitric oxide synthase
EPO	Erythropoietin
HRE	Hypoxia response element
HIF	Hypoxia Inducible factor
PHD	Prolyl hydroxylase domain
FIH	Factor inhibiting HIF-1
ARD	Arrest defective
IRI	Ischaemia and Reperfusion Injury
GFR	Glomerular Filtration rate
MMPs	Metalloproteinases
TIMPs	Tissue inhibitors of metalloproteinases
IGF	Insulin-like growth factor
EGF	Epidermal growth factor
PDGF	Platelet derived growth factor
FGF	Fibroblast growth factor
GDFs	Growth differentiation factors
LAP	Latency-associated peptide
LTBP	Latent TGF-β binding protein
SLC	Small latent complex
ROS	Reactive oxygen species
TSP-1	Thrombospondin-1
R-SMAD	Receptor mediated SMAD proteins
I-SMAD	Inhibitory SMADs
TEC	Tubular epithelial cells

UUO	Unilateral ureteral obstruction
ECM	Extracellular matrix
EDTA	Ethylenediaminetetraacetic acid
SDS-PAGE	Sodium dodecyl sulphate polyacrylamide gel electrophoresis
BSA	Bovine Serum Albumin
DMEM	Dulbecco's Modified Eagle's medium
CoCl2	Cobalt chloride
H2O2	Hydrogen peroxide
HKC8	Human proximal tubular epithelial cell line
HK2	Human kidney cell line
MRC-5	Medical research council cell strain 5
FITC	Fluorescein isothiocyanate
DAPI	4',6-Diamidino-2-Phenylindole, Dihydrochloride
IHC	Immunohistochemistry
IF	Immunofluorescence
FSC	Forward angle light scatter
SSC	Side scatter
ELISA	Enzyme-linked immunosorbent assay
ALK	Activin receptor like kinase
Smurf	SMAD ubiquitination- regulatory factor
BMP	Bone morphogenetic protein
DMSO	Dimethyl sulfoxide
PBS	Phosphate Buffer Saline
RT	Room temperature
BCA	Bicinchoninic Acid
ECL	Enhanced chemiluminescent
EtBr	Ethidium bromide
PCR	Polymerase chain reaction
qRT-PCR	Quantitative real time PCR
CT	Cycle threshold
ΔΔCT	Comparative C_t method
siRNA	Small interfering RNA
Csi	Control siRNA

Table of contents

List of Figures

List of Tables

Chapter 1: Introduction

1.1 The kidney and its function

1.1.1 Anatomy of Kidney

The human kidneys, each weighing around 150 grams, are positioned outside the peritoneal cavity on either side of the spine; with the right kidney usually lower than the left. They account for 2% of human body weight but receive 25% of cardiac output. They consists of a reddish brown cortex surrounding a pale striped cone shaped region, the medulla, and a pelvis that joins with the ureter (Ghori *et al.*, 2016).

1.1.2 The Functional Unit of Kidney: The Nephron

The nephron is the basic functional unit of the kidney, comprising a glomerular capillary network that is surrounded by Bowman's capsule that further connects to a system of tubules transporting filtrate to the collecting duct. Each kidney comprises of around one million nephrons. Based on location of the renal corpuscle and the length of the loop of Henle, nephrons are classified into cortical and juxtamedullary nephrons. The barrier between capillary blood and urine is maintained by specialised endothelial cells, the glomerular basement membrane and epithelial podocytes which allow selective ultrafiltration based on size and charge. Once the filtrate crosses glomerulus, it reaches the tubules for further reabsorption and secretion (Rayner *et al.*, 2016). The tubules are lined by single layer of cells and vary from 4cm to 8cm in length. Tubules are subdivided into proximal tubule, loop of Henle, distal tubule and collecting duct based on cell structure, function and localisation along the nephron. The presence of cellular microvilli/brush border in this segment delivers increased surface area that facilitates maximum reabsorption (Rashid and Schwartz, 2012).

1.1.3 Function of the Kidney

The kidney plays a vital role in maintaining pH homeostasis and electrolyte balance in blood. This is achieved by reabsorption of water, salts, glucose and amino acids by active and passive transport along each segment of nephron. They also facilitate the removal of organic molecules, drugs and nitrogenous waste products such as urea and ammonium from the body. The kidneys produce erythropoietin and renin, and are also involved in the Vitamin D metabolism (Rizzo, 2015).

1.2 Acute and Chronic Kidney Disease

Acute kidney injury (AKI) is characterised by a rapid loss in renal excretory function, resulting accumulation of products of nitrogen metabolism such as creatinine and urea and other clinically unmeasured waste products, electrolytes and fluid (Bellomo *et al.*, 2012). Other common clinical and laboratory manifestations include decreased urine output (not always present), accumulation of metabolic acids, and increased potassium and phosphate concentrations, reduced immunity and dysfunction of non-renal organs (Ostermann and Joannidis, 2016).

1.2.1 Epidemiology of Acute Kidney Injury

The kidney is susceptible to a range of diseases that cause an acute decline in the filtration function. AKI is a global public health problem which it is associated with an increased risk of mortality, up to 50–80% in critically ill patients requiring renal replacement therapy (Molitoris *et al.*, 2007; Ftouh and Thomas, 2013).It is challenging to ascertain an accurate figure for the incidence of AKI. Studies relying on medical data suggest an incidence of 486-630 per million populations per year which tends to increase drastically with age and is more prevalent in males and black populations (Kilbride). AKI can affect 13% to 18% of critically ill patients admitted to hospital in developed countries (Thomas *et al.*, 2013). The incidence of AKI is greater than 60% amongst patients during intensive care unit admission (Hoste and

Schurgers, 2008). Furthermore, the annual cost to the NHS of AKI in secondary care is projected between £434-630 million, which is higher than the cost linked with breast, lung and skin cancer together (Anathhanam and Lewington, 2012). Geographical location might affect the causes of AKI. Cardiac surgery and sepsis are common in developed countries while dehydration is common in developing countries (Bagshaw *et al.*, 2008). Around 2 million deaths occur annually due to AKI worldwide (Murugan and Kellum, 2011).

1.2.2 Aetiology

The condition that causes AKI can be broadly divided into 3 groups pre-renal, intrinsic and post-renal (Figure 1.1).

In pre-renal AKI, the functional integrity of kidney is preserved but glomerular and renal perfusion is decreased. It most commonly occurs in older patients with concurrent illness. In such patients, the glomerular filtration rate decreases as the mean arterial pressure falls. Loss of blood, dehydration, vomiting and nausea may also contribute to a fall in filtration rate. The use of certain anti-inflammatory drugs and antihypertensive that reduce the activity of angiotensin system also predispose to AKI (Abuelo, 2007; Kanbay *et al.*, 2010).

Intrinsic AKI can be categorised by the region of the kidney primarily affected (tubular, glomerular, interstitial or vascular). Acute tubular necrosis (ATN) is a type of intrinsic AKI predominant among hospitalised patients. It usually occurs due to prolonged ischaemia or exposure to nephrotoxic agents that damage the tubular cells. AKI from glomerular damage is most frequently a result of acute inflammation (Rahman *et al.*, 2012). In these conditions, the use of renal biopsy or imaging is often required to confirm the diagnosis before commencing therapy (Singer *et al*., 2011). Post-renal AKI occurs in patients due to obstruction of urinary flow (Basile *et al.*, 2012).

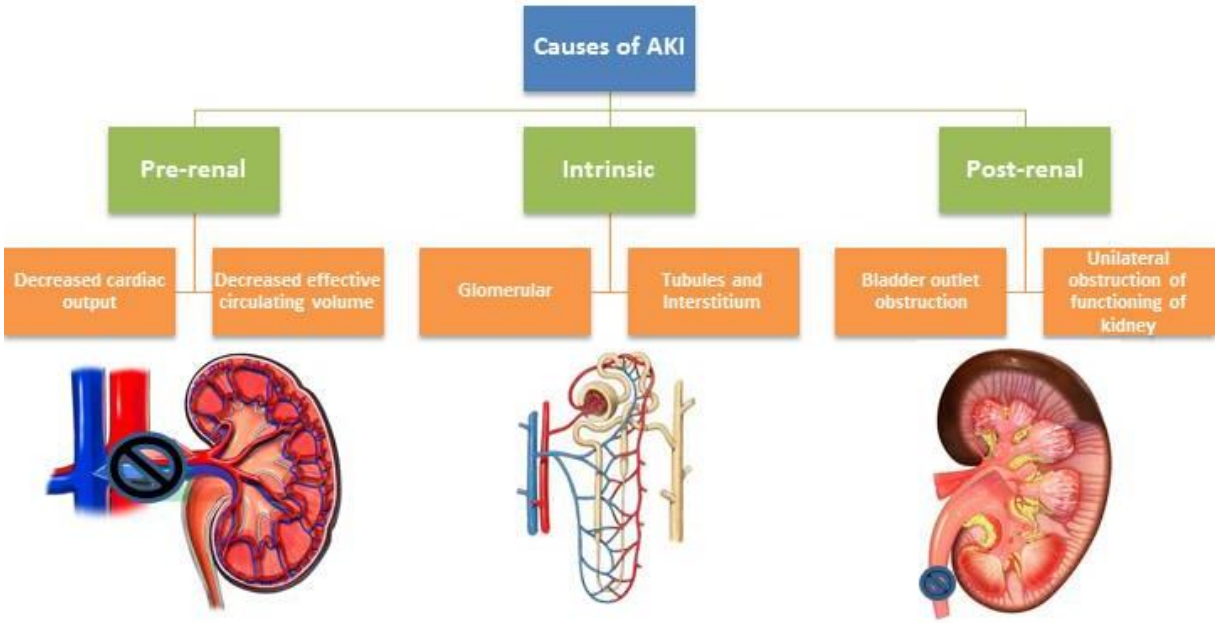

Figure 1.1 Potential causes of AKI.

1.2.3 Pathophysiology of Acute Kidney Injury

Adequate supply of oxygenated blood is necessary for production of mitochondrial adenosine triphosphate (ATP) and homeostatic cell function. The initiation phase of ischaemic AKI occurs when renal blood flow decreases. Lack of oxygen induces structural and functional changes in proximal tubular epithelial cells, disrupting their ability to maintain normal renal function (Sutton *et al.*, 2002).The extension phase of AKI is mediated by prolonged hypoxia after the initial ischaemic event and an inflammatory response (Devarajan, 2006). This is followed by the maintenance phase as cells attempt to maintain cellular and tubular integrity by undergoing repair, dedifferentiation, migration, apoptosis and proliferation (Dirkes, 2015). In order to restore structural and functional integrity of a nephron, tubular repair mechanisms are initiated. During recovery phase, differentiation of cells continues and epithelial cell polarity is re-established to restore cellular and organ function (Nony and Schnellmann, 2003; Schrier *et al.*, 2004) (Figure 1.2).

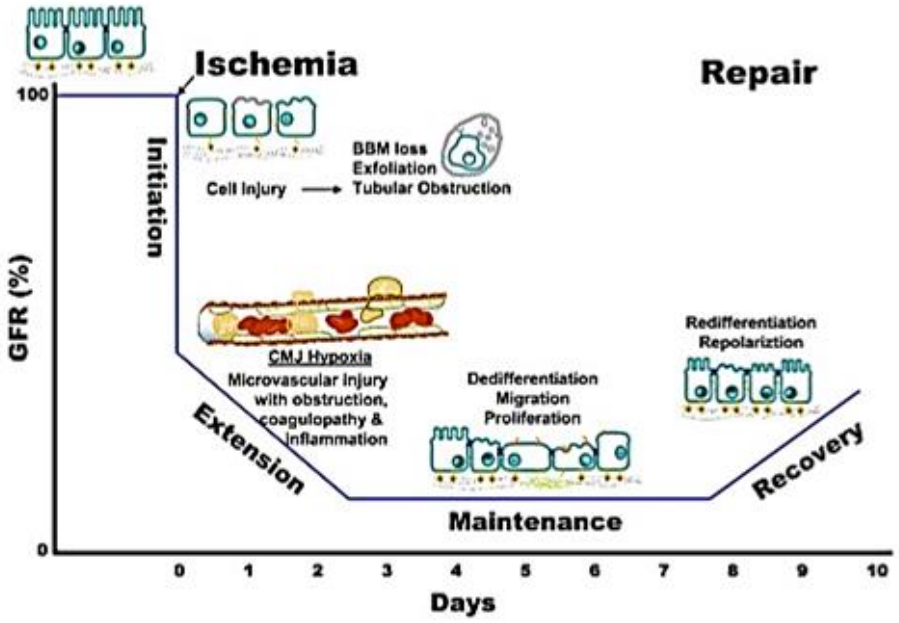

Figure 1.2 Pathophysiology of AKI. Stages of ischemic acute kidney injury depicting the relationship between the clinical phases and the cellular phases of AKI, and the temporal impact on organ function as represented by the GFR. Adapted from (Basile *et al.*, 2012).

1.2.4 Early consequences of Acute Kidney Injury

AKI affects upto 15% of hospitalised patients; it is strongly associated with increased morbidity, mortality and cost. Patients with AKI are unable to control volume status, serum biochemistry and acid base balance. Less severe forms can be managed with supportive care, but more severe forms require renal replacement therapy. Previous studies have shown an increased mortality in critically ill patients requiring dialysis (Lafrance and Miller, 2010; Hoste and De Corte, 2012).

1.2.5 AKI leading to Chronic Kidney disease

The severity of AKI, reversibility of the injury, temporal balance among effective and maladaptive repair and regenerative mechanisms define the course of renal disease after an episode of AKI. An observational study showed that the risk of developing stage 4 or 5 CKD was 28 times higher among patients with AKI necessitating dialysis (Waikar *et al.*, 2006). Furthermore, the risk of developing End Stage Renal Disease (ESRD) was 40 times higher in patients that had both AKI and pre-existing CKD

(Chawla *et al.*, 2014). Recent clinical findings suggest that a single episode of AKI causes irreversible renal damage and these patients have a significant risk for progression to CKD in future with or without coexisting conditions such as hypertension, diabetes, or cardiovascular disease (Coca *et al.*, 2009; Garg and Parikh, 2009).

Although healthy regeneration after AKI should lead to recovery of normal structure and function, maladaptive repair processes associated with dysregulated apoptosis, hypoxia, myofibroblast proliferation and infiltrating immune cells can lead to the loss of nephrons and progression to CKD via a self-perpetuating tubulo-interstitial fibrosis pathway. (Chawla and Kimmel, 2012; Chawla *et al.*, 2014). It is noteworthy that pathology seen in other forms of CKD is indistinguishable from the changes that develop in tubulo-interstitial fibrosis after ischaemic AKI .In addition to clinical findings, data from experimental models of AKI provide insight into biological mechanisms by which AKI contributes to subsequent CKD (Chawla and Kimmel, 2012). Studies have shown that a variety of intrinsic repair processes are activated rapidly after kidney injury induced by several pathophysiological processes such as hypoxia, oxidative stress, epigenetic changes, cell cycle arrest, DNA damage response, and mitochondrial dysfunction (Humphreys *et al.*, 2008). These events initiate an uncontrolled maladaptive repair mechanism that leads to interstitial fibrosis (Basile *et al.*, 2015). Furthermore, the expansion or maintenance of injury–induced interstitial changes may be driven by profibrotic factors such as TGF-β, connective tissue growth factor, and platelet–derived growth factor-B produced by stressed tubular epithelial cells and infiltrating cells (Venkatachalam *et al.*, 2010; Yang *et al.*, 2010b).

1.2.6 Chronic Kidney Disease

Chronic kidney disease is common and associated with an increased risk of end stage kidney disease and a requirement of dialysis and transplantation. In the clinic, CKD is diagnosed when structural or functional abnormalities of the renal tract are present. Functional abnormalities are defined as either a reduced GFR (<60mL/min per 1.73m^2) or albuminuria/haematuria (Jha *et al.*, 2013). In many countries, the incidence of CKD is as high as 200 cases per million per year (Levey *et al.*, 2005).

Over the past decade, the number of patients diagnosed with ESRD in the UK has doubled, thereby increasing the cost of providing renal replacement therapy (RRT) in the form of either dialysis or transplantation (Aitken *et al.*, 2014). In 2014, the number of new patients requiring RRT was 7,411 in the UK, with a rate of ESRD of 115 pmp (Gilg *et al.*, 2016). The incidence rate is higher in men than women. This increase in incidence of ESRD is expected to continue to rise at an annual rate of around 5–8% due to 2 factors (Renal, 2014). Firstly, the risk of developing CKD is higher among patients over 65 years and secondly, the number of patients suffering from diabetes and cardiovascular disease has risen in the last 20 years (Zoccali *et al.*, 2010).

1.2.7 Classification of stages of CKD

According to K/DOQI guidelines, GFR is used to assess the severity of CKD and based on GFR and albuminuria CKD is categorized in 5 main stages (Table 1.1).

Prognosis of CKD by GFR and albuminuria category

Prognosis of CKD by GFR and Albuminuria Categories: KDIGO 2012				Persistent albuminuria categories Description and range		
				A1 Normal to mildly increased <30 mg/g <3 mg/mmol	A2 Moderately increased 30–300 mg/g 3–30 mg/mmol	A3 Severely increased >300 mg/g >30 mg/mmol
GFR categories (ml/min/1.73 m²) Description and range	G1	Normal or high	≥90			
	G2	Mildly decreased	60–89			
	G3a	Mildly to moderately decreased	45–59			
	G3b	Moderately to severely decreased	30–44			
	G4	Severely decreased	15–29			
	G5	Kidney failure	<15			

Green: low risk (if no other markers of kidney disease, no CKD); Yellow: moderately increased risk; Orange: high risk; Red: very high risk

Table 1.1: Stages of CKD. The risk for progression of CKD is determined by colors according to the National Kidney Foundation's Kidney Disease Outcomes Quality Initiative (KDOQI) classification system (Inker *et al.*, 2014).

1.2.8 Management of CKD

In the last 10 years, research into CKD has intensified focusing on the prevention, early detection and treatment before it progresses towards renal failure (Jha *et al.*, 2013).

The risk factors associated with CKD such as diabetes, obesity and hypertension are becoming more prevalent among patients in UK (Stevens *et al.*, 2012). Appropriate treatment should be offered to patients to avoid complications. Randomised control trials suggest angiotensin-converting-enzyme (ACE) inhibitors or angiotensin-receptor blockers are the first line treatment for patients to reduce proteinuria and slow disease progression. Antihypertensive drugs along with ACE inhibitors are

administered to patients to reduce blood pressure (less than 130/80mm Hg) which slows progression of CKD (Cohn and Tognoni, 2001).

1.3 Ischaemia and Reperfusion Injury (IRI)

1.3.1 Ischaemia

An adequate supply of oxygen is critical to renal cell aerobic metabolism, maintenance of high-energy stores and normal renal function. Since the proximal tubule of the nephron has high oxygen consumption, ischaemia primarily influences structure and function of tubular epithelial cells in this region of the kidney. A mismatch of oxygen supply and local tissue demand causes certain cells irreversible cell damage which will eventually lead to cell death (Carden and Granger, 2000; De Groot and Rauen, 2007).

Prolonged deprivation of oxygen inhibits mitochondrial oxidative phosphorylation. This leads to rapid dissociation of ATP molecules to Adenosine monophosphate which may be further metabolised to adenosine and hypoxanthine. ATP depletion leads to rise in intracellular calcium concentration causing activation of proteases and phospholipases and cytoskeletal degradation (De Rosa *et al.*, 2017). Ischaemia induces production of inducible form of nitric oxide synthase (iNOS) that mediates production of high concentration of toxic nitric oxide (NO) from nitrate in proximal tubular epithelial cells (Goligorsky *et al.*, 2002). Generation of nitric oxide in ischemic phase results in formation of a cytotoxic metabolite, peroxynitrite, which can cause lipid peroxidation and nitrotyrosine modification (Devarajan, 2006). Studies have suggested that increased NO via iNOS activity during renal ischemia is deleterious to the kidney and inhibition of iNOS before IRI protects kidneys against IRI (Devarajan, 2005).

1.3.1.1 Hypoxia Inducible factor (HIF)

In an event of hypoxia, cells respond by increasing transcription of genes involved in in angiogenesis, erythropoiesis and anaerobic energy metabolism. Erythropoietin (EPO) maintains the oxygen carrying capacity of the blood by stimulating the production of red blood cells and transcription is increased in response to hypoxia (Haase, 2013). Studies of the EPO gene identified the hypoxia response element (HRE) flanking the 3' enhancer region (Shah and Xie, 2014). Subsequently the protein Hypoxia Inducible Factor-1 (HIF-1) that binds to HRE under hypoxic conditions was identified (Semenza, 2004). HIF-1 is a transcription factor which is constitutively expressed but rapidly degraded by the ubiquitin-proteasome system in the presence of oxygen. In the kidney, activation of HIF-1 provides protection from ischaemia-reperfusion and radiocontrast-induced injury (Semenza *et al.*, 1997; Heyman *et al.*, 2008). Semenza and his colleagues demonstrated that the increased expression of HIF-1α protects kidney from both morphological and functional injury during ischaemic preconditioning (Semenza, 2003).

1.3.1.1.1 HIF-1α and its activation

HIF-1 is a basic helix-loop-helix-Per-ARNT-Sim (bHLH-PAS) protein consisting of two key subunits alpha and beta. HIF-α has 3 isoforms, HIF-1α, HIF-2α and HIF-3α (Wu *et al.*, 2015). HIF-2α shares 48% amino acid sequence identity and structural and functional similarities to HIF-1α. In contrast to HIF-1α expression which is primarily expressed in the tubules, HIF-2α is expressed in endothelial and interstitial cells of the hypoxic kidney (Ke and Costa, 2006). HIF-1β is aryl hydro-carbon nuclear translocator and is constitutively expressed in all cells. Unlike HIF-1β, HIF-1α has a short half-life of 5 minutes (Ke and Costa, 2006). The presence of oxygen-dependent degradation domain facilitates oxygen-regulated stability (Ziello *et al.*, 2007). In normoxic conditions, HIF-1α is continuously synthesised and degraded (Gunaratnam

and Bonventre, 2009). The proline residues (P-402 and P-564) and asparagine (N-803) are hydroxylated by prolyl hydroxylase domain (PHD) and by factor inhibiting HIF-1 (FIH-1) (Bruick and McKnight, 2001). Furthermore, acetylation of lysine residue (K-532) by arrest defective-1 (ARD1) promotes HIF-1α interaction with the von Hippel-Lindau protein. This leads to ubiquitination HIF-1α forming E3 ubiquitin ligase VHL complex leading to proteasomal degradation (Jaakkola *et al.*, 2001).

During ischaemia, HIF-1α is stabilised. The hydroxylation of proline and lysine along with acetylation of asparagine mediated by PHD, FIH-1 and ARD1 is blocked due to lack of oxygen. HIF-1α interacts with CBP/p300 and translocates to nucleus where it dimerizes with HIF-1β and becomes transcriptionally active (Semenza, 2000; Semenza, 2001).

1.3.1.1.2 Downstream effects of HIF-1 signalling

Several biological processes that are essential for kidney function under physiological and pathological conditions are regulated by HIF-1. Although the number of genes directly and indirectly regulated by HIF-1 has grown rapidly, it is still not clear which signalling pathways mediate this protective effect. During hypoxia, HIF-1 exhibits cytoprotective effect by regulating anaerobic glycolysis, protein translation, cellular proliferation, and apoptosis (Higgins *et al.*, 2007). An increased HIF-1α expression was observed in kidneys of rats exposed to various hypoxic stimuli (Rosenberger *et al.*, 2002). Another study showed that knockdown of HIF-1α in mice inhibits fibrosis progression by reducing inflammation and ECM deposition post UUO (Higgins *et al.*, 2007). Moreover, HIF-1α heterozygous mice were more susceptible to renal IRI and suffered substantially more injury post IRI when compared with controls thus proposing a protective role of HIF in IRI to the kidneys (Kojima *et al.*, 2007).

Furthermore, HIF-1 promotes cell proliferation/survival in certain cells types by stimulating the production of several cytokines and growth factors such as insulin-like growth factor-2 (IGF2) and TGF-β (McClintock *et al.*, 2002). Several clinical findings suggest that HIF-1 could potentially lead to a path of renal fibrosis by direct regulation of fibrotic factors and by acting synergistically with TGF-β. Studies suggest that hypoxia promotes fibrosis by increasing SMAD3 mRNA levels and by activating TGF-β signalling via thrombospondin-dependent release of latent TGF- β (Sánchez-Elsner *et al.*, 2004; Heikkinen *et al.*, 2010).

Studies have shown that hypoxia leads to HIF-1 dependent dedifferentiation and transition of renal epithelial to mesenchymal fibroblast-like cells characterised by loss of E-cadherin at intracellular junctions, increase in motility and reorganisation of the actin cytoskeleton (Higgins *et al.*, 2007). Paradoxically, adaptation of a cell to hypoxia assures prolonged proliferation/survival in some circumstances and cell death in other circumstances. Genetic studies using embryonic stem cells have demonstrated that the expression of HIF-1 is significantly correlated with apoptosis since it mediates activation of caspase-3 and Apaf-1-mediated caspase-9, and the release of cytochrome under hypoxic conditions (McClintock *et al.*, 2002).

1.3.2 Reperfusion

Post ischaemia, reperfusion restores the flow of oxygenated blood causing an increase in oxygen levels. This normalisation is associated with damage to tissues. An increase in mitochondrial calcium content, production of ROS and a reduction in antioxidant capacity lead to structural cell injury and cell death. Overall these processes are termed Ischaemia Reperfusion Injury (IRI) (Devarajan, 2005; Devarajan, 2006). Experimental finding suggest that in an event of ischaemia-reperfusion injury, ischaemia accounts for 17% cell death while 73% cell death occurs post ischaemia-reperfusion injury (Padanilam, 2003) (Figure 1.3).

1.3.2.1 Oxidative stress

During the reperfusion phase of IRI, xanthine oxidase catalyses conversion of hypoxanthine to xanthine to yield hydrogen peroxide which forms highly reactive hydroxyl radicals in presence of iron. These free radicals cause renal tissue injury via peroxidation of membrane lipids and oxidative damage to proteins and DNA which contribute to apoptosis and cell death (Malek and Nematbakhsh, 2015).

Recent studies have shown the beneficial effects of supplements containing antioxidants and free radical scavengers on IRI in animals. The antioxidant activity of melatonin prevented free radical-mediated renal damage during the reperfusion period post ischaemia (Mune *et al.*, 2002). Furthermore, the antioxidant activity of Ulinastatin and Propofol protects kidney from IRI by inhibiting apoptosis, neutrophil infiltration, lipid peroxidation and cytokine production. Herbal antioxidants such as picroliv, naringin and aqueous garlic extract have shown protective effects on IRI (Rakesh *et al.*, 2010).

1.3.2.2 Mitochondrial dysfunction

Post ischaemia, the exposure of mitochondria to large amounts of calcium and free radicals contributes to progressive functional deterioration (Szeto *et al.*, 2011). Increased intracellular calcium overload can trigger several calcium mediated pathways that may contribute to cell death (Kosieradzki and Rowiński, 2008). Therapeutic agents with antioxidant properties are being developed to reduce damage caused to mitochondria post IRI (Cho *et al.*, 2007).

1.3.2.3 Nitric oxide

Nitric oxide produced during ischaemia reacts with superoxide to form peroxynitrite leading to protein nitrosylation. The importance of protein nitrosylation in tissue injury

is supported by studies using inhibitors of iNOS which result in in reduced lipid peroxidation and inflammation (Jeong *et al.*, 2008).

1.3.3 Cellular and metabolic consequences of tubular injury

Ischaemia-reperfusion affects cell viability and activates different programs of cell death. Necrosis is a chaotic process characterised by loss of membrane integrity, cytoplasmic swelling followed by fragmentation of a cell and its components. Cells release molecules that stimulate inflammation and tissue damage (Padanilam, 2003). Apoptosis in contrast involves activation of a complex caspase signalling cascade leading to cytoplasmic shrinkage, DNA fragmentation and formation of apoptotic bodies. Loss of tubular cell leads to loss of tubular re-absorptive and excretory function and reduced GFR (Havasi and Borkan, 2011). Animal studies have shown that blocking of pro-apoptotic protein Bax and Bid, caspases (1, 6 and 7) protects mice from cisplatin induced renal injury by reducing tubular apoptosis, neutrophil infiltration, and improved renal function (Faubel *et al.*, 2004; Wei *et al.*, 2007; Yang *et al.*, 2008).

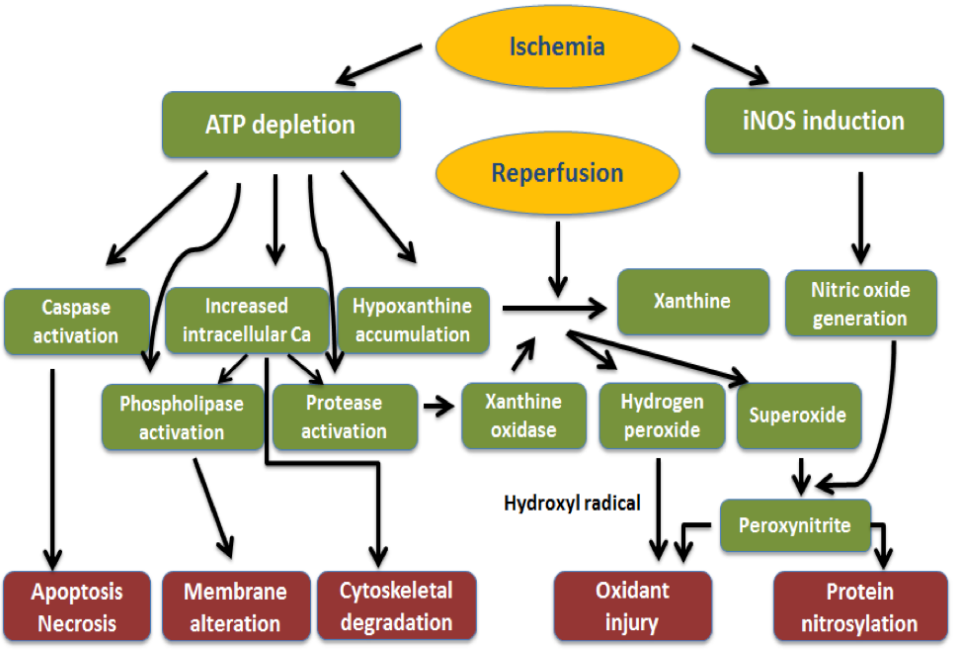

Figure 1.3 Pathophysiology of IRI. Alterations in cell metabolism post IRI. Adapted from (Cao et al., 2013)

1.4 Tissue Repair after IRI

During maladaptive repair post AKI, there is increased numbers of myofibroblasts that contribute to the deposition of fibrotic matrix components such as collagen (Ferenbach and Bonventre, 2015). The different components of extracellular matrix released during kidney injury are discussed below.

1.4.1 Extracellular matrix synthesis

Although kidney can recover form an insult of IRI, there are long term detrimental effects of even brief periods of IRI. To undergo repair, cells initiate signalling pathways that lead to activation of genes causing production and accumulation of extracellular matrix proteins within the interstitial space (Lan, 2003).

1.4.1.1 Collagen

Collagen constitutes the main structural element of the interstitial ECM. In physiological conditions, collagen I and III are expressed at low levels in the glomeruli and the renal interstitium. During fibrosis, collagen I and III accumulates in the tubulointerstitial space, glomeruli and arterial walls thus contributing to development of CKD (Genovese *et al.*, 2014).

1.4.1.2 Glycoproteins

Due to high carbohydrate content, proteoglycans may play an important role in growth factor binding. They are found in the renal extracellular interstitial space where they act as a reservoir of profibrotic growth factors such as the latent forms of TGF-β (Fan *et al.*, 1999). Small leucine rich proteoglycans such as decorin and biglycan are highly expressed in the tubulointerstitium and play an important role in collagen fibrillogenesis. Animal model studies show biglycan upregulation before macrophage infiltration is associated with tubular inflammation (Hsieh *et al.*, 2014)

and decorin modulates the activity of TGF-β1 signaling (Cabello-Verrugio and Brandan, 2007).

1.4.1.3 Metalloproteinases (MMPs)

Metalloproteinases (MMPs) are matrix-degrading enzymes that play a central role in maintaining the homeostasis of the ECM, destruction of the basement membrane, angiogenesis, cell migration and cell apoptosis (Kugler, 1998; Kunugi *et al.*, 2011). An increased expression of MMP-2 and MMP-9 has been reported in animal models of renal fibrosis (Caron *et al.*, 2005; Cheng *et al.*, 2006). These may contribute to the degradation of basement membrane and ECM components (Catania *et al.*, 2007).

1.4.2 Growth factors contributing to the extracellular matrix deposition

Besides their activity on ECM components, MMPs are also known to modulate tubular cell responses by controling the expression of cytokines, chemokines and growth factors that propagate renal injury, facilitate interstitial inflammation and/or directly contribute to fibrosis. Growth factors identified in renal tissue act as potent mediators in the development of fibrosis. These include epidermal growth factor (EGF), TGF-α, TGF-β, platelet derived growth factor (PDGF), fibroblast growth factor (FGF) and insulin-like growth factor IGF and Angiotensin II (Liu, 2010).

TGF-β a key mediator involved in regulating fibrosis and is known to have a direct effect on the turnover of the ECM. Low concentrations of TGF-β are found in a normal functioning kidney. Abnormal expression of TGF-β has been documented in kidney fibrosis. Studies confirm that deposition of fibronectin, laminins, and collagen is facilitated by TGF-β1 and long term increase in TGF-β1 is associated with chronic rejection following organ transplantation in humans (Böttinger and Bitzer, 2002).

1.5 Transforming growth factor

The TGF-β is a member of the transforming growth factor superfamily that plays a fundamental role in cell proliferation and differentiation, in embryological development, oncogenesis, and tissue repair (Verrecchia and Mauviel, 2002). The TGF-β superfamily comprises of nodal, activins, inhibins, bone morphogenetic proteins (BMPs) and growth differentiation factors (GDFs). Increased TGF-β activity is associated with pathophysiological processes including tubular epithelial cell dedifferentiation and ECM deposition that may eventually leads to deterioration in renal function and renal fibrosis. This ubiquitously expressed and multifunctional cytokine is secreted by macrophages, mesengial cells, T cells, tubular epithelial cells and myofibroblast in renal fibrosis (Horiguchi *et al.*, 2012).

In addition to TGF-β, a role for BMP-7 has been suggested in CKD (Meng *et al.*, 2013). Studies have indicated an anti-fibrotic role of BMP-7, largely mediated by opposing the pro-fibrotic effect of TGF-β and reducing ECM formation. It therefore has a therapeutic potential in decreasing acute and chronic renal injury (Zeisberg, 2006; Li *et al.*, 2015).

1.5.1 Latent TGF-β and its activation

The TGF-β superfamily contains three isoforms of TGF-β termed TGF-β1, TGF-β2, and TGF-β3 which display a variety of proliferative, inductive and regulatory functions (Sporn and Roberts, 1992) and exhibit both overlapping and distinct patterns of expression during development (Pelton *et al.*, 1991), wound healing and in disease conditions (Böttinger and Bitzer, 2002). The three isoforms exhibit 71–79% amino acid sequence identity and the function of the different isoforms appears to be similar *in vitro*. However, the phenotype of knockout mice is different for each isoform suggesting distinct functions of the isoforms *in vivo* (Annes *et al.*, 2003).

The activation of TGF-β is localised to sites where its released from its latent form. Each member is synthesised as a large peptide that comprises of N-terminal portion called the latency-associated peptide (LAP), a short C-terminal fragment that is the mature cytokine and a signal peptide to direct TGF-βs to the endoplasmic reticulum. This peptide is subjected to intracellular cleavage by furin to form small latent complex (SLC) that although the amino bonds between LAP and the mature TGF-β are cleaved they remain noncovalently associated (Janssens *et al.*, 2003). The SLC then associates with Latent TGF-β binding protein (LTBP) via interactions with LAP forming the large latent complex. LTBP facilitates binding of the large latent complex to proteins of the extracellular matrix (Kusakabe *et al.*, 2008).

1.5.2 Activation of TGF-β

Latent TGF-β is converted to its active form by changes in pH (2-8), heat (100^0c) or due to action of ROS, plasmin and TSP-1 (Flaumenhaft *et al.*, 1993).

Changes in temperature and pH activate latent TGF-β in biological samples *in vitro*. However, it is not clear whether activation of latent TGF-β by any of these conditions is physiologically relevant (Gleizes *et al.*, 1997).

1.5.2.1 Activation by Plasmin

Plasmin are primarily involved in ECM degradation (Blakytny *et al.*, 2004). Several studies have indicated the activation of Latent TGF-β by plasmin by cleavage of LAP from the latent complex (Khalil, 1999).

1.5.2.2 Activation by Thrombospondin-1

Among the five isoforms of Thrombospondin, Thrombospondin-1 (TSP-1) has been most widely studied (Lawler, 2002). TSP-1 is also expressed in a number of tissues throughout development and facilitates wound repair in several ways: modulation of cell adhesion, promotion of angiogenesis, and reconstruction of the matrix (Midwood

et al., 2004). TSP-1 binds to LAP leading to disrution of the complex and release of boiactive TGF-β. The in vivo role of TSP-1 as an activator of latent TGFβ was suggested when TSP-1 null mice exhibited a similar phenotype as TGFβ null mice (Froese, 2013).

1.5.2.3 Activation by Reactive oxygen species (ROS)

It is hypothesised that ROS leads to TGF-β activation by altering one or several side amino acids such as cysteine or methionine residues in LAP. Oxidation of LAP causes instability resulting in either loss of its noncovalent association with TGF-β or a conformational change thus exposing the TGF-βR binding site. In animal models of ROS generation, increased TGF-β activation is evident (Hegde *et al.*, 2005).

1.5.2.4 Activation by pH

Changing pH causes TGF-β activation by inducing denaturation of the LAP protein, which disturbs the interaction between LAP and TGF-β. No activation of human derived L-TGF-β was observed at a pH above 3.5. A change in pH below 3.1 and above 11.9 led to L-TGF-β activation (Nocera and CHU, 1995).

1.5.2.5 Activation by Heat

Heating is considered more effective and efficient in generating active TGF-β than acid treatment. Activation of TGF-β occurs more when temperature is around 70-80°C for 10 minutes while denaturation occurs if temperature rises above 80°C (Annes *et al.*, 2003).

1.5.3 Structure of TGF-β receptors for TGF-β family

TGF-β transduces its signal by bringing together two transmembrane receptors kinases, TGF-βRI and TGF-βRII (Wrana *et al.*, 1992). Ligand induced oligomerization of type I and II receptors initiates a transphosphorylation cascade (Greenwald *et al.*, 1999). This starts with type II receptor phosphorylation of type I receptor leading to

the activation of its kinase activity. The activated type I kinase receptors in turn activate members of receptor mediated SMAD proteins (R-SMADs) and non-SMAD pathways. This model of signalling involving type I and II receptors and the type II receptor phosphorylation of type 1 receptor is common amongst all proteins of the TGF-β superfamily (Wrana *et al.*, 1994). Furthermore, there are seven human type I receptors and 5 type II receptors to which the individual members of the TGF-β family bind to in different combinations (Table 1.2).

Molecular category	TGFβ pathway*	Activin/inhibin/Nodal pathway*	BMP pathway*
Ligands	TGFβ1, TGFβ2, TGFβ3	Activin A, activin B, inhibin A, inhibin B, Nodal	BMP2, BMP4, BMP5, BMP6, BMP7, BMP8A, BMP8B, BMP9, BMP10
Type I receptors	TβRI (ALK5), ALK1 (ACVRL1 or SKR3)	ALK4 (ACVR1B or ACTRIB), ALK7 (ACVR1C or ACTRIC)	ALK1 (ACVRL1, SKR3), ALK2 (ACVR1, ACTRI), ALK3 (BMPR1A), ALK6 (BMPR1B)
Type II receptors	TβRII	ACTRIIA, ACTRIIB	BMPR2, ACTRIIA, ACTRIIB
Type III receptors	TβRIII (betaglycan), endoglin, CRIPTO3 (TDGF1P3)	CRIPTO1 (TDGF1), CRIPTO3 (TDGF1P3), TβRIII (betaglycan)	RGMA, RGMB (DRAGON), RGMC (HJV or HFE2), endoglin
R-SMADs	SMAD2, SMAD3	SMAD2, SMAD3	SMAD1, SMAD5, SMAD8
Co-SMAD	SMAD4	SMAD4	SMAD4
I-SMADs	SMAD7	SMAD7	SMAD6, SMAD7

*Alternative protein names are listed in brackets. ACTR, activin receptor; ALK, activin receptor-like kinase; BMP, bone morphogenetic protein; BMPR, BMP receptor; RGM, repulsive guidance molecule; TβR, TGFβ receptor; TDGF, teratocarcinoma-derived growth factor.

Table 1.2: List of all ligands, receptors and SMADs involved in the TGF-β superfamily. (Akhurst and Hata, 2012)

For example, the type II activin receptor ActRIIA/B can combine with the type I receptor ActRIB/ALK4 and mediate the downstream activin signalling. Another example of multiple receptor interaction is BMP type II receptor BMP-RII combing to three different type 1 receptors namely BMP-RIA, BMP-RIB and ActRI/ALK2 (Derynck and Feng, 1997). Upon dimerisation of receptors, the ligands TGF-β, activin and nodal induce phosphorylation of SMAD 2 and 3 while BMPs phosphorylate SMAD 1, 5 and 8 (Hinck, 2012; Moustakas and Heldin, 2014).

1.5.4 TGF-β/SMAD signalling pathway

There are eight SMADs i.e. SMAD 1-8. SMAD 2 and SMAD 3 are activated via phosphorylation of carboxyl terminal by TGFβR-I and ActRIIA whereas SMAD 1, 5 and 8 are activated by ALK-1, ALK-2, ALK-3/ BMP-RIA and ALK-6/BMP-RIB in response to ligand binding (Itoh *et al.*, 2000). These activated SMADs are termed receptor-regulated SMADs/ R-SMADs that upon phosphorylation form a complex with SMAD 4 before translocating to the nucleus. Studies suggest that SMAD 4 is not always required to activate the downstream signalling pathways as even in the absence of SMAD 4 some TGF-β responses occur (Sirard *et al.*, 2000; Moustakas *et al.*, 2001). The expression of inhibitory SMADs (I-SMADs), SMAD 6 and SMAD 7 is regulated by extracellular signals. I-SMADs repress the signalling by competing with R-SMADs for their binding to activated type I receptors and preventing phosphorylation of R-SMADs. For example, SMAD 7 strongly binds to the activated type I receptors for TGF- β /Activin and BMP, inhibits phosphorylation of SMAD 1/5 or SMAD 2/3 and represses the signalling cascade. SMAD 6 binds strongly to activated type I receptors for BMP, and only weakly to TGF-β receptors (Nakao, 2006). Antagonists of SMADs such as Smurf 1(SMAD ubiquitination- regulatory factor 1) and Smurf 2 interact with R-SMADs and target them for ubiquitin–proteasome-mediated degradation. Smurf 1 interacts with SMAD 1 and SMAD 5 while Smurf 2 interacts more broadly with different R-SMADs. The former affects BMP responses while the latter interferes with BMP and TGF-β/ activin signalling (Lo and Massagué, 1999)(Figure 1.4).

1.5.5 SMAD independent signalling

TGF-β can also activate other signalling cascades such as MAPK, JNK and ERK pathways via SMAD independent pathways. For example, SMAD4 deficient cells with additional inhibitor of TGF-β type I receptors could induce MAPK pathway activation

in response to TGF-β (Engel *et al.*, 1999). However, the mechanism of MAPK, JNK and ERK kinase pathway activation by TGF-β is not well understood. Furthermore, activation of MAPK pathways by TGF-β may lead to SMAD phosphorylation allowing convergence of TGF- β induced SMAD and MAPK pathways. In this way the balance between the direct and indirect activation of SMADs defines cellular responses to TGF-β (Yu *et al.*, 2002).

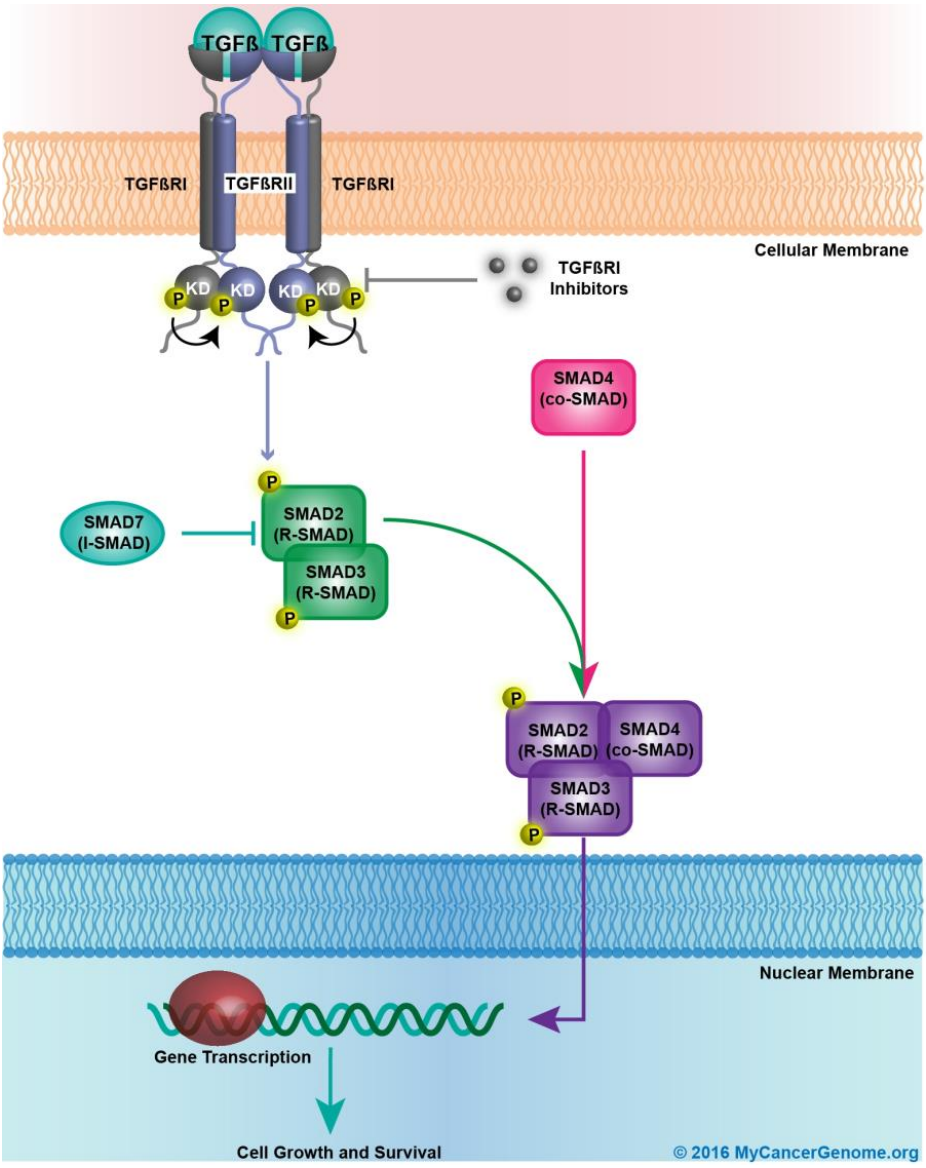

Figure 1.4: Overview of TGF-β receptor activation and SMAD signalling. (Genome, 2016)

1.5.6 TGF-β in kidney diseases

1.5.6.1 Cell culture models of Renal Fibrosis

There is growing evidence that tubular epithelial cells (TEC) can phenotypically and ultra-structurally become myofibroblasts in response to TGF-β *in vitro* that mimics the progression of fibrosis *in vivo*. Thus, cultured cells including those derived from genetically modified animals have been used to study renal fibrosis.

Cell culture 2D and 3D model have been used to assess total ECM accumulation that represents a biological consequence of TGF-β activation. Human derived renal glomerular epithelial cells, tubular epithelial cells and mouse tubular epithelial cells upon stimulation with TGF-β1 have shown to undergo morphological changes and express matrix proteins (Xu *et al.*, 2007). Other studies have used rat derived cells to study the pathophysiological processes of renal disease, for instance TGF-β production and ECM production in response to angiotensin II (Kagami *et al.*, 1994; Ucero *et al.*, 2013).

1.5.6.2 Animal and preclinical models

Animal studies have established the importance of TGF-β in renal fibrosis that is supported by *in vitro* studies, demonstrating that TGF-β not only induces the expression of ECM but also inhibits its degradation by inhibiting matrix metalloproteases MMPs and activating the TIMPs (Ma and Chegini, 1999; Hocevar and Howe, 2000). *In vivo* studies have employed the use of nephrotoxins, such as cyclosporine, to augment the expression of TGF-β1 in renal tubular cells for studying interstitial fibrosis. However, the concentrations of cyclosporine administered was much higher than its used in clinical practice (Yang *et al.*, 2010a; Kim *et al.*, 2012). Furthermore, there are several chemical models for studying renal fibrosis that involve administering chemicals into Sprague-Dawley rats (less resistant to

developing tissue scarring). Although these agents induced renal fibrosis, the model induced liver toxicity.

The unilateral ureteral obstruction (UUO) model is the most widely used interstitial fibrosis model. It shares similar etiology to human obstructive nephropathies and reproduces a sequence of events that is similar to that found in human diseases, including progressive decline in renal blood flow and glomerular filtration rate, tubular epithelial cell damage and a significant increase in renal fibrosis within 1-2 weeks of ureteral obstruction (Tan *et al.*, 2007; Grande *et al.*, 2010). Therefore, UUO mouse model can be used in research to obtain new therapeutic options for effective treatment of renal fibrosis.

1.5.6.3 Inhibition of TGF-β

Blocking TGF-β by using either neutralising antibodies or soluble TBRII alleviates renal fibrosis in rat and murine nephropathy models (Liu *et al.*, 1999; Ucero *et al.*, 2013). However, blockade of SMAD signaling rather than TGF-β may provide more effective therapeutic strategy for renal fibrosis. It is a clear fact that SMAD7 counter regulates TGF/Smad signaling in fibrosis. Several *in vitro* studies have shown that TGF-β stimulates SMAD7 expression to exert a negative feedback mechanism in renal diseases (Uchida *et al.*, 2000; Schiffer *et al.*, 2001). Overexpression of renal SMAD7 by introducing doxycycline-regulated SMAD7 cDNA into the kidney significantly inhibited SMAD 2/3 activation and renal fibrosis in a rat UUO model (Nakao *et al.*, 1999; Lan *et al.*, 2003).

The antifibrotic molecule, Pirfenidone attenuates renal fibrosis in the UUO model by decreasing the level of TGFβ and subsequent synthesis of collagen in the renal tissue. This suggests that pirfenidone may be applied as a treatment of renal fibrosis progression (Shimizu *et al.*, 1998). Although anti-TGFβ therapies are associated with improved renal fibrosis (McCarty, 2006). They should be used cautiously because

TGFβ is also involved in the immune regulation that restricts inflammation during renal injury (Gagliardini and Benigni, 2006). Further studies in animal models are required to confirm whether TGFβ is beneficial for combatting the progression of renal fibrosis, and to assess whether these therapies can be explored in human clinical trials.

1.6 Role of Integrins in kidney injury

Integrins are large, membrane spanning, type I transmembrane heterodimeric glycoprotein receptors that mediate cell-adhesion. The receptor dimer comprises an extracellular head region that traverses the plasma membrane and terminates in short cytoplasmic domains. These domains initiate the assembly of large signalling complexes and thereby bridge between the extracellular space and the intracellular cytoskeleton. Integrin mediated adhesion facilitates migration on ECM, formation of platelet aggregates, establishment of intracellular junctions and modulate signalling cascades that control cell motility, survival, proliferation, and differentiation (Hood and Cheresh, 2002; Danen, 2013).

1.6.1 Integrin structure, expression and function

Integrins are formed through noncovalent association of an α and β subunit. There are 24 different integrins as a result of combinations airing from 18α and 8β known subunits with different binding properties and different tissue distribution. The α subunit forms the globular head region and participates in ligand binding along with the β subunits (Berman and Kozlova, 1999; Springer and Wang, 2004; Xiong *et al.*, 2007)(Figure 1.5).

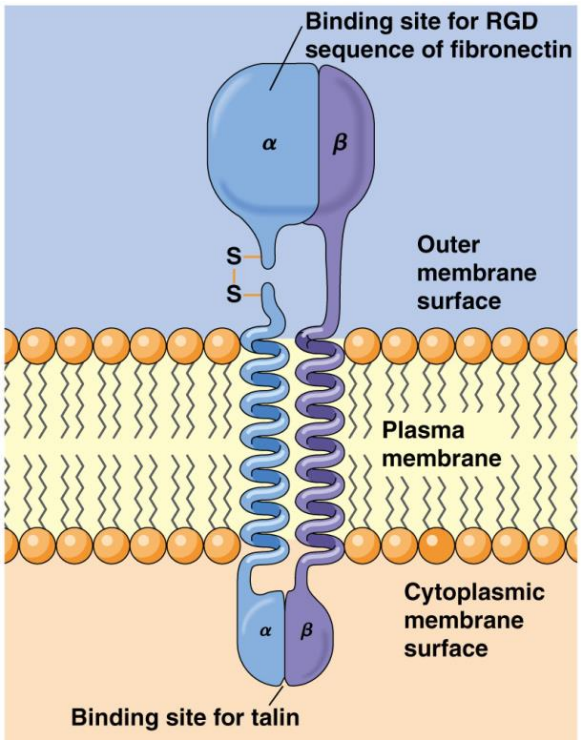

Figure 1.5: Structure of an Integrin. Integrin comprises of α and β subunit. The α subunit forms the globular head region and participates in ligand binding along with the β subunit (Hardin and Bertoni, 2015).

Integrins are expressed by different cell types and play a diverse and important role in most biological processes. Many integrins bind to components of ECM by a common integrin-binding motif, that is expressed by collagen and fibronectin while others bind to receptors present on other on leukocytes and endothelial cells (Ruoslahti, 1991). Mice models provide much insight into the pattern of distribution and functions of specific integrin heterodimers during disease or embryogenesis. Blocking the α1 subunit has shown to increase collagen synthesis while blocking of α2 results in reduced platelet function with increased vascularisation following wounding (Lowell and Mayadas, 2012). Mice lacking α5 have defects in mesoderm and vascular development while αv knockout mice exhibit neuro-epithelial and to cerebral vascular defects (Astrof and Hynes, 2009). The β6 integrin expression is restricted to the epithelia and binds to fibronectin with high specificity (Breuss *et al.*, 1995). The β5 integrin is highly expressed in the glomerulus, juxta glomerular apparatus, proximal convoluted tubules and collecting tubules and epithelial cells of

proximal tubules of the kidney (Pasqualini *et al.*, 1993). This demonstrates that every integrin has a specific expression pattern, different functionality and downstream effect.

1.6.2 Role of integrins in TGF-β activation

In addition to their direct effects on cellular proliferation and survival, integrins interact with a variety of growth factor pathways associated with cell proliferation and differentiation. In vertebrates, αvβ3 integrin interacts with the transmembrane receptors for VEGF, PDGF and IGF while α5β1 integrin interacts with the EGF receptor activating growth factor signalling, ECM deposition and promoting fibrosis. Several studies indicate there is extensive crosstalk between integrins and TGF- β signalling. TGF- β regulates the expression of integrins, their ligands and integrin-associated proteins therefore influencing integrin-mediated cell adhesion and migration. Conversely, several integrins directly control TGF- β activity by interfering with SMAD-dependent and SMAD-independent TGF- β signalling in several ways. This includes regulating the expression of TGF-β signalling pathway components, physical association of integrins with TGF- β receptors and downstream modulation of effectors (Danen, 2013). Once the integrin binds latent TGF-β, the activation occurs by two proposed mechanisms.

The first mechanism involves the use of proteases where integrins serves as a common docking point for latent TGF-β and proteases. The second mechanism involves an interaction between LAP and integrin leading to generation of a mechanical force causing a conformational change in the complex that allows TGF-β to bind to its receptor (Annes *et al.*, 2003; Camelo *et al.*, 2013).

1.6.2.1 Integrin expression in kidney

Integrin αvβ6 is expressed at low levels in normal kidney and regulates the levels of free and active TGF-β in tissues by binding to the LAP/TGF-β complex. Its induction

is evident in a broad range of renal diseases that is coupled with chronic inflammation and fibrosis. Immunohistochemical staining in previous studies has demonstrated prominent αvβ6 staining in the epithelial cell lining, dilated and damaged tubules in biopsies of patients diagnosed with membranous glomerulonephritis, IgA nephropathy and Goodpasture's syndrome (Reiser and Sever, 2013).

The potential regulatory role of αvβ6 in renal fibrosis has been previously investigated by using function-blocking αvβ6 antibodies and a mouse model with genetic ablation of the β6 subunit. Treatment with αvβ6-blocking antibody attenuated accumulation of activated fibroblasts and reduced interstitial collagen matrix deposition and similar inhibition of ECM marker expression was observed in mouse lacking β6- subunit (Hahm *et al.*, 2007; Henderson and Sheppard, 2013). In contrast to the integrin β6 null mice, mice lacking β8 subunit demonstrate subtle renal abnormalities characterised by albuminuria as absence of integrin αvβ8 increases levels of bioactive TGF-β leading to glomerular damage (Pozzi and Zent, 2011)

Integrin α3β1 which is highly expressed in the glomerulus and tubules is involved in podocyte stability and glomerular development. Studies suggest that lack or mutation in the α3 subunit leads to development of renal abnormalities such as atrophic glomeruli and severe proteinuria due to defects in the collecting duct and glomerulus (Kreidberg, 2003). Integrin α1β1 and α2β1 expressed throughout the kidney and on leukocytes binds to collagen and their expression is upregulated during renal disease (Yurchenco, 2011). Blocking α1 subunit has shown to reduce renal scarring by inhibiting leukocyte infiltration while chemical antagonism of α2β1 protects mice from developing glomerular fibrosis by regulating collagen synthesis and ROS production (Cosgrove *et al.*, 2008).

1.7 Hypothesis

IRI was previously thought to be a transient process, with full recovery of function and resolution of the histological lesion, ATN. However, most recent studies suggest that post IRI there is not complete resolution of injury but instead IRI initiates a series of events that can lead to progressive loss of renal function. The null hypothesis of the study was that there is no relationship between TGF-β signalling pathway and hypoxic or free radical stress in human proximal tubular epithelial cells.

1.8 Specific Aims

The main aim of the project was to provide data on the link between AKI and CKD and cell changes that occur and predispose to the subsequent decline in kidney function.

1. Establish an *in vitro* model of renal tubular IRI by using renal tubular proximal epithelial cell lines.

2. Assess whether tubular cells develop a pro-fibrotic phenotype after IRI and determine whether these changes rely on the synthesis of intermediates such as TGF-β.

3. Determining the role of αvβ6 integrin in IRI

Chapter 2: Material and Methods

2.1 General Practise

All experimental procedures were conducted in a containment level II laboratory according to the University Health and Safety policy. Control of Substances Hazardous to Health forms have been reviewed and signed before starting work. All laboratory work and procedures were performed in compliance with the Newcastle University publications ‘Safe Working with Biological Hazards’, and ‘Safe Working with Chemicals in the Laboratory’. Tissue culture was carried out in containment level II microbiological safety cabinets that were routinely cleaned with 70% ethanol prior to use and periodically cleaned by "mycoplasma off" spray. All cell culturing equipment were sprayed with 70% ethanol prior use.

2.2 Materials

Reagents, general chemicals and histological stains were purchased from Sigma Aldrich. Cell culture reagents were purchased from; Lonza, Invitrogen and Sigma Aldrich. General consumables and cell culture consumables were purchased from; Gibco Life Sciences, VWR International and Starlab. GoTaq DNA polymerase was purchased from Promega. Reverse transcription reagents were purchased from Agilent Technologies and SYBR green PCR kit was purchased from Sigma Aldrich.

2.2.1 DNA Buffers

10x Tris-Boric acid EDTA

10.8g of Tris-base, 5.5g of boric acid and 9.3g of EDTA in 1000ml dH_2O with pH adjusted to 8.3.

2.2.2 Western Blot Buffer solutions

10x Tris-glycine Running Buffer

30.3g of Tris-base, 144g of glycine and 10g of SDS was dissolved in distilled water to a total volume of 500ml. For electrophoresis, this buffer was diluted to 1x with distilled water.

10x Transfer Buffer

30.3g of Tris-base and 144g of glycine were dissolved in distilled water to a total volume of 1000ml. To make 1x of Tris-glycine transfer buffer, 100ml of 10x Tris-glycine transfer buffer was added to 200ml of Methanol (ANALAR). The volume was then adjusted to 1000ml with 700ml distilled water.

10x TBS

87.6g of NaCl and 12.1g of Tris-base were dissolved in distilled water to a total volume of 850ml. pH was adjusted to 8.0, and the volume adjusted to 1000ml by adding distilled water.

1x TTBS

To make 1x TTBS solution, 10x TBS was diluted to 1x using distilled water and Tween-20 added to a final concentration of 0.1%.

Blocking Buffer solution

5g of Bovine Serum Albumin (BSA) was dissolved in 100ml of TTBS, and stored at 4^0C.

2.2.3 Flow Cytometry Buffer solutions

Washing solution

2g of BSA was dissolved in 100ml of PBS and stored at 4^0C.

2.2.4 Immunofluorescence Buffer solutions

Blocking Buffer solution

50µl of Goat serum/rabbit serum was dissolved in 950µl of PBS and stored at 4^0C.

2.2.5 Bacterial Transformation

LB agar

Add 35g of LB Broth with agar (Lennox) (Sigma Aldrich) in 1L of water. Autoclave before pouring onto petri dish along with 100μg/ml Ampicillin (Sigma Aldrich).

2.2.6 ELISA (Enzyme Linked Immunosorbent Assay)

Diluent solution

TGF-β1 ELISA- 1.4% BSA in 100ml PBS

TGF-β2 ELISA- 1% BSA in 100ml PBS

Washing Buffer solution

Add 0.05% Tween 20 to 1L of 1XPBS

Blocking Buffer solution

TGF-β1 ELISA- 1-5 % Tween 20 in 100ml PBS

TGF-β2 ELISA- 1% BSA in 100ml PBS

Capture Antibody Solution

TGF-β1 ELISA- 1/120 Dilution in TGF-β1 Diluent

TGF-β2 ELISA- 1/180 Dilution in TGF-β2 Diluent

Acidification and Neutralisation reagents

1 N HCl (100 mL) - To 91.67 mL of deionized water, slowly add 8.33 mL of 12 N HCl.

1.2 N NaOH/0.5 M HEPES (100 mL) - To 75 mL of deionized water, slowly add 12 mL of 10 N NaOH. Mix well. Add 11.9 g of HEPES. Mix well. Bring final volume to 100 mL with deionized water.

For each new lot of acidification and neutralisation reagents, measure the pH of several representative samples after neutralisation to ensure that it is within pH 7.2-7.6. Adjust the volume and corresponding dilution factor of the neutralisation reagent as needed.

2.2.7 Collagen co-culture system

5X DMEM media

25ml of 10X DMEM (Sigma Aldrich), 2.5ml of 10% FBS and 0.5ml of penicillin (100 U/ml) and streptomycin (100 µg/ml) was added to 25ml of DPEC water.

1M NaOH

It was purchased from Sigma Aldrich and was sterile filtered using .2µM filter.

2X $NaHCO_3$ Solution

Since DMEM media contains 3.71g/L of $NaHCo_3$, a 10X stock solution was prepared by adding 1.859g of $NaHCo_3$ in 50ml water. A 2X working solution was further prepared by adding 2ml of 10X stock in 8ml of DPEC water.

2.2.8 ALK5 reconstitution

10mM stock was prepared by dissolving 5mg of ALK5 Inhibitor- SB505124 (Sigma Aldrich) in 1.49ml of 25mg/ml DMSO solution (Sigma Aldrich) to give a working concentration of 10mM. Once dissolved, the aliquots were stored at 2-8^{0}C before further use.

2.2.9 $CoCl_2$ preparation

A 10mM stock solution was prepared by mixing 23.7g of weighed cobalt chloride ($CoCl_2$) powder (Sigma Aldrich) in 10ml of complete media to give a working concentration of 100µM. The stock was sterile filtered prior to use. The stock was further diluted to obtain a working concentration and the stock cannot be used again.

2.2.10 H_2O_2 solution

The molarity of 30% w/w hydrogen peroxide (H_2O_2) was calculated to 8.82M. Based on calculations, a 1mM stock solution was prepared by adding 1.13µl of stock H_2O_2 solution in 10ml of complete media. The stock was further diluted to obtain a working concentration. The stock is freshly prepared for each experiment.

2.3 Cell methodology

2.3.1 Cell culture

For routine culture, adherent cell lines were grown in 25 and 75cm^2 tissue culture flasks or 6, 12 and 24 well plates. The cells were grown in a humidified incubator at 37^{0}C with 5% CO_2 and tissue culture was carried out in a Class II containment cabinet. They were regularly sub-cultured before attaining 80% confluency, with a splitting ratio of 1:3 or 1:4 based on cell density. The cells were washed twice with sterile phosphate buffered saline (PBS; Lonza) and were incubated with 1mM of trypsin-EDTA (Lonza) containing 0.5g/L trypsin and 0.2g/L EDTA at 37^{0}C for 5 minutes. EDTA is a chelating agent that prevents Ca^{2+} (a divalent cation) facilitated adhesion of cells to the flask while trypsin is an enzyme that degrades proteins involved in cell adhesion. Detached cells were diluted with equal volumes of media to neutralize trypsin and collected in a 15ml tube. The cells were centrifuged (5min, 1000xG for HKC8 / 300xG for HK-2 and MRC-5), suspended in tissue culture medium, counted by haemocytometer if necessary and seeded into new flasks or plates.

2.3.2 Culture Media

2.3.2.1 DMEM-HAM F-12 media

DMEM Ham F-12 media (Lonza) was used to grow HKC8 cell line. Complete media was obtained by the addition of 5% FBS, 4 mM L-glutamine, penicillin (100 U/ml) and streptomycin (100µg/ml). HKC8 cells stably transfected with SMAD-Luciferase reporter gene (Courtesy- Dr Ian Logan) were maintained in complete DMEM HAM F12 supplemented with 300µg/ml hygromycin B (Lonza) derived from *Streptomyces hygroscopicus.*

2.3.1.2 DMEM media

This media (Sigma, D5546) was used to support the growth of the HK-2 and MRC-5 cell line. Cells were grown in this medium after the addition of the supplements; 10% FBS, 4 mM L-glutamine, penicillin (100 U/ml) and streptomycin (100 µg/ml).

2.3.3 Cell lines

2.3.3.1 Human kidney epithelial cell lines (HKC8 and HK-2)

HKC8 cell are adherent human cortical kidney tubular epithelial cells immortalised by transfecting with Adenovirus- 12 SV40 vector (Racusen *et al.*, 1997). HK-2 cells (ATCC CRL-2190) were created by transfecting with and human papilloma virus (HPV 16) E6/E7 genes (Ryan *et al.*, 1994). Since they exhibit morphology and activity similar to renal tubular epithelial cells and display renal epithelial makers on immunohistochemistry, they have been widely considered in several *in vitro* studies to understand the basis of renal injury and fibrosis (Racusen *et al.*, 1997; Veerasamy *et al.*, 2009; Prunotto *et al.*, 2011) . HKC8 cells were cultured in complete DMEM Ham F-12 media while HK-2 cells were cultured in complete DMEM media (Figure 2.1).

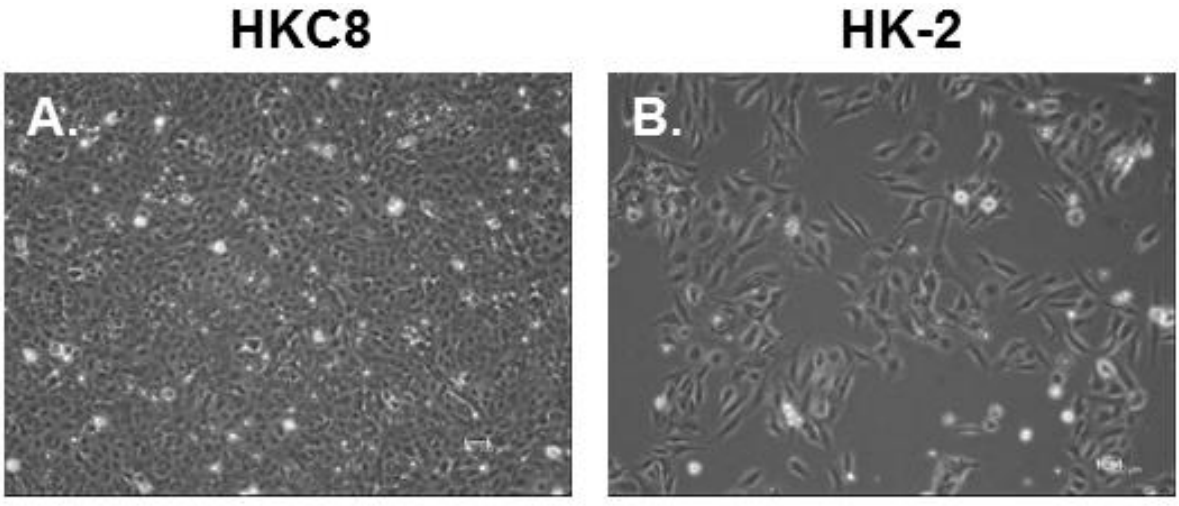

Figure 2.1: Morphology of PTECs.
An image of HKC8 (A) and HK-2 (B) cells acquired at 100X magnification.

2.3.3.2 Human lung fibroblast cell line (MRC-5)

The human lung diploid fibroblast cell line MRC-5 (Medical research council cell strain 5) was derived from lung tissue of a 14 week old aborted Caucasian male foetus by J.P. Jacobs in September of 1966. These cells were cultured in complete DMEM media (Figure 2.2).

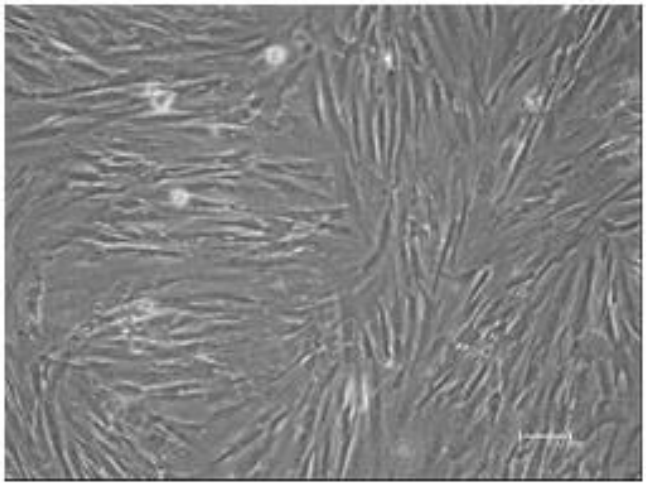

Figure 2.2: MRC-5 cells under bright field microscope.
Inverted microscope analysis of MRC-5 cells grown under normal conditions. Image acquired at 100X magnification.

2.3.4 Cell viability

The cell viability was assessed using typhan blue exclusion assay. 10 µl of cell suspension was mixed with 10µl of 0.4% typhan blue (Sigma Aldrich) and incubated for 2 minutes. The mix was loaded onto a Neubauer chamber haemocytometer covered with a glass slide. The cells were then counted in the corner 4 chambers containing 16 squares using a bright field inverted microscope (100X). The percentage viability of viable cells that appear white against dark blue background was calculated.

2.3.5 Cell Storage

In order to maintain a stock of the cell lines and to retain cells from an early passage, cells are cryopreserved in liquid nitrogen. Cells in their log growth phase (80% confluency) were trypsinised and spun down at 300G-1000G for 5 minutes. The

supernatant was discarded and the cells were resuspended in FBS containing 10% DMSO (Sigma Aldrich). 1 ml of this cell suspension was added to the cryovial (Corning). Before transferring the cryovials to liquid nitrogen, the cells were frozen gradually. The cryovial were transferred to Nalgene Mr. Frosty container containing isopropanol and stored at -80^{0}C. For long-term storage, cells were transferred to liquid nitrogen tank.

For recovery, the frozen cell stock preserved in liquid nitrogen was thawed at 37^{0}C in a water bath. The cells were transferred to a 15 ml falcon tube and were resuspended in 6ml of complete media and centrifuged for 5 minutes. Following the removal of supernatant, the pellet was resuspended in 1 ml of media and transferred to T25 or 75 flasks containing complete media.

2.3.6 Mycoplasma testing

Mycoplasma infection is one of the major risk factors affecting cells in tissue culture. Since mycoplasma is not visible by light microscope, it is difficult to determine the presence of this type of infection which alters cell morphology and function. Every 3 month, a test was performed to confirm the absence of mycoplasma infection in all cell cultures using a Luminometric assay. This assay was performed on supernatants of cells grown for at least 48 h. The cells were tested using MycoAlert™ mycoplasma detection kit (Lonza) in accordance with the manufacturer's instructions.

2.3.7 WST-1 cell proliferation assay

Cell proliferation study was assessed using the WST-1 assay (Roche Applied Sciences). WST-1 assay utilizes tetrazolium salts to measure metabolic activity in active cells. The metabolic activity is largely dependent on the glycolytic production of NADPH in viable cells. The nonradioactive, spectrophotometric quantification of cell was performed in a 96 well plate. Cells (5x10^3) were seeded per well in 100µl medium. Prior treatment, cells were incubated overnight in serum free media. Post

treatment, cells were incubated with 5µl of WST-1 reagent for 120 minutes before reading at 450nm by micro-plate reader (ThermoFisher Scientific).

2.3.8 Establishing co-culture system

An epithelial-fibroblast co-culture system was prepared, consisting of HKC8 and MRC-5 cells. My aim was to develop an *in vitro* model that best mimics the *in vivo* microenvironment during IRI to study the interaction between epithelial cells and fibroblasts. In order to develop a suitable co-culture system, the following experimental parameters were optimised.

2.3.8.1 Collagen concentration

To calculate the optimum collagen concentration, 1.2 x 10^5 of HKC8 cells were used per well in a 12 well plate. A range of rat tail collagen 1 (Corning) concentration was used in order to get a final collagen concentration of 1mg/ml, 2mg/ml, 3mg/ml and 4mg/ml (Table 2.1). Furthermore, the volume of 1N NaOH was also adjusted to allow polymerization of collagen bed within 15 minutes and maintain pH of 7.8 to 8.5. The initial optimisation revealed that 2mg/ml of collagen 1 was optimum to allow HKC8 cells to proliferate (48 h) as a monolayer on the collagen bed and retained the collagen bed structure (without contraction). Therefore, for all experiments, 2mg/ml of collagen was used.

Collagen conc. (mg/ml)	5XDMEM (ml)	2X $NaHCo_3$ (ml)	dH_2O (ml)	1 M NaOH (µl)	Rat Tail Collagen 1 (9.02mg/ml)
1	2	1	5.87	27.71	1.10
2	2	1	4.73	55.25	2.21
3	2	1	3.59	83.14	3.32
4	2	1	2.45	110.86	4.43

Table 2.1: Optimising collagen bed concentration.

2.3.8.2 Cell seeding density

Cell seeding density within the collagen was optimised by culturing 1.2 x 10^5 and 2.5 x 10^5 MRC-5 cells in 3mm and 5mm thick collagen beds (2mg/ml). During the 96 h growth incubation, media was changed and images were captured to monitor cell proliferation. Thereafter, collagen beds were transferred to petri-dishes washed with PBS and digested using 100U/ml collagenase I at 37^{o}C for 2 h on a shaker. The mix was then subjected to centrifugation and RNA was isolated from the cell pellet acquired. RNA quality and quantity was determined using a Nanodrop and suggested that the highest amount of RNA was isolated from 2.5 x 10^5 MRC-5 cells grown in 5mm thick collagen bed.

After optimising the parameters, a 3D co-culture system was prepared that involved culturing HKC8 and MRC-5 cells in a single collagen bed. To prepare the bottom layer of the bed, 2ml 5x DMEM, 1ml of 2x $NaHCO_3$ and 4.73ml of distilled water was added to 2.21ml of rat tail collagen 1(9.02mg/ml). Lastly, 55.25 µl of 1M NaOH was added to the mixture. Once the final mix was prepared, it was added to a pellet of MRC-5 cells and vortexed. To prepare a 5mm collagen bed, 1ml of mix was loaded per well in a 12 well plate and allowed to polymerise for 15 minutes at 37^{o}C. Thereafter, 2.5 x 10^5 HKC8 cells suspended in 1.5ml DMEM media was added to each bed and was placed in the incubator overnight. Next day, 1ml of old media was replaced by new media and this was done consecutively for 3 days. Following 72 h incubation the collagen beds were subjected to quick freezing, H&E staining was performed on 5µ vertical sections and visualised under bright field microscope.

Transwell inserts (Corning) were used to overcome the issue of low cell proliferation in the collagen bed. The polyester inserts allow cells to grow as a monolayer and the small pore size of 0.4 µM permit diffusion of signalling molecules released by cells. To study the paracrine effects of IRI, a system composed of HKC8 cells and MRC-5

cells was set-up. HKC8 cells ($3x10^4$) were seeded on transwell inserts and MRC-5 cells ($6x10^4$) were grown in a 24 well plate in DMEM complete medium (Figure 2.3). Upon reaching confluency, HKC8 cells were stimulated with optimised concentration of H_2O_2 and $CoCl_2$. Post stimulation, HKC8 cells growing on transwell were transferred onto naïve MRC-5 cells pretreated with or without ALK-5 inhibitor.

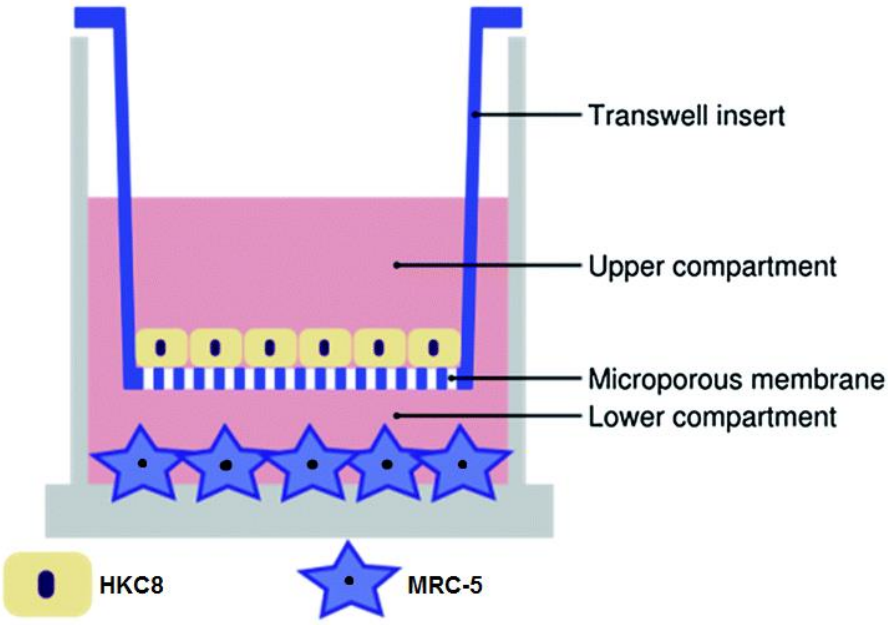

Figure 2.3: Schematic presentation of Transwell mesh Inserts (lateral view is shown). HKC8 cells were seeded at a density of 3 × 104 cells/well in polyester transwell inserts (0.4-μM pore size and a surface area of 0.33 cm2). MRC-5 cells (6 × 104) were added to the lower compartment. There was no direct cell-contact between cell types. HKC8 cells were pre-treated with H_2O_2 and $CoCl_2$ prior to transfer onto wells containing MRC-5 cells. Adapted from Raghnaill et al (Raghnaill et al., 2014)

2.3.9 Bacterial transformation

Bacterial transformation involves introduction of foreign DNA such as plasmid into the bacterial cell for either storing or replicating plasmids. These plasmids carry both bacterial origin of replication sequence and an antibiotic resistance gene to allow selection. Competent *E. coli* cells stored at -80^0C were thawed on ice. 10ng of plasmid DNA was added to 50μl of competent cells and mixed gently by flicking the bottom of the tube followed by incubation of ice for 20-30 minutes. The bacteria were

subjected to heat shock at 42^0C in a water bath for 30 seconds and then incubated on ice for 2 minutes then 950μl of warm LB media was added in each tube. The tubes were incubated for 1 h at 37^0C in shaking incubator (225rpm). 100μl of bacteria was plated onto agar plates containing antibiotics for selection. The plates were incubated overnight at 37^0C to allow bacteria to grow.

2.3.9.1 Bacterial culture

A single bacterial colony was picked and inoculated into a 10ml of LB broth containing antibiotic. The cultures were grown overnight on a shaker at 37^0C. A Plasmid mini kit (Qiagen) was used to isolate plasmid DNA from *E. coli*. Overnight bacterial growths were harvested from LB broth by centrifugation at 4000G for 20 minutes at 4^0C. The bacterial pellet was re-suspended in 0.3ml of buffer P1, P2 and P3. The lysate was centrifuged at 17,900G for 10 minutes. The supernatant was collected and was passed though QIAprep 2.0 spin column to allow plasmid binding to the silica membrane. The membrane was then washed with buffer PB and PE. After washing, the bound plasmid DNA was eluted by adding 50μl of water to the center of membrane and centrifuged for 1 minute. The quality and quantity of isolated plasmid was assessed using Nanodrop 1000 spectrophotometer. 0.8% agarose gel electrophoresis was performed to visualise the quality of plasmids (Figure 2.4).

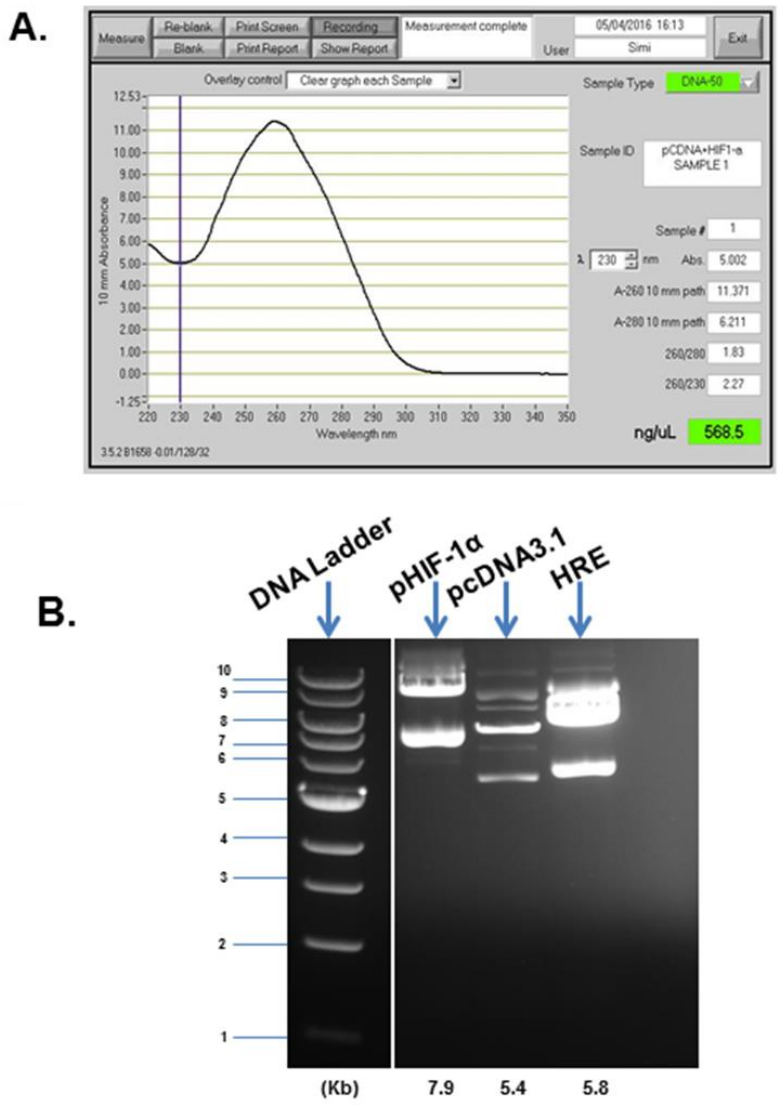

Figure 2.4: Plasmid isolation and agarose gel electrophoresis.
Panel A shows quantity/quality of pHIF-1α plasmid DNA isolated. pHIF-1α, pcDNA3.1 and pHRE were subjected agarose gel electrophoresis (0.8%) (1µg plasmid, B).

2.4 Protein expression

2.4.1 Immunofluorescent cell staining

Immunofluorescence is a robust and broadly applicable laboratory technique that relies on the use of antibodies to identify a specific target antigens by conjugating an antibody with a fluorescent dye such as fluorescein isothiocyanate (FITC). These labelled antibodies allow localisation and expression levels of proteins of interest to be assessed.

For immunofluorescence experiments, cells were seeded on glass coverslips in a 6 well plate with culture medium. The cells were treated once they attain 70-75% confluency. Post treatment, the coverslips were rinsed with PBS and fixed with ice-cold methanol for 5 minutes. After fixing the cells, the coverslips were allowed to dry at room temperature and blocked using 1% BSA prepared in PBS at room temperature for 1 h to maximize non-specific antibody binding.

Coverslips were incubated with primary antibody diluted in PBS at 4^0C overnight (Table 2.2). Cells were then washed with PBS 3 times prior to addition of secondary antibody (Table 2.3) in PBS at 4^0C overnight. Following further washing in PBS, the nuclei were stained with 1μg/ml DAPI (ThermoFisher Scientific) in PBS for 10mins at room temperature. The coverslips were then washed 3 times in PBS and mounted in fluorescence mounting medium (DAKO) and sealed with nail lacquer. Image analysis was performed with Zeiss Axioimager microscope.

Primary Antibody	Manufacturer	Catalogue No.	Species	IF	WB	FACS	IHC
α-SMA	Santa Cruz biotechnology Inc.	sc-32251	Mouse	1:100	1:1000	N/A	N/A
E-Cadherin	BD Transduction Laboratories	610181	Mouse	1:100	1:1000	N/A	N/A
HIF-1α	Santa Cruz biotechnology Inc.	sc-13515	Mouse	1:100	N/A	N/A	N/A
Fibronectin	Santa Cruz biotechnology Inc.	sc-9068	Rabbit	1:100	N/A	N/A	N/A
Col1A1	abcam	ab34710	Mouse	1:100	N/A	N/A	N/A
Integrin β6	R & D systems	MAB4155	Mouse	1:50	N/A	1:50	N/A
Integrin β6	R & D systems	AF4155	Sheep	N/A	N/A	N/A	1:40
GAPDH	Santa Cruz biotechnology Inc.	sc-25778	Sheep	N/A	1:3000	N/A	N/A

Table 2.2: List of primary antibodies used in IF, WB, FACS and IHC.

Secondary Antibody	Manufacturer	Catalogue No.	IF	WB	FACS	IHC
Alexa Fluor 488 goat anti-mouse	ThermoFisher Scientific	R37120	1:200	N/A	1:100	N/A
Alexa Fluor 488 goat anti-rabbit	ThermoFisher Scientific	R37116	1:200	N/A	N/A	N/A
goat anti-mouse IgG-HRP	Santa Cruz biotechnology Inc.	sc-2005	N/A	1:2000	N/A	N/A
goat anti-rabbit IgG-HRP	Santa Cruz biotechnology Inc.	sc-2004	N/A	1:3000	N/A	N/A
Biotinylated Rabbit Anti-Sheep IgG Antibody	Vector Labs	BA-6000	N/A	N/A	N/A	1:200

Table 2.3: List of secondary antibodies used in IF, WB, FACS and IHC.

2.4.1.1 Quantification of Immunofluorescence per Cell (IF/Cell)

Images acquired using a Zeiss Axioimager microscope was subjected to quantification using Image J software. This software was used to count number of nuclei stained with DAPI and calculate the total area of fluorescence (FITC). Parameters such as nuclei size to be detected and fluorescence intensity threshold were adjusted. The software then counted the number of stained nuclei and total fluorescence intensity for each image. Thereafter, total florescence per cell was calculated. A total of 9 images per coverslip were analysed and an average of the same was plotted.

2.4.2 Immunohistochemistry (IHC)

Formalin fixed paraffin embossed 3µm tissue sections were used for IHC analysis. Sections were deparaffinised by immersion in 100% xylene for 10min and rehydrated though graded ethanol (100%, 95% and 70%) to deionised water. Endogenous peroxidase activity was then blocked using 6% H_2O_2 in methanol for 15min at room temperature and then washed with PBS (pH7.6). This is crucial as antigen is detected by peroxidase based methods and the presence of endogenous enzyme may lead to nonspecific background staining. For antigen retrieval, the sections were

incubated with 20µg/ml Proteinase K solution for 35 minutes at 37^0C in humidified chamber. The proteinase K breaks the protein cross-linking; thereby unmasking the antigens in formalin fixed and paraffin embedded tissues. After incubation, the sections were allowed to cool at room temperature for 10 minutes and rinsed with PBS. To avoid background that may occur when using biotinylated antibodies, endogenous avidin and biotin blocking was performed using a streptavidin and biotin blocking kit (Vector Labs) for 20 minutes followed by washing for 5 mins. Sections were then blocked for 30 minutes with 20% swine serum and then incubated with sheep anti-αvβ6 primary antibody (1:40 dilutions in PBS) for 1 h at room temperature and then washed with PBS for 3x5 minutes (Table 2.2). Following this, the sections were incubated with biotinylated rabbit anti-sheep antibody (1:200 dilutions in PBS) for 2 h at room temperature and then washed with PBS for 5 minutes (Table 2.3). The sections were incubated with ABC RTU Elite HP reagent (Vector) for 30 minutes at room temperature and were washed twice with PBS each for 3 minutes. During this time, 3,3-diaminobenzidine (DAB) was prepared using DAB peroxidase substrate kit (Vector) according to manufacturer's instructions. For staining the extracellular matrix, slides were incubated with DAB solution for 7 minutes in the dark conditions. For nucleus staining, sections were incubated with Mayer‟s haematoxylin (TCS Biosciences) and Scott's tap water (Leica). Finally, the sections were taken though series of dehydration steps (50%, 75%, 95% and 100% ethanol), then into xylene before mounting using DPX. Images were acquired using Leica LCM microscope and were quantified using NIS-Elements Microscope Imaging Software (Nikon) as per manufacturers protocol.

2.4.3 Flow cytometry

Flow cytometry is a laser-based technique that can detect characteristics for each cell separately while it passes through a laser light source. This technique uses the

principle of light scattering or emission of light from fluorochomes and can give information on the physical characteristics of the cells. It allows analysis of the expression of cell surface or intracellular molecules, estimating the heterogeneity in a particular cell population, and defining the purity of an isolated cell preparation.

The system comprises of a vibrating mechanism that breaks the stream of cells into individual droplets. As the flow passes though the measuring station, the reflection or refraction of the light according to their size and granularity is measured and detected by different detectors and converted into electrical pulses by optical detectors. Light scattered in the forward direction of the laser beam is captured by forward angle light scatter (FSC) and light scattered perpendicular to the plane of the beam is captured by side scatter (SSC). The FSC represents size and shape of the cell while SSC gives information about the granularity of the cell. Based on these two parameters, a larger size and more granular cell produces higher forward and side scatter signal. Cells can be labelled with different fluorescence dyes that can bind a specific cell component or intercalate within DNA or RNA or with fluorochome-conjugated antibodies that bind to cell surface receptors and allows detection of specific cell surface markers.

In this study flow cytometry has been used to determine the presence of cell surface receptors, using fluorochome-conjugated secondary antibodies that recognise primary antibody bound to an antigen of interest. When the fluorochomes are stimulated at a particular wavelength, they excite from ground state and emit light of lower energy and strong wavelength. After emission, they return to their original unexcited state. This emitted light is split into defined wavelengths and channelled by a set of filters so that each sensor will detect fluorescence only at a specified wavelength.

Adherent cells were washed twice with sterile PBS and then scraped using cell scrapers. These cells were re-suspended in compete media and centrifuged at 100G for 5 minutes. Cells were counted and 2 x 10^5 cells were used per test. The cells were kept on ice throughout the experiment. The cells were washed with 2% FBS in PBS before staining with primary or isotype control antibody (Table 2.2). The antibody concentration was used as per manufacturer's recommendation and incubated at 4^0C for 1 h. Then, the cells were washed twice with 2% FBS-PBS solution by centrifugation at 500G for 5 minutes. Secondary antibody conjugated to fluorochome was added and cells were incubated at 4^0C for 30 minutes (Table 2.3). Finally, the cells were washed twice with FBS-PBS solution at 500G for 5 minutes and re-suspended in 200-300 µl FBS-PBS solution. Cells were analysed on a BD FACSCanto II flow cytometer and data was analysed using FlowJo software v.7.6.4 (Treestar).

2.4.4 Measurement of protein concentration

2.4.4.1 Enzyme linked immunosorbent assay

ELISA a plate-based assay technique is specifically designed for detecting and quantifying proteins. The specific antigen bound to primary antibody is complexed with secondary antibody that is linked to an enzyme. The detection is accomplished by measuring the conjugated enzyme activity via incubation with a substrate to produce a color based product.

The quantitative sandwich ELISA technique was performed as per manufacturers protocol (R&D Systems Ltd). A monoclonal antibody specific for TGF-β1/β2 was diluted to 1:120 and 1:180 in PBS respectively. The wells were coated with 100µl of the diluted capture antibody by incubating overnight on a shaker at room temperature. The coating medium was discarded and unbound antibody was washed using 400µl of wash buffer. Thereafter, 300µl of blocking buffer was added to each

well and the plate was incubated for 2 h. After this, blocking buffer was discarded and washing was performed. To quantify TGF-β1/β2 production, the cell supernatants were collected and centrifuged at 1100G for 4 minutes. To activate latent TGF-β1/β2 to immunoreactive form, 100µl of cell supernatants were incubated with 20µl 1M HCL. Following 10 minutes incubation at room temperature, the acidified samples were neutralized by adding 20µl 1.2N NaOH. As per plate plan, 100µl of sample or standard were added to the wells and incubated for 2h on a shaker at room temperature. After washing away any unbound material, 100µl of detection antibody specific for TGF-β1/β2 was loaded into the wells. Following a wash to remove any unbound antibody-enzyme, 100µl of substrate solution was added and the plates were incubated in dark for 20 minutes at room temperature. The colour development was stopped by adding 50µl of stop solution and the intensity of the colour was measured by reading absorbance at 492 and 540nm.

2.4.4.2 BCA protein assay

Total protein concentration of each sample was assessed calorimetrically using Pierce Bicinchoninic Acid (BCA) Protein assay kit (ThermoFisher Scientific) in accordance with the manufacturer's instructions. The assay employs the principle of Biurets test in which the reduction of copper ions by protein is detected using BCA reagent. The reagent binds to the reduced product to form a coloured product that exhibits strong absorbance at 562nm. The intensity of colour is directly proportional to the protein content in each sample. In my study, 10µl of serial diluted Bovine serum albumin (BSA) standards ranging from 125-2000µg/ml were mixed with 200µl of working solution (mixing reagent A with reagent B in a ratio of 50:1) in a 96 well plate. The plate was incubated at 37^0C for 30 minutes prior to reading the absorbance at 562nm. A BSA standard curve was generated to evaluate protein concentration (Figure 2.5).

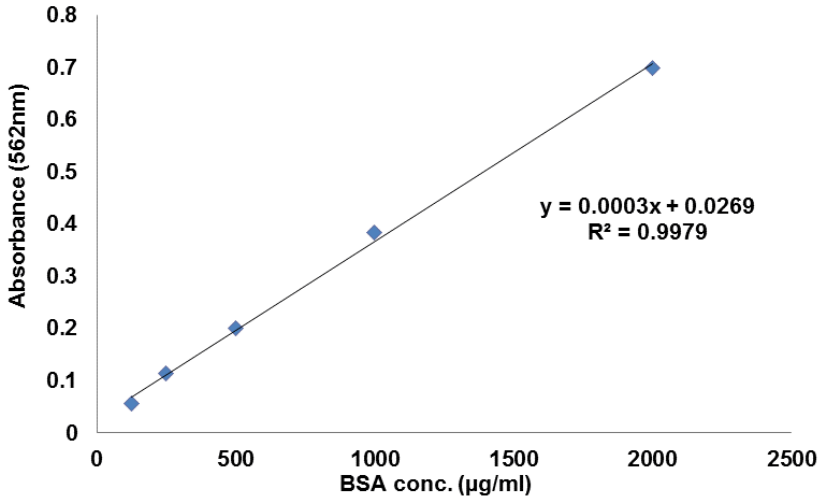

Figure 2.5: Graphical presentation of linear regression model of BSA curve for quantification of protein concentration. Cell lysates acquired from HKC8 cells were added to wells containing working solution (reagent A: reagent B=50:1). A range of diluted BSA (125-2000µg/ml) was added to these wells and the plate was allowed to rest for 30 mins at 370C prior to reading the absorbance at 562nm.

2.4.5 SMAD-Luciferase assay

2.4.5.1 Block TGF-β signalling using ALK-5 inhibitor

ALK5 inhibitor- SB505124 (Sigma Aldrich) was used to block TGF-β signalling in HKC8 cells. HKC8 cells stably transfected with SMAD-Luciferase reporter gene were seeded in 24 well plates. Cells were treated with increasing concentration of ALK5 inhibitor for 1 h prior to treatment with 10ng/ml TGFβ-1 for 24h. Post incubation, media was discarded and SMAD-Luciferase assay was performed to determine the optimum concentration that inhibits TGF-β activity significantly (Figure 2.6). Cells were lysed with 1X Reporter lysis buffer (4 volume of water to 1 volume of 5X Reporter Lysis buffer) (Promega). A single freeze-thaw cycle was performed to aid complete cell lysis. The lysates were centrifuged at 12,000G for 5 minutes to pellet down cell debris and the supernatant was aliquoted into fresh tubes placed on ice. The readings were taken manually using TD20/20 Luminometer (Turner Designs) where 30µl of lysate was added to 70µl of Luciferin reagent. The readings were further corrected for their protein concentration measured from BCA assay. Another

experiment was performed to determine how long a single treatment (1 hr) ALK-5 inhibitor would have an effect on TGF-β activity. For this reason, cells were stimulated with TGF-β1 for 24h. 48h and 72 h post 1h incubation with ALK-5 inhibitor. Thereafter, luminescence/ µg of protein samples were measured (Figure 2.7). WST-1 assay was also performed to assess the effect of ALK5 inhibitor on cell proliferation (Figure 2.8).

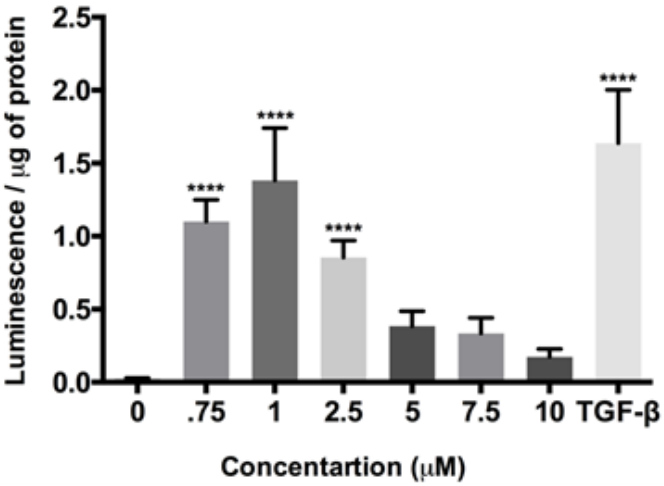

Figure 2.6: Blocking SMAD-Luciferase activity using ALK5 inhibitor. HKC8 cells stably transfected with SMAD-Luciferase reporter gene were treated with varying concentration of ALK-5 inhibitor followed by TGF-β1 stimulation (10ng/ml). Luminescence/ µg of protein sample was measured and compared to the untreated cells. One way ANOVA was used to analyse the data and graphs were plotted using Prism 6 software (****=p≤0.0001; n=3).

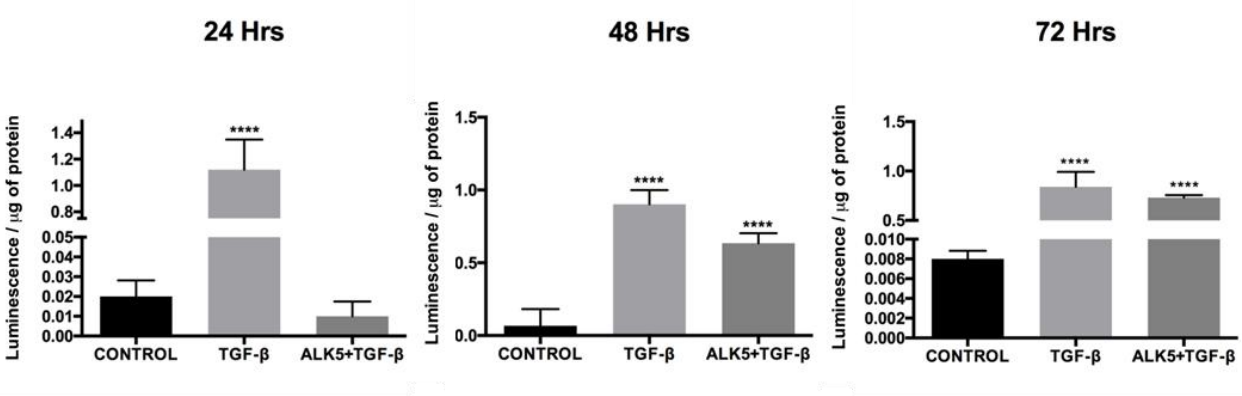

Figure 2.7: TGF-β stimulation for varying time points post ALK5 inhibitor treatment. Cells incubated with ALK-5 inhibitor were treated with 10ng/ml TGF-β for 24 h, 48 h and 72 h. Luminescence/ µg of protein sample was measured. Luminescence/ µg of protein in TGF-β treated cells and ALK5 inhibitor and TGF-β treated cells were compared to the control. One way ANOVA was used to analyse the data and graphs were plotted using Prism 6 software (****=p≤0.0001; n=3).

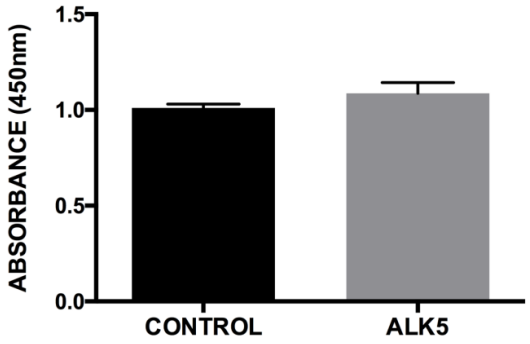

Figure 2.8: WST-1 assay for ALK5 inhibitor treated and untreated cells. Cells were treated with 10μM ALK5 inhibitor for 48 h and WST-1 assay was performed. The controls were untreated cells.

2.4.5.2 Using αVβ6 integrin blocking peptides

The αVβ6 integrin-blocking peptide (RTDLDSLRTYTL) and scrambled control (TLRDYRDTLSLT) that were originally described by Kraft (Kraft, Diefenbach et al. 1999) were synthesised by Isca Biochemicals (Exeter, U.K) for this project. Prior to use, the lyophilised peptides were reconstituted in sterile PBS according to the manufacturer's instructions to a final concentration of 5μM. The blocking peptide were used to determine whether αVβ6 integrin is involved in the regulation of TGF-β in IRI. To optimise the concentration of peptide required to block αVβ6 integrin, HKC8 cells were grown in 24 well plates were exposed to 400μM H_2O_2 for 4 h. Post-treatment, cells were incubated with blocking peptide or the scrambled control in complete media (at final concentrations of 50, 100, 500, 1000 and 2500 nM). After 20 h, the supernatants were collected and transferred onto naïve stably transfected SMAD-Luciferase HKC8 cells. Thereafter, luciferase assay was performed to quantify active TGF-β1 production, which was optimised using BCA protein assay (Figure 2.8-1). No changes in luciferase activity was observed when HKC8 cells were incubated with scrambled peptide or test peptide.

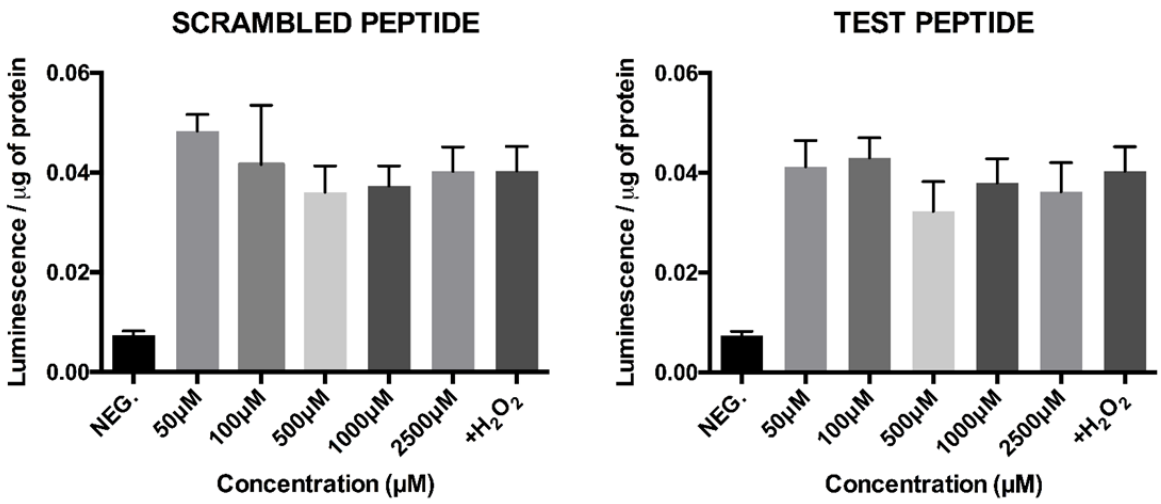

Figure 2.8-1: Effect of αVβ6 integrin blocking peptide on active TGF-β1 production. Post- treatment with 400µM H_2O_2 for 4 h, HKC8 cells were incubated with varying concentrations of scrambled peptide (negative control) and αVβ6 integrin blocking peptide for 20h. Thereafter, supernatants were collected and transferred onto naïve stably transfected SMAD-Luciferase HKC8 cells and luciferase activity was measured.

2.4.6 Western Blotting

Western blotting is used to identify specific protein in a sample of tissue homogenate or a mixture of proteins in a cell lysate. Proteins are separated on the basis of size, charge or isoelectric points followed by transfer of protein onto a membrane followed by identification of the target protein using antibody (Mahmood and Yang, 2012).

2.4.6.1 Preparation of cell lysate

Cells were rinsed with PBS and were detached using trypsin-EDTA. The cells were pipetted into centrifuge tubes where they were mixed with equal volumes on culture media prior to centrifugation for 5 minutes. The resultant pellet of cells was lysed by addition of 500µl lysis buffer (Sigma Aldrich) supplemented with protease inhibitor (Roche). The lysate was sonicated for 10 seconds followed by cooling on ice for 5 minutes to avoid protein denaturation due to heat. The sonicated samples were centrifuged at 10,000G for 10 minutes at 4^0C. The supernatants were aliquoted into

fresh tubes and the protein concentration was estimated using the BSA standard curve (Section 2.4.4.2).

2.4.6.2 SDS PAGE and Immunoblotting

15µg of total protein lysate was mixed with 4X Sample loading buffer (Promega) containing 5% β-mercaptoethanol. Before loading the sample, the mixture was heated at 95^0C for 5 minutes to cleave disulphide bonds and linearise the proteins. 4-12% precast polyacrylamide gels (Life Technologies) were used to separate protein samples. The gel containing cassette was removed from a sealed pack and was gently washed under running tap water to remove traces of unwanted acrylamide. The tape at the bottom of the cassette was removed to allow conductance as failing to remove will present sample migration. After washing, the cassette was placed in an electrophoretic tank, which was filled with 1X running buffer. The comb of the cassette was gently removed and the wells were briefly rinsed with running buffer. Proteins samples and PageRuler Plus Prestained Protein Ladder (ThermoFisher Scientific) were resolved at 180V.

Before transfer, the nitrocellulose membrane (Hybond, Amersham) was equilibrated with absolute methanol for 12 seconds followed by washing with distilled water. The gel was removed from the cassette using spatula. A transfer sandwich comprising of gel and membrane in the middle followed by transfer buffer soaked paper and foam pads on both sides was assembled and enclosed in an electroblotting cassette. The cassette was placed in transfer tank containing 1X Transfer buffer. The protein samples are transferred onto membrane overnight at 30V. During this process, the base of the unit receives constant water flow to avoid overheating. After transfer, the blot is washed with 1X TTBS for 5 minutes. To avoid non-specific antibody binding blots were blocked using blocking buffer solution for 60 minutes at room temperature. Primary antibodies were diluted in blocking buffer solution to optimal concentration

(Table 2.2). The membranes were incubated overnight at 4^0C with continuous shaking on a rocker. After incubation, the blots were washed 3 times with 1X TTBS for 10 minutes and incubated with HP-conjugated secondary antibody at 4^0C overnight with continuous shaking (Table 2.3). After washing 3 times for 10 minutes with 1X TTBS, the blots were developed using Pierce enhanced chemiluminescent (ECL) substrate (ThermoFisher Scientific). The oxidation of luminol substrate by HP-conjugated to secondary antibody allows the detection and visualisation of bound antibodies. Depending upon the intensity of signal, the blots were exposed to X-ray film (Kodak) between 10 seconds to 5 minutes under dark room conditions.

The blots were stripped at room temperature for 15 minutes using Restore™ Western Blot Stripping Buffer (ThermoFisher Scientific) followed by washing with 1 X TTBS for 5 minutes and reprobed for GAPDH (loading control) by the same procedure.

2.5 Molecular biology

In order to decrease the risk of sample contamination, all reagents and consumables used were of molecular biology grade. The reagents used for RNA isolation used were RNase free, only sterile filter tips and autoclaved sterile tubes were used during the entire process. All pipettes were decontaminated with UV light exposure and the RNA isolation area was decontaminated by using RNase removal spray (Sigma Aldrich).

2.5.1 RNA isolation

RNA was extracted from cells using an ISOLATE II RNA mini kit purchased from Bioline according to manufacturer's instructions. A cell pellet generated by centrifugation was lysed by addition of 300µl of cell lysis buffer RLY containing 3.5µl of β-mercaptoethanol. The lysate was transferred to an ISOLATE II filter and spun down at 11,000G for 1 minute. An equal volume of 70% ethanol prepared in RNase free water was added to the filtrate to allow RNA binding to the column and the

solution was mixed by repeated pipetting. The resulting suspension was transferred to an ISOLATE II mini column and centrifuged at 11000G for 30 seconds. The flow-though was discarded and the column containing RNA was washed with desalting buffer followed by treatment with DNases to digest DNA. The column was washed once with buffer RW1 and twice with buffer RW2 and centrifuged between each wash as before. Finally, RNA was eluted by addition of 60µl of RNase free water onto the silica membrane followed by spin at 10000G for 1 minute.

2.5.2 Quantification and integrity of RNA in cells

A Nanodrop spectrophotometer (NanoDrop ND-1000, ThermoFisher Scientific) was used to determine the quantity and purity of RNA. Briefly, 1µl of extracted RNA was applied on to the platform of the Nanodrop after blanking with 1µl of RNase-free water. The machine measures the absorbance at thee wavelengths; 260nm, 230nm and 280nm to quantify nucleic acid purity and concentration. The absorption at 260nm relates to the amount of RNA in samples while absorption at 230 and 280nm define the presence of organic chemicals and contaminant proteins in the isolated RNA. The purity of the isolated RNA sample was evaluated by examining the ratio of absorbance at 260 and 280nm and 260 and 230 nm for each sample. For the 260/280 rate, a reading in the range of 1.8-2.0 was considered satisfactory. The 260/230 ratio was used as a second measure of RNA purity with a reading of 2 considered suitable for cDNA synthesis (Figure 2.9).

In addition to this, the integrity of isolated RNA was assessed by RNA gel electrophoresis. A 1.2% native agarose gel was prepared in 50ml of 1 x TBE buffer by gentle boiling in in a microwave for 2 minutes. Once the molten agar solution was cooled under running tap water, ethidium bromide (EtBr) was added to give a final concentration of 0.5µg/ml. Before loading the sample, RNA sample was mixed with a loading dye and was heated to 65^0C for 5 minutes. When the gel had solidified, it was

immersed in electrophoretic unit containing 1x TBE buffer. The sample and ssRNA ladder (New England Biolabs) was loaded into the wells. The gel was resolved at 90V for 40 minutes and the bands for RNA was detected under UV light using an Alpha Innotech gel dock and alpha image software (Figure 2.10).

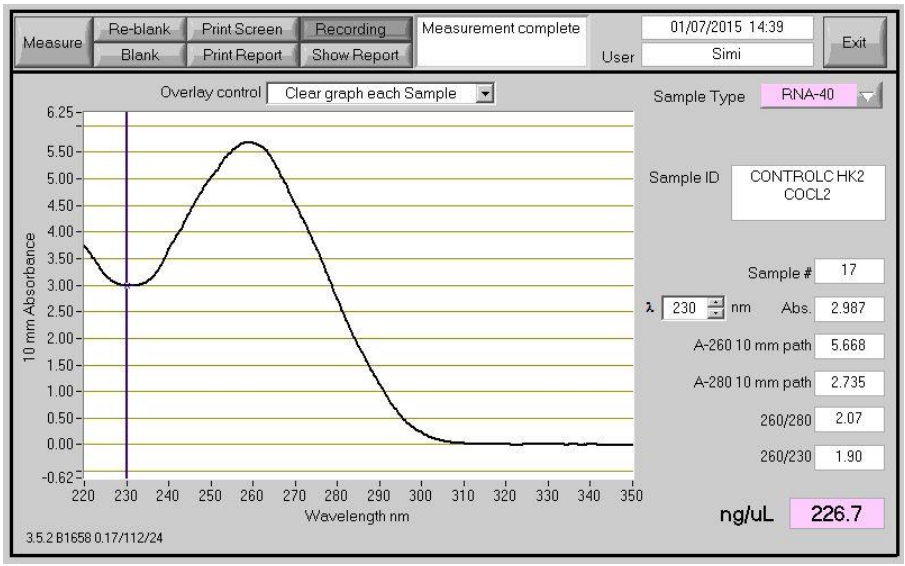

Figure 2.9: Quantification of RNA isolated using NanoDrop ND-1000. RNA quality is shown by 260/280 and 260/230 ratios. Ratios between 2.0 and 1.8 are consistent with good quality and purity of RNA extracted

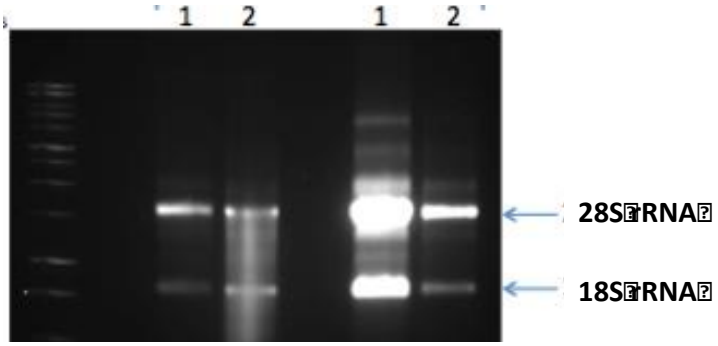

Figure 2.10: RNA quality determination.
The quality of RNA isolated from HKC8 cells was determined by performing agarose gel electrophoresis. RNA samples displayed two prominent bands of 28S rRNA and 18S rRNA. This confirmed that the RNA was intact.

2.5.3 First strand complementary DNA synthesis

Before assessing the gene expression of a gene, mRNA has to be reversed transcribed to obtain cDNA. This step was performed using Affinity Script cDNA synthesis kit purchased from Agilent Technologies. RNase free water was added to 1pg to 5 µg of mRNA to make final volume to 15.7 µl. To this mixture, 1 µl of 0.5 µg/µl

Oligo dT primer or 3µl of 0.1 µg/µl random primer was added and heated to 65^0C for 5 minutes to allow primer annealing. The samples were transferred to ice and a master mix was added (Table 2.4). Thereafter the samples were transferred to thermal cycler and the conditions were as follows: 45^0C for 5 minutes, 55^0C for 1 hour, 72^0C for 10 minutes and then cooled to 4 ^{0}C.

Reagents	Volume
10x AffinityScript buffer	2 µl
100 mM dNTPs (25mM each dNTPs)	0.8 µl
RNase Block Ribonuclease inhibitor (400U/ µl)	0.5 µl
AffinityScript Multiple Temperature Reverse Transcriptase	1 µl

Table 2.4 cDNA synthesis mix

2.5.4 Polymerase chain reaction (PCR)

PCR can be used to measure changes in gene expression by amplifying a specific gene from its cDNA template using primers specific to the gene of interest. Amplification is achieved by repeated cycles that lead to an exponential increase in the amount of PCR product. Every cycle involves 3 steps; 1) denaturation where disruption of double stranded cDNA occurs, 2) an annealing step where binding of primers to single stranded DNA occurs and 3) an elongation step that allows the synthesis of new strand.

Conventional PCR is a semi-quantitative/qualitative technique where levels of amplified product can be visualised by gel electrophoresis. In contrast to this, real time PCR (qRT-PCR) forms an amplification plot that has an early exponential stage of amplification followed by linear stage where the reaction levels off and finally reaching end point plateau stage where the reaction terminates due to exhaustion of reagents. The quantity of PCR product is determined in the exponential phase where

the amount of product doubles at each cycle and crosses the threshold of detection that is called the threshold cycle

2.5.4.1 Conventional PCR

Conventional PCR was performed to amplify/identify a gene of interest. The cDNA obtained was diluted to 100ng/µl. 13µl of master mix containing 12.5µl of GoTaq green mastermix (Promega) and 500nM of each 5' and 3' primer (Table 2.5) were added to the cDNA. The primers used were reconstituted and diluted to their working concentration. To minimise the risk of genomic contamination, exon-spanning primers were chosen. The final volume of 25µl was prepared by adding DEPC water. The samples were loaded onto thermal cycler. The cycle conditions were as follows – 95^0C for 5 minutes, 95^0C for 1 minute, 55-60^0C (as per the primer pair) for 1 minute, 72^0C for 3 minutes(x35), 72^0C for 10 minutes and 4^0C holding temperature. The amplified products were resolved on 2% agarose gel (Figure 2.11).

GENE	5'	3'	Product length	T_m(°C)
GAPDH	5'-GAAGGTGAAGGTCGGAGTC -3'	5'-GAAGATGGTGATGGGATTTC-3'	226bp	55
α-SMA	5'-GCGTGGCTATTCCTTCGTTACT-3'	5'-CCGATGAAGGATGGCTGGAACA-3'	219bp	55
COL1 A1	5'-CAAGAGGAAGGCCAAGTC-3'	5'-CGTTGTCGCAGACGCAGAT-3'	130bp	60
TIMP1	5'-TTATCCATCCCCTGCAAACTG-3'	5'-CAAGGTGACGGGACTGGAA-3'	97bp	55
MMP2	5'-GATACCCCTTTGACGGTAAGGA -3'	5'-CCTTCTCCCAAGGTCCATAGC -3'	112bp	55
TGF-β1	5'-CCCAGCATCTGCAAAGCTC-3'	5'-GTCAATGTACAGCTGCCGCA-3'	101bp	59-61
TGF-β2	5'-TCTTCCCCTCCGAAAATGCC -3'	5'-GCTCAATCCGTTGTTCAGGC-3'	171bp	60-59.9
TGF-β3	5'-TACTATGCCAACTTCTGCTC-3'	5'-AACTTACCATCCCTTTCCTC-3'	522bp	55
β-actin	5'-CAATGAAGATCAAGATCATTG-3'	5'-CTGATCCACATCTGCTGGA-3'	103bp	50-56
18s rRNA	5'-GTAACCCGTTGAACCCCATT-3'	5'-CCATCCAATCGGTAGTAGCG-3'	151bp	58-57.9

Table 2.5 List of primers used in qRT-PCR

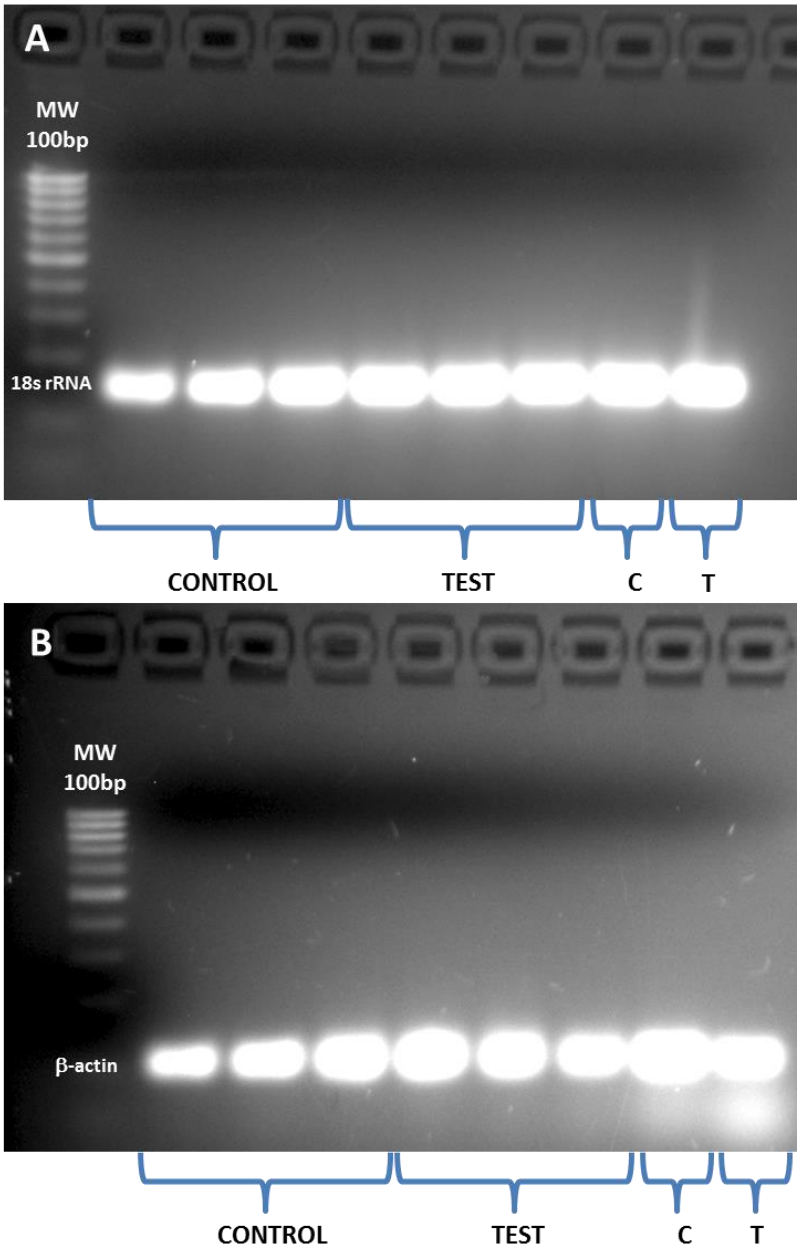

Figure 2.11: Identification of housekeeping gene. Amplified product for 18s rRNA (A) yielded same size bands for control and treated cells as compared to β actin derived amplified products (B).

2.5.4.2 Quantitative real time PCR

In this study, SYBR green fluorescent dye was used for quantification of gene expression. SYBR green binds to the minor groove of the dsDNA of the PCR product and emits a florescent signal at 521nm following excitation at 494nm. The intensity of fluorescence increases with each new copy of dsDNA and is detected during the extension step of qRT-PCR. A major disadvantage of SYBR Green is that it fails to

discriminate the double-stranded DNA from the PCR products and those from the primer-dimers, potentially giving a false positive signal. To overcome this, dissociation curve analysis was additionally performed to confirm the specificity of PCR products. In this step, the temperature was gradually increased from 65^0C to 95^0C after the PCR run was complete. This leads to breaking of dsDNA to ssDNA causing loss of fluorescence as SYBR green only binds to dsDNA (Figure 2.12). SYBR Green JumpStart™ Taq ReadyMix™ (Sigma Aldrich) mastermix was used.

The primers were diluted to 1pmol/µl in nuclease free water. The reaction was performed in triplicates in a 20µl reaction mixture containing the following reagents: SYBR Green JumpStart™ Taq ReadyMix™ 10µl, Forward and reverse primer mix (0.5pmol/µl each) 1µl, Nuclease free water 6µl and cDNA 2µl. The mixture was amplified using StepOnePlus Real-Time PCR system (Applied Biosystems) and was used to analyse the expression of all genes of interest relative to the housekeeping gene. A housekeeping gene is defined as a constitutive gene which is expressed at the same level in all cells during both normal and disease states. The reaction process was carried out for 40 cycles in the following sequential order: 95^0C for 2 minutes to activate Taq polymerase followed by 40 cycles of 95^0C for 15 seconds followed by 1 minute at 55-60^0C. After completing the 40 cycle run, melt curve analysis was performed for all samples.

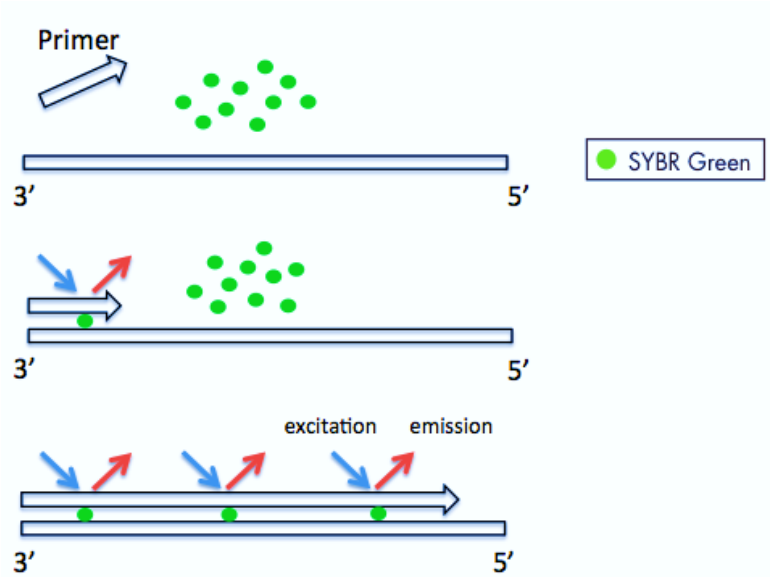

Figure 2.12: SYBR Green principle. SYBR Green is a non-specific dye that binds to double stranded DNA. Upon binding, it emits a fluorescent signal of a defined wavelength. The excitation and emission wavelength of SYBR Green is 494nm and 521 nm respectively.

2.5.4.3 Quantification of gene expression (ΔΔCT value)

The comparative C_t method (ΔΔCT) is a mathematical model used to quantify relative fold difference between a target gene and control gene. Cycle theshold (C_T) is defined as number of PCR cycles required for a fluorescent signal to cross a theshold that exceeds the background fluorescence. C_T values for the target gene and C_T values for the housekeeping gene are subtracted to calculate the ΔCT value for the treated and control group. The ΔCT value for the control group (untreated cells) is subtracted from the ΔCT value of the treated group (ΔΔCT) which is then converted to fold change or relative expression calculated as $2^{-(\Delta CT \text{ treated group} - \Delta CT \text{ control group})}$.

2.6 Transfection of epithelial cells

Cells ($3x10^4$ cells /well) were seeded in 24 well plates. Once the cells attained 70-80% confluency, a transfection reaction was prepared in 1.5ml tubes comprising of Opti-MEM media, Lipofectamine LTX and plasmid as per manufacturers guidelines (Table 2.6).

Components	Vol. per well	Total vol. (4 wells+1)
Basal media (no AB, no serum)	500uL	2.5mL
Lipofectamine LTX	1.5uL	7.5uL
Plasmids	500ng	2.5ug

Table 2.6 Plasmid transfection mix

The eppendorfs were incubated at room temperature for 5 minutes prior to transfection. Following 6 h incubation with transfection mix, cells were incubated with complete media for 18 h. To quantify HIF-1α expression in HKC8 cells, luminescence was measured to determine whether co-transfecting HKC8 cells with HRE-Luciferase (hypoxia response element containing plasmid) and pHIF-1α (plasmid containing HIF-1α insert) leads to an increase in luciferase activity due to overexpression of HIF-1α (Figure 2.13 & 2.14).

A

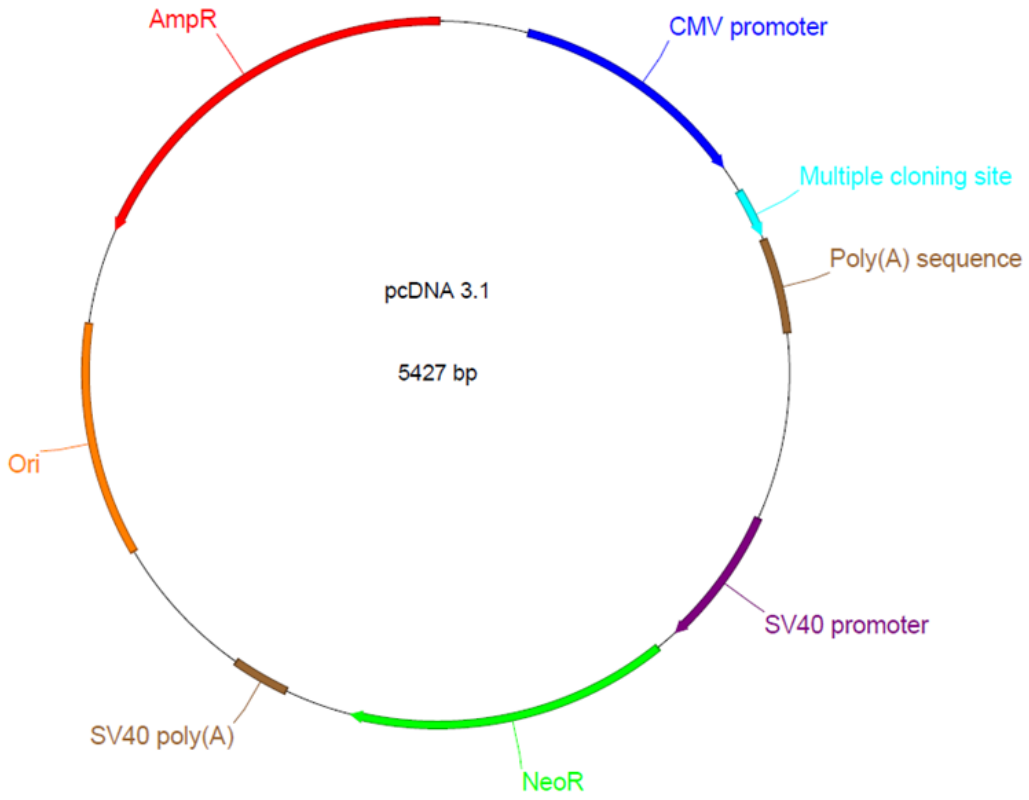
AmpR
CMV promoter
Multiple cloning site
Poly(A) sequence
pcDNA 3.1
5427 bp
Ori
SV40 promoter
SV40 poly(A)
NeoR

B

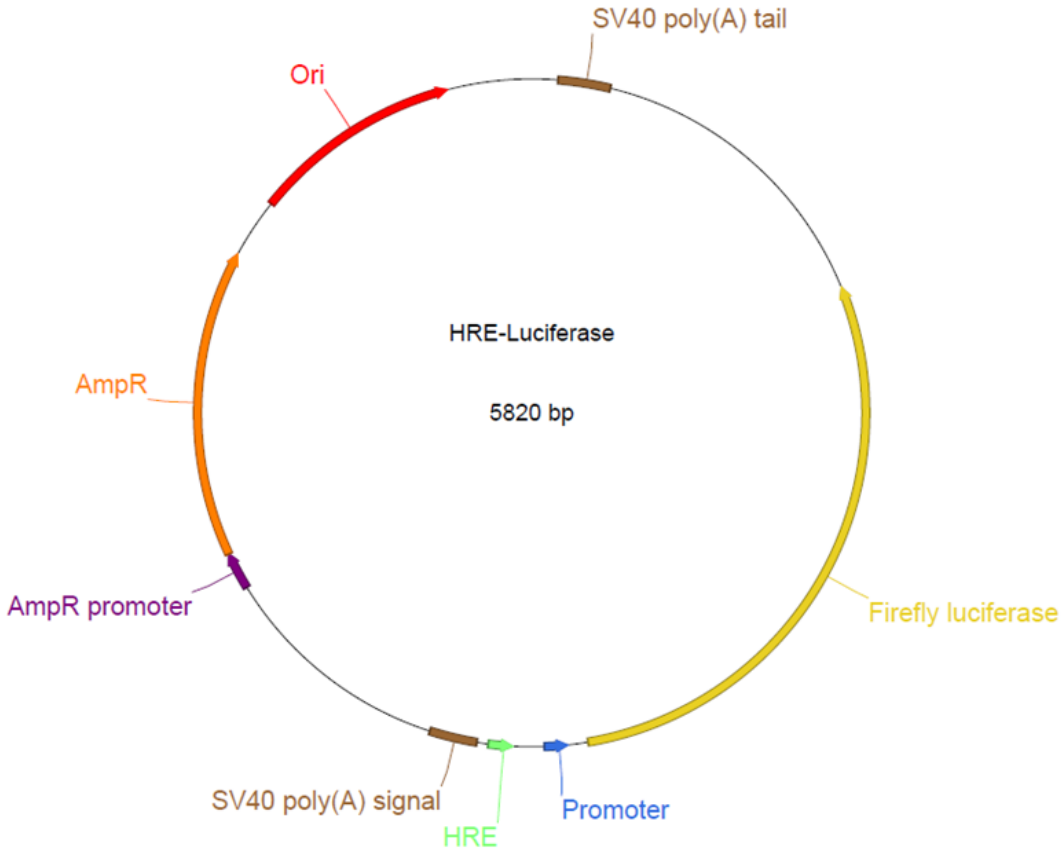
SV40 poly(A) tail
Ori
HRE-Luciferase
5820 bp
AmpR
AmpR promoter
Firefly luciferase
SV40 poly(A) signal
HRE
Promoter

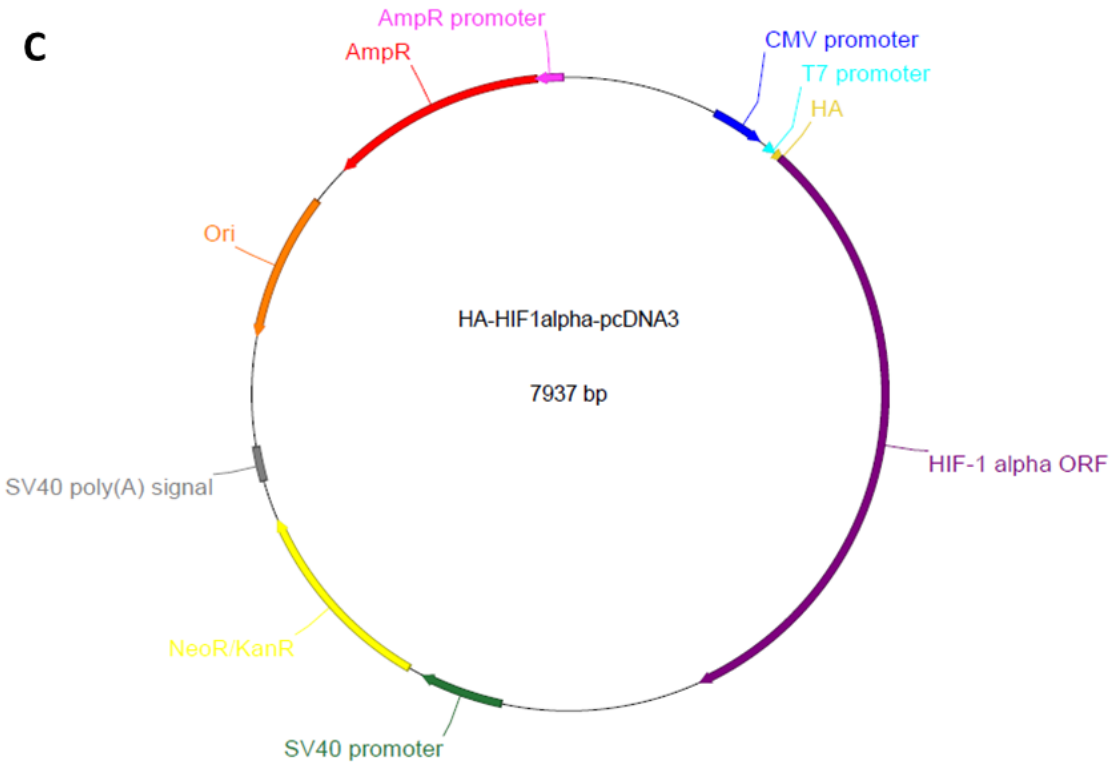

Figure 2.13: Plasmid maps of pcDNA 3.1 (A, negative control), HRE-Luciferase (B) and HA-HIF1alpha-pcDNA3 (C). Plasmids were purchased from Addgene, USA

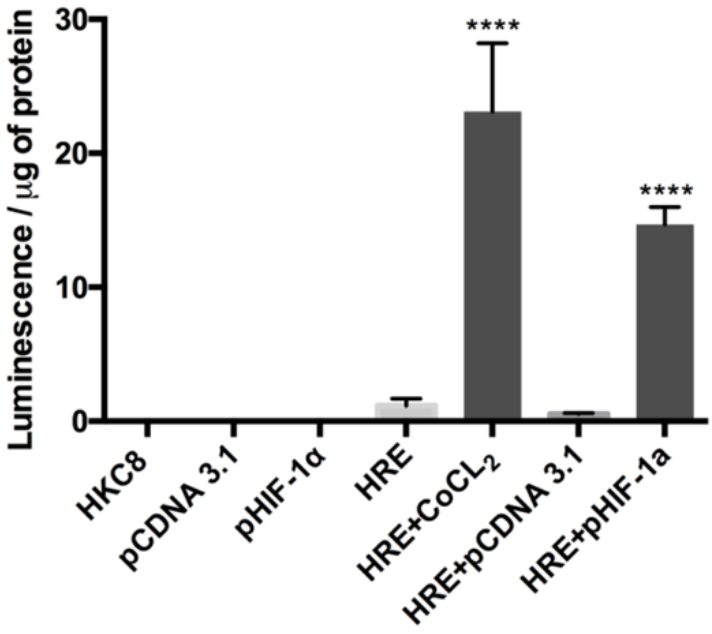

Figure 2.14: Quantification of HIF-1α expression in HKC8 cells.
HKC8 cells were transfected with pHIF-1α, HRE-Luciferase and pCDNA 3.1 (negative control) plasmids. In addition, cells were also co-transfected with HRE-Luciferase and pHIF-1α plasmid and HRE-Luciferase and pCDNA 3.1 plasmid. Cells were then treated with 100 µM $CoCl_2$. Luciferase assay was performed and luminescence/ µg of protein sample was plotted using Prism 6 software (n=3). (****=$p \leq 0.0001$)

2.6.1 siRNA transfection

SiRNA transfection involves introducing small interfering RNA (siRNA) or other small RNAs into the cells using cationic lipids such as Lipofectamine transfection reagents (ThermoFisher Scientific). The positively charged lipid molecules encapsulate the siRNA by forming liposomes that facilitate entry into the cell via endocytosis. The siRNA enters the cytosol, where it interacts with the mRNA and silences the target gene (Chesnoy and Huang, 2000; Hirko *et al.*, 2003).

Transfection can be categorised as stable and transient transfection. Stable transfection leads to long-term incorporation of the nucleic acid that persists in subsequent generations. In transiently transfected cells, the DNA/RNA is introduced into the nucleus. However, the gene does not integrate into the chromosome. Since the outcome is short lived, transiently transfected cells have to be analysed within 96 h of transfection (Kim and Eberwine, 2010).

2.6.1.1 Transfection efficiency using fluorescently labelled siRNA

Human silencer cy3 labelled GAPDH siRNA (Applied Biosystems) was used to optimise transfection conditions, where cy3 labelling allowed monitoring the localisation of the siRNA. A 20μM stock solution was prepared by resuspending lyophilised siRNA in RNase free water. A lipid based transfection reagent, Lipofectamine® RNAiMAX Reagent (ThermoFisher Scientific) was used to facilitate transfection of siRNA into cells. HKC8 cells ($5x10^3$ / well) were seeded in a chamber slide (Applied Biosystems) containing 400μl of complete media and allowed to adhere to the surface overnight. Thereafter, the complete media was replaced by Opti-MEM (Applied Biosystems, Table 2.7). The siRNA stock was diluted to a final concentration of 10, 30 and 50nM in Opti-MEM. The siRNA concentration was optimised by incubating HKC8 cells with 10nM, 30nM and 50nM control siRNA for 24, 48 and 72 h while keeping Lipofectamine volume constant (1 μl). After 8 h

incubation, the cells were washed with PBS, fixed using ice-cold methanol and counterstained with DAPI. The uptake of siRNA was then visualised using Axioimager Fluorescence microscope (Zeiss) at DAPI and rhodamine channel (Figure 2.15).

Concentration	siRNA volume (µl)	Opti-MEM volume (µl)
10nM	5	45
30nM	15	35
50nM	25	25

Table 2.7 siRNA Transfection reagent preparation (using 1µM stock)

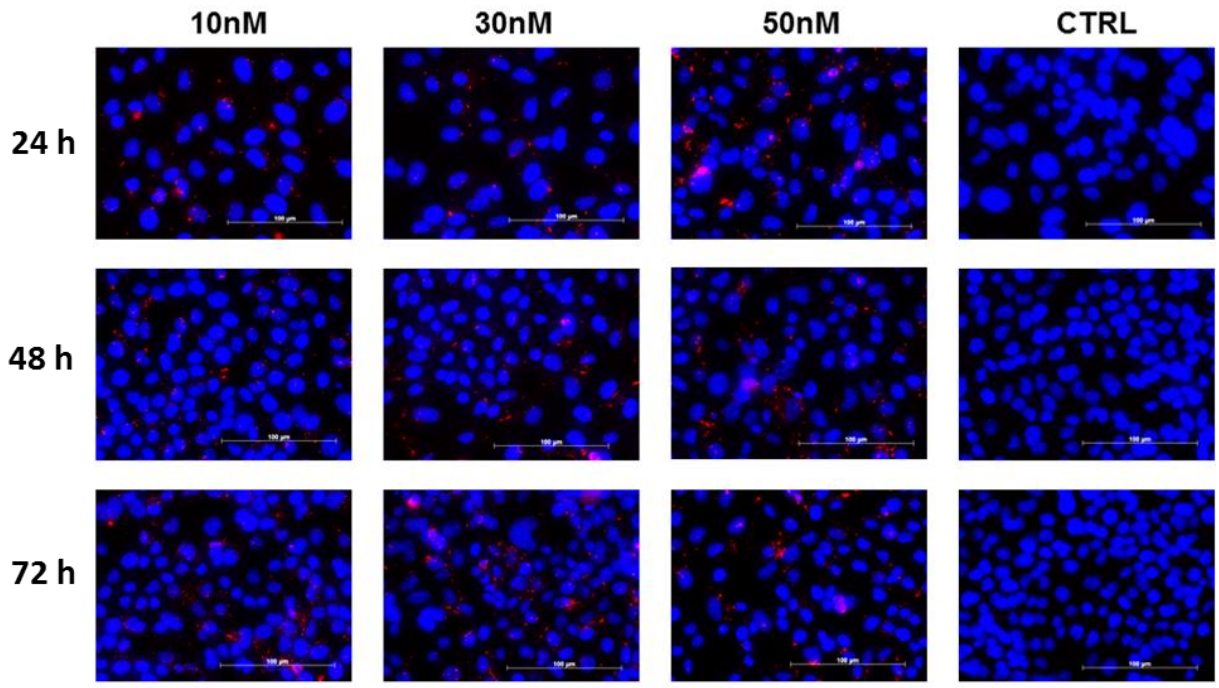

Figure 2.15 Optimising transfection control concentration using Cy3 labelled GAPDH control siRNA. HKC8 cells were seeded on a 8 well chamber slide and transfected with 10nM, 30nM and 50nM cy3 labelled GAPDH control siRNA for 24, 48 and 72 h using 1 µl transfection reagent for optimising transfection control concentration.

2.7 Statistics

Statistical analysis of data was performed using Prism 6.0 (Graph Pad software, San Diego USA) software. For evaluating any statistical significance between two groups (control versus treated) unpaired t-test was performed. One way Anova with Bonferroni correction was used to compare more than two groups (Control versus treatment 1/treatment 2). A p value less than or equal to 0.05 was regarded as statistically significant and the error bars showed the standard error of mean for each sample. Further it was assumed that the same data for each experiment was normally distributed.

The Western blots shown are the best images obtained and not necessarily representative of all the data.

Chapter 3: Ischaemia and reperfusion injury induces a profibrotic phenotype in proximal tubular epithelial cells and lung fibroblast cells

3.1 Introduction

IRI is one of the major inducers of AKI and is associated with increased morbidity and mortality. It involves a series of complex events involving tissue and organ injury, in part, though alterations in tissue blood flow and the production of reactive oxygen species. In addition, renal tubular epithelial cells are injured, tissue resident leucocytes are activated and endothelial cell functionality is impaired. Upon reperfusion there is production of H_2O_2 derived ROS that further facilitate DNA damage and cause considerable tissue injury (Dagher *et al.*, 2003; Just, 2007). The epithelial damage is further accelerated due to immune activation. Therefore, IRI seeds the early development of potentially irreversible cell damage and tubular injury with the proximal tubular epithelial cells being most susceptible (Weight *et al.*, 1996; Sutton, 2009; Munshi *et al.*, 2011; Denecke and Tullius, 2014).

Hypoxia inducible factors such as HIF-1α play an important in the progression of renal fibrosis. During ischaemia, HIF-1α expression significantly increases and this in turn regulates the downstream expression of several genes related to angiogenesis, cell growth and differentiation (Weidemann and Johnson, 2008). Studies have also indicated increased deposition of interstitial collagen in response to low oxygen in human renal fibroblasts, suggesting that hypoxia-regulating factors increase matrix production in renal fibroblasts (Ruthenborg *et al.*, 2014).

To determine the effects of IRI on proximal tubular cell phenotype, an *in vitro* model of hypoxia and free radical stress was established by subjecting proximal tubular cells to H_2O_2 or $CoCl_2$.

3.2 Results

3.2.1 Establishing an *in-vitro* model of Ischaemia and reperfusion injury

3.2.1.1 Optimising conditions for H_2O_2 treatment in HKC8 cells

To mimic oxidative stress in vitro, cells were treated with H_2O_2**.** A pragmatic approach was taken to determine the H_2O_2 concentration that induces maximal oxidative stress with minimum impact upon cell viability. Cells were incubated with varying concentration (200, 400, 600, 800 & 800 µM) of H_2O_2 for 4 h. Following this, cells were incubated with fresh complete media for upto 20 h. Cell viability was assessed using trypan blue dye exclusion assay. 85% or greater viability was chosen an arbitrary cut off with lower viability suggesting excessive early cell death. When compared to untreated group, ≥85% viability was demonstrated at 200 and 400µM concentrations of H_2O_2. Less than 85% viability was observed at higher concentrations of H_2O_2 compared to untreated control cells (Figure 3.1).

The long-term effects of 200 and 400µM H_2O_2 on viability was assessed at various time points. Following 200µM H_2O_2 treatment, HKC8 cells maintained ≥85% viability for 72 h when compared to the untreated cells. However, cells stimulated with 400µM concentration showed a reduction in cell viability after 48 h incubation as compared to the untreated control cells due to increased cell death (Figure 3.2). Images of HKC8 cells were captured to visualise the effect of oxidative stress on cell morphology Morphological changes were not evident at earlier time points. At 72h treatment with 200µM H_2O_2, cells adopted spindle shaped morphology consistent with a more fibroblast-like phenotype. Higher concentration of H_2O_2 resulted in a significant reduction in cell number due to cell death (Figure 3.3).

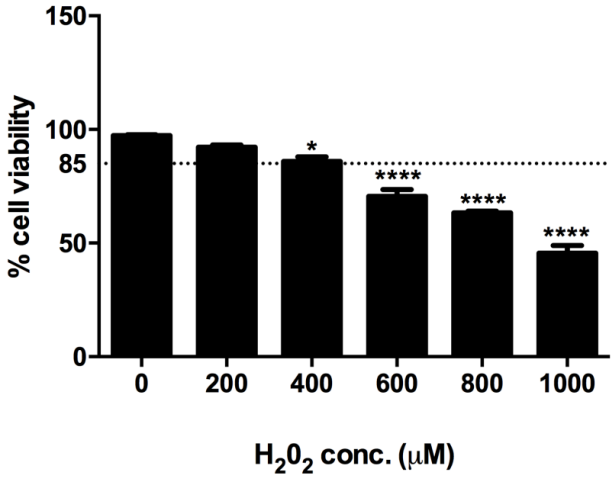

Figure 3.1: Percentage cell viability assessment with increasing H_2O_2 treatment. Following 4 h H_2O_2 treatment, cells were incubated with complete media for 20 h. The viability was measured using Trypan blue dye exclusion assay and compared to the untreated control. One way ANOVA was used to analyse the data and graphs were plotted using Prism 6 software (n=3). (*p≤0.05) (****p≤0.0001)

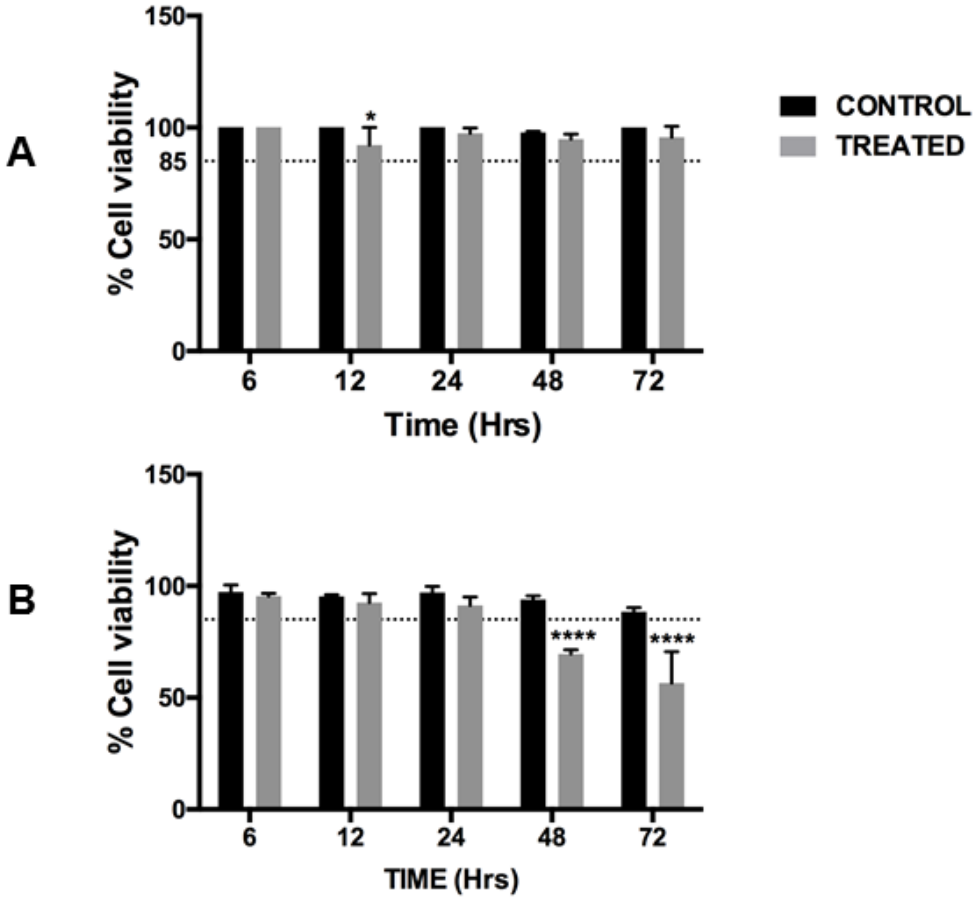

Figure 3.2: Percentage cell viability post 200μM and 400μM H_2O_2 treatment. HKC8 cells were treated with 200μM (A) and 400μM (B) H_2O_2 for various time points and the percentage viability was assessed using Trypan blue dye exclusion assay and compared to the respectively untreated control (n=3; unpaired t-test). (*p≤0.05) (****p≤0.0001)

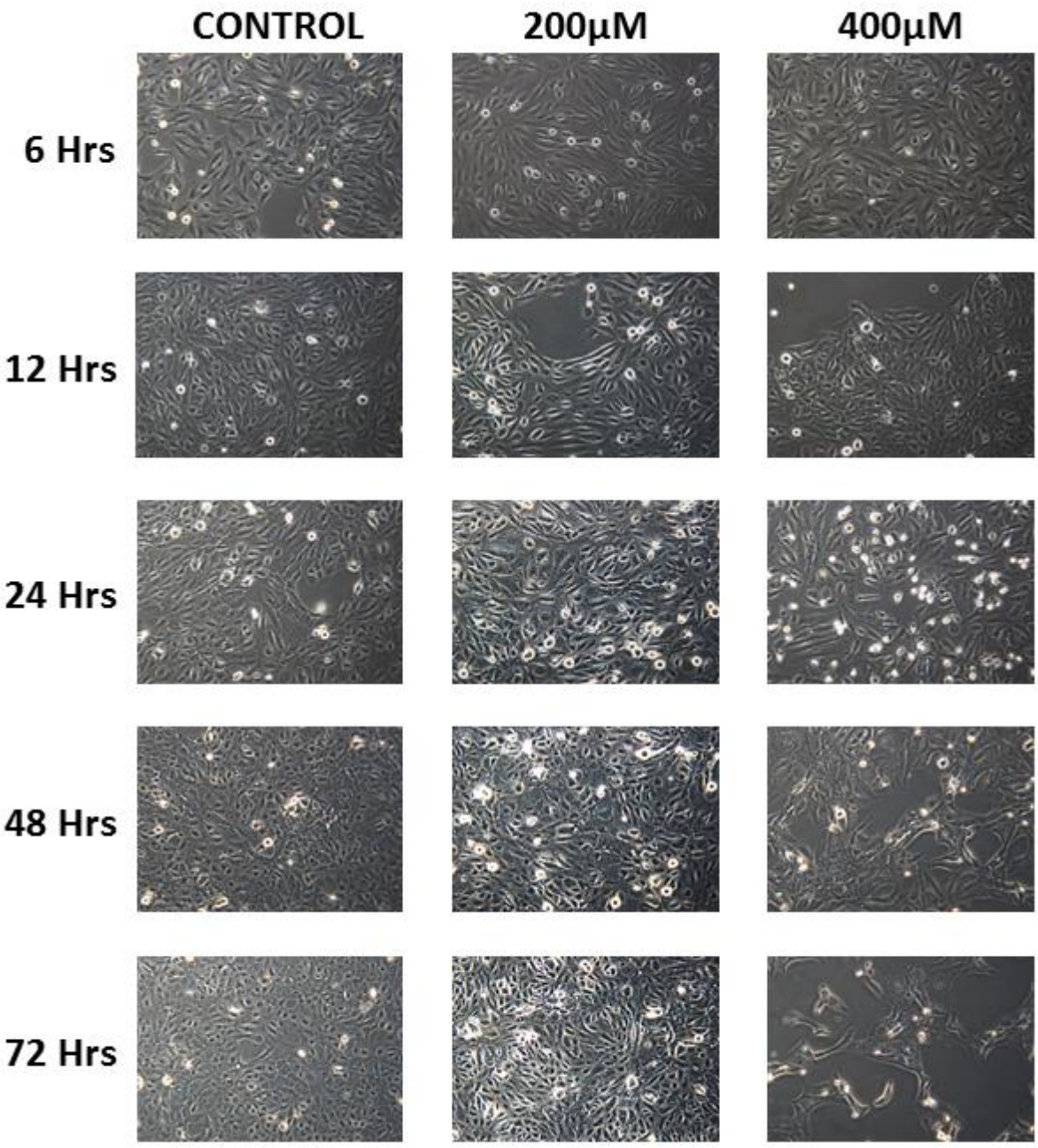

Figure 3.3: Morphological changes in HKC8 cell line following H_2O_2 treatment. Following H_2O_2 treatment, cells were incubated with complete media for several time points. Images were captured at 6 h, 12 h, 24 h, 48 h and 72 h using Leica bright field microscope (100X).

3.2.1.2 ROS generation during H_2O_2 treatment of HKC8 cells

To assess whether treatment of HKC8 cells with H_2O_2 resulted in free radical production as predicted, I used a fluorescent probe, CM2-H2DCFDA (ROS Indicator) which is oxidised by free radicals in cells to yield a fluorescent adduct. Cells were incubated with varying concentration (200, 400, 600 & 800 µM) of H_2O_2 for 4 h. Following this, cells were incubated with fresh complete media for upto 20 h. After 24 h treatment, the assay was performed as per manufacturer's protocol. The result suggested there was an increase in fluorescence in response to higher H_2O_2 concentration up to 400µM followed by a decline at 600-800µM due to increased cell death (Figure 3.4).

Due to decreased cell viability beyond 24h with 400µM treatment as demonstrated in Figure 3.1, the long-term effect of H_2O_2 on ROS generation was studied at 200µM. Time course experiments revealed an increase in ROS production in cells post-treatment with 200µM H_2O_2 compared to untreated control cells (Figure 3.5). These observations suggest that H_2O_2 successfully mimics oxidative stress by increasing ROS production in cells. Treatment with H_2O_2 can therefore be used to understand the effects of ROS on gene and protein expression.

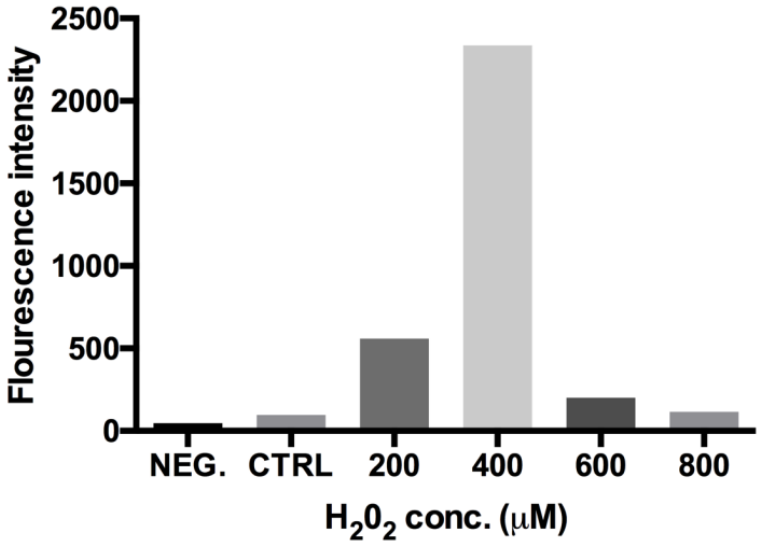

Figure 3.4: Median intensity emission of CM2-H2DCFDA probe in HKC8 following H_2O_2 treatment. Free radical injury was induced by treating HKC8 cells with varying concentration of H_2O_2 for 4 h followed by incubation in complete media for 24 h. Cells were stained with CM-H2DCFDA. Fluorescence was measured using FACS Canto II flow cytometer (BD Biosciences).

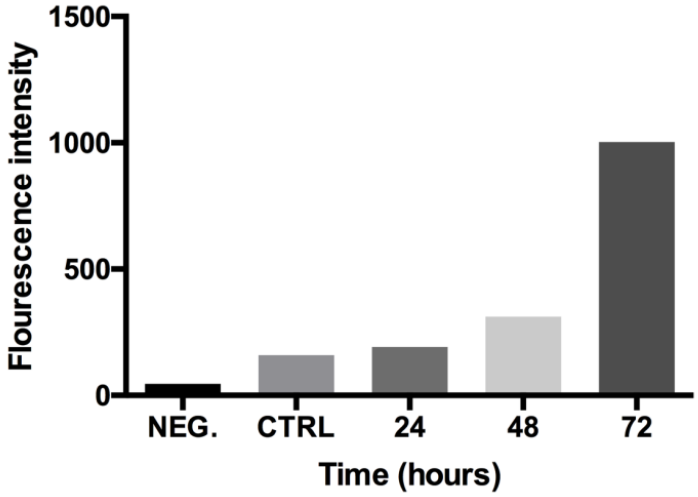

Figure 3.5: An increase in CM2-H2DCFDA emissions following 200μM H_2O_2 treatment. Following 4 h incubation with 200μM H_2O_2, the cells were incubated in normal media for 24, 48 and 72 h before staining with CM-H2DCFDA. Fluorescence was measured using FACS Canto II flow cytometer (BD Sciences; n=1)

3.2.1.3 The effect of Ischaemia on HKC8 cells

Ischaemia was induced in HKC8 cells initially using a hypoxic incubator. The percentage viability was assessed after exposing HKC8 cells to 1% oxygen. The results indicate equivalent viability for hypoxic cells when compared to control cells

(Figure 3.6A). Cells were imaged at 24, 48, 72 and 96 h post hypoxic incubation. Cells acquired an elongated phenotype by 72 h (Figure 3.6B) suggesting that hypoxia induces cytoskeletal re-organisation.

MTT assay was performed to evaluate whether hypoxia has an effect on cell proliferation. The results indicated significantly reduced cell proliferation in hypoxia treated cells as compared to their respective control after 48 h incubation in hypoxic conditions ($p \leq 0.0001$)(Figure 3.7).

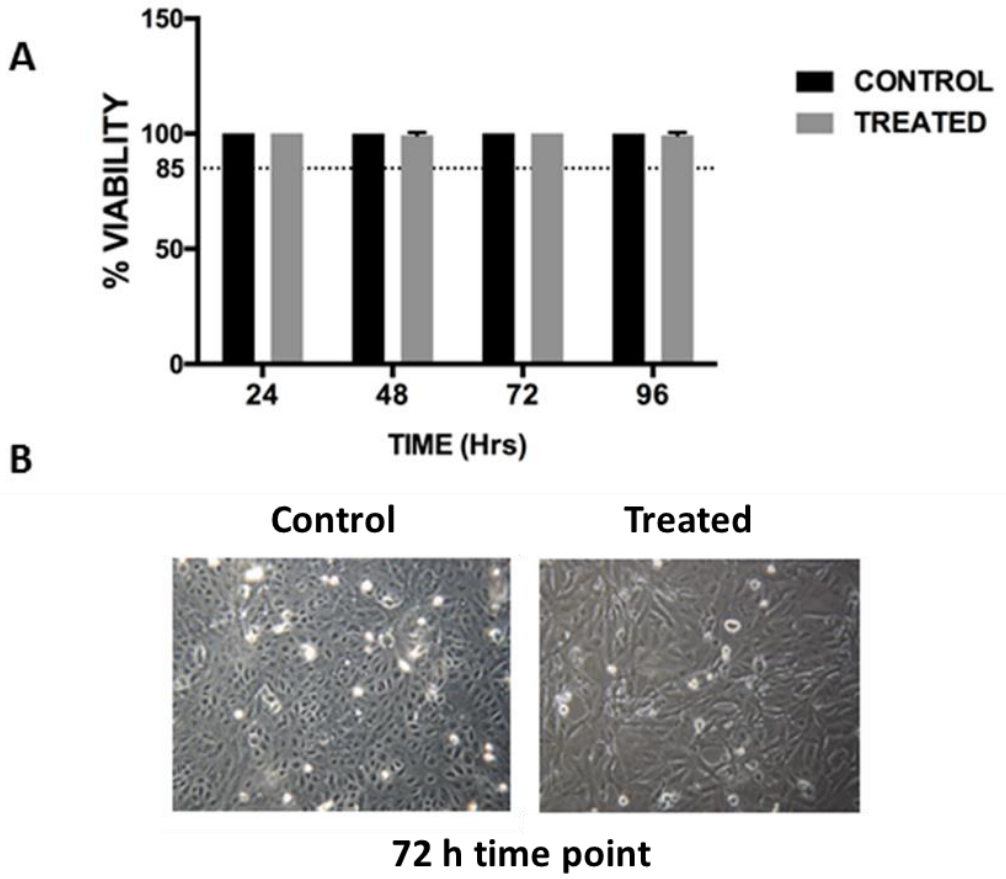

Figure 3.6: Cell viability following hypoxic stress (1% oxygen). HKC8 cells were incubated in a hypoxic chamber for time points up to 96 h and cell viability was evaluated by Trypan blue dye exclusion assay (n=3; Mean +/- SD). Images were captured at 72 h Leica bright field microscope (100X).

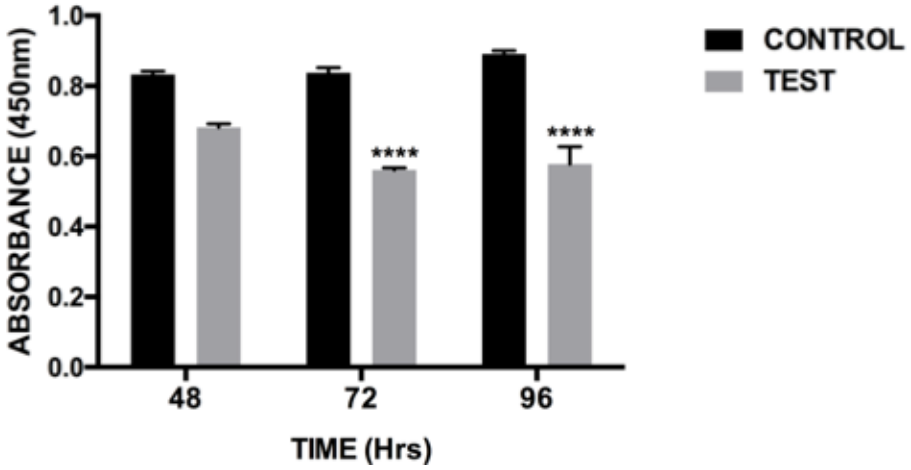

Figure 3.7: Reduced cell proliferation in HKC8 cells during hypoxia incubation. Following growth in control or hypoxic conditions a MTT assay was performed to evaluate cell number after 48, 72 and 96 h. Readings were acquired using Multiskan FC microplate photometer and compared with baseline/control cells at the same time point.(n=2; Mean +/- SD)(****$p \leq 0.0001$, unpaired t test)

During normoxia, the α-subunits of HIF transcription factors (including HIF-1α and HIF-2α) are hydroxylated and degraded by binding to tumour suppressor pVHL. In hypoxic conditions, proline hydroxylation is blocked leading to HIF-1α stabilisation. Studies have shown that cobalt mimics hypoxia by inhibiting pVHL binding to HIF-α and causing accumulation HIF-1α and HIF-2α (Yuan *et al.*, 2003; Chachami *et al.*, 2004).

Therefore, cells were treated with $CoCl_2$ to induce ischemic changes mediated by HIF-1α. To optimise $CoCl_2$ concentration, cells were seeded onto a 6 well plate and treated with variable concentrations of $CoCl_2$ (25, 50, 75 and 100μM) in 2 ml media for various time points. Following incubation, the cell viability was assessed. Changes in percentage cell viability were observed post treatment with 75 and 100μM of $CoCl_2$ at 96 h only (Figure 3.8). However, change in cell morphology was noted at 72 and 96 h incubation from a typical cobblestone epithelial type to a spindle cell (Figure 3.9).

To study the effect of $CoCl_2$ on cell proliferation, a MTT assay was performed. This suggests that $CoCl_2$ can lead to an increase in HKC8 cell number upto 48h

(**=$p \leq 0.01$) and arrested growth at 72 h. Based on results, I hypothesise that HIF-1α activation by $CoCl_2$ may lead to an increase in cell proliferation upto 48h followed by toxicity of $CoCl_2$ at 96h (Figure 3.10 A).

An alternative technique was also used to assess cell number. HKC8 cells were grown on glass coverslips in a 6 well plate. Cells were incubated with 25, 50, 75 and 100 µM $CoCl_2$ containing media for 24, 48, 72 and 96 h. Following incubation, the coverslips were fixed and the cell nuclei were stained with DAPI. Images were taken and the number of stained cells per field were counted using Velocity cell imaging software. A significant reduction in cell number was observed as early as 24 h following 75 and 100µM of $CoCl_2$ treatment ($p \leq 0.0001$) (Figure 3.10B).

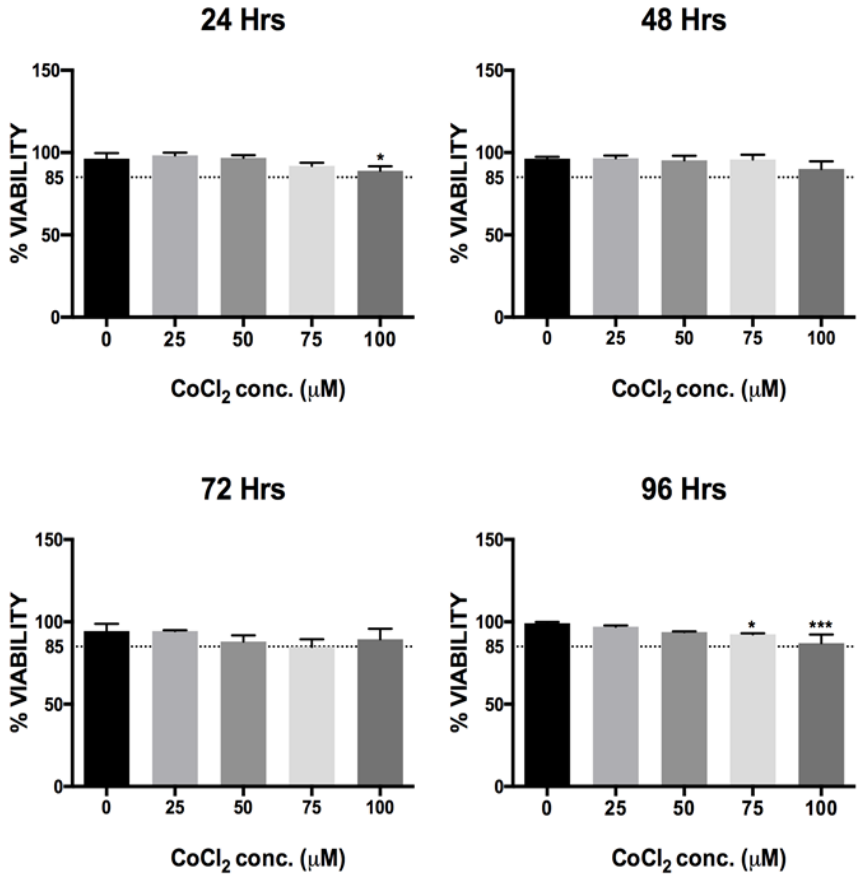

Figure 3.8: HKC8 cells maintain viability post $CoCl_2$ treatment.
HKC8 cells were incubated with various concentrations of $CoCl_2$ upto 96 h and cell viability was assessed Trypan blue dye exclusion assay and compared to the untreated control cells (n=3; Mean +/- SD). One-way ANOVA with Bonferroni method was used for analysis. (*=$p \leq 0.05$) (****=$p \leq 0.0001$)

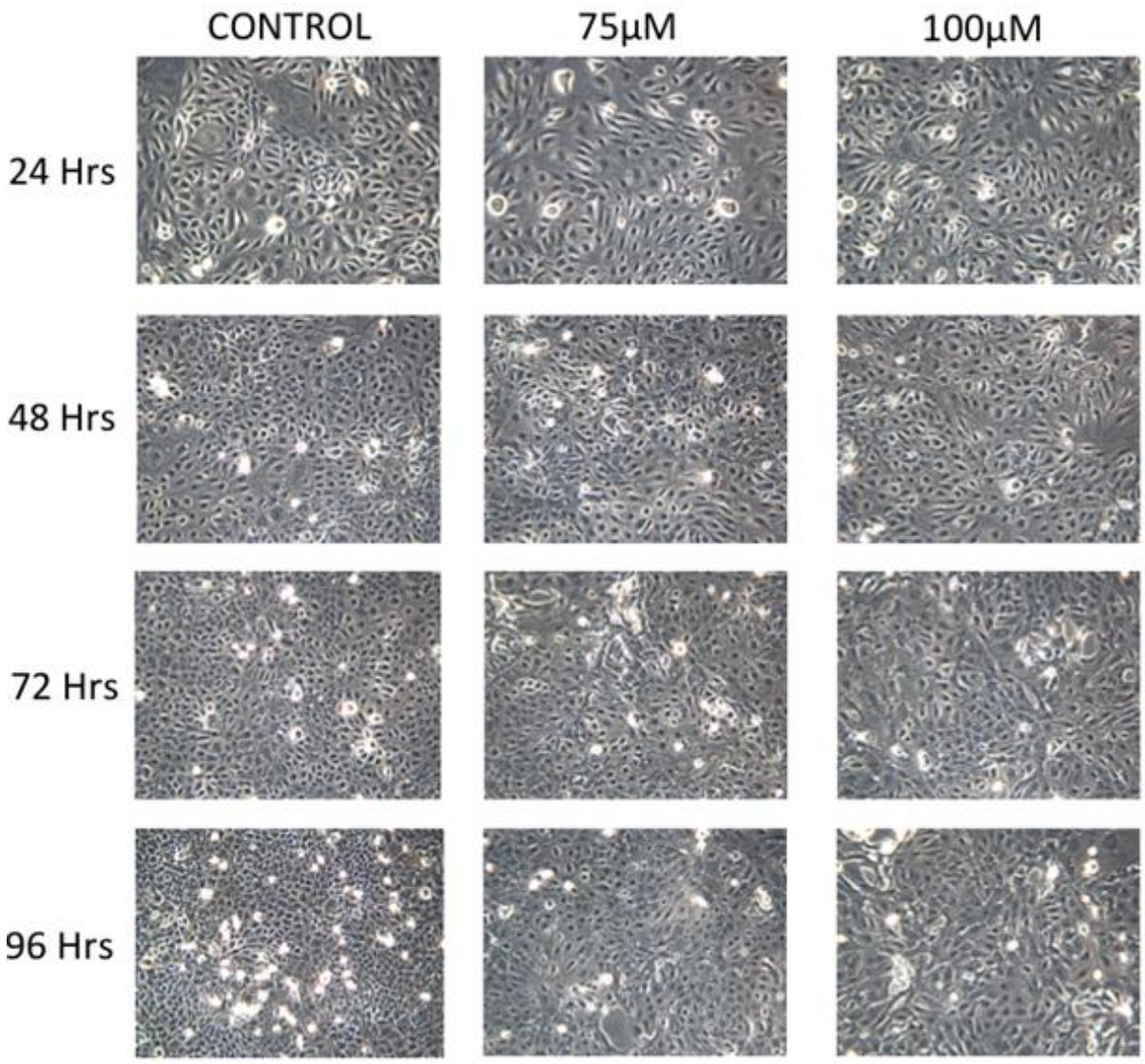

Figure 3.9: Altered cell morphology following $CoCl_2$ treatment. Images were captured at 24, 48, 72 and 96 h post 75 and 100 µM $CoCl_2$ treatment using a bright field microscope (X100).

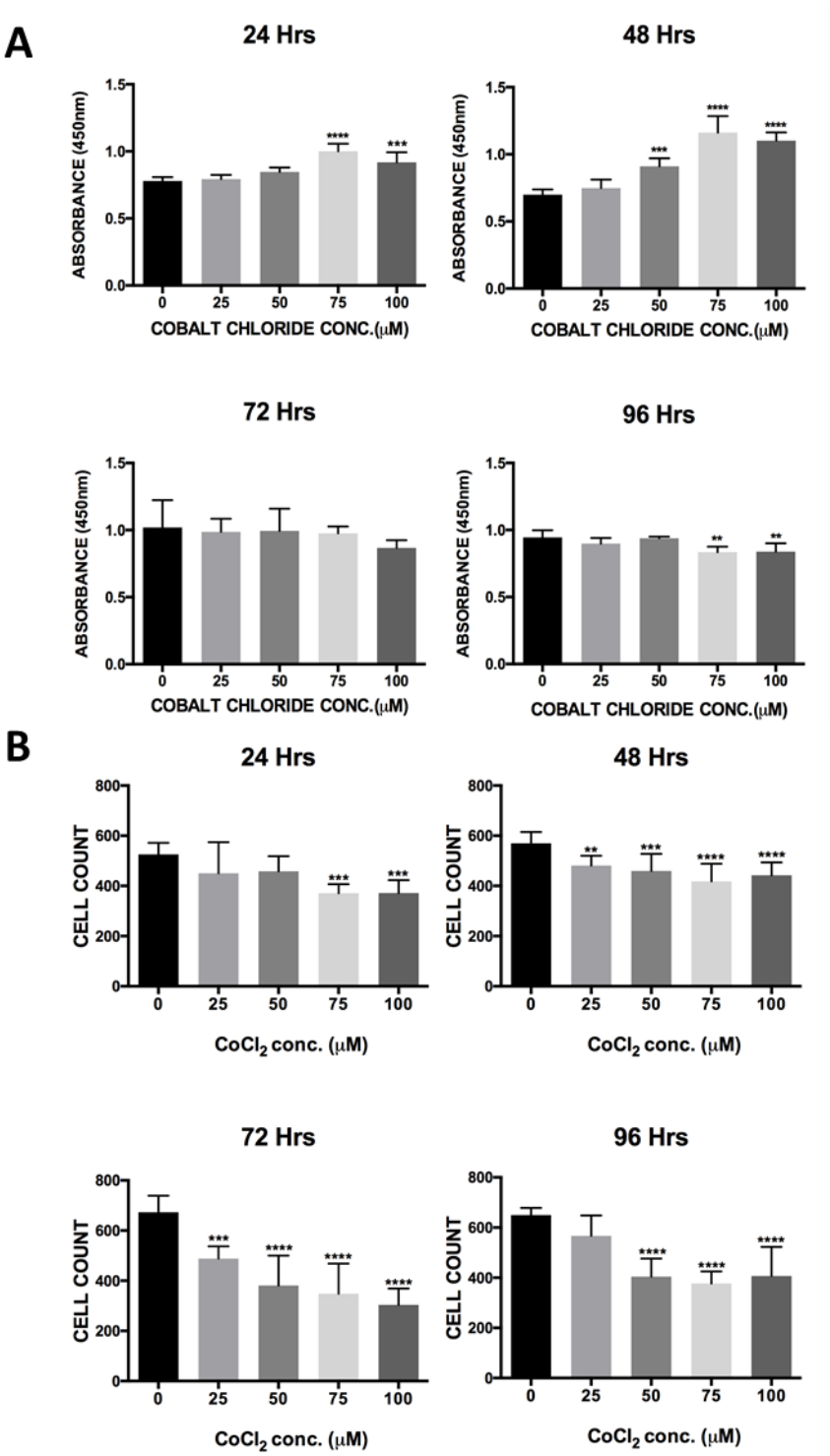

Figure 3.10: Cell proliferation assay post $CoCl_2$ incubation. Following growth in $CoCl_2$ containing media, MTT assay was performed to assess cell proliferation at 24, 48, 72 and 96 h. MTT assay indicated an increase in cell number upto 48h in $CoCl_2$ treated cells followed by a decline at 96 h compared to their respective control untreated cells (n=3; Mean +/- SD) (**=$p \leq 0.01$, One-way Anova) (A). The alternative technique employed staining of nuclei to count HKC8 cells post treatment with 25, 50, 75 and 100 μM $CoCl_2$ containing media at various time points (n=3; Mean +/- SD) (****=$p \leq 0.0001$, One-way Anova)(B).

HIF-1α level in response to $CoCl_2$ was assessed by immunofluorescence. Cells treated with $CoCl_2$ displayed an increased expression and nuclear localisation of HIF-1α in $CoCl_2$ stimulated cells compared to control cells (Figure 3.11). Similar expression was observed in cells following 96 h stimulation with $CoCl_2$ (data not shown).

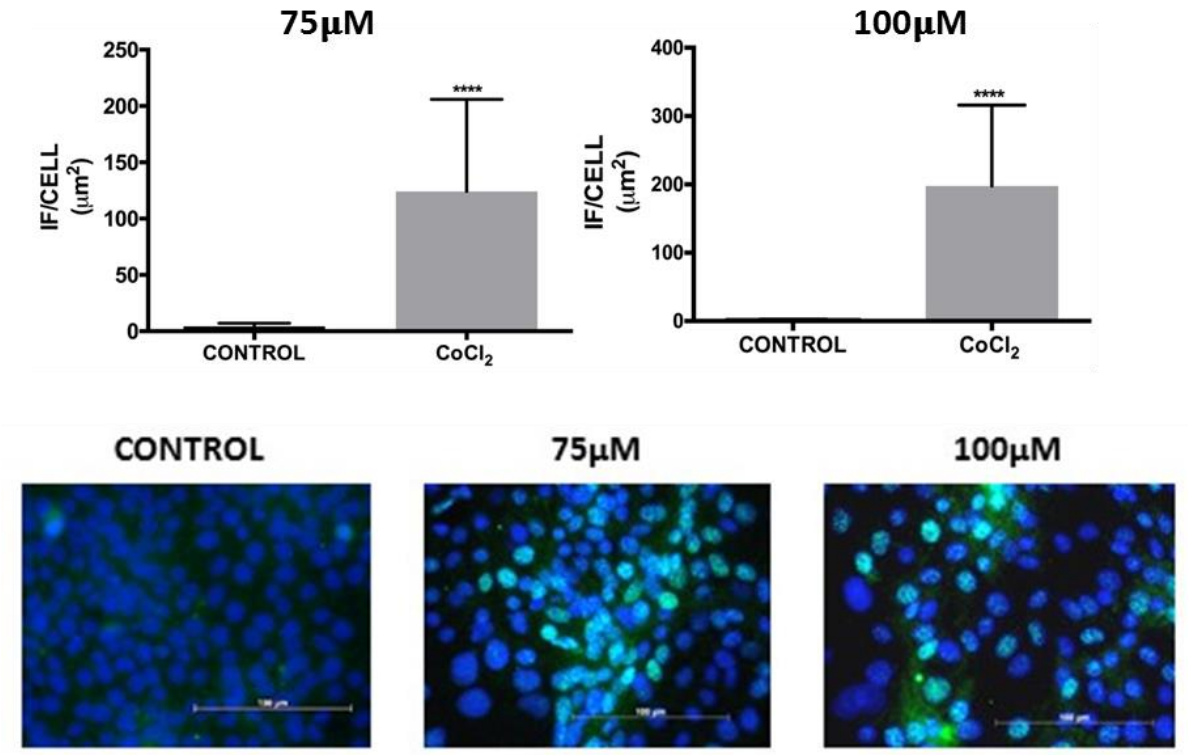

Figure 3.11: Increased nucleolar localisation of HIF-1α in HKC8 cells following treatment with $CoCl_2$. Immunofluorescence (n=3; Mean +/- SD, Unpaired t test) shows increased HIF-1α expression in cells stimulated with $CoCl_2$ at 72 h compared to the untreated control (****=$p \leq 0.0001$). Images were taken at 400X magnification using Leica AF imaging unit. The images were analysed using Image J and are represented as bar graphs of fluorescence per cell.

3.2.1.4 Optimising conditions for H_2O_2 treatment in HK2 cells

Experiments were also performed in a second cell line to ensure that my findings were reproducible. HK2 cells were treated with various concentrations of H_2O_2 for 4 h followed by incubation with complete media for upto 20 h. HK2 cells maintained 85% viability at 50 and 100µM H_2O_2 concentration when compared to untreated control.

Increased cell death was observed with H_2O_2 concentrations above this level ($p \leq 0.01$; $p \leq 0.0001$) (Figure 3.12 A).

The cells were photographed upto 72 h to monitor morphological changes in phenotype (data not shown). As with HKC8 cells, treated HK2 cells demonstrated a change in epithelial phenotype when compared to untreated cell (Figure 3.12 B).

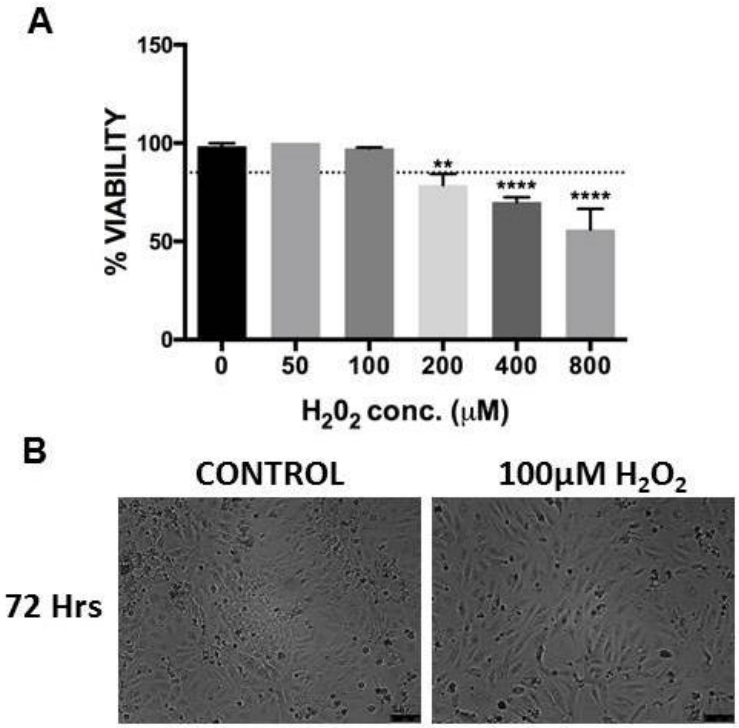

Figure 3.12: Percentage HK2 cell viability following H_2O_2 treatment.
HK2 cells were treated with various concentration of H_2O_2 for 4 h followed by 20 h incubation with complete media. The cell viability was subsequently evaluated by Trypan blue dye exclusion assay and compared to the untreated control cells (n=3; Mean +/- SD) (3.12 A). Images were captured at 72 h using Zeiss Axioimager microscope (100X)(3.12 B). (**=$p \leq 0.01$, ****=$p \leq 0.0001$; One-way Anova)

3.2.1.5 The effect of $CoCl_2$ on HK2 cells

The effect of $CoCl_2$ on HK2 cell viability was also assessed. Once confluent, HK2 cells were subjected to treatment 25, 50, 75, 100, 200 µM of $CoCl_2$ upto 72 h. HK2 cells were viable for all concentrations of $CoCl_2$ at 72 h (Figure 3.13 A). However, HK2 cells appeared spindle shaped and elongated following 72 h incubation with 100µM of $CoCl_2$ (Figure 3.13 B).

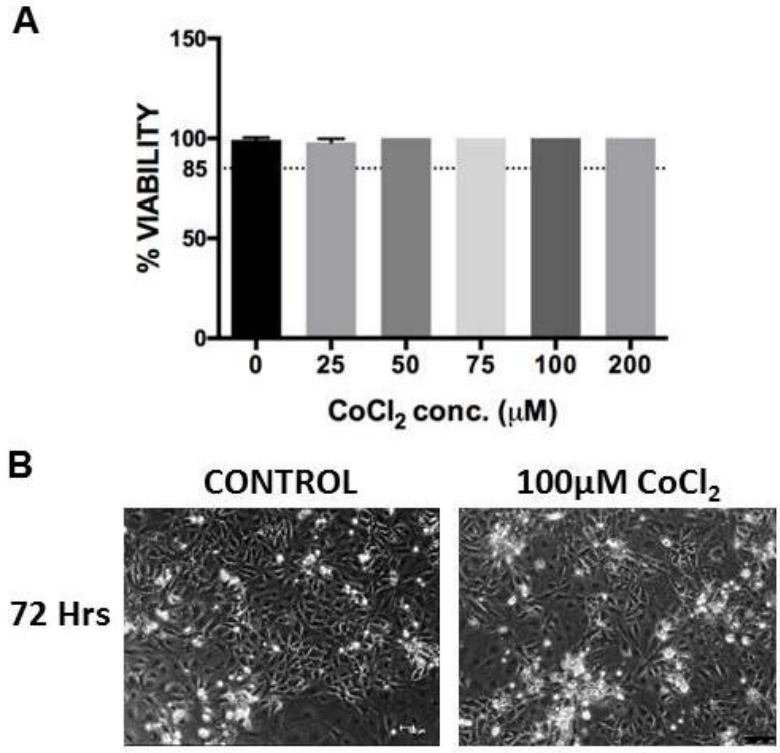

Figure 3.13: Viability of HK2 cells following 72 h $CoCl_2$ treatment.
HK2 cells were stimulated with varying concentration of $CoCl_2$ for upto 72 h and cell viability was measured by Trypan blue dye exclusion assay and compared to the untreated control cells (n=3; Mean +/- SD)(3.13 A). Images were captured at 72 h using Zeiss Axioimager microscope (100X)(3.13 B).

3.2.2 Changes in expression of pro-fibrotic markers in H_2O_2, hypoxia and $CoCl_2$ in PTECs and fibroblasts.

3.2.2.1 α-SMA and E-cadherin expression following H_2O_2 stimulation of HKC8 cells

HKC8 cells were treated with concentrations of H_2O_2 that induced production of oxygen free radicals. To study acute effects of free radical injury, HKC8 cells were treated with 400μM H_2O_2 for 4 h after cells attained 80% confluency followed by incubation for 20 h in complete media. Immunofluorescence and Western blot data suggests a significant upregulation of α–SMA in treated cells compared to untreated control cells (Figure 3.14 A and B).

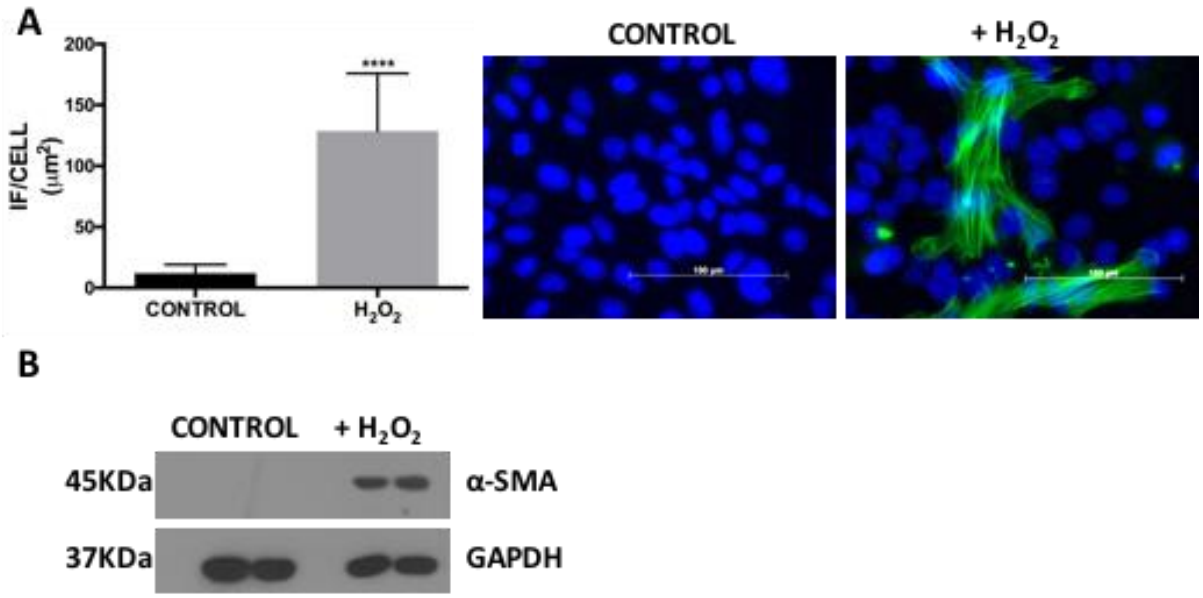

Figure 3.14: α–SMA expression in HKC8 cells 24 h following 400μM H_2O_2 treatment. HKC8 cells were incubated with 400μM of H_2O_2 in complete media for 4 h followed by substitution with fresh media for 20 h. Immunofluorescence (A, n=3; Mean +/- SD) and Western blot (B, n=2) was performed to study the expression at protein level. Compared to control cells, α-SMA was significantly increased (****=$p \leq 0.0001$) post treatment. Images were taken at 400X magnification for α-SMA using Leica AF imaging unit. The images were analysed using Image J and data is represented as bar graphs of fluorescence per cell.

The longer-term effects of free radical injury on epithelial cell phenotype was studied by subjecting HKC8 cells to 200μM H_2O_2 treatment for 4 h followed by incubation with complete media for 48 and 72 h. Cells stimulated with H_2O_2 showed a consistent upregulation of α–SMA (Figure 3.15) with clear decrease in E-Cadherin expression at (Figure 3.16) 48 h and 72 h. The expression of E-cadherin was low at baseline when cells have been grown for 48 h and only increased when cells were over 90% confluent (control 72h).

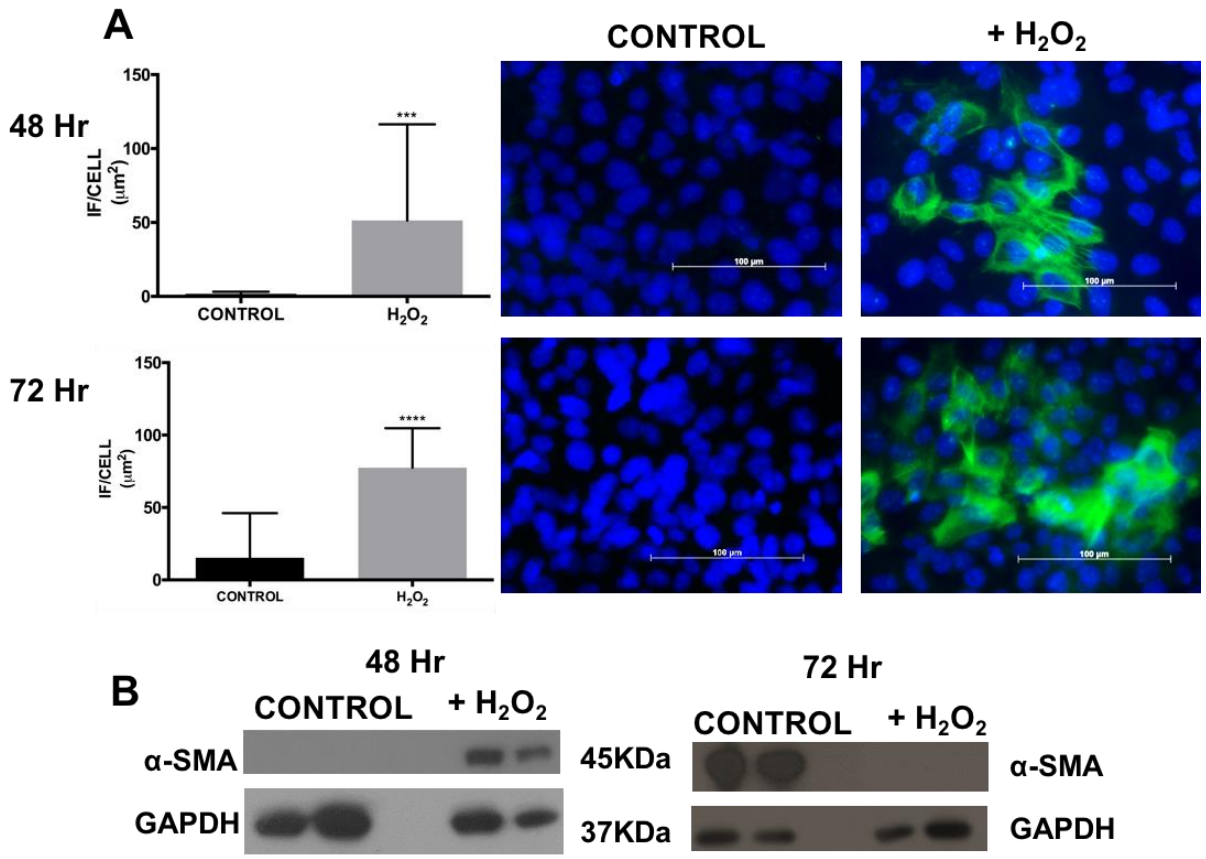

Figure 3.15: α–SMA expression HKC8 cells 48 and 72 h after exposure to H_2O_2. Immunofluorescence (A, n=3; Mean +/- SD, Unpaired t test) and Western blot (B, n=2) studies suggest a significant increase in α-SMA expression following 200µM treatment for 48 and 72 h compared to their respective control (**=$p \leq 0.01$, ****=$p \leq 0.0001$). Images were taken at 400X magnification for α-SMA using Leica AF imaging unit. The images were analysed using Image J and data is represented fluorescence per cell.

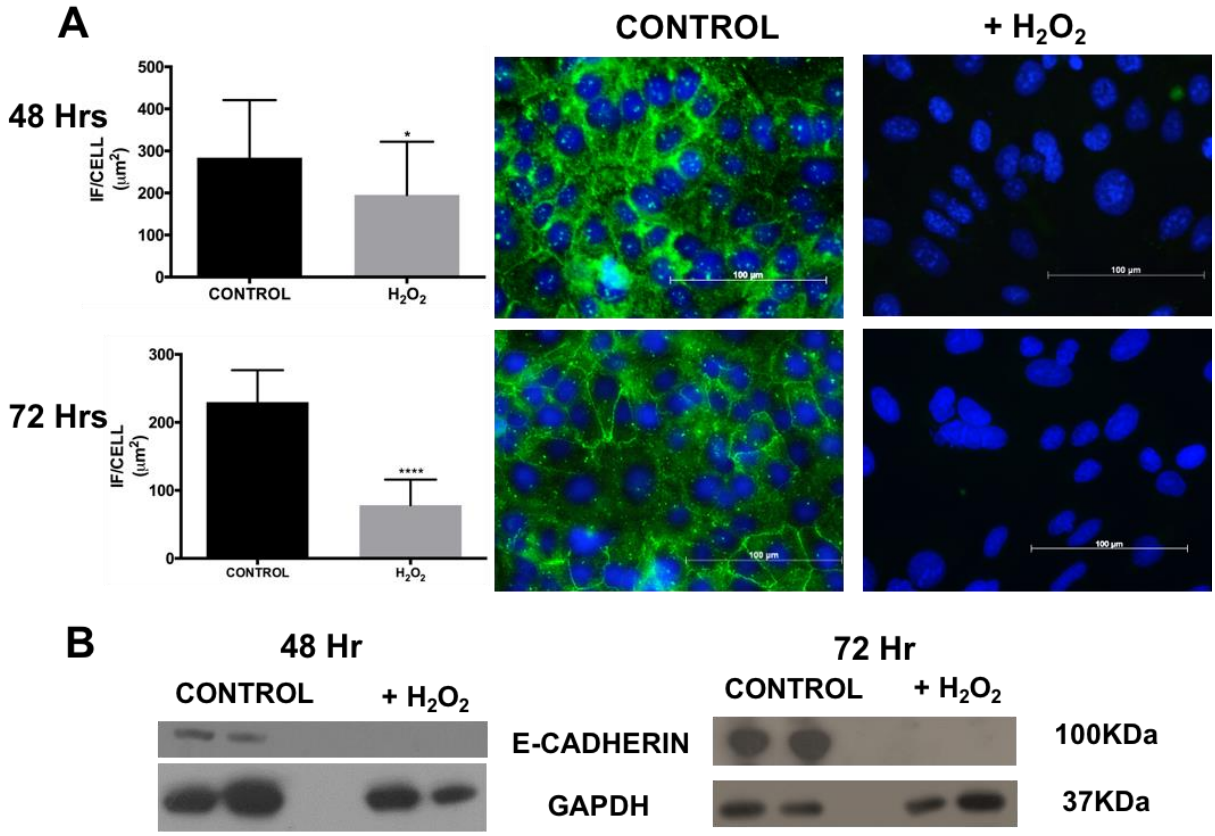

Figure 3.16: E-cadherin expression following H_2O_2 treatment. 200µM H_2O_2 treatment significantly reduced E-cadherin expression (*=$p \leq 0.05$, ****=$p \leq 0.0001$) (A). Similar trend was observed with Western blot (B, n=2) studies. Unpaired T test was used to analyse the data. Images were taken at 400X magnification for E-cadherin using Leica AF imaging unit.

3.2.2.2 α-SMA and E-cadherin expression in HKC8 cells in hypoxic conditions

Cells were subjected to 1% oxygen and the expression of α-SMA and E-cadherin was examined. HKC8 cells were cultured in 6 well plates and grown until they reached 80% confluency, incubated in a hypoxic chamber (1% O_2) for 72 h. Protein studies showed an increased α-SMA expression and reduced E-cadherin expression (Figure 3.17) in the treated cells compared to the control cells. A similar pattern was observed after 96 h in hypoxic conditions.

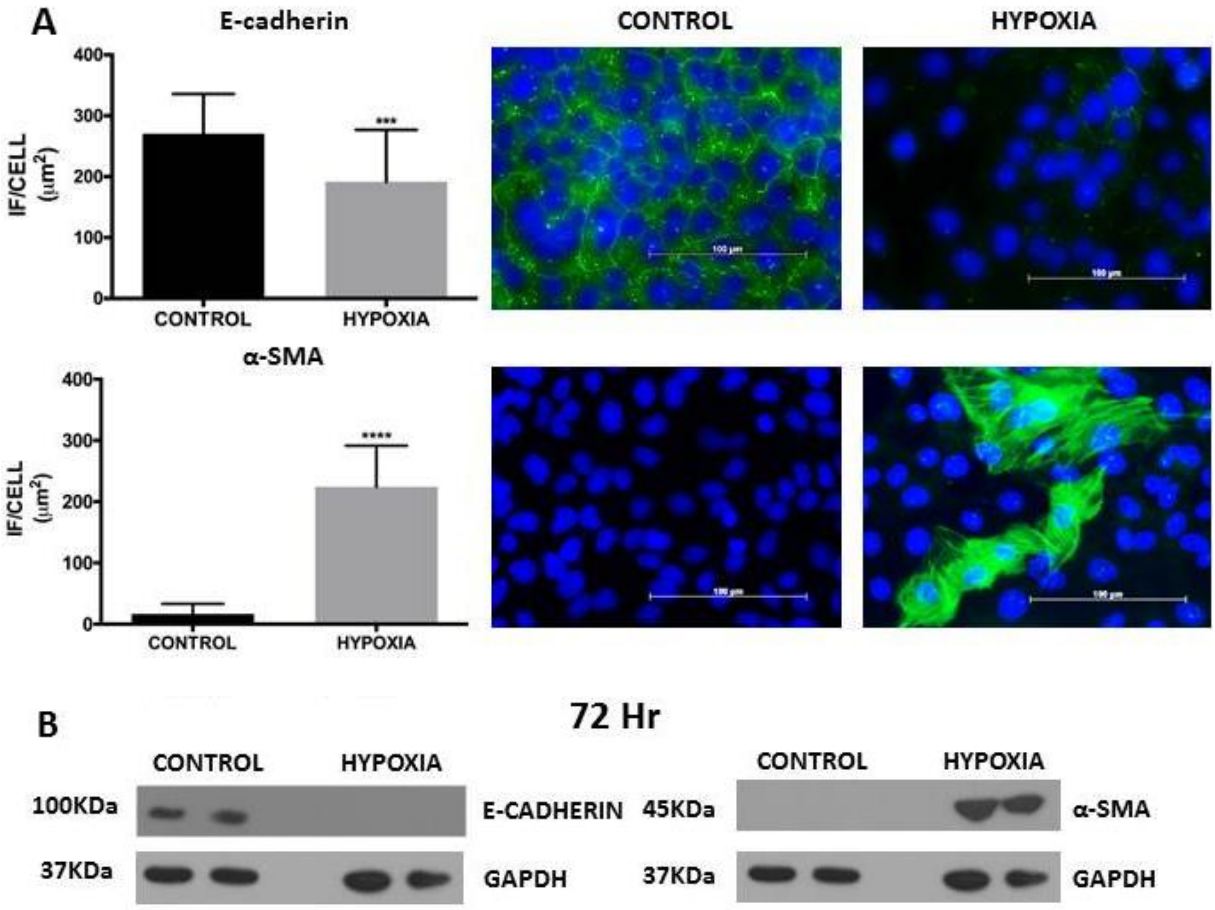

Figure 3.17: Protein expression following hypoxic incubation. Following hypoxic incubation, protein studies using immunofluorescence (A, n=3; Mean +/- SD, Unpaired t test) and Western blot (B, n=2) suggested that hypoxia induced a significant increase in α-SMA expression (***=$p \leq 0.001$) and reduced E-cadherin expression (****=$p \leq 0.0001$) in treated cells when compred to control. Images were taken at 400X magnification for α-SMA and E-cadherin using Leica AF imaging unit. The images were quantitatively analysed using Image J and are represented as bar graphs of fluorescence per cell.

3.2.2.3 α-SMA and E-cadherin expression after $CoCl_2$ treatment in HKC8 cells.

$CoCl_2$ mimics hypoxia by stabilising HIF-1α and prevents its degradation. HKC8 cells were treated with 100μM $CoCl_2$ for 72 h. Immunofluorescence and Western blots (Figure 3.18) studies showed an increase in α-SMA and decrease in E-Cadherin expression at 72 h suggesting a profibrotic phenotype due to HIF-1α stabilisation. Similar change was observed at 96 h treatment (data not shown).

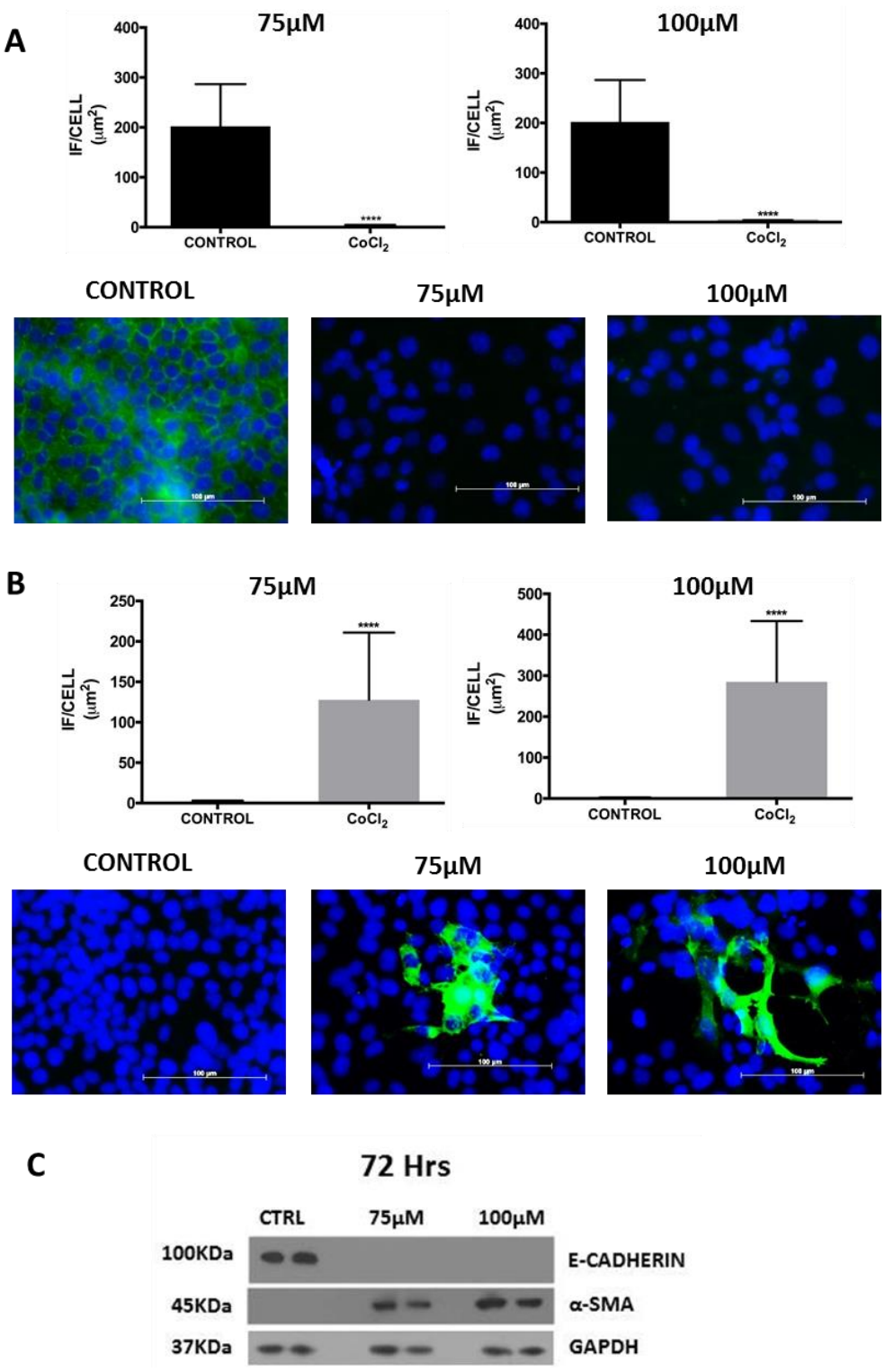

Figure 3.18: $CoCl_2$ treated HKC8 cells show increased α-SMA and reduced expression of E-Cadherin. HKC8 cells were treated with 100µM $CoCl_2$ 72 h. The expression of E-cadherin and α-SMA was assessed using immunofluorescence (A and B, n=3; Mean +/- SD, Unpaired t test) and Western blots (C, n=2). Compred to control, $CoCl_2$ induced an increase in expression of α-SMA (****=$p \leq 0.0001$) and a decrease in E-Cadherin expression in treated cells (****=$p \leq 0.0001$). Images were taken at 400X magnification for α-SMA and E-cadherin using Leica AF imaging unit. The images were quantitatively analysed using Image J and are represented as bar graphs of fluorescence per cell.

3.2.2.4 Overexpression of HIF-1α induces a fibrotic phenotype in HKC8 cells

To determine whether overexpression of HIF-1α can shift epithelial phenotype to more fibrotic one, cells were transfected with pHIF-1α and control pCDNA 3.1 followed by incubation in complete media for 72 h. The protein expression of E-cadherin, α–SMA and HIF-1α were investigated. Compared to transfection control, overexpression of HIF-1α increased α–SMA and reduced E-cadherin expression (Figure 3.19). These observations suggest a clear shift in protein expression - from a largely epithelial pattern, to an intermediate or fibrotic pattern.

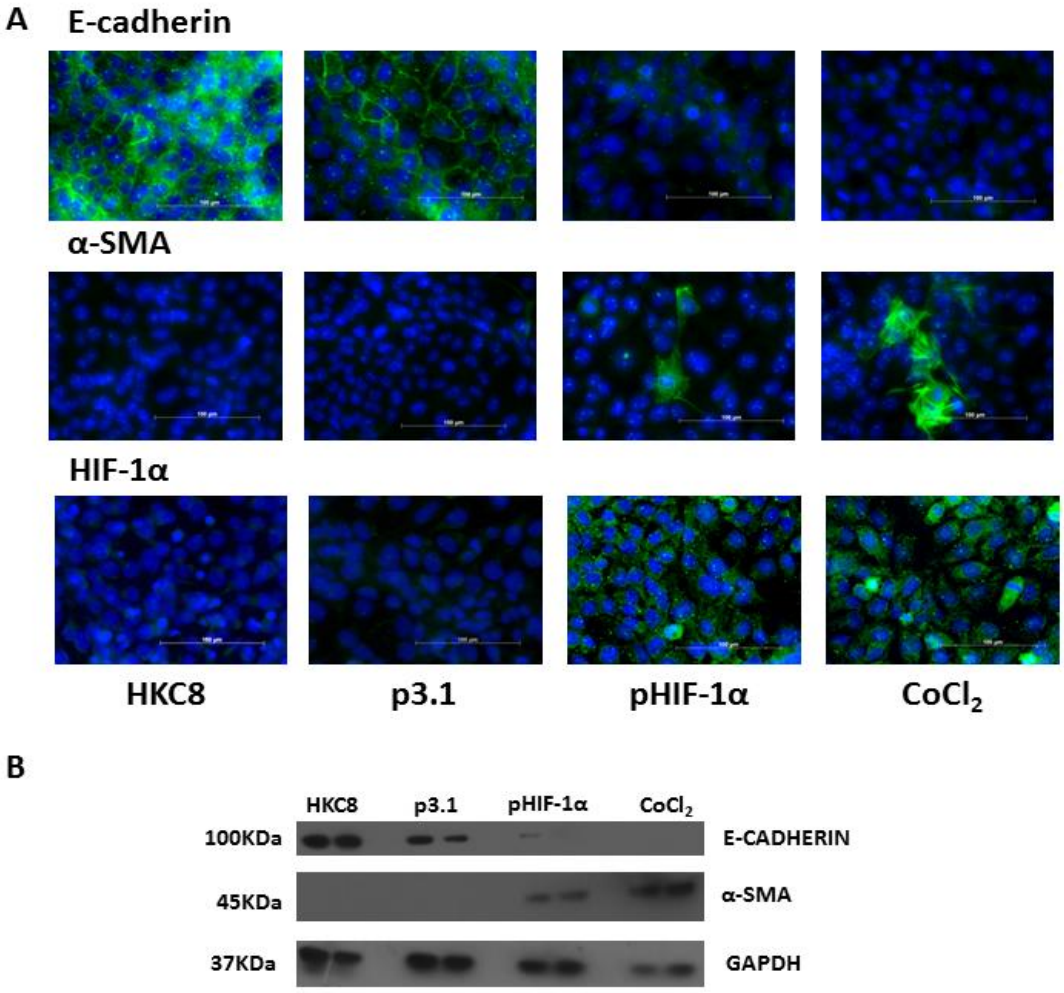

Figure 3.19: HIF1-α overexpression reduced E-cadherin and increased α-SMA expression. Immunofluorescence (A) and Western blot (B) demonstrates reduced E-cadherin and increased α–SMA and HIF-1α expression post transfection with pHIF-1α compared to control (untransfected and pcDNA3.1 vector transfected). Images were taken at 400X magnification for α-SMA, HIF-1α and E-cadherin using Leica AF imaging unit.

3.2.2.5 Protein expression in HK2 cells treated with H_2O_2 and $CoCl_2$

Experiments performed in HKC8 cells were replicated in a second human proximal tubular epithelial cell, HK2. Cells were treated with 100μM H_2O_2 for 72 h and the expression of ECM markers was analysed using Western blot and immunofluorescence. A significant increase in α-SMA expression ($p \leq 0.0001$) along with reduced E-cadherin expression ($p \leq 0.0001$) was seen in H_2O_2 treated cells (Figure 3.20). HK2 cells were treated with 100μM CoCl2 treatment for 72 h. Immunofluorescence results suggested a significant increase in α-SMA ($p \leq 0.0001$) and a significant decrease in E-cadherin ($p \leq 0.0001$) in treated cells compared to controls. Western blotting confirmed these changes (Figure 3.21). These results further support the role of HIF-1α in modulating fibrotic phenotype in renal proximal tubular epithelial cells.

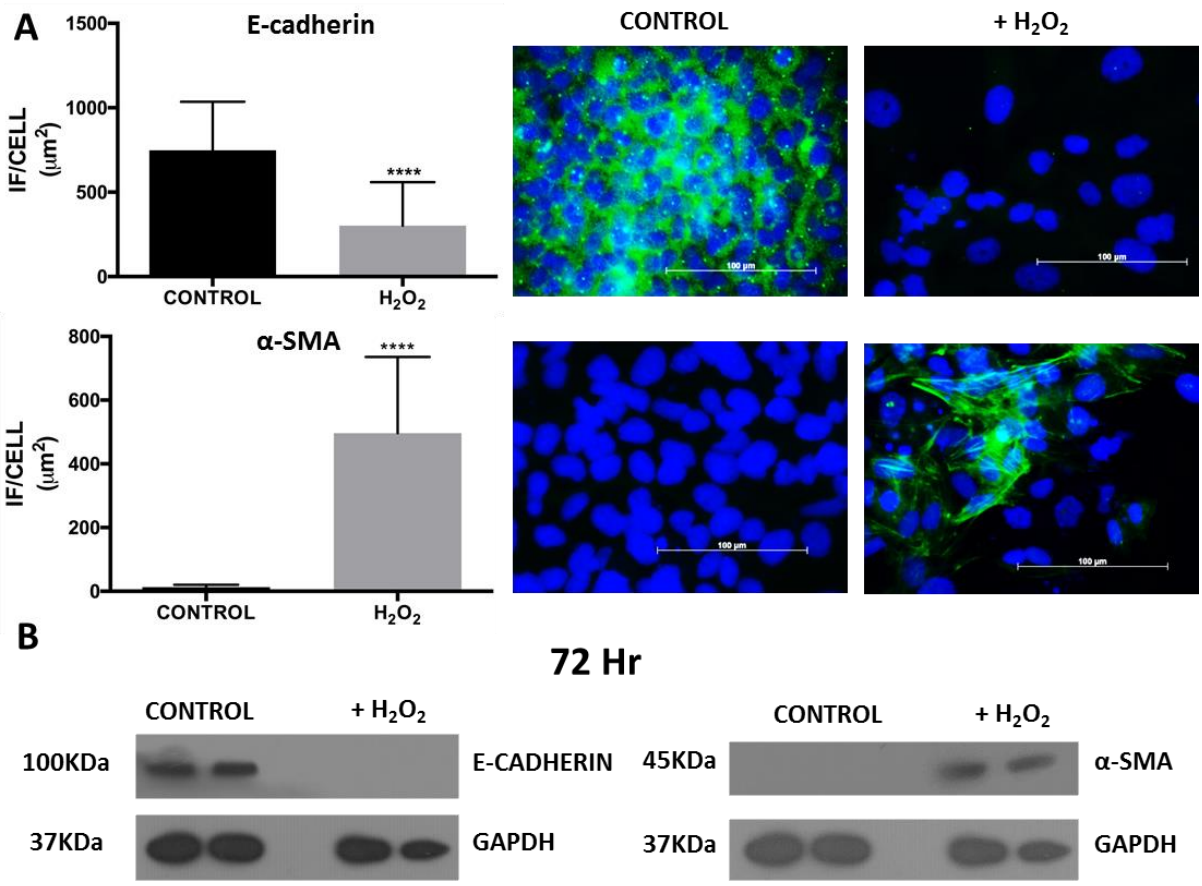

Figure 3.20: H_2O_2 induces fibrotic phenotype characteristics in HK2 cells.
HK2 cells were treated with 100μM H_2O_2 for 4 h followed by incubation with complete media for 72 h. Protein expression of α-SMA and E-cadherin was analysed by immunofluorescence (A, n=3; Mean +/- SD) and Western blots (B, n=2). Cells stimulated with H_2O_2 show reduced E-cadherin expression (****=$p \leq 0.0001$) with an increased α-SMA expression compared to the controls (****=$p \leq 0.0001$). Western blotting data suggested a similar expression pattern. Images were taken at 400X magnification for α-SMA and E-cadherin using Leica AF imaging unit. The images were quantitatively analysed using Image J and are represented as bar graphs of fluorescence per cell.

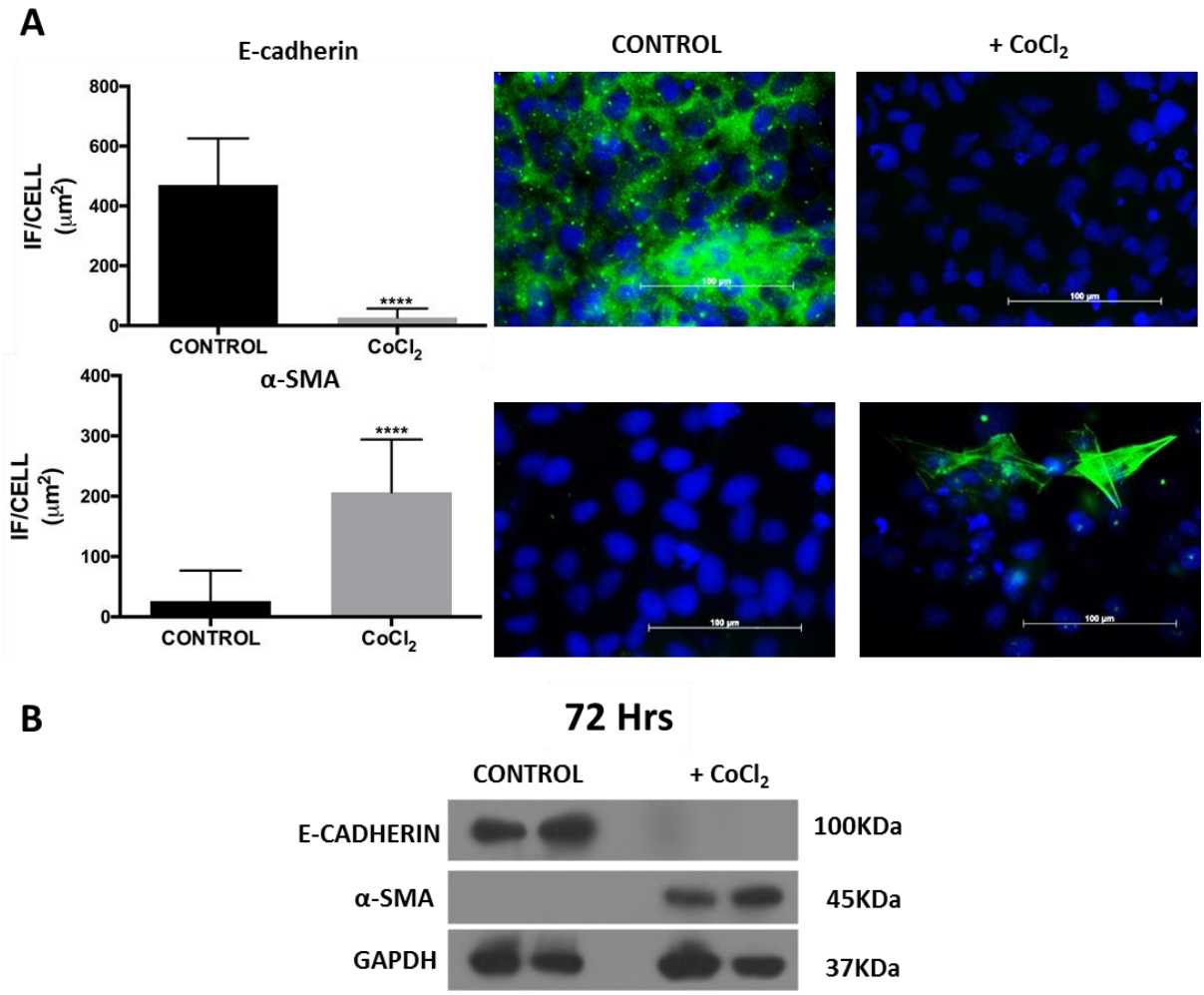

Figure 3.21: $CoCl_2$ treated HK2 cells showed reduced E-cadherin and increased α-SMA expression. HKC8 cells were stimulated with 100 μM $CoCl_2$ for 72 h. Protein studies using Immunofluorescence data (A, n=3; Mean +/- SD, Unpaired t test) and Western Blots (B, n=2) suggest an increased α-SMA expression (****=$p \leq 0.0001$) with reduced E-Cadherin (****=$p \leq 0.0001$) expression post stimulation with $CoCl_2$ compared with control. Images were taken at 400X magnification for α-SMA and E-cadherin using Leica AF imaging unit. The images were quantitatively analysed using Image J and are represented as bar graphs of fluorescence per cell.

3.2.2.6 H_2O_2 and $CoCl_2$ stimulates myofibroblast generation in MRC-5 cells

The aim of this work was to establish an in-vitro co-culture system with both fibroblast and epithelial cells. The effects of H_2O_2 and $CoCl_2$ on fibroblast cell line MRC-5 were assessed. MRC-5 cells exposed to H_2O_2 for 4 h followed by 20h incubation in complete media and $CoCl_2$ for 24 h show an increased myofibroblast features characterised by increased α-SMA expression ($p \leq 0.0001$)(Figure 3.22).

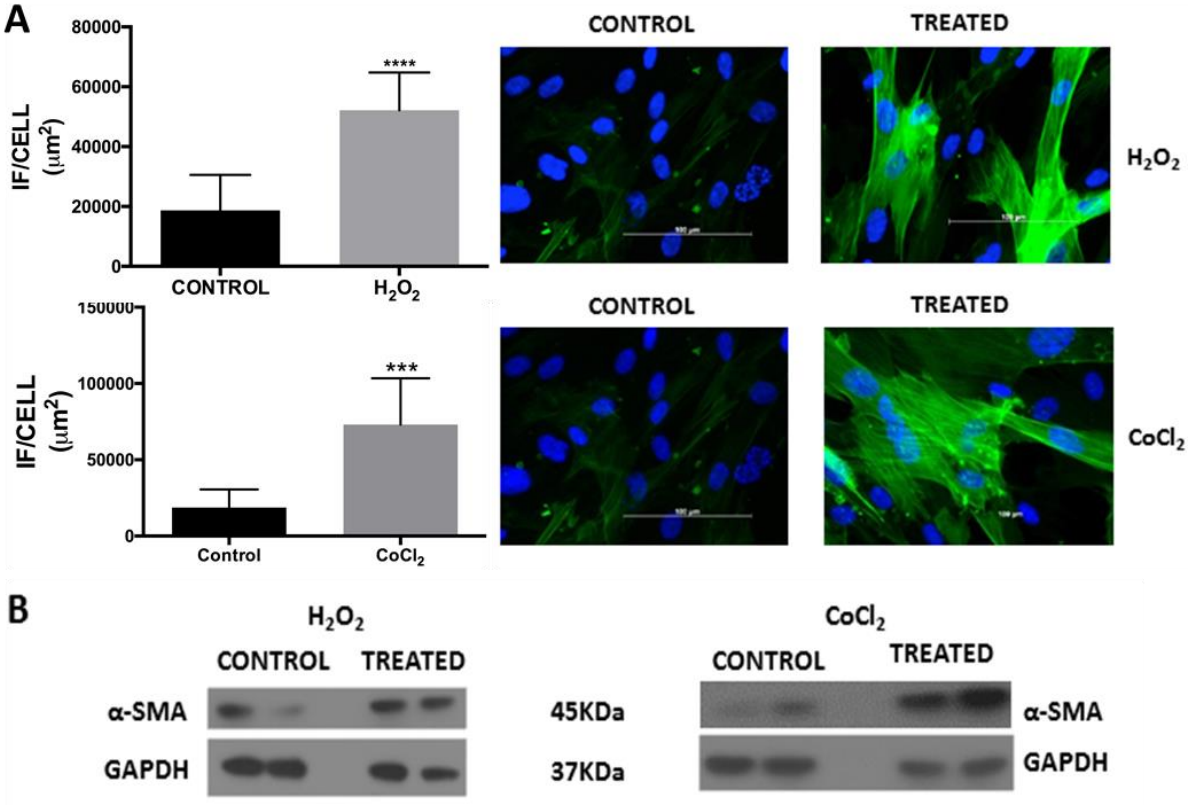

Figure 3.22: Treatment with 100μM H_2O_2 and 100μM $CoCl_2$ induces an increased α-SMA expression in MRC-5 cells.
MRC-5 cells were stimulated with 100μM H_2O_2 and $CoCl_2$. Protein studies performed using (A, n=3; Mean +/- SD, Unpaired t test) and Western blots (B, n=2) displays a significant increase in α-SMA expression (****=$p \leq 0.0001$) compared to untreated control. Images were taken at 400X magnification for α-SMA and E-cadherin using Leica AF imaging unit. The images were quantitatively analysed using Image J and are represented as bar graphs of fluorescence per cell.

3.2.3 Gene expression following $CoCl_2$ and H_2O_2 treatment

3.2.3.1 Quantitative RT-PCR analysis of fibrotic markers in HKC8 cells

QRT-PCR was used to evaluate changes in gene expression of fibrotic markers following H_2O_2 and $CoCl_2$ treatment in HKC8 cells. However no significant changes in the expression of fibrotic markers were observed.

3.2.3.2 Changes in fibrotic gene expression at RNA level in HK2 cells

HK2 cells stimulated with 100μM H_2O_2 for 4 h followed by incubation in complete media upto 72 h displayed a significant increase in expression of the fibrotic markers α-SMA ($p \leq 0.01$), MMP2 ($p \leq 0.0001$), COL1A1 ($p \leq 0.01$), TGF-β1 and TGF–β2 ($p \leq 0.05$) when compared to controls. No change in expression was observed in TIMP1 expression (Figure 3.23). A significant increase in MMP2 ($p \leq 0.01$) and TGF-β2 ($p \leq 0.05$, $p \leq 0.01$) expression was seen at 72 and 96 h of incubation with 100μM $CoCl_2$. TGF-β1 ($p \leq 0.05$) and COL1A1 expression ($p \leq 0.0001$) was significantly upregulated at 96 h incubation (Figure 3.24). These results suggest that H_2O_2 and $CoCl_2$ increase fibrotic gene expression in HK2 cells at RNA and protein level.

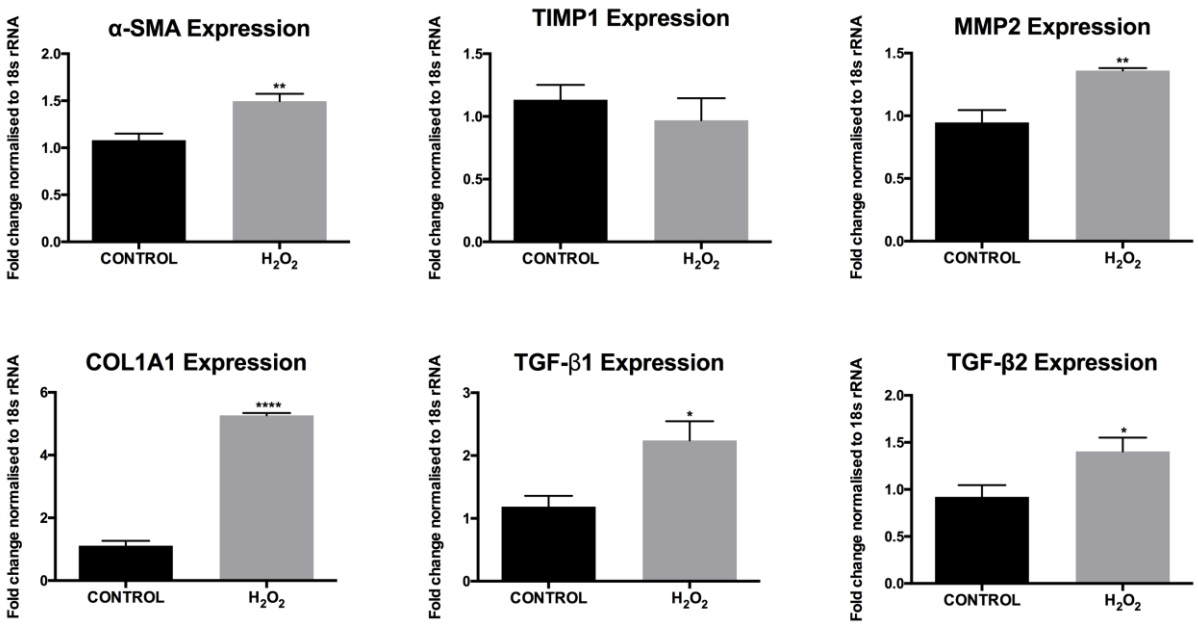

Figure 3.23: Gene profiling in HK2 cells following H_2O_2 treatment.
Expression of α–SMA, TIMP1, MMP2, COL1A1, TGF-β1 and TGF-β2 was analysed at 72 h post 100μM H_2O_2 treatment normalised to 18srRNA and expression levels compared to untreated control (N=3). Following 72 h incubation, a significant increase in α-SMA, MMP2, COL1A1, TGF-β1 and TGF–β2 expression was observed. Unpaired T test was used to analyse the data and graphs were plotted using prism 6 software. (*=$p \leq 0.05$, **=$p \leq 0.01$, ****=$p \leq 0.0001$)

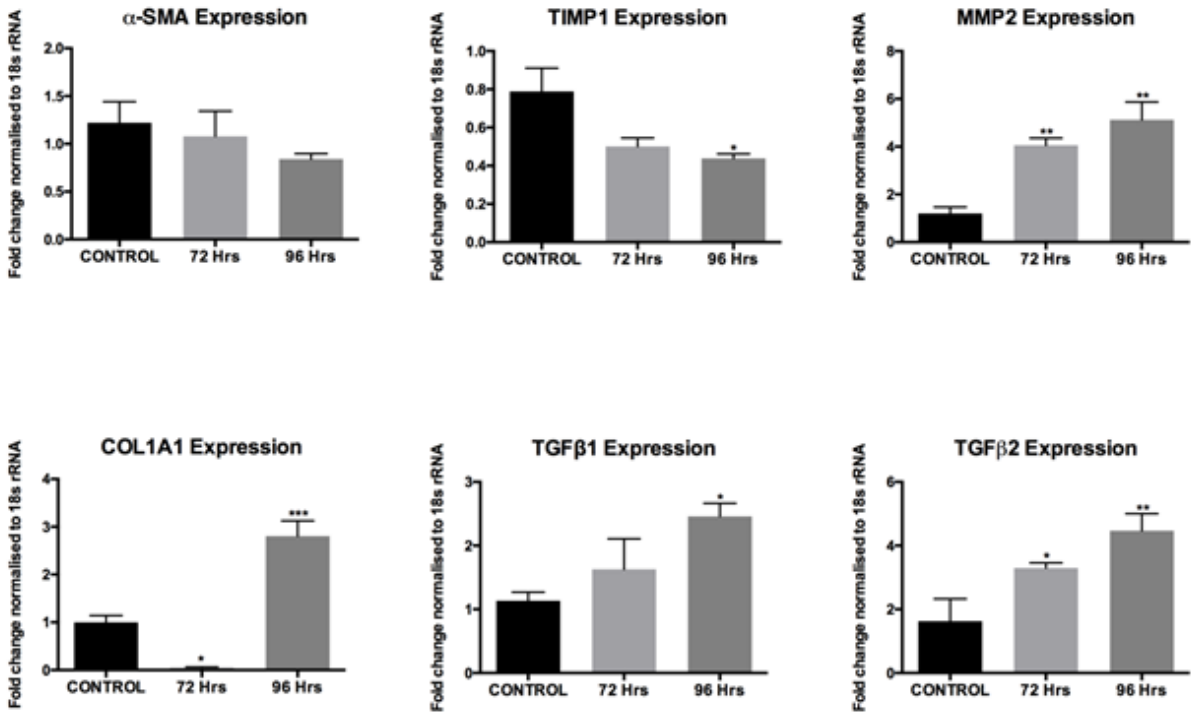

Figure 3.24: Gene expression in HK2 cells post 100μM $CoCl_2$ treatment.
The graphs show expression of α–SMA, TIMP1, MMP2, COL1A1, TGF-β1 AND TGF-β2 at 72 and 96 h $CoCl_2$ treatment normalized to 18srRNA and expression levels compared to untreated control (N=3). A significant fold change in COL1A1, MMP2, TIMP1, TGF-β1 and TGF-β2 expression observed. One-way Anova Bonferroni method was used to analyse the data and graphs were plotted using prism 6 software. (*=$p \leq 0.05$, **=$p \leq 0.01$)

3.2.3.3 Increased expression of fibrotic genes in MRC-5 cells

MRC-5 cells stimulated with H_2O_2 and $CoCl_2$ showed a significant increase in fibronectin ($p \leq 0.05$) and α-SMA ($p \leq 0.001$, $p \leq 0.05$) expression (Figure 3.25 and 3.26).

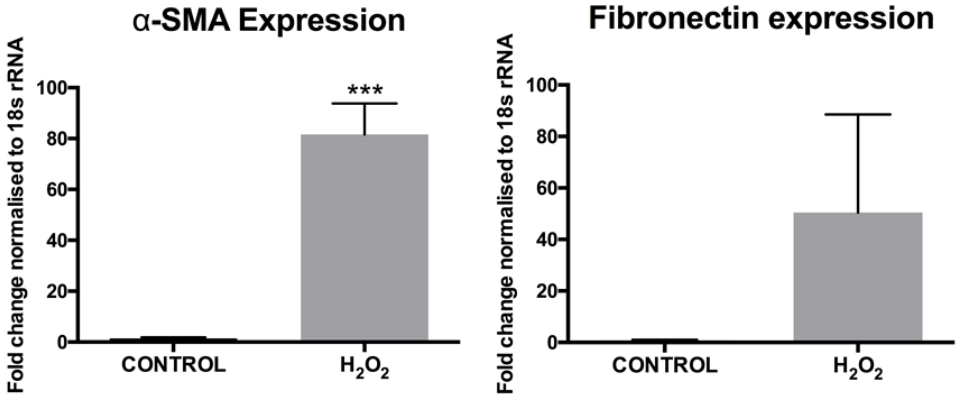

Figure 3.25: RT-PCR analysis in MRC-5 cells post H_2O_2 treatment.
The graphs show expression of α–SMA and Fibronectin expression at 24 h post 100μM H_2O_2 treatment normalised to 18srRNA and expression levels compared to untreated control (N=3). A significant increase in α-SMA expression (*p*≤0.001) was observed post H_2O_2 treatment. Unpaired T test was used to analyse the data and graphs were plotted using prism 6 software.

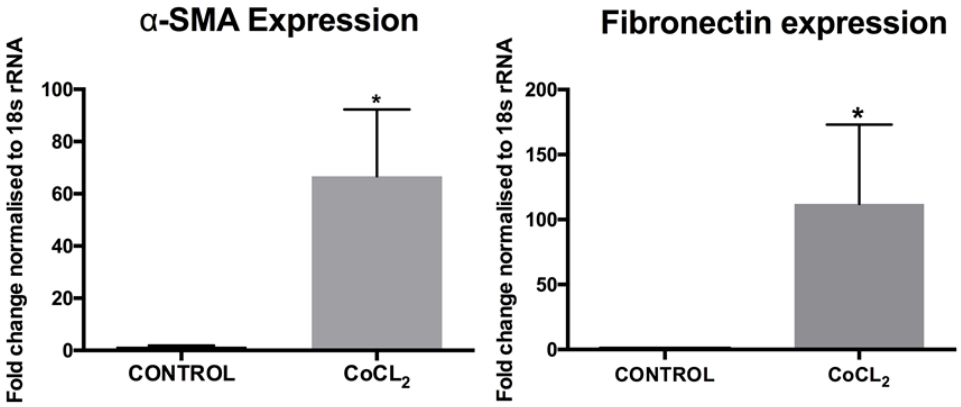

Figure 3.26: RT-PCR analysis in MRC-5 cell post $CoCl_2$ treatment.
The graphs show expression of α–SMA and Fibronectin expression at 24 h post 100μM $CoCl_2$ treatment normalized to 18srRNA and expression levels compared to untreated control (N=3). A significant increase in fibronectin and α–SMA expression (*=*p*≤0.05) was analysed when compared to untreated control. Unpaired T test was used to analyse the data and graphs were plotted using prism 6 software.

3.3 Discussion

Reactive oxygen species, such as H_2O_2 upon accumulation over extended periods of time causes oxidative stress and IRI induce tissue damage. H_2O_2 is more stable than other ROS because it is not itself a free radical (Bae *et al.*, 2015). Studies suggest that H_2O_2 may affect cell-signalling survival pathways and is responsible for the modulation of transcription factors involved in cellular response to stress stimuli such as hypoxia and oxidative stress (Nakamura *et al.*, 2003). Therefore, in my study, I used H_2O_2 to treat HKC8 and HK2 cells prior to studying the effect of ROS generation. Previous studies have used higher concentrations of H_2O_2 in human proximal tubular epithelial cells (500μM H_2O_2)(Rhyu *et al.*, 2005) and in an *in vitro* rodent model (1000 μM H_2O_2)(Armogida *et al.*, 2012). In my study, the optimum concentration of H_2O_2 treatment in HKC8 cells was found out to be 200 and 400μM. Whereas for HK2 cells, cells retained >85% cell viability at 100μM concentration. Although higher concentrations of H_2O_2 heightened changes in cell morphology, it was also associated with increased cell death. Therefore, further studies were conducted using lower concentrations of H_2O_2 that induced phenotypic changes in the cells but kept the cell viability constant.

Preclinical studies have indicated increased ROS production during progressive kidney inflammation and fibrosis, wherein persistent ROS production has been linked increased production of fibrotic markers such as α-SMA and decrease in the epithelial marker E-Cadherin (Shen *et al.*, 2016). My study demonstrated similar results: H_2O_2 significant increased the expression of α–SMA and reduced E-Cadherin expression in HKC8 cells. For instance, there was 3 fold increase in α–SMA expression (Figure 3.15) and 2.5 fold decrease in E-Cadherin expression (Figure 3.16) in 72 hrs H_2O_2 (200μM) treated HKC8 cells as compared to the untreated control. Similar results were seen using HK2 cells. Changes in fibrotic marker

expression were also evaluated at RNA level. A significant increase in α-SMA, TGF-β1 and 2, COL1A1 and MMP2 was observed in HK2 cells. Similar changes in expression of α-SMA and type-I collagen post ROS generation has been reported in studies of Idiopathic Pulmonary Fibrosis indicating that oxidative-stress promotes changes in fibrotic markers (Bocchino *et al.*, 2010).

Previous studies have used different methods including enzymatic, chemical and incubation in an anaerobic chamber to mimic the clinical setting of tissue hypoxia and to unravel the underlying mechanisms (Lièvre *et al.*, 2000; Askoxylakis *et al.*, 2011; Saxena *et al.*, 2012). However, most models established have drawbacks. They either could not induce rapid and/or terminate hypoxia or were not able to exclude side effects such as excessive cell death. To overcome this problem, a hypoxic chamber and $CoCl_2$ treatment were used to induce or mimic hypoxia. To mimic hypoxic conditions in kidney tubular epithelial cells *in vitro*, HKC8 cells were incubated in hypoxic incubator (1% oxygen) for upto 96 h. There was no significant change in cell viability. Previous studies have also indicated that incubating cells with 1% oxygen has no effect on cell viability and morphology in renal fibroblasts (Norman *et al.*, 2000).

Previous studies have shown that $CoCl_2$ mimics hypoxia via HIF-1α stabilisation *in vitro* in a mouse myoblast cell line (Chen *et al.*, 2017) and rat-derived PTECs (Weidemann *et al.*, 2008; Koeners *et al.*, 2014). Therefore, $CoCl_2$ was used as an alternative treatment to induce hypoxia. Percentage cell viability was assessed post treatment with varying concentrations of $CoCl_2$ at various time points. HKC8 and HK2 cells treated with 100μM of $CoCl_2$ looked elongated, although this is difficult to quantify. The results suggested a shift in the phenotypic characteristics of the cells from epithelial to fibrotic as has also been demonstrated in rat derived tubular epithelial cells by other researchers (Higgins *et al.*, 2007). Changes have also been

reported in renal carcinoma cell lines upon treatment with 50 μM - 200μM $CoCl_2$ (Zhang *et al.*, 2017). Furthermore, this change in phenotype also correlated with increased MMP2 expression at 72 h and TGF-β2 gene expression at 96-h following hypoxia incubation at the RNA level. Previous studies have also reported an increase in TGF-β2 post 48 h of hypoxic incubation in human endothelial cells (Chu *et al.*, 2004). Post hypoxic stress there was an increased expression of the fibrotic marker α-SMA (10 fold) and reduction in epithelial cell marker E-cadherin (2 fold) in HKC8 cells (Figure 3.17). Similar trend was observed in HK2 cells. Treatment with $CoCl_2$ elevated the expression of EMT-related transcription factors such as fibronectin, snail and downregulated E-Cadherin in hepatocytes supporting the results observed in my study (Kong *et al.*, 2015). Furthermore, these experiments clearly demonstrated 25 fold increase in HIF1α expression post 100μM $CoCl_2$ treatment at the protein level compared to untreated control (Figure 3.11). These observations suggest that the change in cell phenotype could be induced by HIF1α, rather than other cellular effects of hypoxia.

There are no available human renal fibroblast lines that could be used in this series of experiments. The use of a human lung fibroblast line, as a responder line to demonstrate potential fibroblast responses, was thought more appropriate that the use of a renal fibroblast line from another species to avoid differences in TGF-β signalling pathways that may be present in different species. The transcriptome data for MRC-5 cells is available and has been compared to other fibroblast cell lines, where data suggests that MRC-5 cells show similar clusters (Giannakakis *et al.*, 2015; Marthandan *et al.*, 2015; Marthandan *et al.*, 2016). Furthermore, MRC-5 cells have been extensively used to study the effects of oxidative stress (Sitte *et al.*, 1998; Chen *et al.*, 2015; Romeo *et al.*, 2016) and hypoxia (Dai *et al.*, 2003; Mathieu *et al.*, 2014). Therefore, in my study MRC-5 cells were stimulated with H_2O_2 or $CoCl_2$ and

fibrotic marker expression was examined. Oxidative stress and hypoxia induced two fold and four fold increased expression of fibrotic markers in MRC-5 cells respectively (Figure 3.22) that has also been previously described in literature (Hamblin and Huang, 2013). Overall the results suggested that H_2O_2 and $CoCl_2$ induced oxidative stress and hypoxia in human renal epithelial cell lines and MRC-5 cells.

Chapter 4: Role of transforming growth factor in ischaemia and reperfusion injury induced renal fibrosis in proximal tubular epithelial cells

4.1 Introduction

The previous chapter demonstrates that inducing ischaemic stress by hypoxia and $CoCl_2$ and reperfusion stress by H_2O_2 effectively replicates the *in vivo* conditions. Cells displayed an increased expression of α-SMA and reduced E-cadherin expression at protein level. Since TGF-β acts as a central mediator in the progression of renal fibrosis (Lan, 2011), further investigation and understanding of the effects of TGF-β in response to IRI is required (Gerritsma *et al.*, 1998). SB-505124 is an activin receptor-like kinase (ALK-5) inhibitor that inhibits downstream signal transducers such as Smad 3, Smad 2 of TGF-β signalling. My studies showed that SB-505124 reduced expression of α-SMA and maintained the expression of E-Cadherin in H_2O_2 or $CoCl_2$ treated HKC8 cells.

4.2 Results

4.2.1 TGF-β treatment of PTECs

Treating cells directly with TGF-β1 offers insight into the role of TGF-β1 in progression of renal fibrosis. Experimental findings show that PTECs exposed to 10ng/ml of recombinant TGF-β1 appear morphologically altered when compared to untreated controls (Yu *et al.*, 2003; Xu *et al.*, 2007). I observed that PTECs exposed to 10ng/ml of TGF-β1 for 24 h appeared elongated and spindle shaped compared to untreated control cells (Figure 4.1).

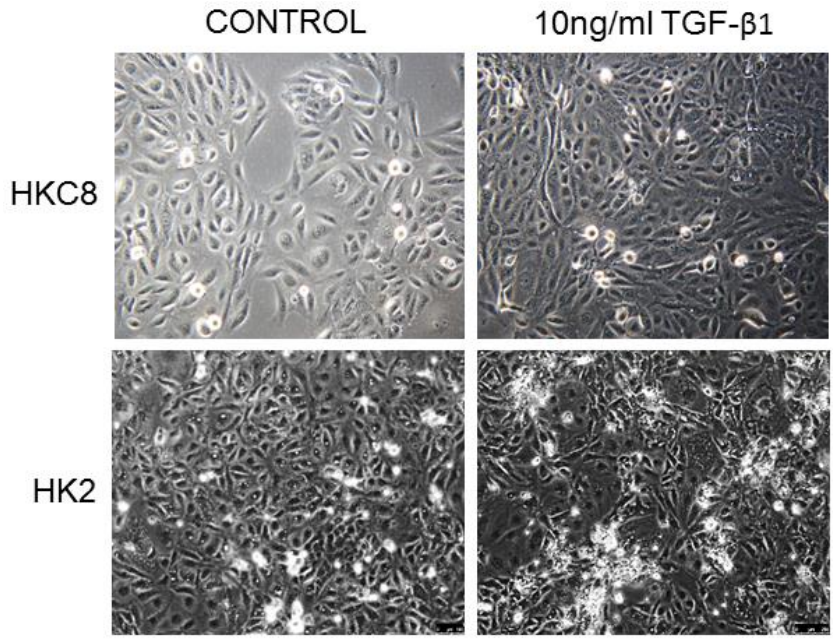

Figure 4.1: Morphological changes in epithelial cells post TGF-β1 treatment. HKC8 and HK-2 cells were incubated with 10ng/ml of recombinant TGF-β1 for 24 h. Images were acquired at 24 h using a Leica bright field microscope (Magnification X100).

Changes at transcriptional level also assessed after TGF-β1 treatment. QRT-PCR was performed on RNA isolated from cultured HKC8 cells subjected to 10ng/ml TGF-β1 for 24 h. A significant fold increase in α–SMA expression (p≤0.01) with no change in TIMP1 expression was seen. TGF-β1 expression was upregulated in stimulated HKC8 cells but this change was not statistically significant (Figure 4.2).

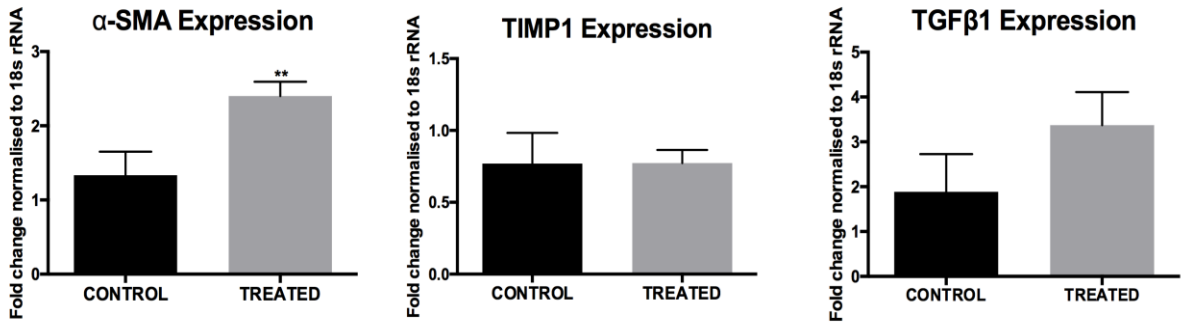

Figure 4.2: Gene expression in HKC8 cell line after 24h of TGF-β1 treatment. The graphs show analysis of α–SMA, TIMP1 and TGF-β1 expression at 24h post 10ng/ml TGF-β1 treatment normalised to 18srRNA expression and compared to untreated control (N=3). A significant fold increase in α–SMA expression *(**=p≤0.01)* was seen. Unpaired T test was used to analyse the data and graphs were plotted using prism 6 software.

Due to lack of availability of a suitable human renal fibroblast cell line, a cell line derived from human lung fibroblasts were used (MRC-5). MRC5 cells were stimulated with 10ng/ml TGF-β1 was studied using conventional and qRT-PCR. Data obtained from gel electrophoresis (Figure 4.3 A) suggests an increased expression of α–SMA and Fibronectin after 24 h TGF-β1 treatment and qRT-PCR data suggests a significant fold increase in α–SMA, Fibronectin, COL1A1 and TGF-β1 ($p \leq 0.01$)(Figure 4.3 B).

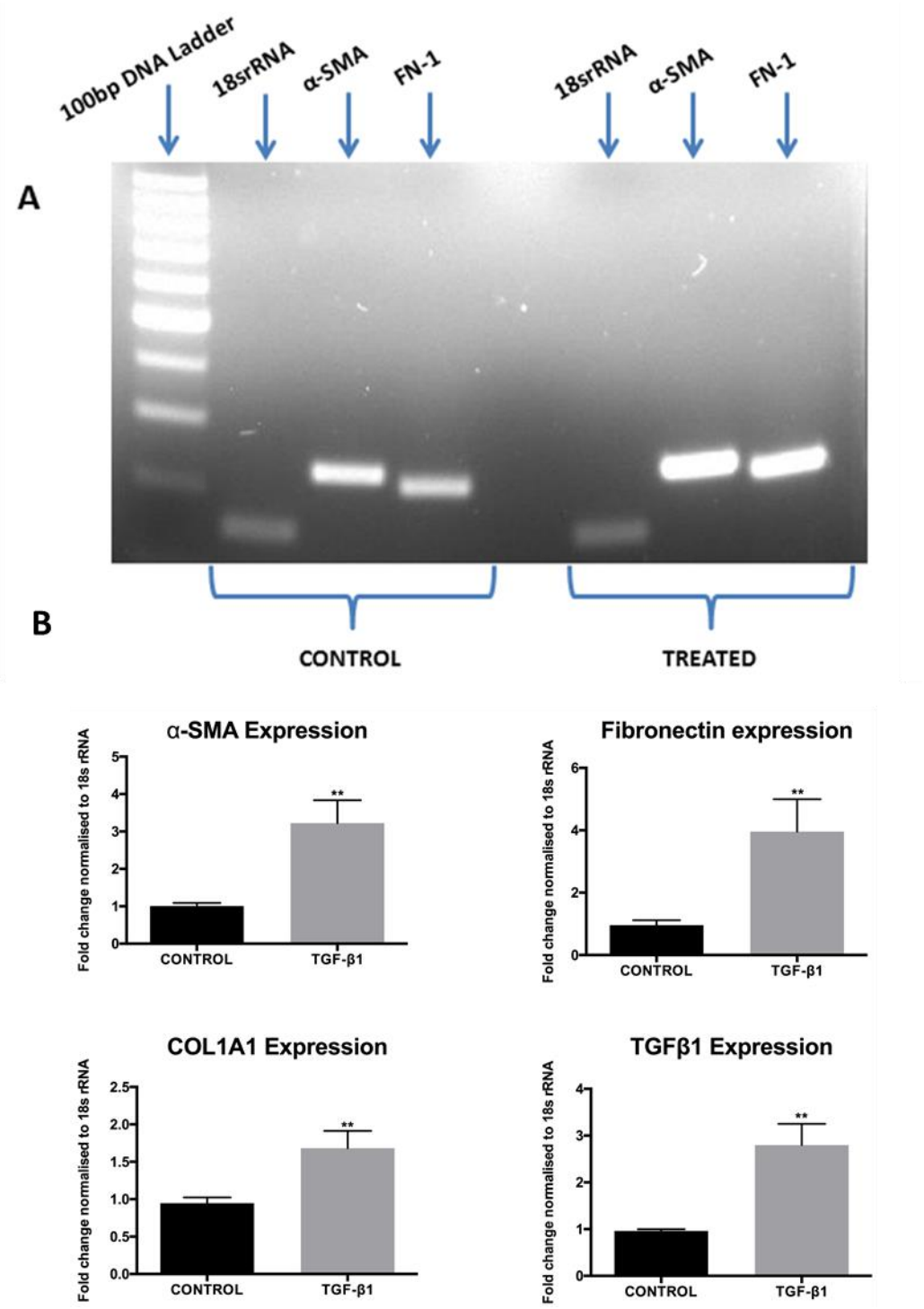

Figure 4.3: Gene expression in MRC-5 cells following TGF-β1 treatment.
The expression of fibrotic markers α–SMA and fibronectin was initially examined by conventional PCR and 18S rRNA was used as a housekeeping gene (A). The graphs (B) show analysis of α–SMA, fibronectin, COL1A1 and TGF-β1 expression at 24h following 10ng/ml TGF-β1 treatment using q-RT-PCR. The expression was normalised to 18srRNA expression levels and compared to the untreated control (N=3). Unpaired T test was used to analyse the data and graphs were plotted using prism 6 software. *(**=p≤0.01)*

4.2.2 Expression of pro-fibrotic proteins following TGF-β treatment

TGF-β1 treatment induced morphological alterations in epithelial cell phenotype along with changes in expression of fibrotic markers at mRNA level. The effect TGF-β1 treatment on protein expression was further examined.

HKC8 cells were grown until they acquired 70% confluency. This was followed by overnight incubation in serum free media. Following this, cells were incubated with complete media containing 10ng/ml TGF-β1 for 24 h. Western blot and immunofluorescence was performed to examine the expression of fibrotic marker α–SMA and epithelial marker E-cadherin. Treatment with TGF-β1 increased α–SMA ($p \leq 0.0001$) expression and reduced E-cadherin ($p \leq 0.0001$) expression in PTECs at protein level (Figure 4.4, 4.5).

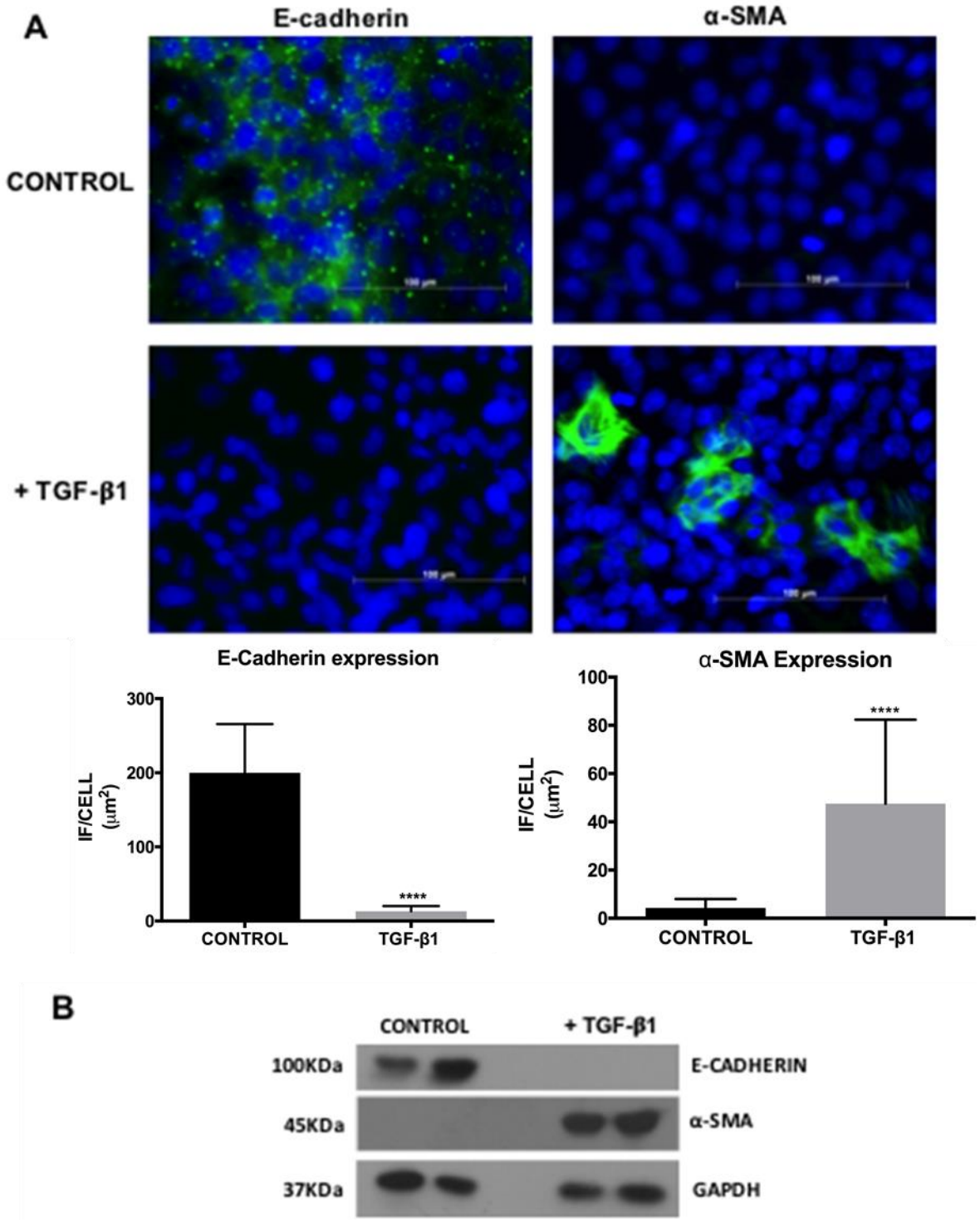

Figure 4.4: Protein expression in HKC8 cells following TGF-β1 treatment. HKC8 cells were treated 10ng/ml TGF-β1 for 24 h. Immunofluorescence data (A, N=3) showed a significant increase in α-SMA expression (****=$p \leq 0.0001$) and significant decrease in E-Cadherin (****=$p \leq 0.0001$) in treated cells when compared to control. Similarly, Western blots (B, N=2) showed a decrease in E-Cadherin and increase in α-SMA expression. Immunofluorescence data was presented as IF/cell, unpaired T test was used to analyse the data and graphs were plotted using prism 6 software. Images were taken at 400X magnification using a Leica AF imaging unit.

Protein expression was also examined in MRC-5 cells. Results obtained from Immunofluorescence and western blot data were consistent with gene expression. A significant increase in α–SMA ($p \leq 0.05$) and COL1A1 expression ($p \leq 0.0001$) indicates that MRC-5 cells stimulated with TGF-β1 acquire myofibroblast like characteristics (Figure 4.6).

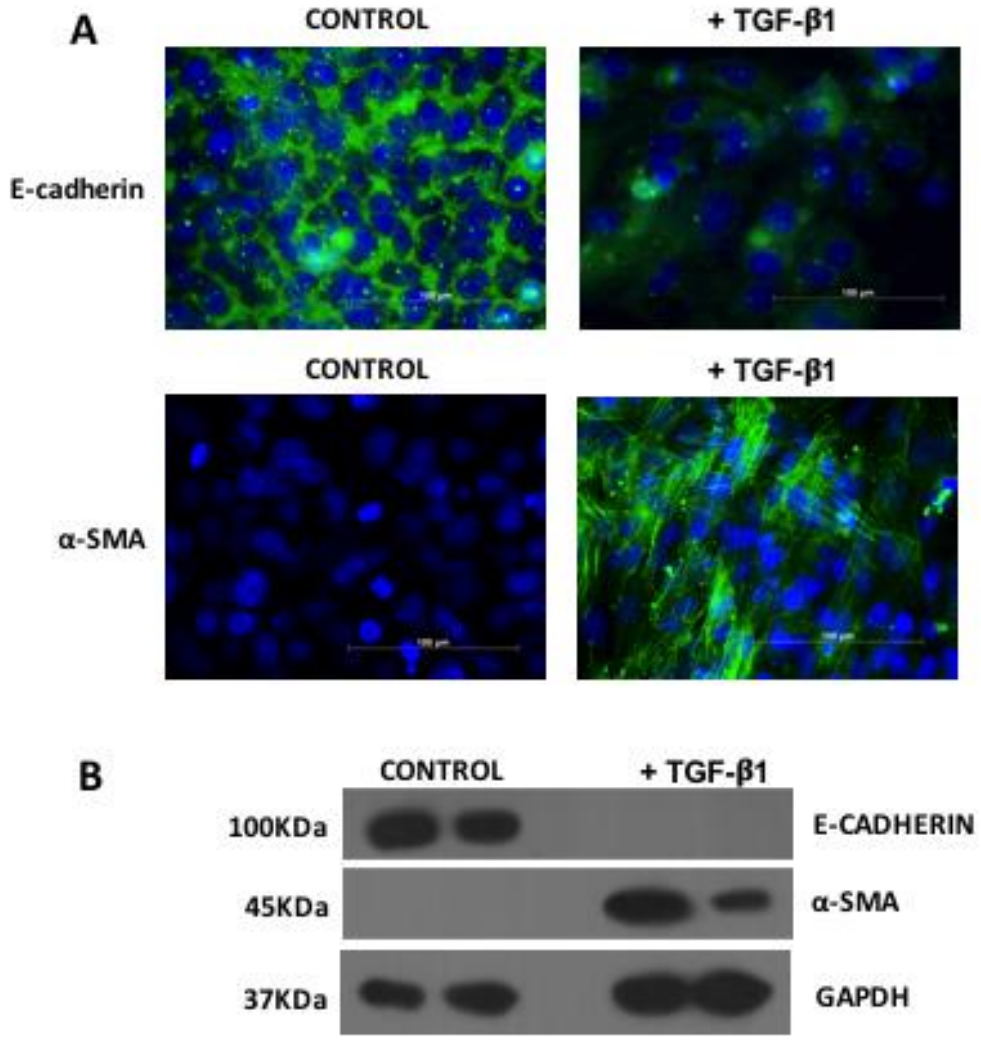

Figure 4.5: Protein expression in HK-2 cells following TGF-β1 treatment. Immunofluorescence data (A) and Western blot (B, N=2) show an increased expression of fibrotic marker along with reduced epithelial marker in HK-2 cells stimulated with TGF-β1 for 24 h compared to corresponding control. Immunofluorescence images were taken at 400X magnification using Leica AF imaging unit.

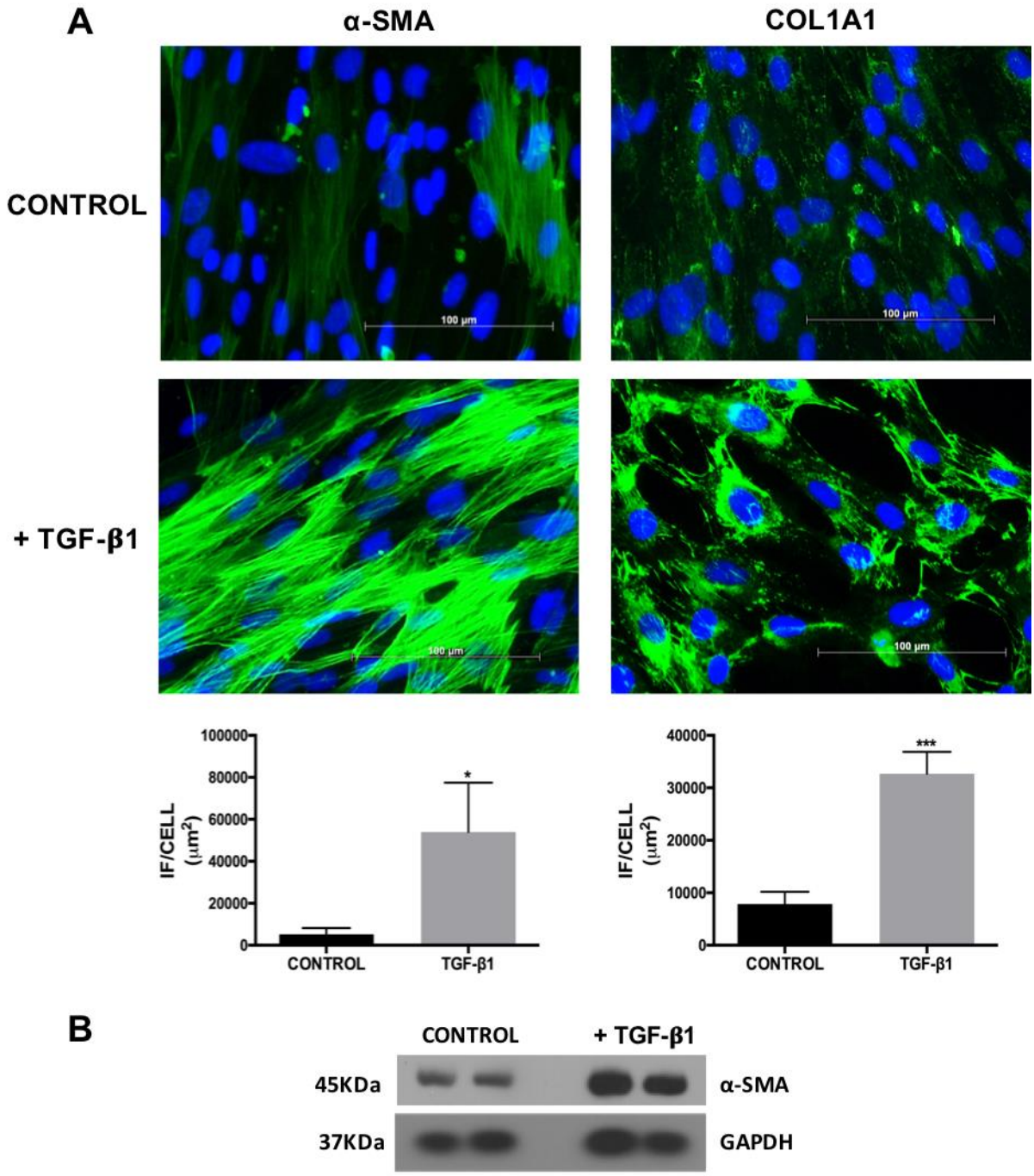

Figure 4.6: Expression of profibrotic markers in MRC-5 cells in response to TGF-β1 treatment.

Following TGF-β1 treatment, Immunofluorescence data (A, N=3) suggest a significant increase in α–SMA (*=$p \leq 0.05$) and COL1A1 expression (***=$p \leq 0.0001$) in stimulated cells while Western blot (B, N=2) data shows an increased expression of in MRC-5 stimulated with TGF-β1 for 24 h compared to corresponding control. Immunofluorescence images were taken at 400X magnification using Leica AF imaging unit and bar graphs were plotted (as IF/cell) and analysed (unpaired t test) using Prism 6.

4.2.3 The role of ALK-5 inhibitor in supressing TGF-β signalling

4.2.3.1 ALK-5 inhibitor blocks TGF-β mediated profibrotic phenotypic change in HKC8 cells

SB-505124 (Sigma) is a potent inhibitor of TGF-β1 receptor and it inhibits ALK-4, 5 and 7 mediated activation of SMAD2 and SMAD3. The concentration of SB-505124 was initially optimized prior to conducting experiments. Results suggested a significant increase in TGF-β stimulated cells pre-treated with 0.75μM, 1μM and 2.5μM ALK-5 inhibitor when luminescence/ μg of protein sample were compared to untreated control. However, 10μM ALK-5 inhibitor treatment followed by TGF-β stimulation showed a inhibition in luminescence similar to that seen in untreated cells suggesting efficient reduction in TGF-β activity (Section 2.5.4.1, Figure 2.6). Next, the duration of TGF-β1 stimulation post ALK-5 inhibitor treatment was optimized (Figure 2.7). Pre-treatment with ALK-5 inhibitor could maintain low TGF-β activity for only upto 24h. Therefore, further experiments involved stimulating cells with TGF-β1 for only upto 24 h. WST-1 assay demonstrated that ALK5 inhibitor had no effect on the cell proliferation upto 48 h of treatment (Figure 2.8).

HKC8 cells were treated with 10μM SB-505124 for 1 h followed by 24 h TGF- β1 treatment. Protein studies suggest that TGF-β1 induction of α-SMA and suppression of E-cadherin expression was successfully attenuated by SB-505124 pre-treatment (S+TGF-β/ALK5; $p \leq 0.001$; Figure 4.7).

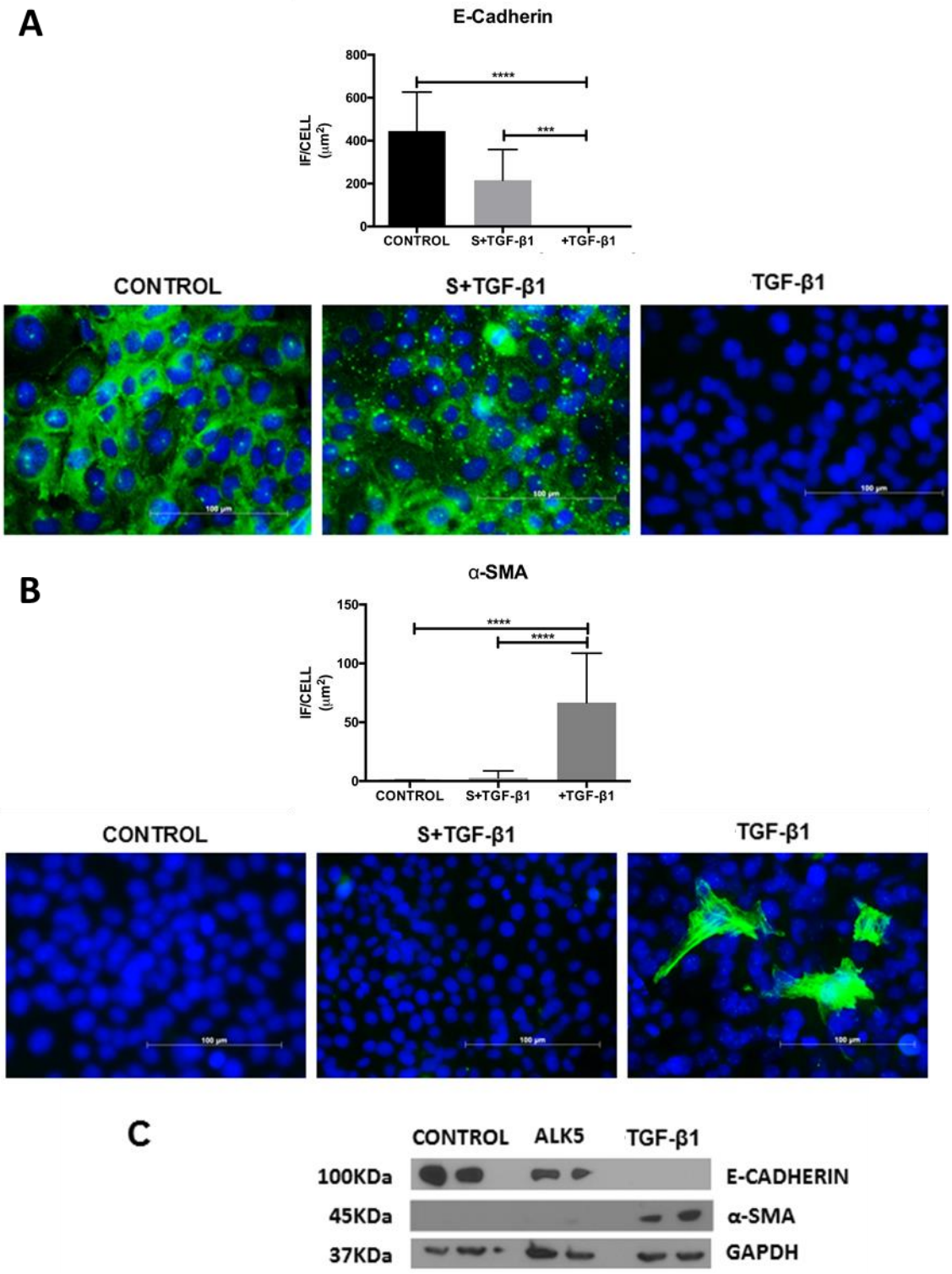

Figure 4.7: Protein expression in TGF-β1 and ALK-5 inhibitor treated HKC8 cells. HKC8 cells were treated with and without 10μM SB-505124 (S) for 1 h followed by treatment with 10ng/ml TGF-β1 for 24 h. Immunofluorescence (A, N=3) and Western blot (B, N=2) was performed. One-way ANOVA with Bonferroni method was used to analyse the data and graphs were plotted using prism 6 software. Images were taken at 400X magnification for α-SMA and E-cadherin using Leica AF imaging unit and are represented as bar graphs of fold change in fluorescence per cell. (****=$p \leq 0.0001$)

4.2.3.2 The effect of ALK5 inhibition on ischaemia and reperfusion induced changes

It was shown in the previous chapter that PTEC's adopt a profibrotic phenotype in conditions that mimic IRI. To ascertain whether the observed changes were driven by TGF-β, HKC8 cells were pre-treated by incubation with 10μM of SB-505124 for 1 h before treatment with 400μM H_2O_2 for 4 h and incubation for 20 h. SB-505124 and H_2O_2 treated cells (S+H_2O_2) retained E-Cadherin expression (Figure 4.8 A) and prevented an increase in α-SMA expression when expression was compared to H_2O_2 treated cells only ($p \leq 0.0001$) (Figure 4.8 B).

A similar experiment was performed using 200μM $CoCl_2$ treatment for 24 h. Although pharmacological inhibition of TGF-β/SMAD signaling preserved epithelial phenotype by maintaining E-cadherin expression (Figure 4.9 A) and prevented α-SMA expression (Figure 4.9 B), a significant increase in HIF-1α expression was observed in SB-505124 and $CoCl_2$ stimulated cells (S+$CoCl_2$) ($p \leq 0.0001$) as compared to the control (Figure 4.9 C). This confirms that TGF-β induces the expression of a profibrotic phenotype in epithelial cells that may contribute to progression of renal fibrosis.

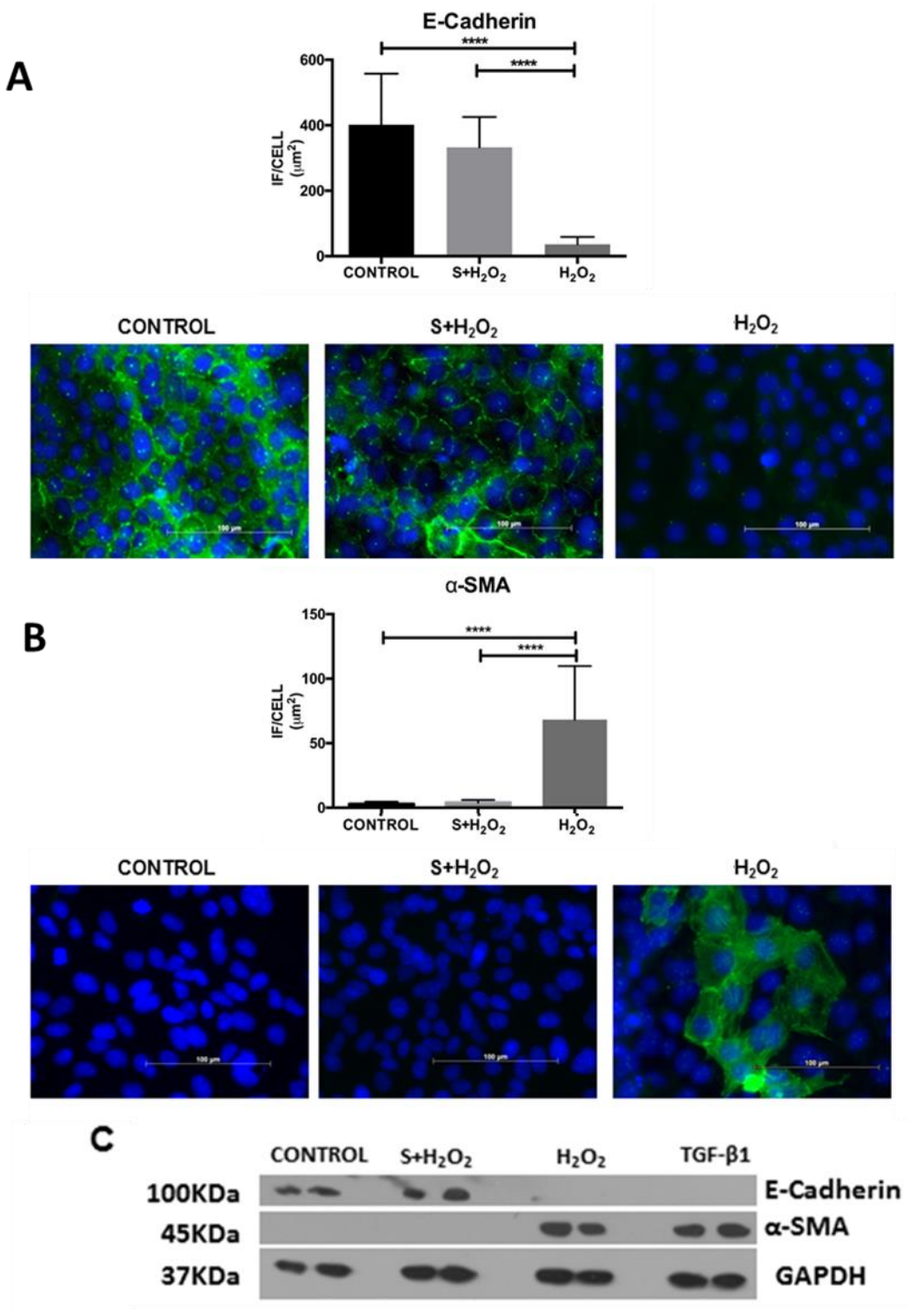

Figure 4.8: Protein expression in H_2O_2 and ALK-5 inhibitor treated HKC8 cells. HKC8 cells were treated with and without 10μM SB-505124 (S) for 1 h followed by treatment with 400μM H_2O_2 (4 h + 20 h). Protein expression of E-cadherin and α-SMA was analysed using Immunofluorescence (A and B, N=3) and Western blots (C, N=2). ALK5 inhibitor prevented the increase in α-SMA expression and maintained expression of E-Cadherin in H_2O_2 treated cells and expression was compared untreated cells. One-way ANOVA with Bonferroni method was used to analyse the data and graphs were plotted using prism 6 software. Immunofluorescence images were taken at 400X magnification using Leica AF imaging unit. (****=$p \leq 0.0001$)

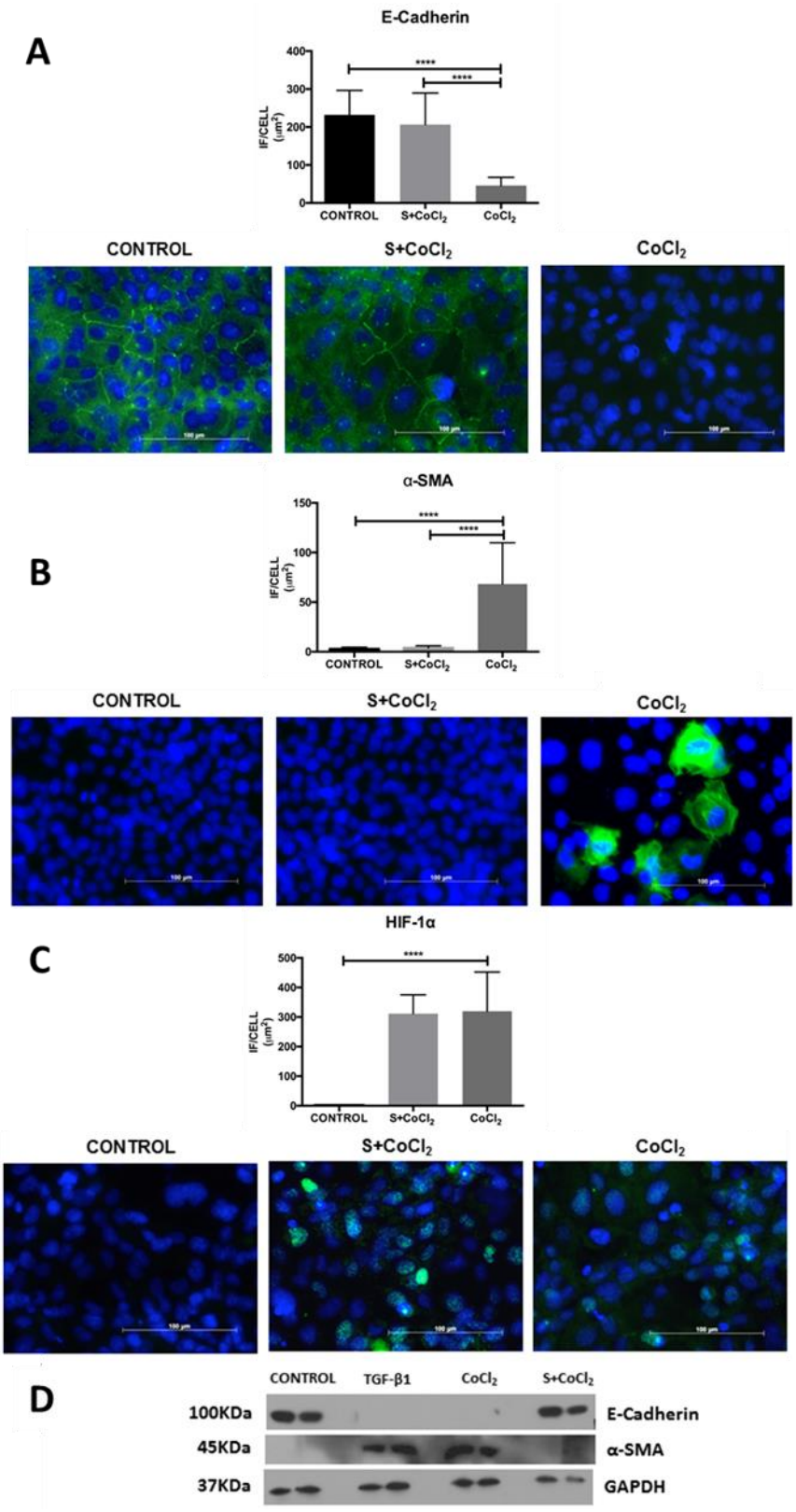

Figure 4.9: Protein expression in $CoCl_2$ and ALK-5 inhibitor treated HKC8 cells. HKC8 cells were treated with and without 10μM SB-505124 (S) for 1 h followed by 24h treatment with 200μM $CoCl_2$. Immunofluorescence (N=3, A, B and C) and Western Blot (N=2, D) were performed. One-way ANOVA with Bonferroni method was used to analyse the data and graphs were plotted using prism 6 software. Images were taken at 400X magnification using Leica AF imaging unit. (****=$p \leq 0.0001$)

4.2.3.3 ALK-5 inhibitor reduces fibrotic marker expression in a co-culture study

Several attempts were made to establish a co-culture system with epithelial cells growing on the upper surface of the collagen matrix with the fibroblast suspended within the matrix. Since MRC-5 cells failed to proliferate in the matrix, an alternative approach was designed.

4.2.3.3.1 Media transfer studies

An *in-vitro* co-culture model comprising of HKC8 and MRC-5 cells was established to investigate the signalling mechanism leading to progression of fibrosis in *in-vivo*. In this model, HKC8 cells were grown on a 6 well plate. Once confluent, the cells were stimulated with 400μM H_2O_2 for 4h followed by incubation in complete media for 20h. Post incubation, the supernatants were collected and transferred to naïve MRC-5 cells (Figure 4.10). Cells were also culture with 200μM $CoCl_2$ for 24 h the media was then replaced by fresh complete media and incubated for 24 h. Media was again collected and transferred to wells containing MRC-5 cells.

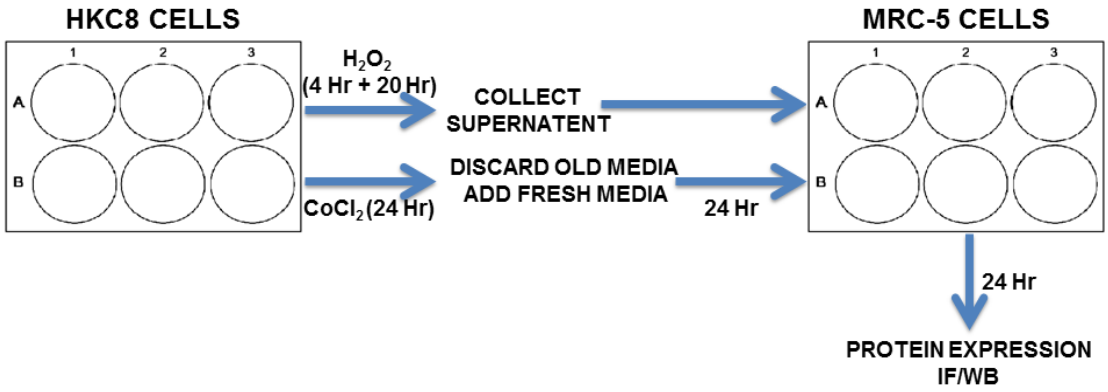

Figure 4.10: Schematic diagram of media transfer study involving MRC-5 cells

Protein data illustrates a significant increase in α-SMA expression in MRC-5 cells incubated with pre-conditioned media obtained from with H_2O_2 (+H_2O_2) ($p \leq 0.001$) or $CoCl_2$ (+$CoCl_2$) ($p \leq 0.01$) stimulated cells compared to MRC-5 cells incubated with control media (Figure 4.11).

Also, RT-PCR data suggests a significant fold increase in α-SMA ($p \leq 0.05$) and Fibronectin ($p \leq 0.01$) expression in MRC-5 cells with preconditioned treated cell media compared to control (Figure 4.12).

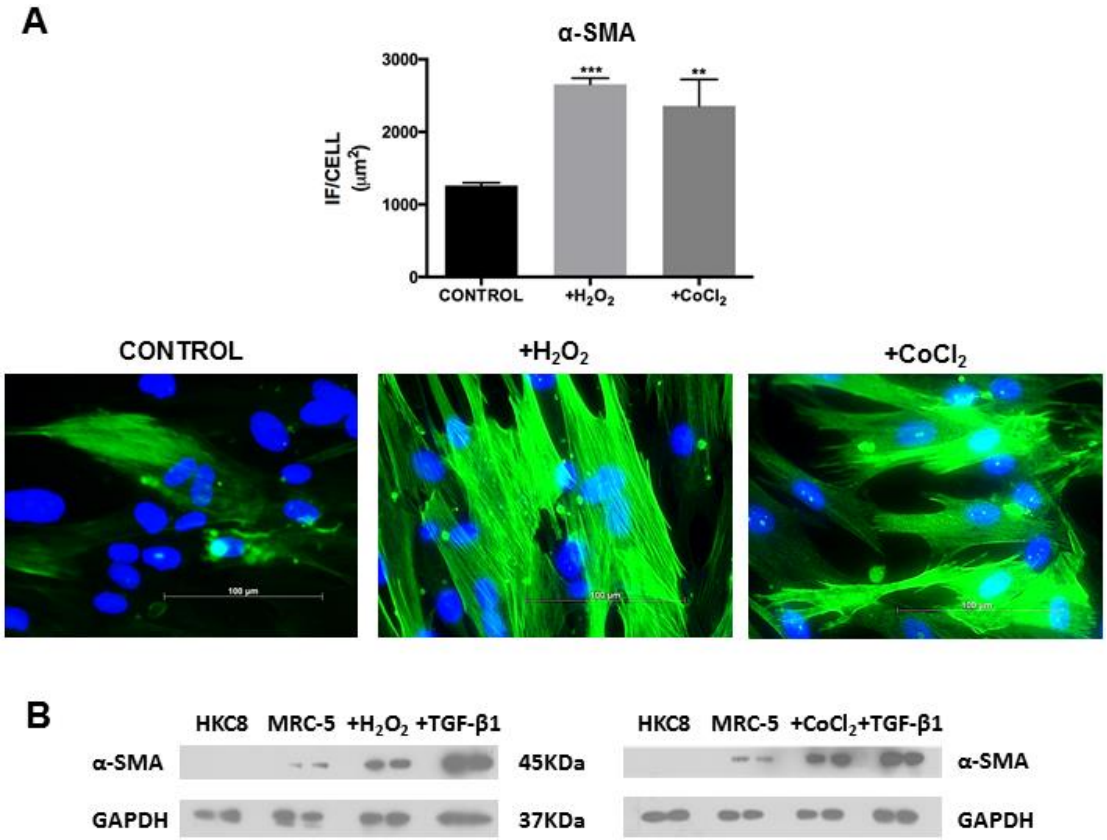

Figure 4.11: Protein expression in MRC-5 cells following media transfer. Preconditioned media collected from HKC8 cells treated with H_2O_2 (4h treatment + 20 h incubation) or $CoCl_2$ (24h) were transferred onto naïve MRC-5 cells for 24h. Immunofluorescence (A, N=3) and Western blot (B, N=2) show that α–SMA expression was significantly upregulated in MRC-5 cells incubated with preconditioned media obtained from H_2O_2 or $CoCl_2$ stimulated cells compared to unstimulated control (***=p≤0.001)(**=p≤0.01)(A and B). One-way ANOVA with Bonferroni method was used to analyse the data and graphs were plotted using prism 6 software. Images were taken at 400X magnification using Leica AF imaging unit.

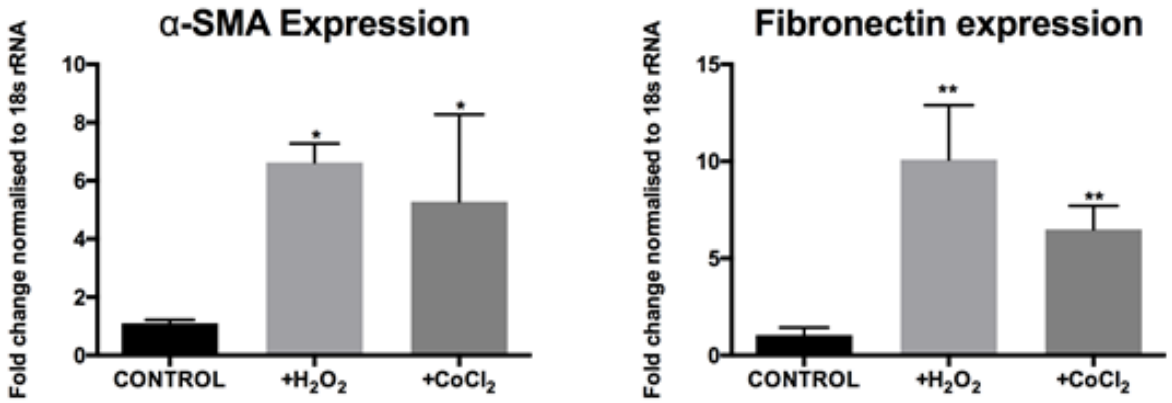

Figure 4.12: Gene expression in MRC-5 cells following media transfer. Following 24 h incubation with preconditioned media collected from HKC8 cells stimulated with H_2O_2 or $CoCl_2$, RNA was isolated to study gene expression. A significant increase in α–SMA (*=$p \leq 0.05$) and Fibronectin (**=$p \leq 0.01$) expression was seen in MRC-5 cells post 24 h incubation when expression was compared to the control cells. Expression was normalised to 18srRNA and expression levels compared to untreated control (N=3). One-way ANOVA with Bonferroni method was used to analyse the data and graphs were plotted using prism 6 software.

To identify the molecule responsible for driving the changes in MRC5 cells, cells were pre-treated with 10μM SB-505124 for 1 h before 24 h incubation with pre-conditioned media. When compared to MRC-5 cells incubated with preconditioned media from HKC8 cells stimulated with H_2O_2 or $CoCl_2$ only, α–SMA expression was significantly reduced (*=p≤0.05, **=p≤0.01) in MRC-5 cells pre-treated with 10μM SB-505124 when expression was compared to MRC5 cells treated with H_2O_2 or $CoCl_2$ preconditioned media (Figure 4.13). At mRNA level, MRC-5 cells treated with SB-505124 and H_2O_2 or $CoCl_2$ (S+H_2O_2 and S+$CoCl_2$) demonstrated similar expression of α–SMA and fibronectin when compared to control cells which was significantly lower than that seen in cells stimulated with preconditioned media without ALK-5 pre-treatment (+H_2O_2 and +$CoCl_2$) (Figure 4.14).

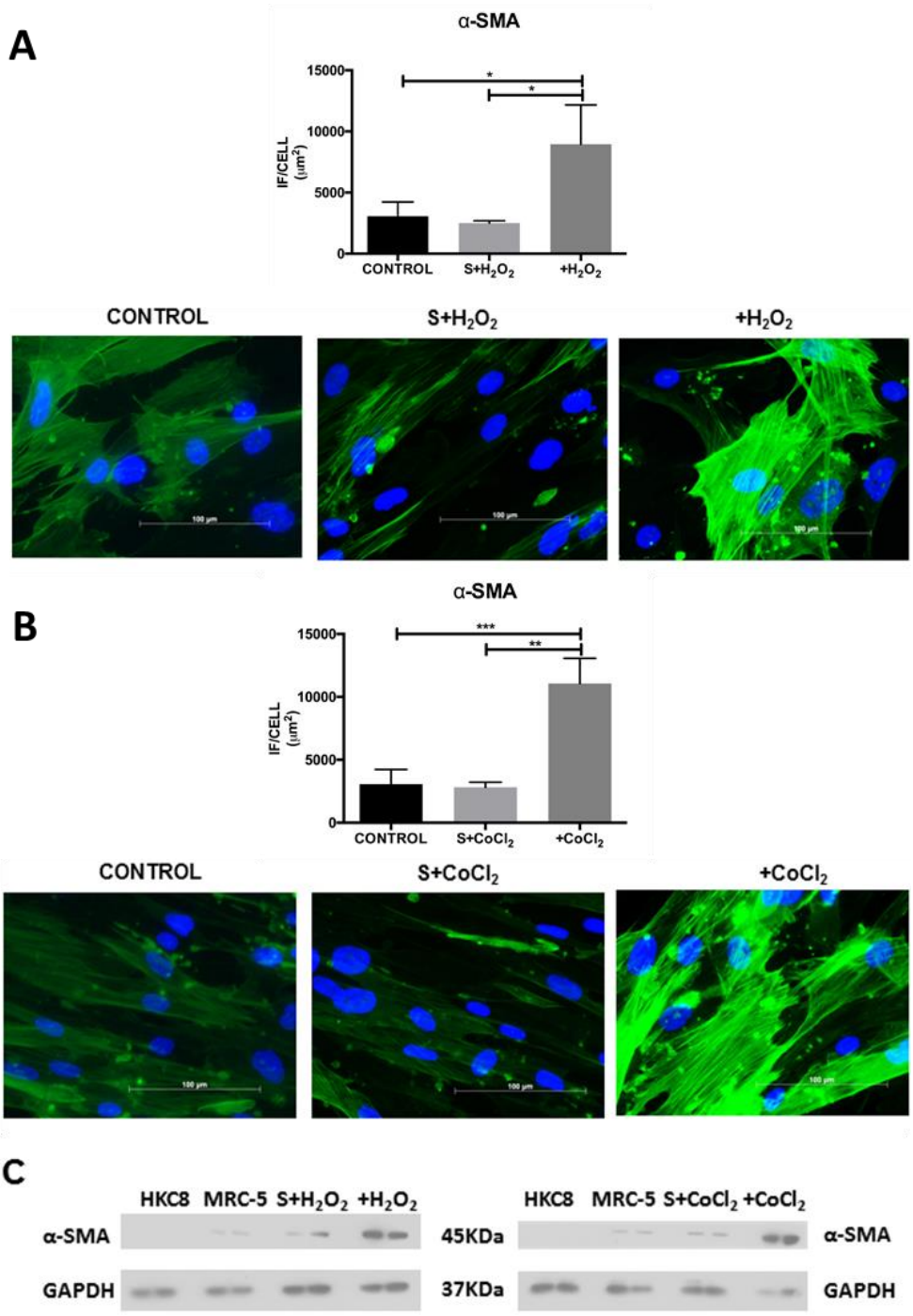

Figure 4.13: MRC-5 cells pre-treated with ALK-5 showed reduced α-SMA expression following media transfer. MRC-5 cells were treated with and without SB-505124 (S) for 1 h followed by incubation with preconditioned media for 24 h. The expression of α–SMA was examined using immunofluorescence (A, N=3) and Western blot (B, N=2) studies were performed. Treatment with SB-505124 maintained the expression of α–SMA when MRC-5 cells were incubated with preconditioned media and expression was compared to cells incubated with preconditioned media only. One-way ANOVA with Bonferroni method was used to analyse the data and graphs were plotted using prism 6 software. Images were taken at 400X magnification for α-SMA using Leica AF imaging unit and are represented as bar graphs of fold change in fluorescence per cell. (*=$p \leq 0.05$, **=$p \leq 0.01$, ***=$p \leq 0.001$)

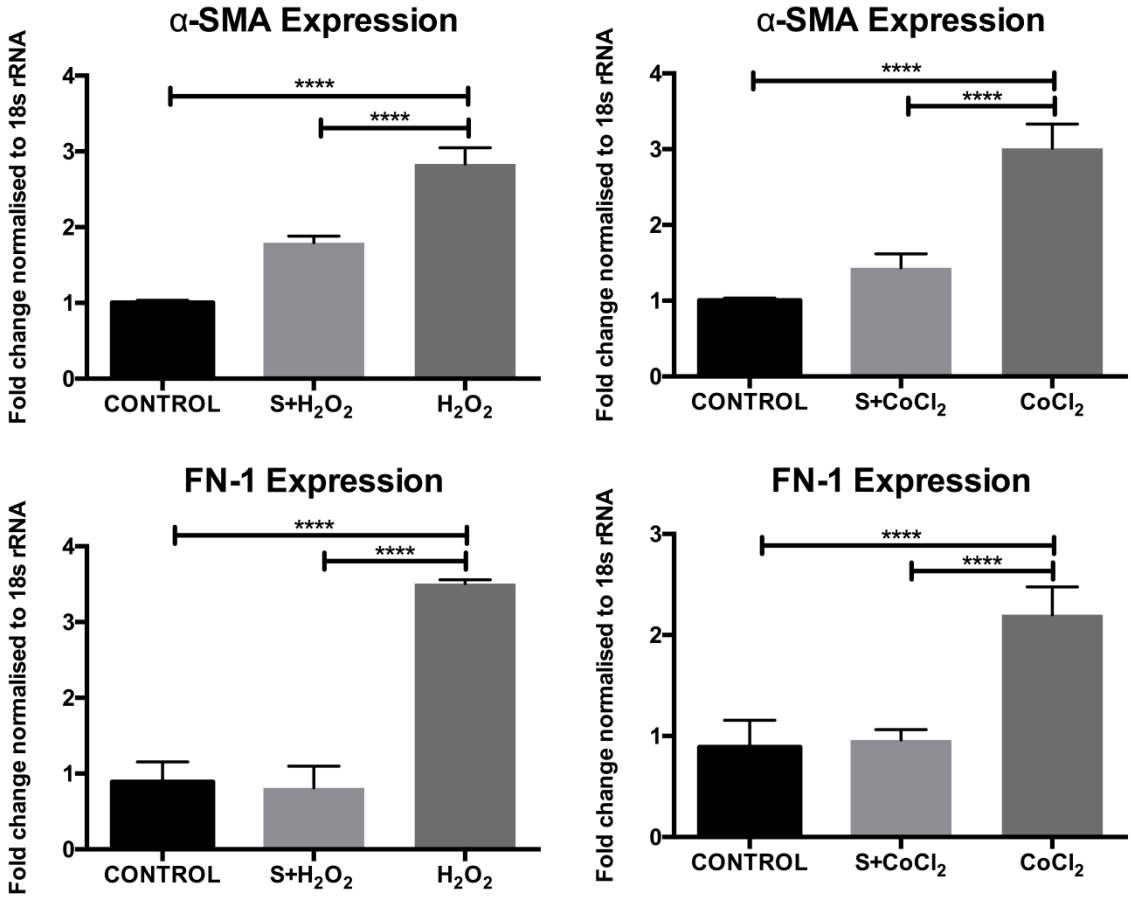

Figure 4.14: ALK5 inhibitor maintained low expression of fibrotic markers in H_2O_2 or $CoCl_2$ treated MRC5 cells
Analysis of α–SMA and fibronectin expression in MRC-5 cells treated with and without SB-505124 followed by incubation with preconditioned media from HKC8 cells stimulated with H_2O_2 or $CoCl_2$. Expression was normalised to 18srRNA (N=3). Cells treated with SB-505124 and preconditioned media showed a significant reduction in α–SMA and fibronectin expression when expression was compared to MRC5 cells incubated with preconditioned media only (H_2O_2 or $CoCl_2$). One-way ANOVA with Bonferroni method was used to analyse the data and graphs were plotted using prism 6 software. (****=$p \leq 0.0001$)

4.2.3.3.1 Transwell inserts

I propose that even after the ischaemia and reperfusion insult, cells continue to produce growth factors that may drive the progression of injury leading to fibrosis. To confirm whether stressed epithelial cells continue to produce active TGF-β even after a brief ischaemic or reperfusion insult, HKC8 cells were grown on transwell inserts. Once the cells were confluent, they were stimulated with 400μM H_2O_2 or 200μM $CoCl_2$. Post stimulation, the inserts were transferred onto the 6 well plates containing

naïve MRC-5 cells. The MRC-5 cells were pre-treated with and without SB-505124 prior to insert transfer. Following 24 h incubation, the expression of fibrotic markers in MRC-5 cells was assessed. This model allowed us to confirm whether the epithelial cells continue to produce active TGF-β that will signal to MRC-5 cells. Protein studies suggest that treated HKC8 cells induce profibrotic changes in MRC-5 cells which were successfully inhibited upon SB-505124 pre-treatment (Figure 4.15).

A similar trend in fibrotic marker expression was observed at the RNA level. There was no change in α-SMA and fibronectin expression in cells treated with SB-505124 and co-incubated with stimulated HKC8 cells (S+H_2O_2 or S+$CoCl_2$) and MRC-5 cells incubated with untreated HKC8 cells. This showed that SB-505124 treated cells did not differ from control cells even in the presence of external stimuli thus confirming the role of active TGF-β production in the phenotypic changes observed (Figure 4.16).

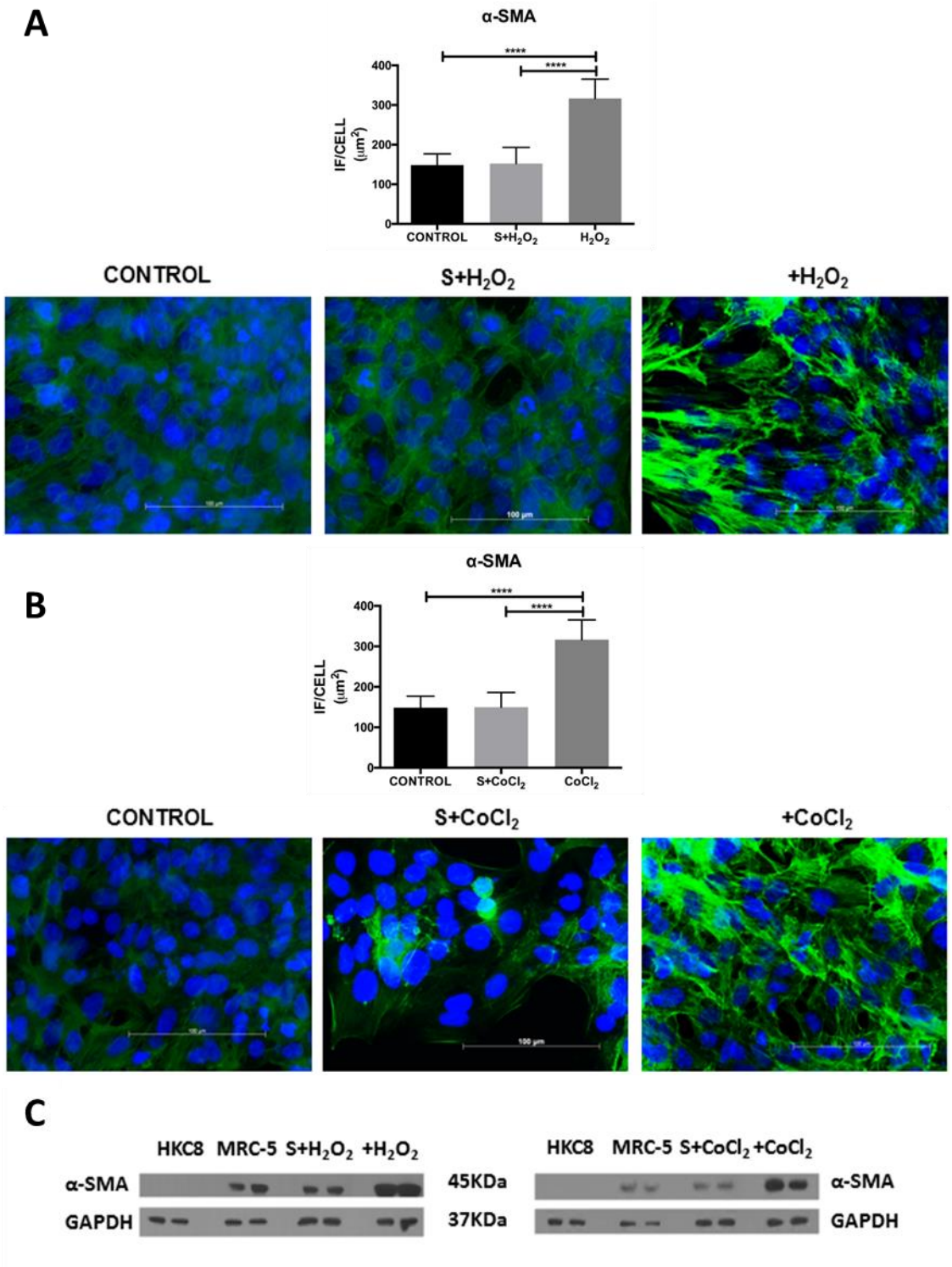

Figure 4.15: ALK-5 treated MRC-5 cells co-incubated with HKC8 cells. Immunofluorescence (A and B, N=3) and Western blot (C, N=2) demonstrate similar α–SMA expression in control and SB-505124 (S) treated MRC-5 cells compared to untreated cells incubated with a transwell containing stimulated HKC8 cells. One-way ANOVA with Bonferroni method was used to analyse the data and graphs were plotted using prism 6 software. Images were taken at 400X magnification for α-SMA using Leica AF imaging unit. (****=p≤0.0001)

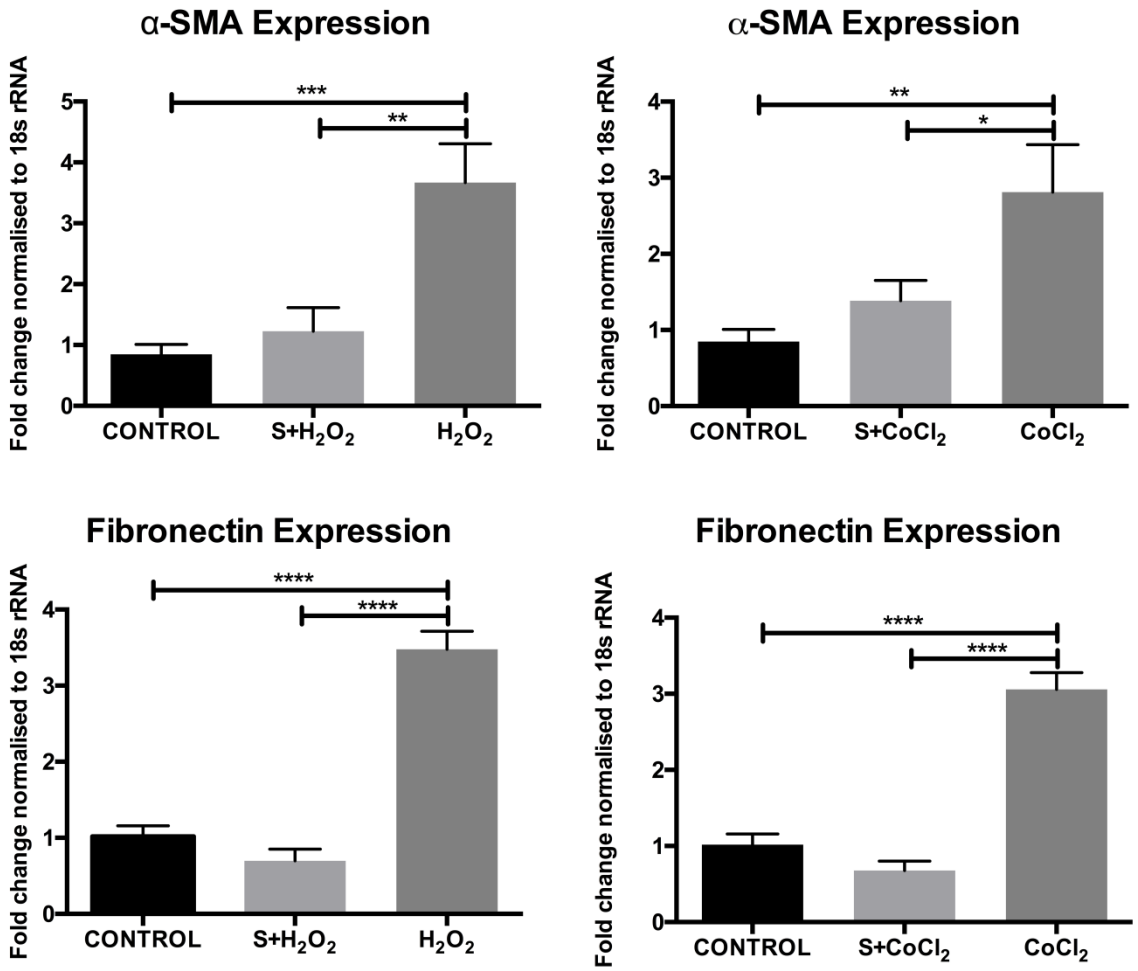

Figure 4.16: Gene expression in MRC-5 cells following mesh transfer. An analysis of α–SMA and Fibronectin expression in MRC-5 cells treated with and without SB-505124 followed by 24 h incubation with mesh containing HKC8 cells stimulated with 400μM H_2O_2 (4h+20h) or 200μM $CoCl_2$ (24h). Expression was normalised to 18srRNA (N=3). MRC-5 cells treated with ALK-5 inhibitor maintained similar expression of fibrotic markers at mRNA level. One-way ANOVA with Bonferroni method was used to analyse the data and graphs were plotted using prism 6 software. (****=$p \leq 0.0001$) (***=$p \leq 0.001$)(**= $p \leq 0.01$)

4.2.4 SMAD-Luciferase reporter gene studies

To confirm active TGF-β production by HKC8 cells, a luciferase reporter gene assay was used. Stable transfected SMAD-Luciferase HKC8 cells were used in this study that show an increased luciferase production in response to active TGF-β. To identify if ischaemia and reperfusion injury induces SMAD signalling, SMAD-Luciferase cells were grown in a 6 well plate in hygromycin containing media until they are 70% confluent. Prior to treatment, cells were incubated overnight in

hygromycin free media. The cells were then stimulated with 400μM H_2O_2 (4h treatment + 20h incubation). After 24 h incubation, the cells were lysed and luciferase activity was measured. BCA protein assay was performed to calculate luciferase activity/μg protein sample. A significant increase in SMAD-luciferase activity was seen in cells treated with H_2O_2 ($p \leq 0.01$) compared to unstimulated control (Figure 4.17).

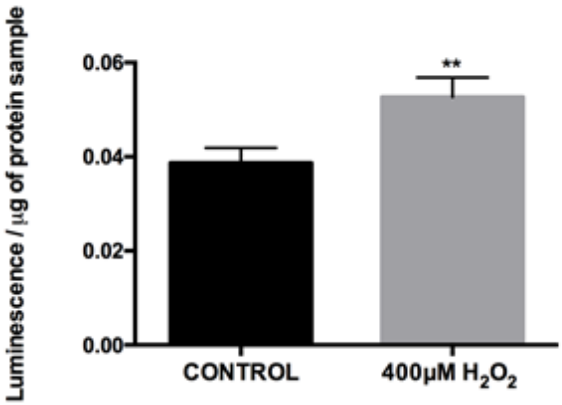

Figure 4.17: SMAD-Luciferase activity following H_2O_2 treatment. SMAD-Luciferase transfected HKC8 cells treated with 400μM H_2O_2 (4h+20h) show a significant (**=$p \leq 0.01$) increase in luciferase activity (controlled by a SMAD promoter) compared to control cells (N=4). Unpaired T-test was used to analyse the data and graphs were plotted using prism 6 software. (**=$p \leq 0.01$)

To further quantify if HKC8 cells produce active TGF-β, media transfer studies were performed where supernatants were collected from 200μM $CoCl_2$ stimulated HKC8 cells or HKC8 cells transiently transfected with HIF1-α plasmid. These supernatants were transferred to naïve SMAD-Luciferase cells. Following 24 h incubation with preconditioned media, there was increased luciferase activity consistent with increased TGF-β production in cells stimulated with $CoCl_2$ or transfected with HIF1-α when compared to their respective controls (Figure 4.18).

HKC8 cells were subjected to 400μM H_2O_2 (4h treatment + 20h incubation) or 200μM $CoCl_2$ (24h) stimulation. Supernatants were transferred onto naïve SMAD-luciferase cells treated with and without 10μM SB-505124 inhibitor for 1 h. The increase in

luciferase activity on transfer of pre-conditioned media was blocked in cells pre-treated with SB-505124 (Figure 4.19).

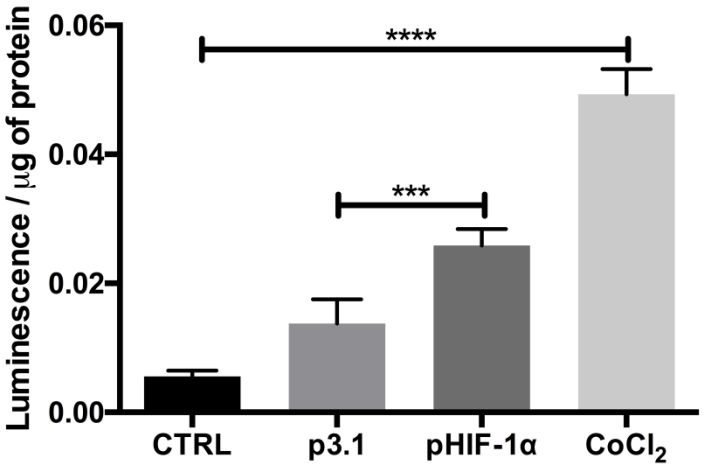

Figure 4.18: SMAD-Luciferase activity post $CoCl_2$ treatment. Supernatants collected from 24 h $CoCl_2$ stimulated or HIF-1α transfected cells were transferred onto naïve SMAD-Luciferase cells for 24 h. Results showed a significant (***=$p \leq 0.001$) (****$p \leq 0.0001$) increased TGF-β production in $CoCl_2$ stimulated and HIF1-α transfected cells compared to untreated cells and transfection control (p3.1) respectively (N=4). Unpaired T-test was used to analyse the data and graphs were plotted using prism 6 software. (****$p \leq 0.0001$)(***=$p \leq 0.001$)

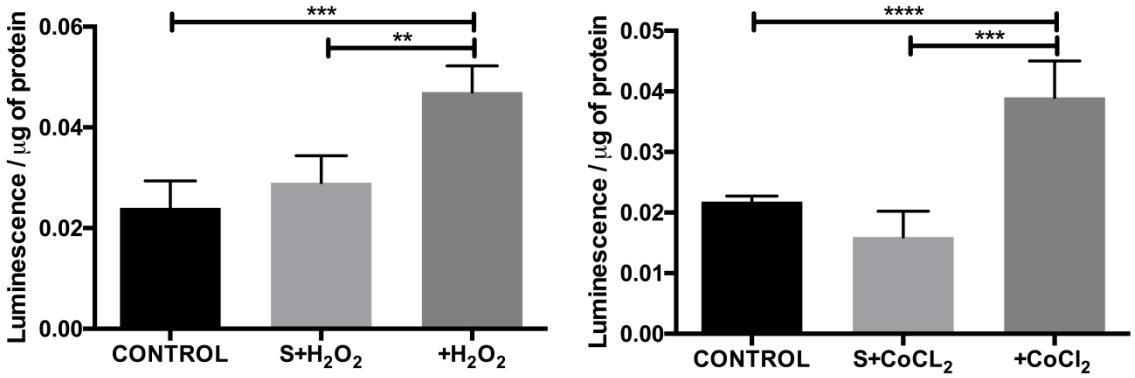

Figure 4.19: Effect of ALK5 inhibitor on SMAD-luciferase activity following media transfer. Supernatants collected from HKC8 stimulated with 400µM H_2O_2 (4h treatment + 20h incubation) or 200µM $CoCl_2$ (24h) were transferred into wells containing naïve SMAD-Luciferase treated with and without SB-505124. A significant increase in luciferase activity (controlled by a SMAD promoter) was observed. H_2O_2 and $CoCl_2$ stimulated cell media compared to cells treated with SB-505124 (N=4). One-way ANOVA with Bonferroni method was used to analyse the data and graphs were plotted using prism 6 software. (**=$p \leq 0.01$, ***=$p \leq 0.001$, ****=$p \leq 0.0001$)

Cell transfer studies were performed to quantify active TGF-β production. Post stimulation with 400μM H_2O_2 (4h treatment + 20h incubation) or 200μM $CoCl_2$ (24h), the inserts housing HKC8 cells were transferred onto naïve SMAD-Luciferase cells. Increased luciferase activity was seen in cells incubated with stimulated HKC8 cells ($p \leq 0.001$) compared to cells with control (Figure 4.20).

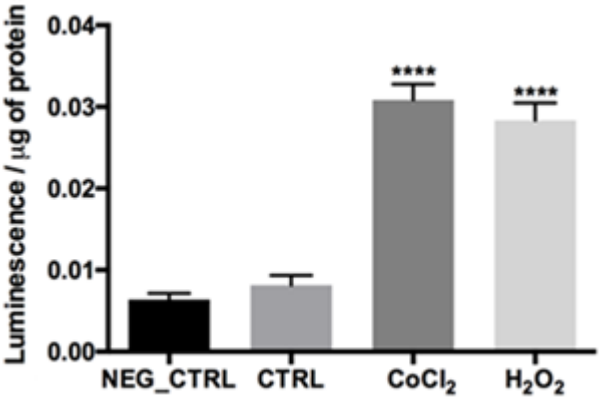

Figure 4.20: SMAD-luciferase activity following cell transfer. Inserts containing HKC8 cells stimulated with H_2O_2 and $CoCl_2$ were transferred onto naïve SMAD-Luciferase cells for 24h. There was a significant (****=$p \leq 0.0001$) increase in luciferase activity post treatment with H_2O_2 or $CoCl_2$ compared to control (N=3). One-way ANOVA with Bonferroni method was used to analyse the data and graphs were plotted using prism 6 software. (****=$p \leq 0.0001$)

4.3 Discussion

TGF-β exerts a wide range of biological activities including its role in progression of renal fibrosis. Numerous studies have recognised proximal tubular epithelial cells as a potential source of TGF-β that may affect the renal morphology (Morrisey *et al.*, 2001). My data confirms that stimulation of proximal tubular epithelial cells with recombinant TGF-β1 led to acquisition of fibrotic spindle-shaped morphology along with a decrease in E-Cadherin expression and loss of cell-cell contact. Previous work by Tian *et al* demonstrated that stimulating HK-2 cells with 10ng/ml of recombinant TGF-β1 induced reorganisation of the actin cytoskeleton and the formation of dense focal adhesion plaques (Tian *et al.*, 2003). Another study by Deyi luo *et al* showed that 3D colonies of HKC8 cells subjected to 10ng/ml TGF-β1 treatment showed an

increased cell movement due to appearance of finger-like pseudopodia (Luo *et al.*, 2017). Therefore, supporting data confirms that TGF-β1 induces phenotypic changes in fibrotic cells.

There was a significant increase in α-SMA expression (1.6 fold) post TGF-β1 treatment in HKC8 cells (Figure 4.2). This is consistent with a recent study that demonstrated an increased expression of MMP-2, FN-1 and TGF-β2 in TGF-β1 stimulated HKC8 cells (Luo *et al.*, 2017). Protein studies using HKC8 (Figure 4.4) post TGF-β1 treatment exhibited a significant increase in α-SMA expression (5 fold) and reduced E-cadherin expression (9 fold). Similar trend was observed in HK2 cells. My results were in line with previous studies showing that TGF-β1 induces *de novo* transformation of epithelial cells to myofibroblast morphology orchestrated by loss of epithelial cell adhesion characteristics (Yang and Liu, 2001).

The ALK-5 inhibitor was used to confirm the role of TGF-β in the changes that were observed (Byfield *et al.*, 2004). My result demonstrated that, pre-treatment with ALK-5 inhibitor blocked TGF-β mediated phenotypic changes in epithelial cells reducing α-SMA whilst preserving E-cadherin expression.

To investigate the role of TGF-β in ischemia and reperfusion injury, HKC8 cells were treated with the ALK5 inhibitor for 1 h followed by H_2O_2 and $CoCl_2$ treatment. Pre-treatment with ALK5 inhibitor prevented the changes induced by oxidative and hypoxic stress. This result implied a significant role of TGF-β in changes that occur in the renal tubular epithelium during IRI. This is also consistent with findings in pulmonary epithelium which undergo TGF-β- dependent EMT in response to free radical stress (Gorowiec *et al.*, 2012). My study demonstrated that ALK5 inhibition blocked the changes induced by the hypoxic mimetic $CoCl_2$. However, increased HIF-1α expression (30 fold) was seen in HKC8 cells pre-treated with ALK5 inhibition and stimulated with $CoCl_2$ (Figure 4.9C).

To investigate whether TGF-β1 released by H_2O_2 or $CoCl_2$ stimulated HKC8 cells could lead to fibrosis by stimulating fibroblast activity naïve MRC-5 cells were incubated with conditioned medium. Increased expression of α-SMA expression (2.2 fold & 1.8 fold respectively) was observed in MRC-5 cells incubated with preconditioned media (acquired from stimulated HKC8 cells; Figure 4.11). In addition, MRC-5 cells pre-treated with ALK5 inhibitor prior to exposure to conditioned media did not show upregulation of myofibrotic markers.

To mimic the *in vivo* cross talk and understand the role of PTEC derived TGF-β1 production in the progression of fibrosis, an *in vitro* co-culture model consisting of HKC8 and MRC-5 cells was established. HKC8 cells were grown onto 3μM transwell inserts. Following stimulation with H_2O_2 or $CoCl_2$, the inserts were transferred into a chamber with MRC-5 cells that were pre-treated with and without ALK5 inhibitor. As with media transfer studies, ALK5 inhibitor treatment significantly reduced α-SMA expression at gene and protein level in H_2O_2 (1.5 & 4 fold decrease) or $CoCl_2$ (2 & 4.4 fold decrease) treated MRC5 cells when compared to cells treated with H_2O_2 or $CoCl_2$ only (Figure 4.13 & 4.14). A similar approach was adopted by Chiovaro *et al* to examine the role of TGF-β1 in inducing Tenascin W expression in BMSCs. MDA cells cultured in transwell inserts were transferred into BMSCs preincubated with and without ALK5 inhibitor. Increased Tenascin W expression was seen in BMSCs incubated with a transwell insert housing MDA cells. This expression was blocked in BMSCs preincubated with ALK5 inhibitor (Chiovaro *et al.*, 2015). Investigating the effect of radiation on TGF-β/SMAD2 signalling, Xiaoming Yin *et al* performed co-culture studies where keratinocytes cells cultured in transwell were pretreated with ALK5 inhibitor prior to irradiation. Following irradiation, HeCaT cell lines were co-cultured with WS1 fibroblast cells. Protein studies confirm that WS1 cells pretreated

with ALK5 inhibitor prior to irradiation significantly inhibited pSMAD2 expression in WS1 cells (Yin *et al.*, 2015).

To assess active TGF-β production post ischaemia and reperfusion stress, SMAD-luciferase assays were performed. Following H_2O_2 or $CoCl_2$ treatment, cells released active TGF-β post that was coupled with increase in HIF-1α. Studies have shown that increase in HIF-1α further accelerates the production of TGF-β1 (Li *et al.*, 2009; Heikkinen *et al.*, 2010; Chaston *et al.*, 2011; Jiao *et al.*, 2015).

In this study, inducing ischaemia using $CoCl_2$ and reperfusion stress using oxidative free radicals leads to changes in HKC8 cells as observed *in vivo* during IRI. The results also provide conclusive evidence that changes induced in IRI are TGF-β mediated and that release of TGF-β by stressed cells during hypoxia and reperfusion could have detrimental consequences. For instance, its role in modulating fibroblast phenotype and promoting fibrosis has been well defined in myocardial infarction and cardiac remodelling (Frangogiannis, 2017) and hepatic IRI(Xu *et al.*, 2016). Therefore, considering the significance of TGF-β-mediated actions *in vivo*, study of signalling pathways is needed to design strategies for effective blockage of TGF-β to protect against damage caused due to fibrosis.

Chapter 5: Blocking αvβ6 integrin protects epithelial cell phenotype post ischemia and reperfusion injury

5.1 Introduction

The first two results chapters of this thesis have already illustrated the role of active TGF-β in an *in vitro* model of IRI. It has previously been demonstrated that pharmacological blocking of TGF-β signaling pathway by treatment with an ALK5 inhibitor significantly reduced pro-fibrotic marker expression in the presence of H_2O_2 or $CoCl_2$ (Section 4.4).

αvβ6 integrin–dependent activation of latent TGF-β in pulmonary epithelial cells was proposed to be an underlying mechanism for experimental lung fibrosis (Kanwar, 2012). Wang et al also demonstrated that the β6 integrin–null phenotype conferred protection from TGF-β–mediated hepatic fibrosis (Wang *et al.*, 2007). Therefore, by eliminating the effects of αvβ6 integrin the profibrotic effects of TGF-β1 could be reduced.

TGF-β1–mediated fibrosis has been proposed in a variety of human chronic kidney diseases that also exhibit increased αvβ6 integrin expression. This increase of αvβ6 integrin could be due to TGF-β signalling (Hahm *et al.*, 2007). This would mean that increased αvβ6 integrin expression and active TGF-β production form a positive self-sustaining loop that reinforces TGF-β signalling. These data identify a novel mechanism for local regulation of TGF-β function *in vivo* by regulating expression of the αvβ6 integrin. Therefore, the the role of αvβ6 integrin in IRI was further investigated.

5.2 Results

5.2.1 Effect of IRI on the expression of αvβ6 integrin expression

Under normal conditions, epithelial cells do not express significant levels of Integrin αvβ6. To investigate αvβ6 integrin expression in proximal tubular epithelial cells post injury, HKC8 cells were treated with 200μM H_2O_2 (4 h+68 h) or 100μM $CoCl_2$ (72 h). Post incubation, protein expression of αvβ6 integrin was examined by flow cytometry and immunofluorescence. Under resting condition, HKC8 cells did not express αvβ6 integrin but expression was upregulated in response to stimulation with H_2O_2 and $CoCl_2$. TGF-β1 treatment also increased the expression of αvβ6 integrin (Figure 5.1). In this experiment, TGF-β1 treated cells were used as a positive control.

The expression of αvβ6 integrin was also analysed in HKC8 cells transfected with HIF-1α plasmid which leads to increased HIF-1α protein expression. Compared to the transfection control, overexpression of HIF-1α in HKC8 cells caused a detectable increase in αvβ6 integrin expression (Figure 5.2). A similar trend of expression was observed in HK-2 cells subjected to H_2O_2 and $CoCl_2$ treatment compared to unstimulated control cells (Figure 5.3).

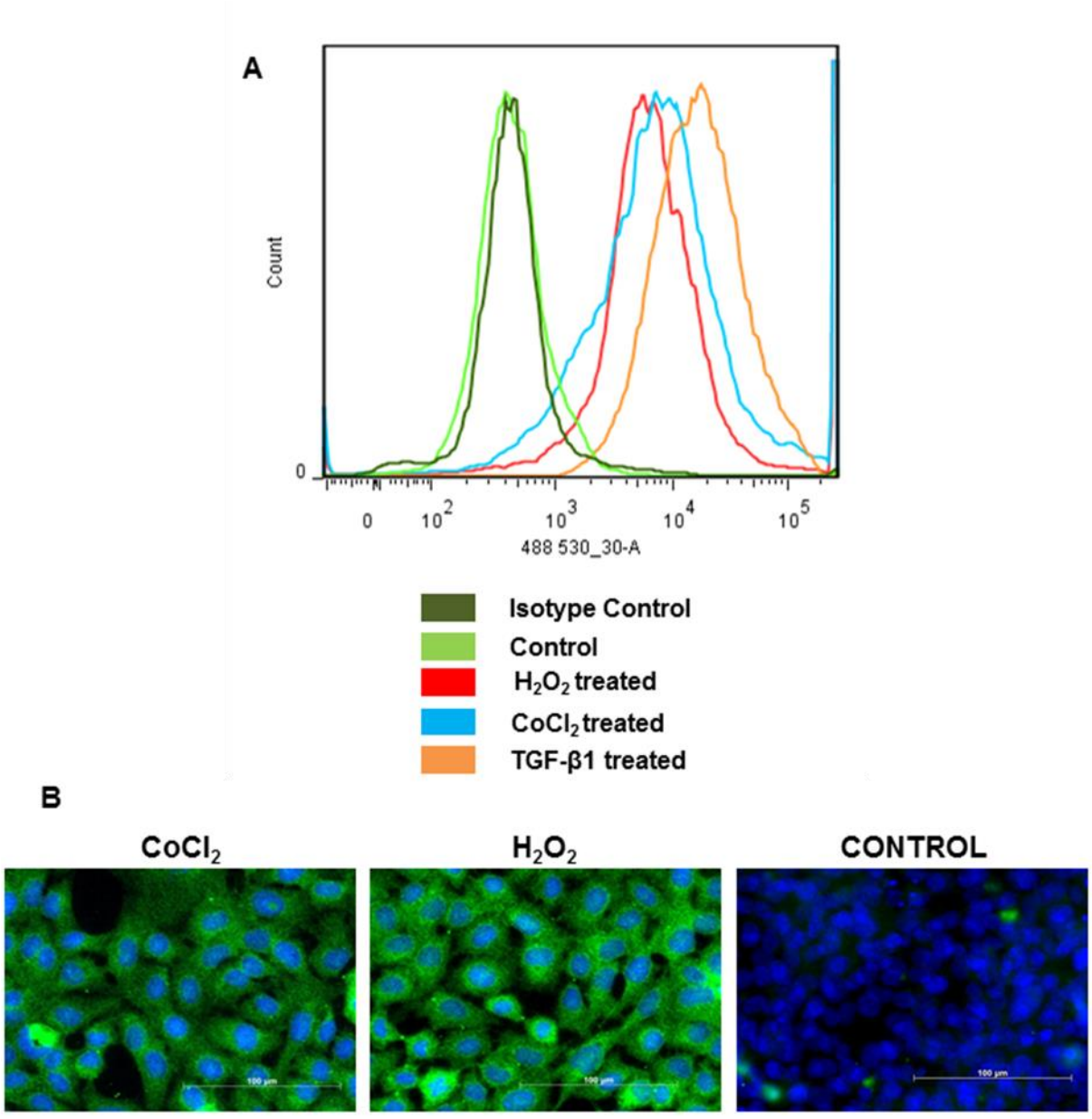

Figure 5.1: Increased αVβ6 expression in HKC8 cells.
HKC8 cells stimulated with 200μM H_2O_2 (4h + 68h) or 100μM $CoCl_2$ (72h) show an increased expression of αvβ6 integrin compared to control. Flow cytometry (A, N=2) and Immunofluorescence (B, N=1) studies were performed to study the expression at protein level. Images were taken at 400X magnification using Leica AF imaging unit.

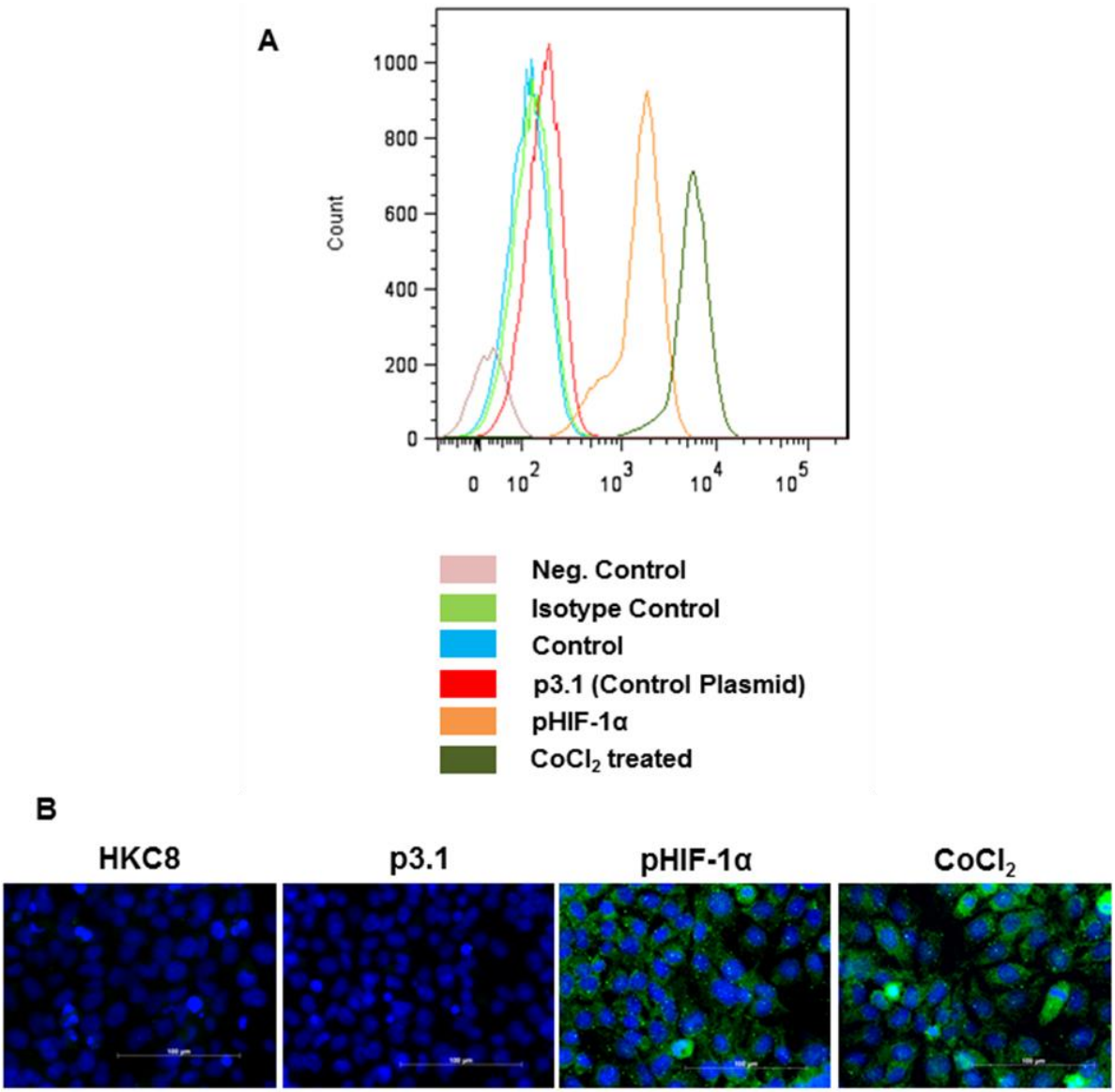

Figure 5.2: Effect of overexpression of HIF-1α on αvβ6 integrin expression. Flow cytometry (A, N=2) and Immunofluorescence (B, N=1) show an increased expression of αvβ6 integrin in cells transfected with HIF-1α compared to control. Images were taken at 400X magnification for αVβ6 integrin using Leica AF imaging unit.

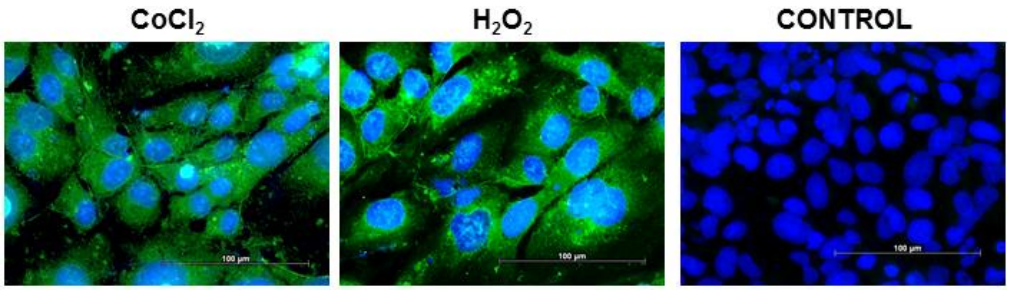

Figure 5.3: Effect of $CoCl_2$ or H_2O_2 on αVβ6 expression in HK-2 cells. HK-2 cells stimulated with 100μM H_2O_2 (4h + 68h) or 100μM $CoCl_2$ (72h) displayed an increased expression of αvβ6 integrin compared to control (N=1). Images were taken at 400X magnification for αVβ6 integrin using Leica AF imaging unit.

5.2.2 Immunohistochemical analysis of αVβ6 integrin

Immunohistochemical analysis was performed to examine the expression of αvβ6 integrin in human kidney biopsies from patients with acute tubular necrosis. There was prominent αVβ6 integrin staining in the epithelial lining of the dilated and damaged (proximal and distal) tubules (Figure 5.4).

To understand the dynamics of αVβ6 integrin expression in the kidneys of mice with IRI, immunohistochemical analysis of αVβ6 integrin expression was analysed in kidney early post IRI (25 mins ischaemia + 24 h reperfusion; n=7) and at a later stage (35 mins ischaemia + 28 days reperfusion; n=5). Mice sections were obtained from previous IRI study perfomed by Dr Anna Moles (Fearn *et al.*, 2017). There was a significant increase in expression of αVβ6 in mouse kidney sections (early p≤0.001 and late stage p≤0.05 of IRI) as compared to the control sections (Figure 5.5).

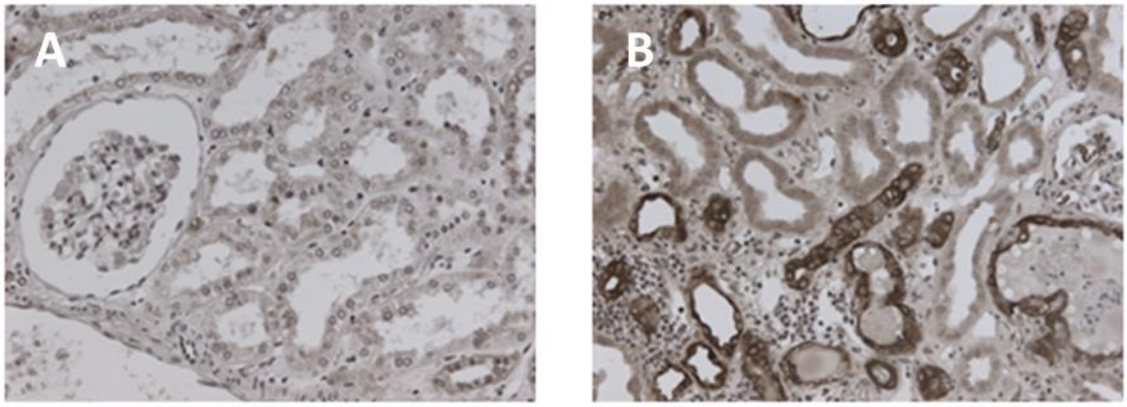

Figure 5.4: αvβ6 integrin immunostaining in human kidney tissue.
Paraffin embedded human kidney sections immunostained for αVβ6 integrin. An increased staining was evident in dilated and damaged tubules (B, n=11) compared to normal kidney (A, n=3). Photos were taken at 200X magnification using Leica AF imaging unit and are representative of images obtained from the other biopsy samples.

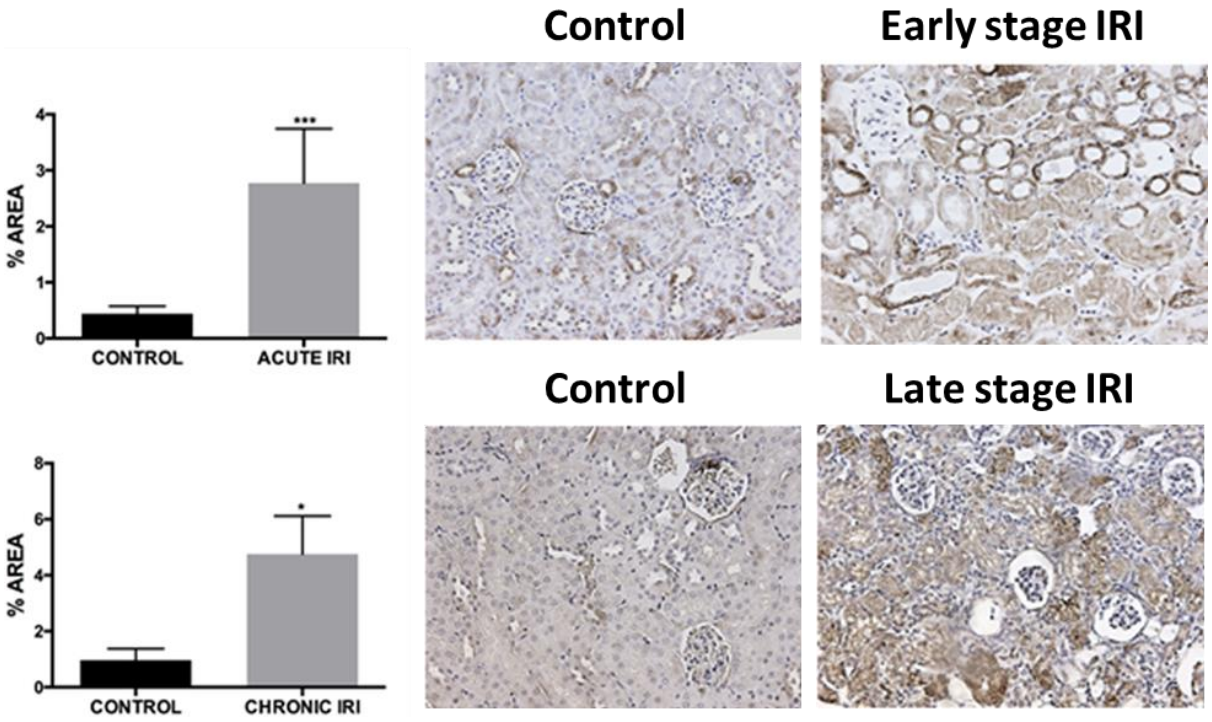

Figure 5.5: Immunohistochemical analysis of αvβ6 expression in mice following IRI. Paraffin embedded mouse kidney sections were immunostained for αVβ6. An increase in the expression of αVβ6 was observed in mouse kidney early post IRI (25 mins ischaemia + 24 h reperfusion; n=7) and at a later stage (35 mins ischaemia + 28 day reperfusion; n=5) as compared to the control (n=6). This persisted as fibrosis developed. Images (15 images/slide) were taken at 100X magnification for αVβ6 using Leica AF imaging unit. (*=p≤0.05)(**=p≤0.001)

5.2.3 The effect of ITGB6 sequence specific siRNA by HKC8 cells

A αVβ6 integrin-blocking peptide was initially used to determine whether αVβ6 integrin is involved in the regulation of TGF-β in IRI. However, since no significant difference in TGF-β activity was observed (Figure 2.8-1). Further experiments were performed using ITGB6 siRNA that suppresses β6 integrin activity (Section 2.6.1.1).

HKC8 cells were transfected with sequence specific siRNA for ITGB6 at concentrations of 10nM, 30nM and 50nM or a control siRNA for 24 hours followed by stimulation with 10ng/ml of exogenous TGF-β1 for 48 h. Immunofluorescence staining and FACS data demonstrates that HKC8 cells stimulated with TGF-β1 express αvβ6 integrin. Silencing of αvβ6 using 10nM, 30nM and 50nM of ITGB6 specific siRNA induced a significant reduction in expression (Figure 5.6 A and B). Transfection of HKC8 cells with control siRNA (Csi) produced no significant effect on αvβ6 expression compared to stimulated, untransfected cells (Figure 5.6). RT-PCR data suggests that 10nM concentration can effectively block β6 expression upto 48 h post-TGF-β1 treatment compared to transfection control (Figure 5.7).

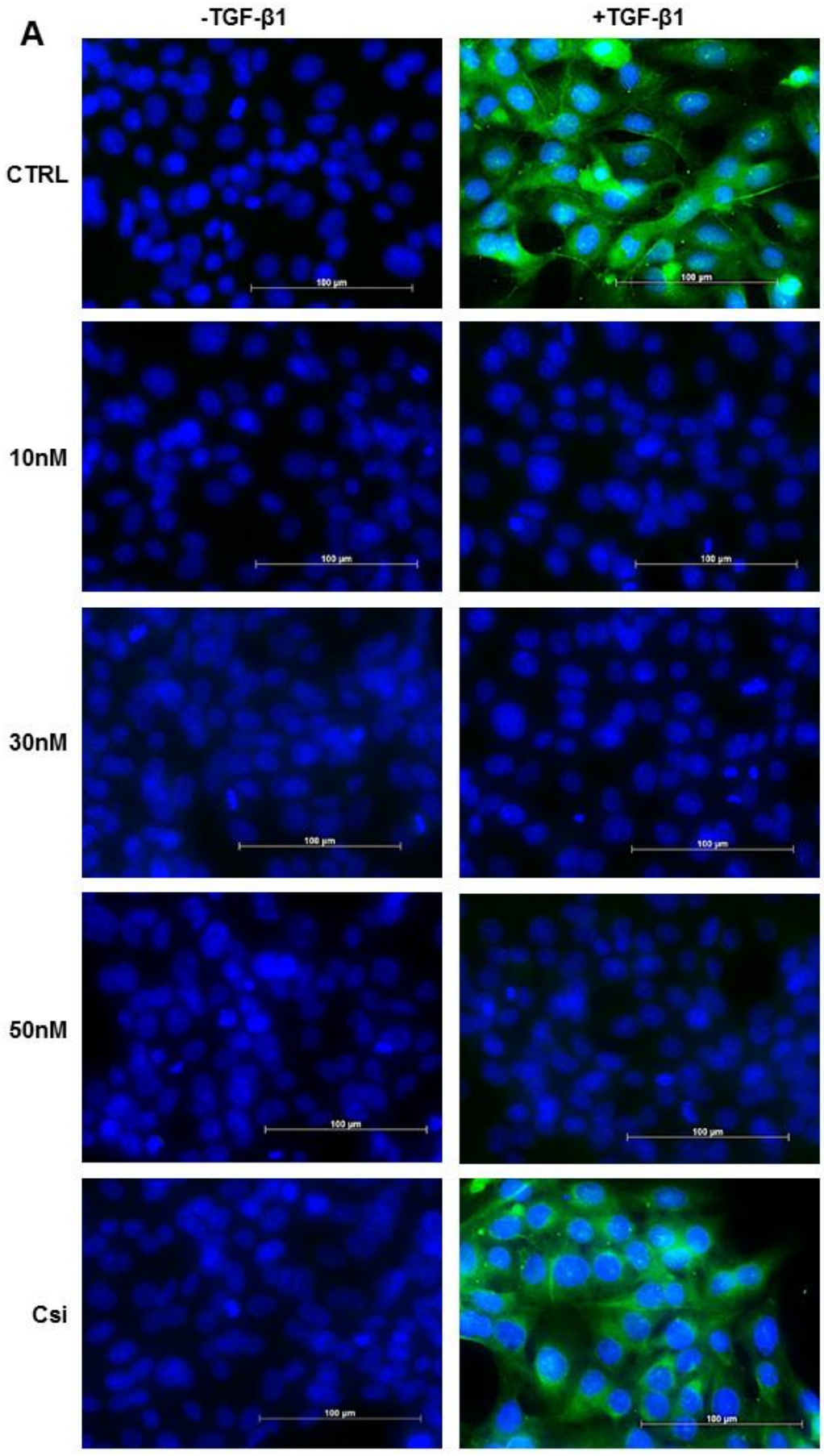
A
-TGF-β1
+TGF-β1
CTRL
10nM
30nM
50nM
Csi
100 µm

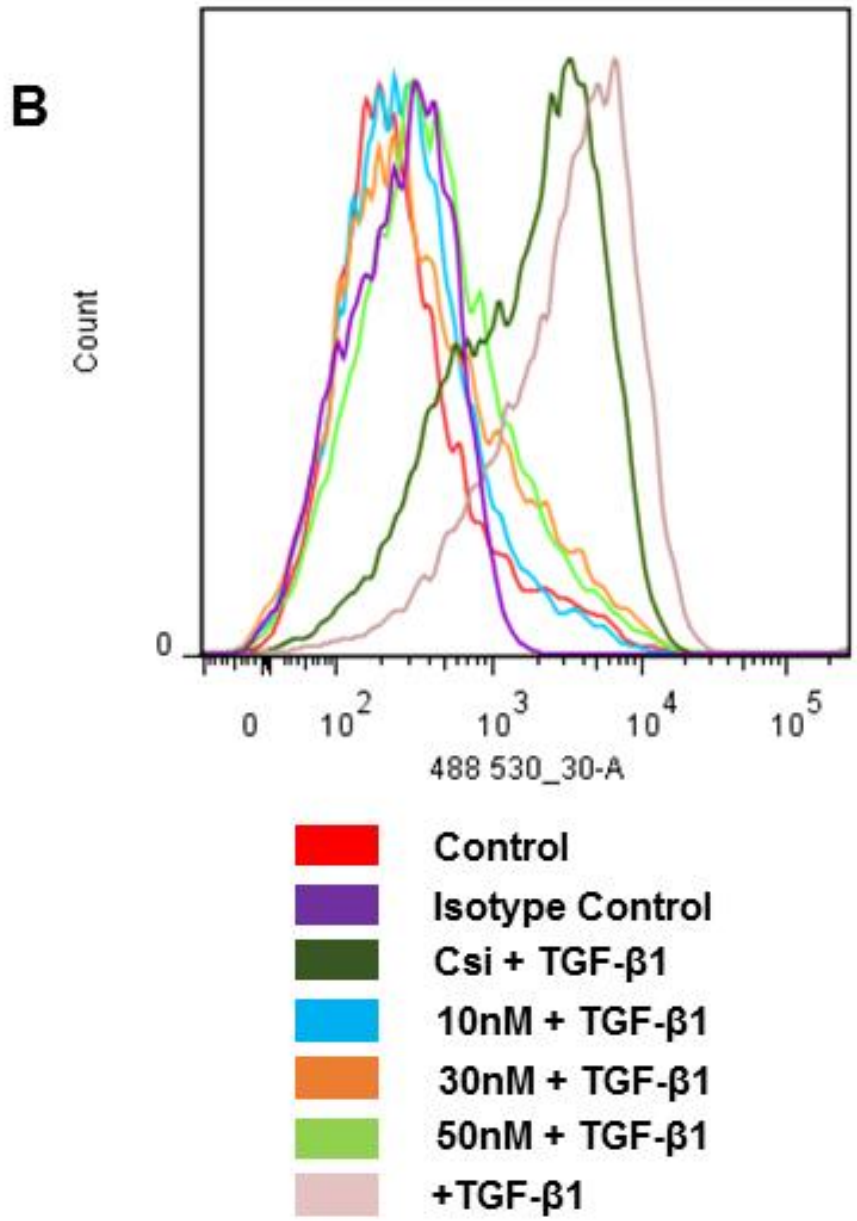

Figure 5.6: αvβ6 integrin expression in transfected HKC8 cells post TGF-β1 treatment.

HKC-8 cells were seeded and transfected with 10nM, 30nM and 50nM ITGB6 siRNA or a control siRNA (Csi) for 24h and then treated TGF-β1 for 48h. Immunofluorescence (A, N=1) and flow cytometry (B, N=2) studies were performed to study αvβ6 expression at protein level. Reduced αVβ6 expression was observed in HKC8 cells transfected with ITGB6 siRNA (10nM/30nM/50nM + TGF-β1) compared to corresponding control. Images were taken at 400X magnification for αvβ6 using Leica AF imaging unit.

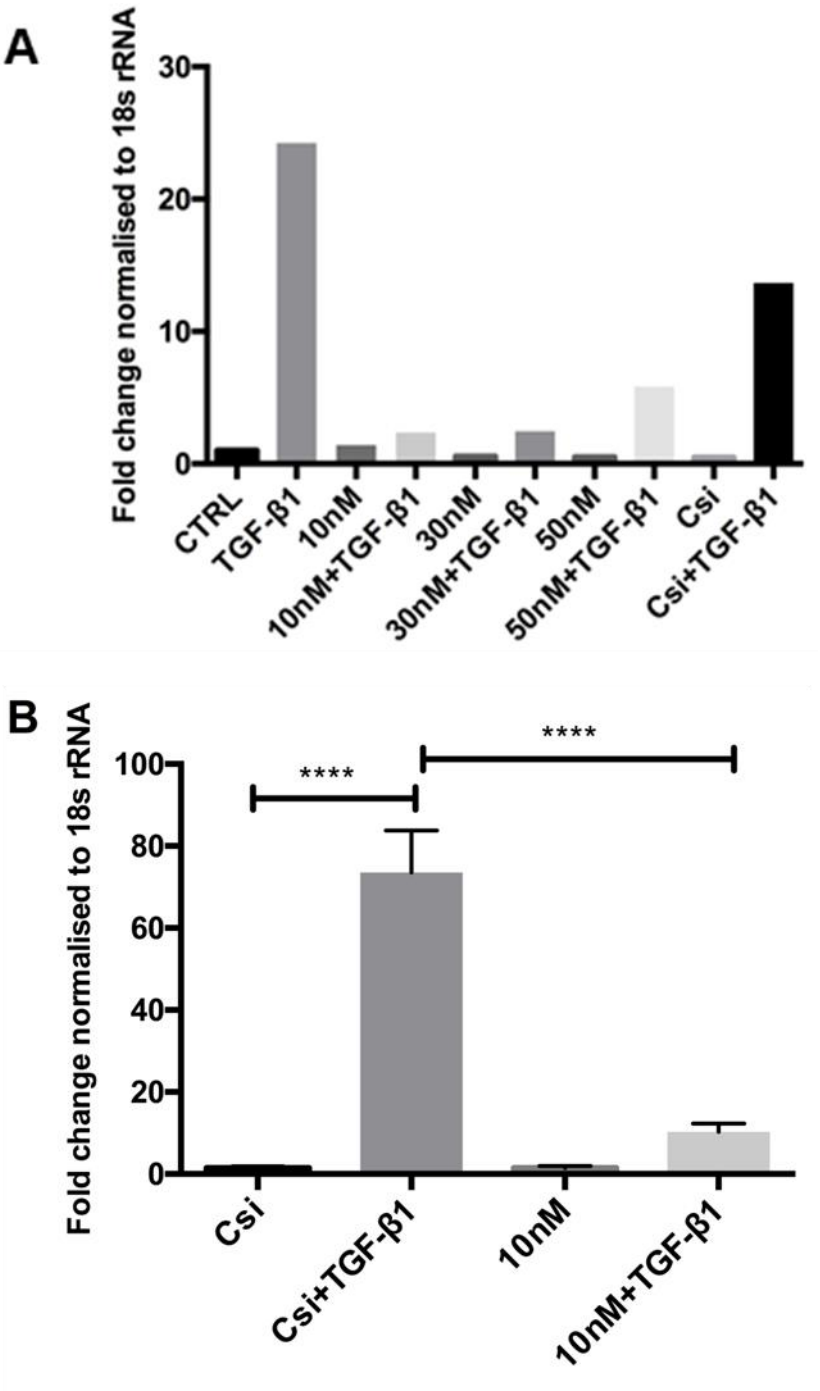

Figure 5.7: ITGB6 sequence specific siRNA inhibits the expression of β6 mRNA
Expression levels of β6 mRNA determined by qRT-PCR upon transfection with 10nM, 30nM and 50nM ITGB6 siRNA or a control siRNA (Csi) for 24h followed by treatment with 10ng/ml of TGF-β1 for 48h. The experiment was normalised to 18srRNA and expression levels compared to untreated control (A, N=1; B, N=3). Results indicate that TGF-β induces αvβ6 expression with largest effect at 10nM concentration. One-way Anova was used to analyse the data and graphs were plotted using Prism 6 software. (****=p≤0.0001)

5.2.4 Effect of αvβ6 knockdown on epithelial phenotype of HKC8 cells

Previous data (Chapter 4) suggests the role of TGF-β in progression of fibrosis post IRI. I next assessed whether ECM component expression by PTEC post IRI can be manipulated by ITGB6 siRNA transfection in HKC8 cells. Confluent HKC8 cells were transiently transfected with 10nM ITGB6 sequence specific siRNA for 24h prior to treatment with 400μM H_2O_2 (4h+20h) or 200μM $CoCl_2$ (24h). Cells transfected with control siRNA and stimulated with H_2O_2 or $CoCl_2$ showed increased expression of α-SMA and reduced E-cadherin expression. Introduction of ITGB6 siRNA preserved E-cadherin expression ($p \leq 0.001$ and $p \leq 0.0001$) and curtailed expression of α-SMA expression ($p \leq 0.0001$ and $p \leq 0.01$) post stimulation (Figure 5.8-1 A and 5.8-2 A). The change in expression of E-Cadherin and α-SMA was further confirmed by Western blotting (Figure 5.8-1 B and 5.8-2 B). Silencing of αvβ6 integrin using 10nM of ITGB6 sequence specific siRNA before treatment attenuated α-SMA expression and maintained E-cadherin expression. Transfection of HKC8 cells with control siRNA produced similar expression level compared to stimulated, untransfected cells. This suggests that ITGB6 siRNA, similar to SB-505124, maintains epithelial marker expression and reduces α-SMA expression post stimulation.

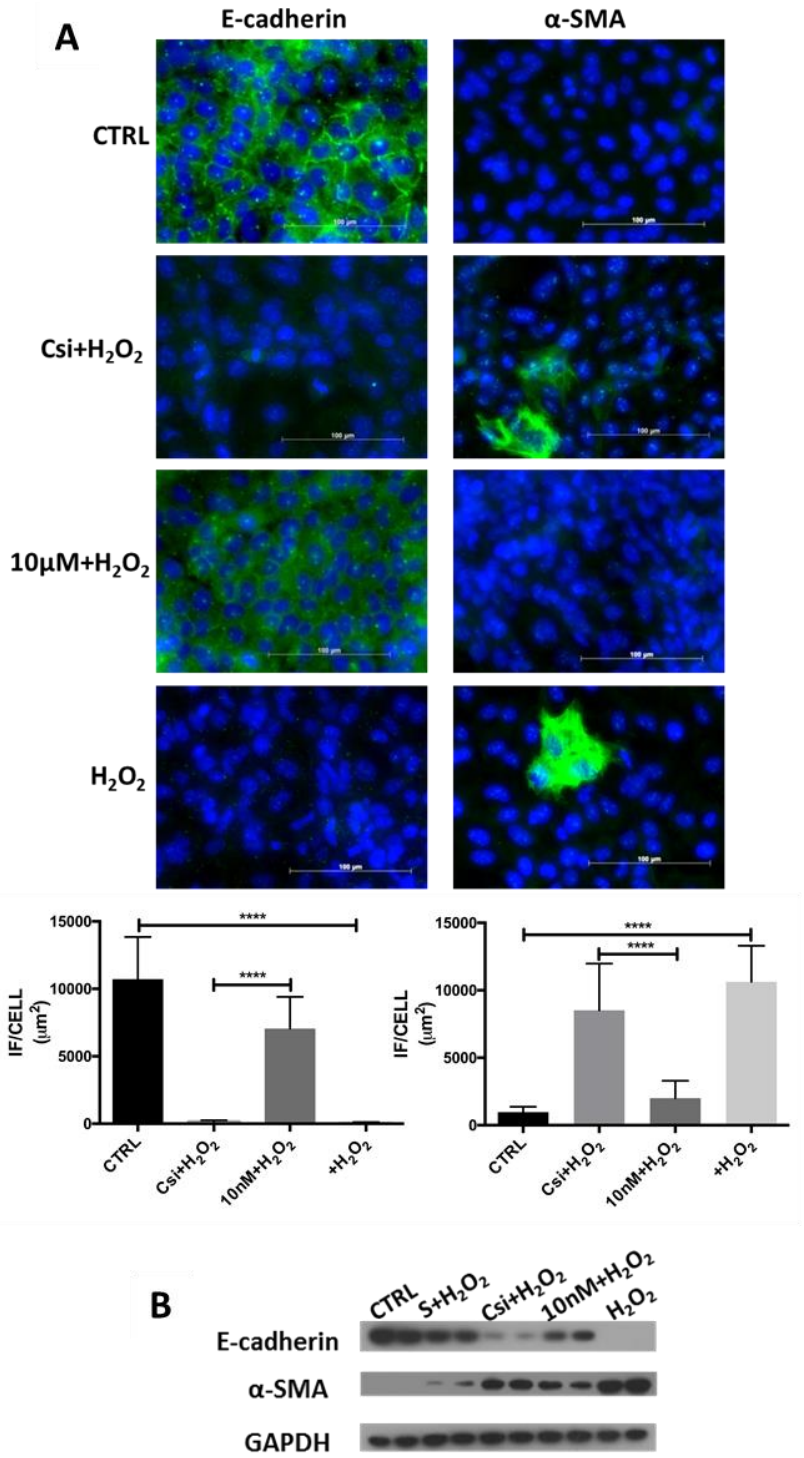

Figure 5.8-1: ITGB6 sequence specific siRNA decreases the expression of profibrotic markers in response to H_2O_2 in HKC8 cells.
HKC-8 cells were transfected with 10nM of ITGB6 sequence specific siRNA or control siRNA (Csi) for 24h. Cells were treated with or without 400μM H_2O_2 for 24h. Immunofluorescence (A, N=3) and Western blotting (B) confirmed that ITGB6 sequence specific siRNA preserves epithelial phenotype by maintaining E-cadherin expression and reducing α-SMA expression after stimulation, compared to non-silencing control siRNA. One-way Anova Bonferroni method was used to analyse the data and graphs were plotted using Prism 6 software. Images were taken at 400X magnification for E-cadherin and α-SMA using Leica AF imaging unit. *(****=p≤0.0001)*

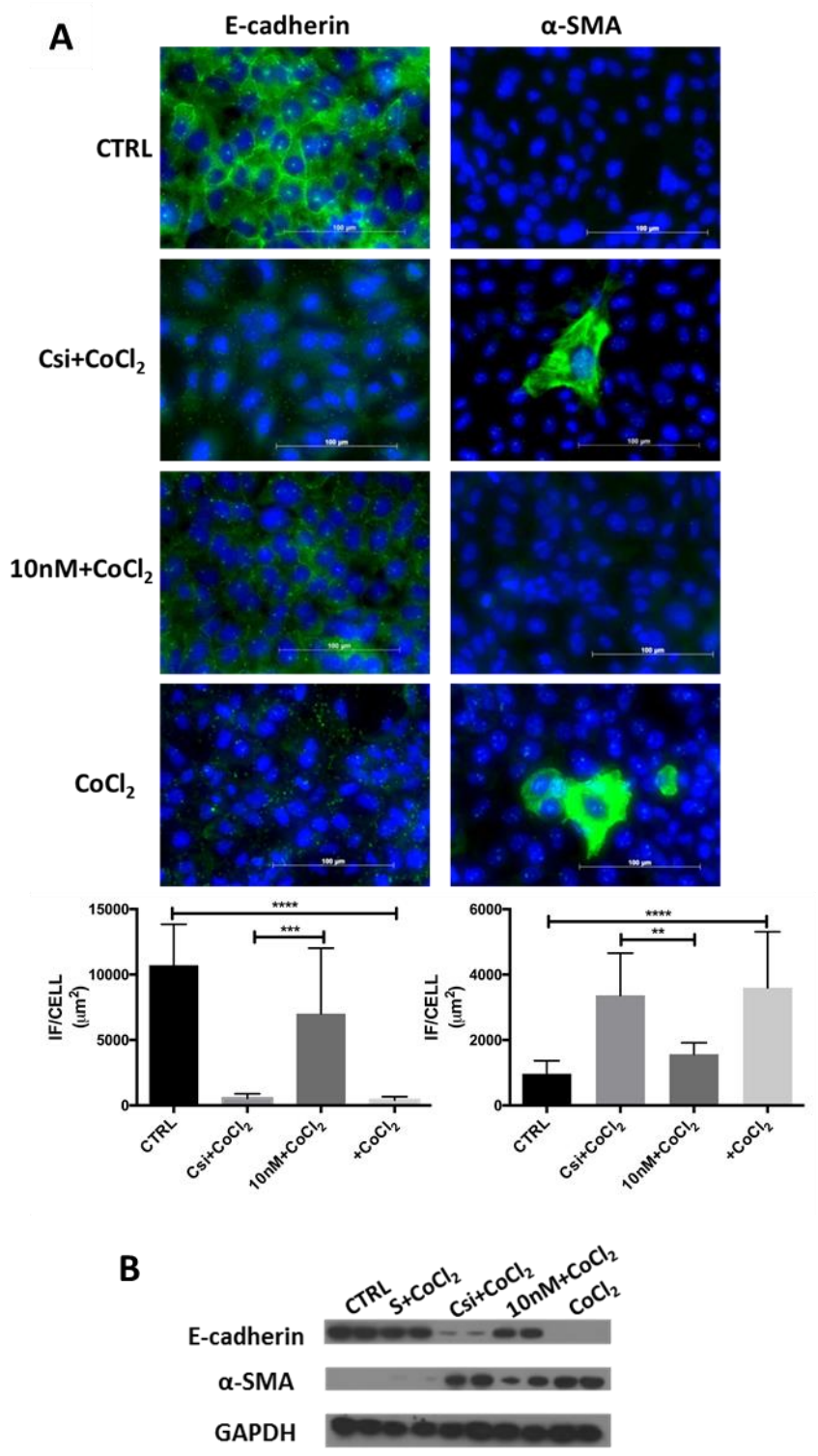

Figure 5.8-2: Knockdown of αvβ6 integrin in HKC8 cells decreases the expression of profibrotic markers in response to $CoCl_2$.
HKC-8 cells were transfected with 10nM of ITGB6 sequence specific siRNA or control siRNA (Csi) for 24h. Cells were treated with or without 200µM $CoCl_2$ for 24h. Immunofluorescence (A, N=3) and Western blotting (B) confirmed that ITGB6 sequence specific siRNA preserves epithelial phenotype by maintaining E-cadherin expression and reducing α-SMA expression after stimulation, compared to non-silencing control siRNA. One-way Anova Bonferroni method was used to analyse the data and graphs were plotted using Prism 6 software. Images were taken at 400X magnification using Leica AF imaging unit. (***=p≤0.01, ***=p≤0.001, ****=p≤0.0001*)

5.2.5 Transfection with ITGB6 sequence specific siRNA depletes active TGF-β bioavailability post $CoCl_2$ and H_2O_2 treatment

5.2.5.1 SMAD-Luciferase activity is reduced upon αvβ6 integrin knockdown

Having demonstrated that blocking αvβ6 integrin reduced profibrotic maker expression in epithelial cells, SMAD-Luciferase assay was performed to ascertain that transient blocking of αvβ6 integrin could regulate active TGF-β production post $CoCl_2$ and H_2O_2 treatment. HKC8 cells were transfected with ITGB6 sequence specific siRNA or control siRNA 24h prior to stimulation with 400μM H_2O_2 (4h+20h) or 200μM $CoCl_2$ (24h). After 24h incubation, the conditioned media was collected and was transferred to SMAD-reporter HKC8 cells pretreated with or without 10μM ALK5 inhibitor for 1h.

Transfection of the ITGB6 siRNA resulted in abrogation of TGF-β induced luciferase activity ($p \leq 0.05$) that was evident when media was transferred from cells transfected with control siRNA. This induction of luciferase activity was not seen if the cells were pre-treated with SB505124 (Figure 5.9). These observations confirm that TGF-β is released following treatment with $CoCl_2$ and H_2O_2 treatment and knockdown of αvβ6 reduces active TGF-β bioavailability.

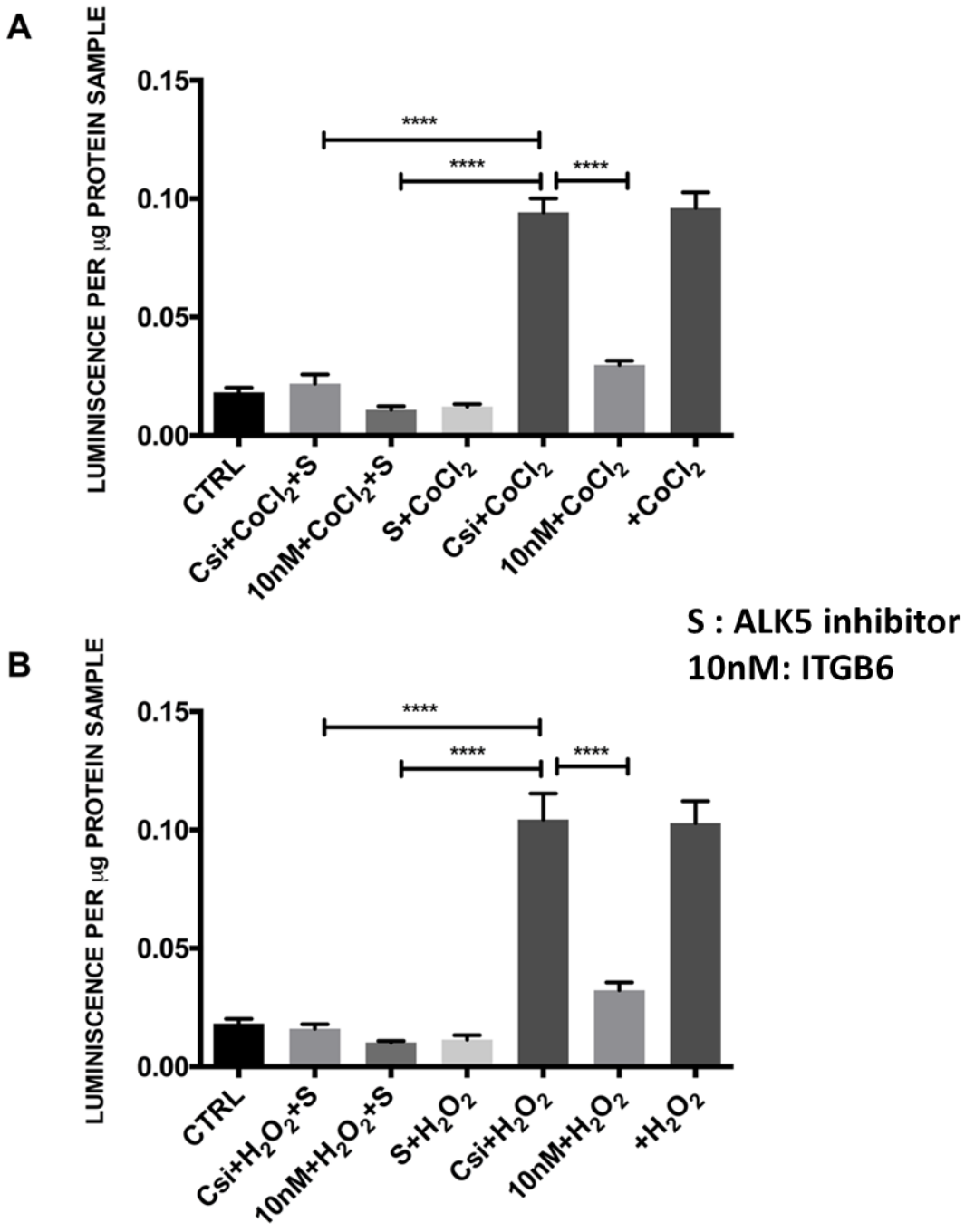

Figure 5.9: Silencing αvβ6 integrin minimizes active TGF-β production post IRI. Conditioned media obtained from ITGB6 (10nM) or control siRNA (Csi) transfected HKC8 cells post stimulation were transferred to naïve HKC8 SMAD-reporter cells pre-treated with or without 10µM ALK5 inhibitor (S) for 1h (N=4). Treatment with ITGB6 siRNA (*=p≤0.05) reduced active TGF-β bioavailability in response to $CoCl_2$ and H_2O_2 treatment compared to control siRNA. One-way Anova Bonferroni method was used to analyse the data and graphs were plotted using Prism 6 software (****=*p*≤0.0001)

5.2.5.2 Co-culture model system

Having developed an efficient co-culture system to replicate the *in vivo* environment, the following experiment was performed to assess whether knocking down the expression of αvβ6 integrin in PTEC can attenuate profibrotic changes induced in MRC5 cells post $CoCl_2$ and H_2O_2 treatment. Conditioned media from HKC8 cells was transferred onto naïve MRC-5 cells and protein expression was assessed using Western blotting and immunofluorescence. Although a marked increase in α-SMA expression was observed in MRC-5 cells incubated with control siRNA transfected cell media, αvβ6 knockdown in HKC8 cells prior to stimulation lead to a significant reduction in TGF-β induced α-SMA expression in MRC-5 cells suggesting that αvβ6 integrin has a functional effect on mechanisms that are recognised to mediate fibrosis (Figure 5.10).

In addition to protein expression, expression of Fibronectin and α-SMA was assessed at mRNA level. αvβ6 integrin knockdown in HKC8 cells prior to stimulation and media transfer attenuated TGF-β induced expression of ECM associated genes in MRC-5 cells , demonstrating that αvβ6 mediated activation of TGF-β can alter fibrosis though paracrine effects on surrounding cells (Figure 5.11).

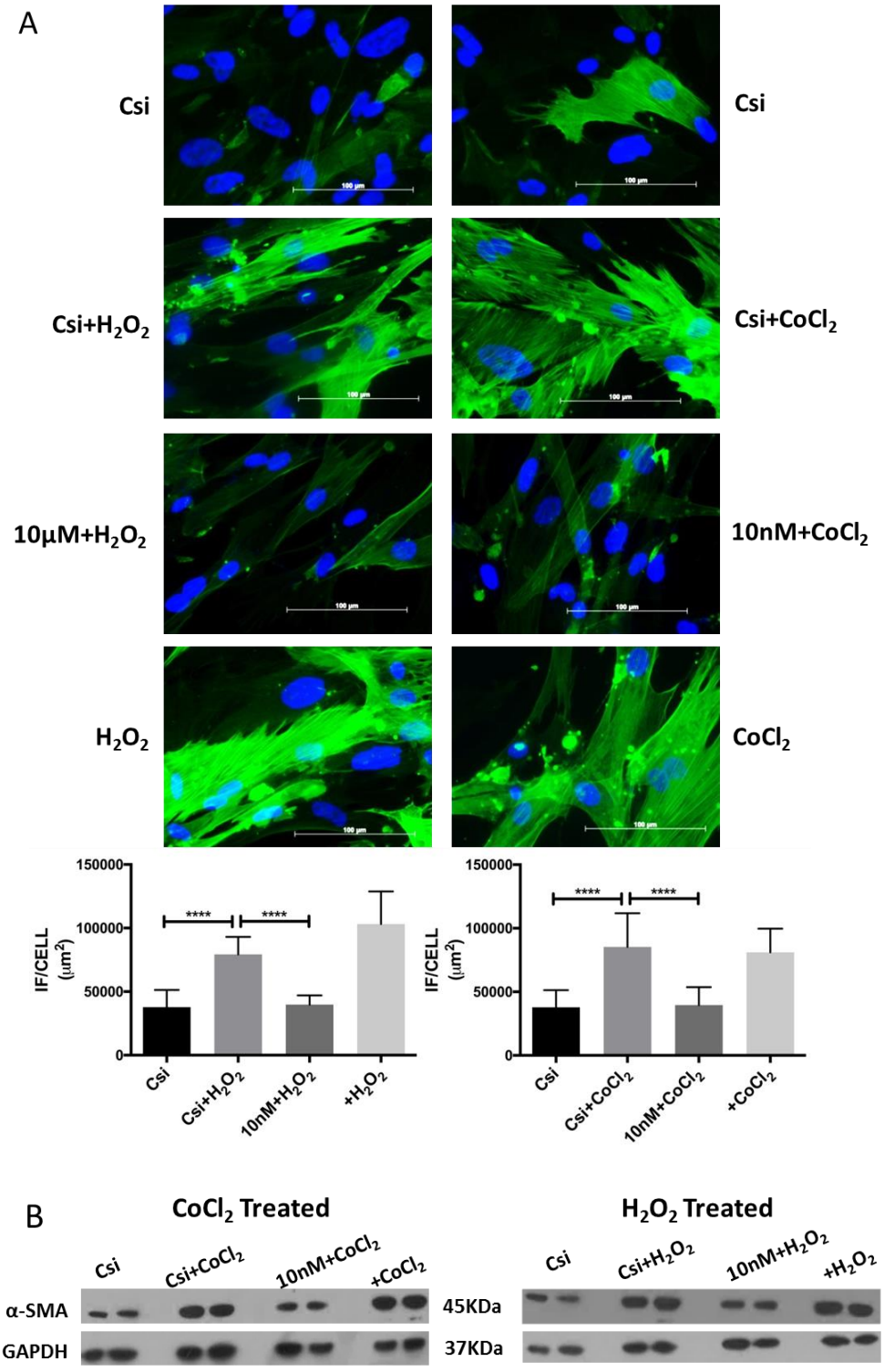

Figure 5.10: Blocking of αvβ6 integrin reduces α-SMA expression in co-culture model.

HKC8 cells were transfected with 10nM of ITGB6 sequence specific siRNA or control siRNA (Csi) for 24h and then treated with 400µM H_2O_2 or 200µM $CoCl_2$ for 24h. Supernatants collected were transferred onto naïve MRC-5 cells. Protein studies involving Western blotting (N=2) and immunofluorescence (N=3) demonstrate that silencing αvβ6 integrin reduced α-SMA compared to control siRNA-treated cells. One-way Anova Bonferroni method was used to analyse the data and graphs were plotted using Prism 6 software. Images were taken at 400X magnification for α-SMA using Leica AF imaging unit. (****=p≤0.0001)

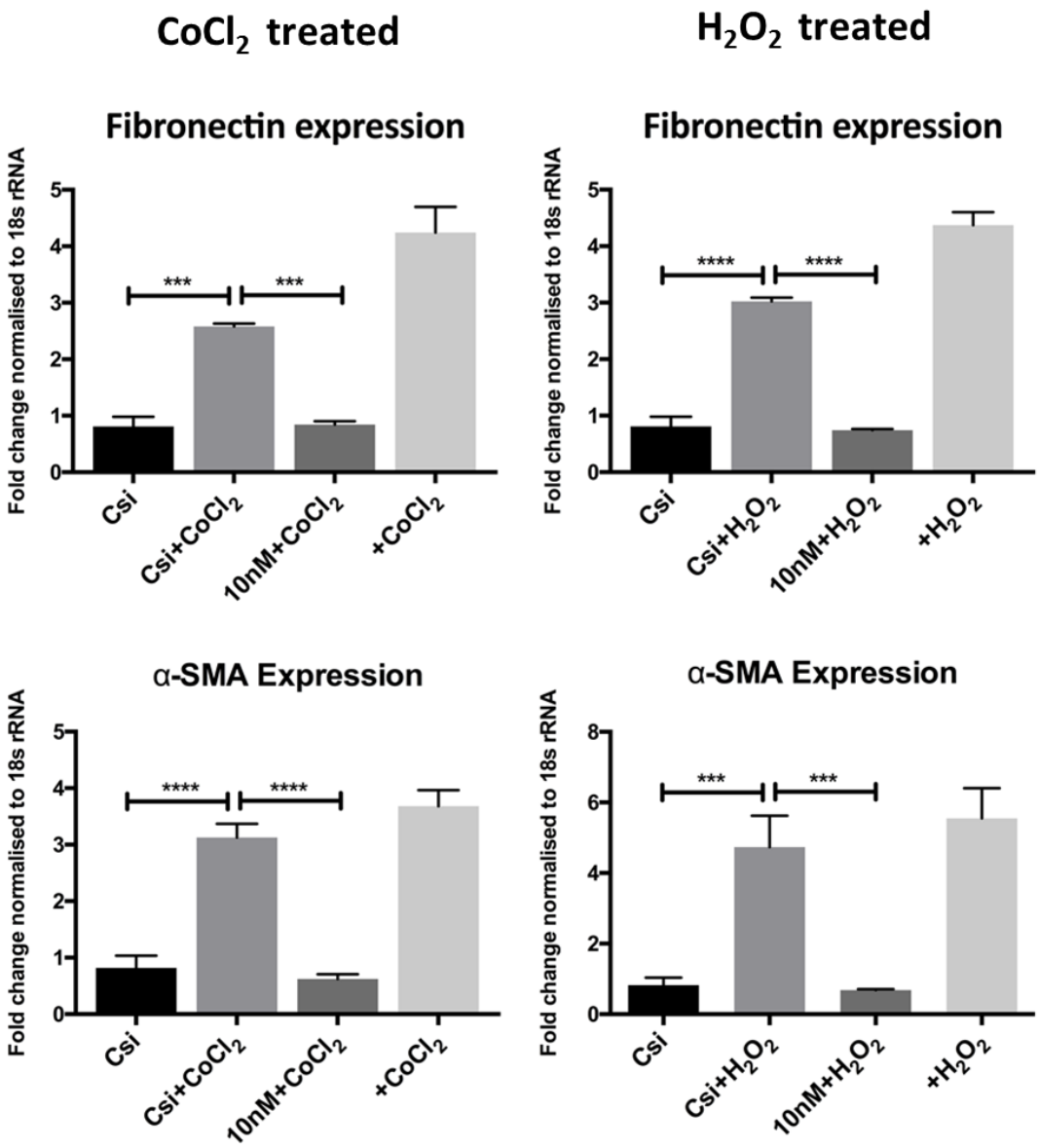

Figure 5.11: Blocking of αvβ6 integrin reduced expression of fibrotic gene expression. Gene expression of α-SMA and fibronectin was analysed in MRC-5 cells post incubation with HKC8 cells transfected with ITGB6 (10nM) or control siRNA (Csi) and subjected to stimulation by 400μM H_2O_2 (4h+20h) or 200μM $CoCl_2$ (24h). The experiment was normalised to 18srRNA (A and B, N=3). Inhibition of αvβ6 integrin prior to stimulation abrogated the expression of α-SMA and fibronectin in MRC-5 cells when compared to MRC5 cells incubated with control siRNA transfected preconditioned media (Csi+H_2O_2 or Csi+ $CoCl_2$). One-way Anova Bonferroni method was used to analyse the data and graphs were plotted using Prism 6 software. (****=p≤0.0001)(***=p≤0.001)

5.3 Discussion

Published data has demonstrated the role of αvβ6 integrin in disease and injury, however little is known about the contribution of αvβ6 integrin during IRI (Betensley *et al.*, 2016; Song *et al.*, 2016). The last part of my PhD work explored the contribution of αvβ6 integrin towards IRI and to determine whether blocking αvβ6 integrin could reduce the progression of fibrosis. αvβ6 integrin is expressed at relatively low levels in normal PTECs however, expression is increased during tissue remodeling, injury, and neoplasia (Okada and Kalluri, 2005). Cytokines such as EGF and TGF-β that regulate epithelial remodeling are capable of inducing an increased expression of the αvβ6 integrin in cultured epithelial cells (Hynes, 2002). It has been shown that active TGF-β stimulation increases expression of αvβ6 integrin in a prostate cancer cell line suggesting that active TGF-β can stimulate αvβ6 expression *in vitro* (Dutta *et al.*, 2015).

Activation of latent TGF-β by the αvβ6 integrin can only occur via direct association with the epithelial cells since αvβ6 integrin is an epithelial restricted integrin. This further leads to αvβ6 integrin binding to and activating TGF-β (Tatler *et al.*, 2012). My IHC data shows an increased αvβ6 integrin expression in human renal biopsies with ATN. A previous study on human renal biopsies has shown that αvβ6 integrin is upregulated in distal tubules during acute rejection and end-stage chronic allograft nephropathy (Trevillian *et al.*, 2004).

αvβ6 integrin binds to the RGD domains on fibronectin, tenascin, the LAP1 and 3 and the N-terminal fragments of the latent precursor forms of TGF-β1. Direct interaction between αvβ6 integrin and RGD motif contained within LAP1 and 3 converts TGF-β precursor into a receptor binding-competent state. Blocking RGD- domain prevents the subsequent binding of αvβ6 to the transforming growth factor-β1 latency-associated peptide. However, mature TGF-β1 does not contain the RGD motif and

thus an additional ligand binding pocket distinct from RGD domain has been documented (Annes *et al.*, 2002; Williams *et al.*, 2004). For αvβ6, a non-RGD ligand recognition motif (DLXXL) has been described that is also detected on several proteins including collagen and fibrinogen. A sequence with 70% similarity to the recognition motif has also been detected in the LAP and mature TGF-β1(Kracklauer *et al.*, 2003). In my study, DLXXL was used to block the binding of αvβ6 integrin and TGF-β1 and prevent the subsequent activation of mature TGF-β1. However, no significant change in active TGF-β production by HKC8 cells was observed.

The use of siRNA technique has been reported in several studies where siRNA knockdown of αvβ6 significantly blocked the invasion of cancer cell line though matrigel compared to antibody mediated blocking (Niu *et al.*, 2010; Moore *et al.*, 2014). In my study, I successfully silenced the expression of αvβ6 in HKC8 cells using sequence specific siRNA. Dutta *et al* made similar observations where silencing of αvβ6 integrin prior to 10ng/ml TGF-β1 stimulation did not increase αvβ6 integrin in prostate cancer cells compared to non-transfected or cells transfected with a control siRNA (Dutta *et al.*, 2015).

The β6 knockdown model was used to assess the expression of epithelial and fibrotic markers post H_2O_2 and $CoCl_2$ treatment. H_2O_2 or $CoCl_2$ treated β6 knockdown HKC8 cells preserved E-cadherin expression and reduced α-SMA expression compared to control siRNA cells. This result is supported by a mouse study where β6 knockout mice were protected from UUO induced tubulointerstitial fibrosis. These mice expressed low levels of collagen, PAI-1 and pSMAD2 at a protein and mRNA level compared to wild type (Ma *et al.*, 2003).

A SMAD-luciferase assay was performed to examine active TGF-β production in β6 knockout cells. My data shows that transient knockdown of αvβ6 integrin reduces active TGF-β bioavailability in conditioned media. To mimic the *in vivo* effects of

blocking αvβ6 integrin on progression of fibrosis a co-culture system was used that showed reduced active TGF-β production, reduced α-SMA expression and fibroblast activation post αvβ6 blocking (Munger *et al.*, 1999; Hahm *et al.*, 2007; Allen *et al.*, 2014). I performed media transfer studies where results confirmed that αvβ6 integrin plays a major role in mediating TGF-β activation. Knockdown of αvβ6 blocked the paracrine auto-activation effect exhibited by TGF-β in mediating fibrosis.

Chapter 6: Discussion

6.1 Specific aims and outcomes

1. Establish an *in vitro* model of renal tubular IRI by using renal tubular proximal epithelial cell lines.

The *in vitro* model of hypoxia and free radical stress established in this study allowed the investigation of the effects of IRI on proximal tubular epithelial cell phenotype. Various concentrations of hydrogen peroxide and cobalt chloride were used to induce free radical injury and hypoxia respectively. This was followed by measurement of the expression of fibrotic markers such as α-SMA and the epithelial cell marker E-Cadherin was studied using qRT-PCR, Western blotting and immunofluorescence in HKC8 and HK2 cells. Furthermore, the effect of hypoxia and free radical stress was also studied in lung fibroblast cells (MRC-5) with an aim to establish an *in vitro* system comprising epithelial cells and fibroblasts. Results suggested that H_2O_2 and $CoCl_2$ induced oxidative stress and hypoxia in HKC8, HK2 and MRC-5 cells, increasing the expression of fibrotic markers and stimulating myofibroblast characteristics.

2. Assess whether tubular cells develop a pro-fibrotic phenotype after IRI and determine whether these changes rely on the synthesis of intermediates such as TGF-β.

Since TGF-β is implicated in mediating renal fibrosis, the effects of TGF-β on proximal tubular epithelial cells and fibroblasts were investigated at RNA and protein level. This was done by studying the changes in expression of epithelial and fibrotic markers. The effect of TGF-β on epithelial cell phenotype was also determined in the presence of a potent inhibitor of TGF-β signalling. SB-505124 blocked the effect of TGF-β1 on PTECs. ALK5 inhibition also prevented the changes induced by H_2O_2 and

$CoCl_2$, retaining epithelial cell markers and inhibiting the expression of fibrotic markers. These results were in line with data from SB-505124 and TGF-β1 treated cells, suggesting the involvement of TGF-β in changes induced by $CoCl_2$ and H_2O_2. This was further investigated in a co-culture system wherein media collected from H_2O_2 and $CoCl_2$ stimulated HKC8 cells was transferred to wells containing MRC-5 cells. This led to increased α-SMA expression which was inhibited in MRC-5 cells pre-treated with SB-505124. To confirm that stressed cells produce active TGF-β after stimulation that mimics IRI, HKC8 cells cultured in transwell were stimulated with H_2O_2 and $CoCl_2$. The transwells were then transferred into wells containing naïve MRC-5 cells pre-treated with and without SB-505124. Transfer of stimulated cells led to an increase in α-SMA, a response that was inhibited by treatment with SB-505124. This suggests that bioactive TGF-β is released by HKC8 cells post IRI injury.

3. Determining the role of αvβ6 integrin in IRI

Since αvβ6 integrin regulates TGF-β activity, its role in IRI was investigated. Free radical stress and hypoxia increased the expression of αvβ6 integrin *in vitro*. Its expression in biopsy samples acquired form patients and mouse kidney following IRI was increased. Furthermore, the effect of αvβ6 integrin knockdown on epithelial responses was investigated using ITGB6 siRNA. Knockdown of αvβ6 integrin in HKC8 cells not only decreased the expression of profibrotic markers but also reduced the bioavailability of active TGF-β following $CoCl_2$ and H_2O_2 treatment. This confirmed that bioactive TGF-β is produced following IRI and siRNA knockdown of αvβ6 integrin blocks its production.

6.2 Overall discussion

Data from this thesis has demonstrated a prominent role of TGF-β in kidney tubular epithelial cell responses post-IRI. Prior to the current study, investigation into injured PTECs has demonstrated that recovery of renal function is largely dependent on the

restoration of proximal tubular cells integrity and function. The repair mechanism in response to injury can lead to complete recovery (adaptive) or may lead to fibrosis and CKD (maladaptive). Adaptive repair is initially dependent on restoring the population of proximal tubular cells occurring 1 to 3 d post-injury (Tian and Phillips, 2003; Humphreys *et al.*, 2008). During maladaptive repair, epithelial cell cycle arrest and failure to repopulate the tubules can lead to fibrosis, thus providing a link between acute injury and CKD. This occurs when the injury is more severe, or repeated, and the stimulated cells cannot complete the cell cycle efficiently leading to arrest in the G2/M phase. Apoptosis of these cells is often blocked so that they survive and pro-fibrotic gene transcription is initiated. This repair process leads to incomplete structural and recovery with accumulation of pro-fibrotic factors, increased production of extracellular matrix, and development of fibrosis (Yang *et al.*, 2010b). A study has demonstrated that moderate IRI is followed by repair without fibrosis, but severe IRI leads to fibrosis (Bonventre, 2014). Since one of the main causes of AKI is IRI, in this thesis an attempt to develop an *in vitro* model was undertaken to investigate the underlying mechanism involved in maladaptive repair and tissue fibrosis (Figure 5.12).

Using an *in vitro* model instead of *in vivo* models has its benefits, as it allows the exact response of specific cells to be measured accurately. However, *in vitro* models have drawbacks as there is no assessment of the interaction between various cell types and some cells might show different behaviour *in vitro* than *in vivo* (Russ *et al.*, 2007). Nevertheless, well-designed *in vitro* models are crucial in understanding molecular mechanisms underlying disease and providing a foundation to subsequent *in vivo* work (Russ *et al.*, 2007; Kurian and Pemaih, 2014).

Previous studies have standardised *in vitro* cell based model of kidney IRI in rat (Williams *et al.*, 1997) and mouse (Oxburgh and de Caestecker, 2012) tubular

proximal epithelial cells, renal epithelial cells of Hampshire pigs (Kurian and Pemaih, 2014) and cultured human PTECs (Turman and Bates, 1997). HKC8 and HK2 have been used in *in vitro* models of IRI in this study. This is because culturing cell lines is much more efficient and less time consuming but may not maintain all features of the original cell than primary cells. Importantly it is the renal tubular epithelial cells that are most affected by IRI due to their high metabolic demands (Bonventre and Weinberg, 2003)

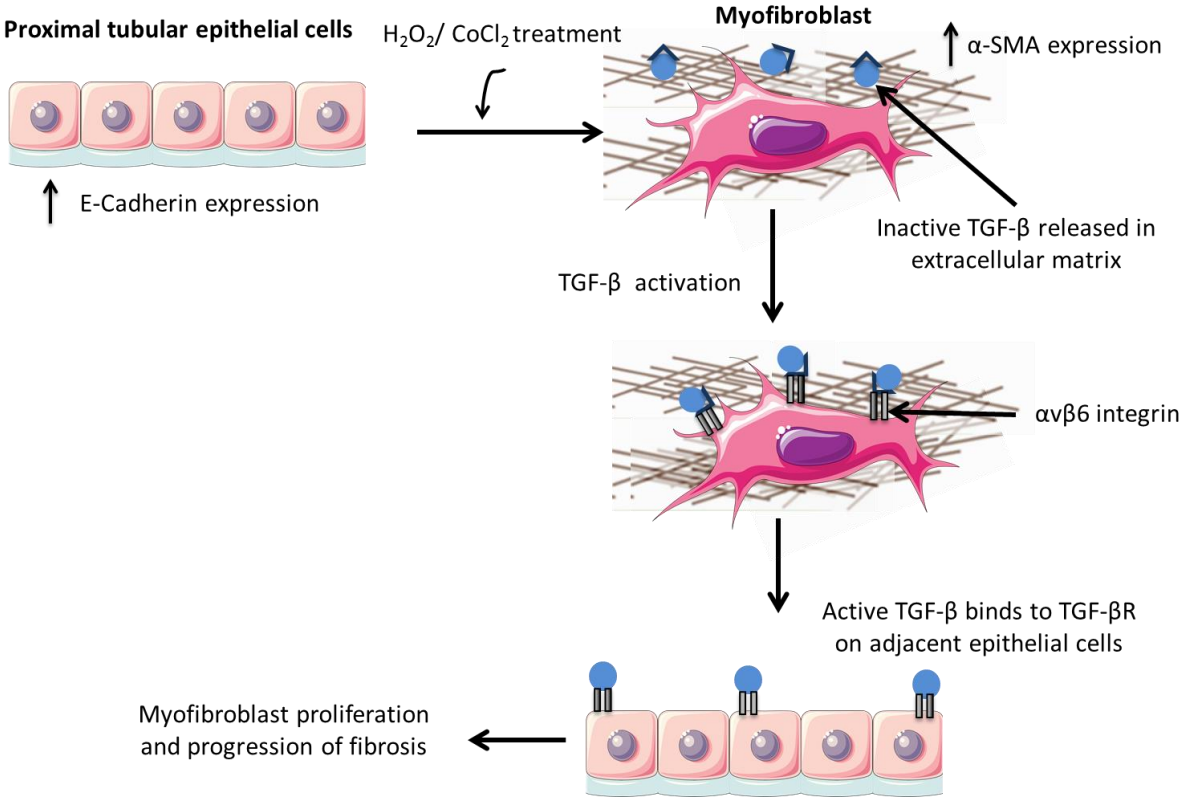

Figure 5.12: Proposed model of IRI in human proximal epithelial cells.

Ischaemia is associated with oxygen deprivation that leads to decline in ATP production and increase in HIF-1α stabilisation (Kurian and Pemaih, 2014). Several studies have used a hypoxic chamber to induce ischaemia in PTECs (Turman and Bates, 1997; Leonard *et al.*, 2003; Xu *et al.*, 2010; Ramamoorthy and Shi, 2014). Therefore, HKC8 cells were initially subjected to hypoxic conditions and the duration of incubation was optimised. $CoCl_2$ was also used to replicate ischaemia as it has the

advantage to be inexpensive, fast and mimics hypoxia without the risk of hypoxia/re-oxygenation as in the case of using hypoxic chambers (Wu and Yotnda, 2011; Dai *et al.*, 2014). HKC8 and HK2 cells, when treated with 100µM $CoCl_2$, increase HIF-1α and developed a pro-fibrotic phenotype. Previous studies have reported similar induction of HIF-1α in Balb/c mice injected with $CoCl_2$ (Zhang *et al.*, 2014) and increased α-SMA expression in human coronary artery endothelial cells treated with $CoCl_2$ (Xu *et al.*, 2015).

To induce free radical injury, HK2 and HKC8 cells were treated with H_2O_2 which is a source of ROS and implicated in renal IRI (Lee *et al.*, 2013). H_2O_2 increased the expression of α–SMA and reduced E-Cadherin expression in HKC8 and HK2 cells. *In vivo* mice work has demonstrated that renal PTECs produce ROS during IRI and the extent of tubular damage correlates with H_2O_2 production (Wang *et al.*, 2011).

Hypoxia has been previously studied in mouse Embryonic Fibroblasts (Vengellur and LaPres, 2004), human dermal fibroblasts (Eleftheriadis *et al.*, 2011) and human lung fibroblasts (MRC-5) (Mathieu *et al.*, 2014) while ROS generation effects have been extensively studied in human dermal fibroblasts (Bladier *et al.*, 1997) and MRC-5 cells (Teramoto *et al.*, 2001; Romeo *et al.*, 2016). Due to unavailability of an appropriate human kidney fibroblast cell line, MRC-5 cells were used to study the effects of hypoxia and ROS in fibroblasts. Results showed a similar response as previously seen in HKC8 and HK2 cells following $CoCl_2$ treatment.

It has been recently reported that up-regulation of TGF-β and the downstream SMAD cascade is evident in injured tubular epithelial cells arrested at the G2/M phase of cell cycle (Yang *et al.*, 2010b). To study the progression of renal fibrosis post IRI, PTECs (HKC8 and HK2) were stimulated with TGF-β1. Changes in α-SMA and E-Cadherin expression suggested a shift from an epithelial to fibrotic like phenotype as previously shown in an *in vitro* culture model of HKC8 cells (Phanish *et al.*, 2006).

Several strategies have been proposed to inhibit TGF-β and enhance re-epithelialization of cutaneous wounds and reduce scarring fibrosis. This includes the use of neutralising antibodies against TGF-β and small-molecule inhibitors for receptor serine/threonine kinases. While neutralising antibodies against TGF-β is the most intensively studied approach, the inhibitors of TGF-β signalling pathway developed for therapeutics are powerful tools in dissecting this complex pathway and studying the cross talk with other signalling pathways (Yanagita, 2012). In the present study, SB505124 which inhibits the TGF-β type I receptor serine/threonine kinase (ALK5 inhibitor) , was used (Byfield *et al.*, 2004). The effect of ALK5 inhibition was not only apparent in TGF-β treated HKC8 cells but also on IRI induced changes. The latter was done to ascertain that the changes in epithelial cell phenotype observed post IRI are mediated by TGF-β (Kapoor *et al.*, 2016).

Epithelial cells can control and regulate fibroblast phenotype and both primary cells and cell lines are being used in different culture matrices and co-culture models (Moll *et al.*, 2013). To study the interaction between epithelial cells and fibroblasts, an *in vitro* model comprising of HKC8 and MRC-5 cells was established. Here, MRC-5 cells were incubated with H_2O_2 and $CoCl_2$ pre-conditioned media (from HKC8 cells) and the expression of fibrotic markers was assessed in the presence and absence of SB505124. Increase in fibrotic markers was observed in cells stimulated only with the preconditioned media suggesting fibroblast activation. Similar results were reported when media from Cisplastin treated HKC8 cells increased level of key fibrotic markers α-SMA, TGF- β1 and Collagen 1α1 in WS-1 dermal fibroblasts (Moll *et al.*, 2013). Additionally, SB505124 prevented effects of HKC8 preconditioned media on MRC-5 cells. This suggests that stressed epithelial cells produce active TGF-β post IRI insult (Geng *et al.*, 2009). This was confirmed by stimulating HKC8 cells grown in transwell inserts with H_2O_2 and $CoCl_2$ prior to transferring the cell into wells containing

MRC-5 cells. Under these conditions α-SMA expression in MRC-5 cells was increased. SB505124 inhibited this change. This was also validated using luciferase assay studies (Section 4.5).

There are sequences within the β6 subunit of αvβ6 integrin that bind the LAP (Munger *et al.*, 1999). Subsequently, cell culture studies showed that fibroblasts and epithelial cells can use integrins to activate latent TGF-β (Wipff *et al.*, 2007; Giacomini *et al.*, 2012). Since αvβ6 integrin is implicated in TGF-β induced pulmonary fibrosis (M Teoh *et al.*, 2015), the role of αvβ6 integrin was investigated in renal IRI.

Stimulating HKC8 cells with H_2O_2 and $CoCl_2$ resulted in an increase of αvβ6 integrin. This could be due to the fact that active TGF-β production by virtue of cell activation due to H_2O_2 and $CoCl_2$ results in upregulation of TGF-β which increases αvβ6 integrin that then leads to a positive feedback loop in TGF-β signalling (Cagle, 2010 434). Furthermore high expression of αvβ6 integrin was also demonstrated in patients and mouse kidney tissue (acute IRI and chronic IRI model) as previously reported (Trevillian *et al.*, 2004). Subsequently, using sequence specific siRNA for αvβ6 integrin in HKC8 cells prior to stimulation with H_2O_2 and $CoCl_2$ not only reduced the expression of profibrotic marker expression but also reduced TGF-β bioavailability. Similar results were observed in co-culture model (Section 5.2.5.2). This model established an *in vitro* system to replicate the *in vivo* effects of αvβ6 integrin in the progression of fibrosis.

6.2 Conclusion

In this study an *in vitro* and co-culture model was established. The *in vitro* model was designed to stimulate both phases of IRI whereas the co-culture model allowed studying the downstream effects of stressed epithelial cells on fibroblasts. The model was also able to examine the repair period post IRI that involves TGF-β signalling.

Lastly the use of ALK5 inhibitor and αvβ6 siRNA suggests that TGF-β has a significant role to play in the progression of renal fibrosis post IRI.

6.3 Limitations

Gene expression profile of fibrotic markers did not yield similar results as seen in protein studies. The reason for this is unclear. Furthermore, only key experiments could be replicated in HK2 cells as they were only available during the last year of my study. MRC-5 cells were used due to unavailability of a human renal fibroblast cell line.

Although several attempts were made to optimise the concentration and protocol for Western blotting using HIF-1α, this could not be performed due to excessive background staining. An attempt to create stable transfectants (HKC8 cells) overexpressing HIF-1α (for co-culture model) also failed due to excessive cell death. I also attempted to use collagen gels concentration to generate co-culture beds. However, the fibroblast cells failed to proliferate and lead to poor RNA quality and inconsistent gene expression profiling. Lastly, αvβ6 blocking peptides were used prior to using αvβ6 siRNA. However, αvβ6 blocking peptides had no effect on TGF-β production.

6.4 Future directions

Future work would emphasis on the use of β6 integrin knockout mice to study the progression of TGF-β induced renal fibrosis post IRI. This would involve examining the expression of fibrotic markers in epithelial cells and adjacent fibroblasts post inducing acute and chronic IRI in β6 integrin knockout mice versus wildtype mice. Furthermore, pharmacological blocking of αVβ6 integrin using inhibitor peptides in mice would allow validating whether inhibition of αVβ6 integrin could alter the renal microenvironment during both homeostasis and IRI leading to reduced renal injury

and improved survival. Lastly, the role of αVβ6 integrin as a biomarker of renal fibrosis would be evaluated in cells derived from patient urine.

References

Abuelo, J.G. (2007) 'Normotensive Ischemic Acute Renal Failure', *N Engl J Med*, 357, pp. 797-805.

Aitken, G.R., Roderick, P.J., Fraser, S., Mindell, J.S., O'Donoghue, D., Day, J. and Moon, G. (2014) 'Change in prevalence of chronic kidney disease in England over time: comparison of nationally representative cross-sectional surveys from 2003 to 2010', *BMJ open*, 4(9), p. e005480.

Akhurst, R.J. and Hata, A. (2012) 'Targeting the TGFβ signalling pathway in disease', *Nature reviews. Drug discovery*, 11(10), p. 790.

Allen, M.D., Thomas, G.J., Clark, S., Dawoud, M.M., Vallath, S., Payne, S.J., Gomm, J.J., Dreger, S.A., Dickinson, S. and Edwards, D.R. (2014) 'Altered microenvironment promotes progression of preinvasive breast cancer: myoepithelial expression of αvβ6 integrin in DCIS identifies high-risk patients and predicts recurrence', *Clinical Cancer Research*, 20(2), pp. 344-357.

Anathhanam, S. and Lewington, A.J. (2012) 'Acute kidney injury', *The journal of the Royal College of Physicians of Edinburgh*, 43(4), pp. 323-8; quiz 329.

Annes, J.P., Munger, J.S. and Rifkin, D.B. (2003) 'Making sense of latent TGFβ activation', *Journal of cell science*, 116(2), pp. 217-224.

Annes, J.P., Rifkin, D.B. and Munger, J.S. (2002) 'The integrin αVβ6 binds and activates latent TGFβ3', *FEBS letters*, 511(1-3), pp. 65-68.

Armogida, M., Nisticò, R. and Mercuri, N.B. (2012) 'Therapeutic potential of targeting hydrogen peroxide metabolism in the treatment of brain ischaemia', *British journal of pharmacology*, 166(4), pp. 1211-1224.

Askoxylakis, V., Millonig, G., Wirkner, U., Schwager, C., Rana, S., Altmann, A., Haberkorn, U., Debus, J., Mueller, S. and Huber, P.E. (2011) 'Investigation of tumor hypoxia using a two-enzyme system for in vitro generation of oxygen deficiency', *Radiation Oncology*, 6(1), p. 35.

Astrof, S. and Hynes, R.O. (2009) 'Fibronectins in vascular morphogenesis', *Angiogenesis*, 12(2), pp. 165-175.

Bae, S., Kang, C., Park, M., Samad, M.A., Kang, T., Ke, Q., Lee, D. and Kang, P.M. (2015) 'Hydrogen Peroxide-Responsive Nanoparticles Reduce Myocardial Ischemia/Reperfusion Injury'. Am Heart Assoc.

Bagshaw, S.M., George, C. and Bellomo, R. (2008) 'Early acute kidney injury and sepsis: a multicentre evaluation', *Critical Care*, 12(2), p. R47.

Basile, D.P., Anderson, M.D. and Sutton, T.A. (2012) 'Pathophysiology of acute kidney injury', *Comprehensive Physiology*.

Basile, D.P., Bonventre, J.V., Mehta, R., Nangaku, M., Unwin, R., Rosner, M.H., Kellum, J.A. and Ronco, C. (2015) 'Progression after AKI: understanding maladaptive repair processes to predict and identify therapeutic treatments', *Journal of the American Society of Nephrology*, p. ASN. 2015030309.

Bellomo, R., Kellum, J.A. and Ronco, C. (2012) 'Acute kidney injury', *The Lancet*, 380(9843), pp. 756-766.

Berman, A. and Kozlova, N. (1999) 'Integrins: structure and functions', *Membrane & cell biology*, 13(2), pp. 207-244.

Betensley, A., Sharif, R. and Karamichos, D. (2016) 'A systematic review of the role of dysfunctional wound healing in the pathogenesis and treatment of idiopathic pulmonary fibrosis', *Journal of clinical medicine*, 6(1), p. 2.

Bladier, C., Wolvetang, E.J., Hutchinson, P., De Haan, J.B. and Kola, I. (1997) 'Response of a primary human fibroblast cell line to H2O2: senescence-like growth arrest or apoptosis?', *Cell growth & differentiation: the molecular biology journal of the American Association for Cancer Research*, 8(5), pp. 589-598.

Blakytny, R., Ludlow, A., Martin, G.E.M., Ireland, G., Lund, L.R., Ferguson, M.W.J. and Brunner, G. (2004) 'Latent TGF-β1 activation by platelets', *Journal of cellular physiology*, 199(1), pp. 67-76.

Bocchino, M., Agnese, S., Fagone, E., Svegliati, S., Grieco, D., Vancheri, C., Gabrielli, A., Sanduzzi, A. and Avvedimento, E.V. (2010) 'Reactive oxygen species are required for maintenance and differentiation of primary lung fibroblasts in idiopathic pulmonary fibrosis', *PLoS One*, 5(11), p. e14003.

Bonventre, J.V. (2014) 'Primary proximal tubule injury leads to epithelial cell cycle arrest, fibrosis, vascular rarefaction, and glomerulosclerosis', *Kidney international supplements*, 4(1), pp. 39-44.

Bonventre, J.V. and Weinberg, J.M. (2003) 'Recent advances in the pathophysiology of ischemic acute renal failure', *Journal of the American Society of Nephrology*, 14(8), pp. 2199-2210.

Böttinger, E.P. and Bitzer, M. (2002) 'TGF-ß signaling in renal disease', *Journal of the American Society of Nephrology*, 13(10), pp. 2600-2610.

Breuss, J.M., Gallo, J., DeLisser, H.M., Klimanskaya, I.V., Folkesson, H.G., Pittet, J.F., Nishimura, S.L., Aldape, K., Landers, D.V. and Carpenter, W. (1995) 'Expression of the beta 6 integrin subunit in development, neoplasia and tissue repair suggests a role in epithelial remodeling', *Journal of cell science*, 108(6), pp. 2241-2251.

Bruick, R.K. and McKnight, S.L. (2001) 'A conserved family of prolyl-4-hydroxylases that modify HIF', *Science*, 294(5545), pp. 1337-1340.

Byfield, S.D., Major, C., Laping, N.J. and Roberts, A.B. (2004) 'SB-505124 is a selective inhibitor of transforming growth factor-β type I receptors ALK4, ALK5, and ALK7', *Molecular Pharmacology*, 65(3), pp. 744-752.

Cabello-Verrugio, C. and Brandan, E. (2007) 'A novel modulatory mechanism of transforming growth factor-β signaling through decorin and LRP-1', *Journal of Biological Chemistry*, 282(26), pp. 18842-18850.

Cagle, P.T. (2010) *Molecular pathology of lung diseases*. Springer Science & Business Media.

Camelo, A., Dunmore, R., Sleeman, M.A. and Clarke, D.L. (2013) 'The epithelium in idiopathic pulmonary fibrosis: breaking the barrier', *Frontiers in pharmacology*, 4.

Cao, Y., Yi, Z.-W., Zhang, H., Dang, X.-Q., Wu, X.-C. and Huang, A.-W. (2013) 'Etiology and outcomes of acute kidney injury in Chinese children: a prospective multicentre investigation', *BMC urology*, 13(1), p. 41.

Carden, D.L. and Granger, D.N. (2000) 'Pathophysiology of ischaemia–reperfusion injury', *The Journal of pathology*, 190(3), pp. 255-266.

Caron, A., Desrosiers, R.R. and Béliveau, R. (2005) 'Ischemia injury alters endothelial cell properties of kidney cortex: stimulation of MMP-9', *Experimental cell research*, 310(1), pp. 105-116.

Catania, J.M., Chen, G. and Parrish, A.R. (2007) 'Role of matrix metalloproteinases in renal pathophysiologies', *American Journal of Physiology-Renal Physiology*, 292(3), pp. F905-F911.

Chachami, G., Simos, G., Hatziefthimiou, A., Bonanou, S., Molyvdas, P.-A. and Paraskeva, E. (2004) 'Cobalt induces hypoxia-inducible factor-1α expression in airway smooth muscle cells by a reactive oxygen species–and PI3K-dependent mechanism', *American journal of respiratory cell and molecular biology*, 31(5), pp. 544-551.

Chaston, T.B., Matak, P., Pourvali, K., Srai, S.K., McKie, A.T. and Sharp, P.A. (2011) 'Hypoxia inhibits hepcidin expression in HuH7 hepatoma cells via decreased SMAD4 signaling', *American Journal of Physiology-Cell Physiology*, 300(4), pp. C888-C895.

Chawla, L.S., Eggers, P.W., Star, R.A. and Kimmel, P.L. (2014) 'Acute kidney injury and chronic kidney disease as interconnected syndromes', *New England Journal of Medicine*, 371(1), pp. 58-66.

Chawla, L.S. and Kimmel, P.L. (2012) 'Acute kidney injury and chronic kidney disease: an integrated clinical syndrome', *Kidney international*, 82(5), pp. 516-524.

Chen, J., Wang, G., Li, L. and Zhang, P. (2015) 'Protective effect of Astragalus polysaccharide on MRC-5 cells from oxidative damage induced by hydrogen peroxide', *Xi bao yu fen zi mian yi xue za zhi= Chinese journal of cellular and molecular immunology*, 31(8), pp. 1062-1066.

Chen, R., Jiang, T., She, Y., Xu, J., Li, C., Zhou, S., Shen, H., Shi, H. and Liu, S. (2017) 'Effects of Cobalt Chloride, a Hypoxia-Mimetic Agent, on Autophagy and Atrophy in Skeletal C2C12 Myotubes', *BioMed research international*, 2017.

Cheng, S., Pollock, A.S., Mahimkar, R., Olson, J.L. and Lovett, D.H. (2006) 'Matrix metalloproteinase 2 and basement membrane integrity: a unifying mechanism for progressive renal injury', *The FASEB journal*, 20(11), pp. 1898-1900.

Chesnoy, S. and Huang, L. (2000) 'Structure and function of lipid-DNA complexes for gene delivery', *Annual review of biophysics and biomolecular structure*, 29(1), pp. 27-47.

Chiovaro, F., Martina, E., Bottos, A., Scherberich, A., Hynes, N.E. and Chiquet-Ehrismann, R. (2015) 'Transcriptional regulation of tenascin-W by TGF-beta signaling in the bone metastatic niche of breast cancer cells', *International journal of cancer*, 137(8), pp. 1842-1854.

Cho, J., Won, K., Wu, D., Soong, Y., Liu, S., Szeto, H.H. and Hong, M.K. (2007) 'Potent mitochondria-targeted peptides reduce myocardial infarction in rats', *Coronary artery disease*, 18(3), pp. 215-220.

Chu, H.W., Balzar, S., Seedorf, G.J., Westcott, J.Y., Trudeau, J.B., Silkoff, P. and Wenzel, S.E. (2004) 'Transforming growth factor-β2 induces bronchial epithelial mucin expression in asthma', *The American journal of pathology*, 165(4), pp. 1097-1106.

Coca, S.G., Yusuf, B., Shlipak, M.G., Garg, A.X. and Parikh, C.R. (2009) 'Long-term risk of mortality and other adverse outcomes after acute kidney injury: a systematic review and meta-analysis', *American Journal of Kidney Diseases*, 53(6), pp. 961-973.

Cohn, J.N. and Tognoni, G. (2001) 'A randomized trial of the angiotensin-receptor blocker valsartan in chronic heart failure', *New England Journal of Medicine*, 345(23), pp. 1667-1675.

Cosgrove, D., Meehan, D.T., Delimont, D., Pozzi, A., Chen, X., Rodgers, K.D., Tempero, R.M., Zallocchi, M. and Rao, V.H. (2008) 'Integrin α1β1 regulates matrix metalloproteinases via P38 mitogen-activated protein kinase in mesangial cells: implications for Alport syndrome', *The American journal of pathology*, 172(3), pp. 761-773.

Dagher, P.C., Herget-Rosenthal, S., Ruehm, S.G., Jo, S.-K., Star, R.A., Agarwal, R. and Molitoris, B.A. (2003) 'Newly developed techniques to study and diagnose acute renal failure', *Journal of the American Society of Nephrology*, 14(8), pp. 2188-2198.

Dai, S., Huang, M.L., Hsu, C.Y. and Chao, K.S.C. (2003) 'Inhibition of hypoxia inducible factor 1α causes oxygen-independent cytotoxicity and induces p53 independent apoptosis in glioblastoma cells', *International Journal of Radiation Oncology* Biology* Physics*, 55(4), pp. 1027-1036.

Dai, Y., Li, W., Zhong, M., Chen, J., Liu, Y., Cheng, Q. and Li, T. (2014) 'Preconditioning and post-treatment with cobalt chloride in rat model of perinatal hypoxic–ischemic encephalopathy', *Brain and Development*, 36(3), pp. 228-240.

Danen, E.H.J. (2013) 'Integrins: an overview of structural and functional aspects'.

De Groot, H. and Rauen, U. (2007) *Transplantation proceedings*. Elsevier.

De Rosa, S., Antonelli, M. and Ronco, C. (2017) 'Hypothermia and kidney: a focus on ischaemia–reperfusion injury', *Nephrology Dialysis Transplantation*, 32(2), pp. 241-247.

Denecke, C. and Tullius, S.G. (2014) 'Innate and adaptive immune responses subsequent to ischemia-reperfusion injury in the kidney', *Progrès en urologie*, 24, pp. S13-S19.

Derynck, R. and Feng, X.-H. (1997) 'TGF-β receptor signaling', *Biochimica et Biophysica Acta (BBA)-Reviews on Cancer*, 1333(2), pp. F105-F150.

Devarajan, P. (2005) 'Cellular and molecular derangements in acute tubular necrosis', *Current opinion in pediatrics*, 17(2), pp. 193-199.

Devarajan, P. (2006) 'Update on mechanisms of ischemic acute kidney injury', *Journal of the American Society of Nephrology*, 17(6), pp. 1503-1520.

Dirkes, S.M. (2015) 'Acute kidney injury: causes, phases, and early detection', *Am Nurse Today*, 10(7), pp. 20-24.

Dutta, A., Li, J., Fedele, C., Sayeed, A., Singh, A., Violette, S.M., Manes, T.D. and Languino, L.R. (2015) 'αvβ6 integrin is required for TGFβ1-mediated matrix metalloproteinase2 expression', *Biochemical Journal*, 466(3), pp. 525-536.

Eleftheriadis, T., Liakopoulos, V., Lawson, B., Antoniadi, G., Stefanidis, I. and Galaktidou, G. (2011) 'Lipopolysaccharide and hypoxia significantly alters interleukin-8 and macrophage chemoattractant protein-1 production by human fibroblasts but not fibrosis related factors', *Hippokratia*, 15(3), p. 238.

Engel, M.E., McDonnell, M.A., Law, B.K. and Moses, H.L. (1999) 'Interdependent SMAD and JNK signaling in transforming growth factor-β-mediated transcription', *Journal of Biological Chemistry*, 274(52), pp. 37413-37420.

Fan, J.-M., Ng, Y.-Y., Hill, P.A., Nikolic-Paterson, D.J., Mu, W., Atkins, R.C. and Lan, H.Y. (1999) 'Transforming growth factor-&bgr; regulates tubular epithelial-myofibroblast transdifferentiation in vitro', *Kidney international*, 56(4), pp. 1455-1467.

Faubel, S., Ljubanovic, D., Reznikov, L., Somerset, H., Dinarello, C.A. and Edelstein, C.L. (2004) 'Caspase-1–deficient mice are protected against cisplatin-induced apoptosis and acute tubular necrosis', *Kidney international*, 66(6), pp. 2202-2213.

Fearn, A., Situmorang, G.R., Fox, C., Oakley, F., Howarth, R., Wilson, C.L., Kiosia, A., Robson, M.G., Mann, D.A. and Moles, A. (2017) 'The NF-κB1 is a key regulator of acute but not chronic renal injury', *Cell Death & Disease*, 8(6), p. e2883.

Ferenbach, D.A. and Bonventre, J.V. (2015) 'Mechanisms of maladaptive repair after AKI leading to accelerated kidney ageing and CKD', *Nature Reviews Nephrology*, 11(5), pp. 264-276.

Flaumenhaft, R., Kojima, S., Abe, M. and Rifkin, D.B. (1993) 'Activation of latent transforming growth factor ß', *Advances in pharmacology*, 24, pp. 51-76.

Frangogiannis, N.G. (2017) 'The role of transforming growth factor (TGF)-β in the infarcted myocardium', *Journal of thoracic disease*, 9(Suppl 1), p. S52.

Froese, A. (2013) 'MECHANISMS OF TGFβ ACTIVATION IN LUNG FIBROSIS'.

Ftouh, S. and Thomas, M. (2013) 'Acute kidney injury: summary of NICE guidance', *BMJ: British Medical Journal*, 347(7924).

Gagliardini, E. and Benigni, A. (2006) 'Role of anti-TGF-β antibodies in the treatment of renal injury', *Cytokine & growth factor reviews*, 17(1), pp. 89-96.

Garg, A.X. and Parikh, C.R. (2009) 'Yin and Yang: acute kidney injury and chronic kidney disease', *Journal of the American Society of Nephrology*, 20(1), pp. 8-10.

Geng, H., Lan, R., Wang, G., Siddiqi, A.R., Naski, M.C., Brooks, A.I., Barnes, J.L., Saikumar, P., Weinberg, J.M. and Venkatachalam, M.A. (2009) 'Inhibition of autoregulated TGFβ signaling simultaneously enhances proliferation and differentiation of kidney epithelium and promotes repair following renal ischemia', *The American journal of pathology*, 174(4), pp. 1291-1308.

Genome, M.C. (2016) *TGF-β Signaling*. Available at: https://www.mycancergenome.org/content/molecular-medicine/pathways/TGF-beta-signaling (Accessed: 18 Aug).

Genovese, F., Manresa, A.A., Leeming, D.J., Karsdal, M.A. and Boor, P. (2014) 'The extracellular matrix in the kidney: a source of novel non-invasive biomarkers of kidney fibrosis?', *Fibrogenesis & tissue repair*, 7(1), p. 4.

Gerritsma, J.S., van Kooten, C., Gerritsen, A.F., van Es, L.A. and Daha, M.R. (1998) 'Transforming growth factor-β1 regulates chemokine and complement production by human proximal tubular epithelial cells', *Kidney international*, 53(3), pp. 609-616.

Ghori, I., Ahmed, I., Bukhari, F. and Tohid, H. (2016) 'Cardiac Output and Renal Function: An Association', *J Cell Sci Ther*, 7(252), p. 2.

Giacomini, M.M., Travis, M.A., Kudo, M. and Sheppard, D. (2012) 'Epithelial cells utilize cortical actin/myosin to activate latent TGF-β through integrin α v β 6-dependent physical force', *Experimental cell research*, 318(6), pp. 716-722.

Giannakakis, A., Zhang, J., Jenjaroenpun, P., Nama, S., Zainolabidin, N., Aau, M.Y., Yarmishyn, A.A., Vaz, C., Ivshina, A.V. and Grinchuk, O.V. (2015) 'Contrasting expression patterns of coding and noncoding parts of the human genome upon oxidative stress', *Scientific reports*, 5.

Gilg, J., Caskey, F. and Fogarty, D. (2016) 'UK Renal Registry 18th Annual Report: Chapter 1 UK Renal Replacement Therapy Incidence in 2014: National and Centre-specific Analyses', *Nephron*, 132(Suppl. 1), pp. 9-40.

Gleizes, P.E., Munger, J.S., Nunes, I., Harpel, J.G., Mazzieri, R., Noguera, I. and Rifkin, D.B. (1997) 'TGF-β Latency: Biological Significance and Mechanisms of Activation', *Stem Cells*, 15(3), pp. 190-197.

Goligorsky, M.S., Brodsky, S.V. and Noiri, E. (2002) 'Nitric oxide in acute renal failure: NOS versus NOS', *Kidney international*, 61(3), pp. 855-861.

Gorowiec, M.R., Borthwick, L.A., Parker, S.M., Kirby, J.A., Saretzki, G.C. and Fisher, A.J. (2012) 'Free radical generation induces epithelial-to-mesenchymal transition in lung epithelium via a TGF-β1-dependent mechanism', *Free Radical Biology and Medicine*, 52(6), pp. 1024-1032.

Grande, M.T., Pérez-Barriocanal, F. and López-Novoa, J.M. (2010) 'Role of inflammation in tubulo-interstitial damage associated to obstructive nephropathy', *Journal of inflammation*, 7(1), p. 19.

Greenwald, J., Fischer, W.H., Vale, W.W. and Choe, S. (1999) 'Three-finger toxin fold for the extracellular ligand-binding domain of the type II activin receptor serine kinase', *Nature Structural & Molecular Biology*, 6(1), pp. 18-22.

Gunaratnam, L. and Bonventre, J.V. (2009) 'HIF in kidney disease and development', *Journal of the American Society of Nephrology*, 20(9), pp. 1877-1887.

Haase, V.H. (2013) 'Regulation of erythropoiesis by hypoxia-inducible factors', *Blood reviews*, 27(1), pp. 41-53.

Hahm, K., Lukashev, M.E., Luo, Y., Yang, W.J., Dolinski, B.M., Weinreb, P.H., Simon, K.J., Wang, L.C., Leone, D.R. and Lobb, R.R. (2007) 'αvβ6 integrin regulates renal fibrosis and inflammation in Alport mouse', *The American journal of pathology*, 170(1), pp. 110-125.

Hamblin, M.R. and Huang, Y. (2013) *Handbook of photomedicine*. Taylor & Francis.

Hardin, J. and Bertoni, G.P. (2015) *Becker's World of the Cell*. Pearson.

Havasi, A. and Borkan, S.C. (2011) 'Apoptosis and acute kidney injury', *Kidney international*, 80(1), pp. 29-40.

Hegde, P.S., Rajasekaran, N.S. and Chandra, T. (2005) 'Effects of the antioxidant properties of millet species on oxidative stress and glycemic status in alloxan-induced rats', *Nutrition Research*, 25(12), pp. 1109-1120.

Heikkinen, P.T., Nummela, M., Leivonen, S.-K., Westermarck, J., Hill, C.S., Kähäri, V.-M. and Jaakkola, P.M. (2010) 'Hypoxia-activated Smad3-specific dephosphorylation by PP2A', *Journal of Biological Chemistry*, 285(6), pp. 3740-3749.

Henderson, N.C. and Sheppard, D. (2013) 'Integrin-mediated regulation of TGFβ in fibrosis', *Biochimica et Biophysica Acta (BBA)-Molecular Basis of Disease*, 1832(7), pp. 891-896.

Heyman, S.N., Khamaisi, M., Rosen, S. and Rosenberger, C. (2008) 'Renal parenchymal hypoxia, hypoxia response and the progression of chronic kidney disease', *American journal of nephrology*, 28(6), pp. 998-1006.

Higgins, D.F., Kimura, K., Bernhardt, W.M., Shrimanker, N., Akai, Y., Hohenstein, B., Saito, Y., Johnson, R.S., Kretzler, M. and Cohen, C.D. (2007) 'Hypoxia promotes fibrogenesis in vivo via HIF-1 stimulation of epithelial-to-mesenchymal transition', *The Journal of clinical investigation*, 117(12), pp. 3810-3820.

Hinck, A.P. (2012) 'Structural studies of the TGF-βs and their receptors–insights into evolution of the TGF-β superfamily', *FEBS letters*, 586(14), pp. 1860-1870.

Hirko, A., Tang, F. and Hughes, J.A. (2003) 'Cationic lipid vectors for plasmid DNA delivery', *Current medicinal chemistry*, 10(14), pp. 1185-1193.

Hocevar, B.A. and Howe, P.H. (2000) 'Analysis of TGFβ-mediated synthesis of extracellular matrix components', *Transforming Growth Factor-Beta Protocols*, pp. 55-65.

Hood, J.D. and Cheresh, D.A. (2002) 'Role of integrins in cell invasion and migration', *Nature Reviews Cancer*, 2(2), pp. 91-100.

Horiguchi, M., Ota, M. and Rifkin, D.B. (2012) 'Matrix control of transforming growth factor-β function', *Journal of biochemistry*, 152(4), pp. 321-329.

Hoste, E.A.J. and De Corte, W. (2012) 'Clinical consequences of acute kidney injury', in *Controversies in Acute Kidney Injury*. Karger Publishers, pp. 56-64.

Hoste, E.A.J. and Schurgers, M. (2008) 'Epidemiology of acute kidney injury: how big is the problem?', *Critical care medicine*, 36(4), pp. S146-S151.

Hsieh, L.T.-H., Nastase, M.-V., Zeng-Brouwers, J., Iozzo, R.V. and Schaefer, L. (2014) 'Soluble biglycan as a biomarker of inflammatory renal diseases', *The international journal of biochemistry & cell biology*, 54, pp. 223-235.

Humphreys, B.D., Valerius, M.T., Kobayashi, A., Mugford, J.W., Soeung, S., Duffield, J.S., McMahon, A.P. and Bonventre, J.V. (2008) 'Intrinsic epithelial cells repair the kidney after injury', *Cell stem cell*, 2(3), pp. 284-291.

Hynes, R.O. (2002) 'Integrins: bidirectional, allosteric signaling machines', *Cell*, 110(6), pp. 673-687.

Inker, L.A., Astor, B.C., Fox, C.H., Isakova, T., Lash, J.P., Peralta, C.A., Tamura, M.K. and Feldman, H.I. (2014) 'KDOQI US commentary on the 2012 KDIGO clinical practice guideline for the evaluation and management of CKD', *American Journal of Kidney Diseases*, 63(5), pp. 713-735.

Itoh, S., Itoh, F., Goumans, M.J. and ten Dijke, P. (2000) 'Signaling of transforming growth factor-β family members through Smad proteins', *European Journal of Biochemistry*, 267(24), pp. 6954-6967.

Jaakkola, P., Mole, D.R., Tian, Y.-M., Wilson, M.I., Gielbert, J., Gaskell, S.J., von Kriegsheim, A., Hebestreit, H.F., Mukherji, M. and Schofield, C.J. (2001) 'Targeting of HIF-α to the von Hippel-Lindau ubiquitylation complex by O2-regulated prolyl hydroxylation', *Science*, 292(5516), pp. 468-472.

Janssens, K., ten Dijke, P., Ralston, S.H., Bergmann, C. and Van Hul, W. (2003) 'Transforming growth factor-β1 mutations in Camurati-Engelmann disease lead to increased signaling by

altering either activation or secretion of the mutant protein', *Journal of Biological Chemistry*, 278(9), pp. 7718-7724.

Jeong, K.H., Lee, T.W., Ihm, C.G., Lee, S.H., Moon, J.Y. and Lim, S.J. (2008) 'Effects of sildenafil on oxidative and inflammatory injuries of the kidney in streptozotocin-induced diabetic rats', *American journal of nephrology*, 29(3), pp. 274-282.

Jha, V., Garcia-Garcia, G., Iseki, K., Li, Z., Naicker, S., Plattner, B., Saran, R., Wang, A.Y.-M. and Yang, C.-W. (2013) 'Chronic kidney disease: global dimension and perspectives', *The Lancet*, 382(9888), pp. 260-272.

Jiao, G., Pan, B., Zhou, Z., Zhou, L., Li, Z. and Zhang, Z. (2015) 'MicroRNA‐21 regulates cell proliferation and apoptosis in H2O2‐stimulated rat spinal cord neurons', *Molecular medicine reports*, 12(5), pp. 7011-7016.

Just, A. (2007) 'Mechanisms of renal blood flow autoregulation: dynamics and contributions', *American Journal of Physiology-Regulatory, Integrative and Comparative Physiology*, 292(1), pp. R1-R17.

Kagami, S., Border, W.A., Miller, D.E. and Noble, N.A. (1994) 'Angiotensin II stimulates extracellular matrix protein synthesis through induction of transforming growth factor-beta expression in rat glomerular mesangial cells', *Journal of Clinical Investigation*, 93(6), p. 2431.

Kanbay, M., Kasapoglu, B. and Perazella, M.A. (2010) 'Acute tubular necrosis and pre-renal acute kidney injury: utility of urine microscopy in their evaluation-a systematic review', *International urology and nephrology*, 42(2), pp. 425-433.

Kanwar, Y.S. (2012) 'TGF-β and renal fibrosis: a Pandora's box of surprises', *The American journal of pathology*, 181(4), pp. 1147-1150.

Kapoor, R., Kirby, J., Logan, I. and Sheerin, N. (2016) 'MP178ISCHEMIA REPERFUSION INJURY INDUCES A PRO-FIBROTIC PHENOTYPE IN HUMAN PROXIMAL TUBULAR EPITHELIAL CELLS', *Nephrology Dialysis Transplantation*, 31(suppl 1), pp. i400-i401.

Ke, Q. and Costa, M. (2006) 'Hypoxia-inducible factor-1 (HIF-1)', *Molecular pharmacology*, 70(5), pp. 1469-1480.

Khalil, N. (1999) 'TGF-β: from latent to active', *Microbes and Infection*, 1(15), pp. 1255-1263.

Kilbride, H. 'Clinical Review: Acute kidney injury'.

Kim, J.Y., Ghee, J.Y., Lim, S.W., Piao, S.G., Chung, B.H., Yoon, H.E., Hwang, H.S., Choi, B.S., Kim, J. and Yang, C.W. (2012) 'Comparison of early and late conversion of sirolimus in experimental model of chronic cyclosporine nephropathy', *Journal of Korean medical science*, 27(2), pp. 160-169.

Kim, T.K. and Eberwine, J.H. (2010) 'Mammalian cell transfection: the present and the future', *Analytical and bioanalytical chemistry*, 397(8), pp. 3173-3178.

Koeners, M.P., Vink, E.E., Kuijper, A., Gadellaa, N., Rosenberger, C., Mathia, S., van den Meiracker, A.H., Garrelds, I.M., Blankestijn, P.J. and Joles, J.A. (2014) 'Stabilization of hypoxia inducible factor-1α ameliorates acute renal neurogenic hypertension', *Journal of hypertension*, 32(3), pp. 587-597.

Kojima, I., Tanaka, T., Inagi, R., Kato, H., Yamashita, T., Sakiyama, A., Ohneda, O., Takeda, N., Sata, M. and Miyata, T. (2007) 'Protective role of hypoxia-inducible factor-2α against ischemic damage and oxidative stress in the kidney', *Journal of the American Society of Nephrology*, 18(4), pp. 1218-1226.

Kong, D., Zhang, F., Shao, J., Wu, L., Zhang, X., Chen, L., Lu, Y. and Zheng, S. (2015) 'Curcumin inhibits cobalt chloride-induced epithelial-to-mesenchymal transition associated with interference with TGF-β/Smad signaling in hepatocytes', *Laboratory Investigation*.

Kosieradzki, M. and Rowiński, W. (2008) *Transplantation proceedings*. Elsevier.

Kracklauer, M.P., Schmidt, C. and Sclabas, G.M. (2003) 'TGFβ 1 signaling via α V β 6 integrin', *Molecular cancer*, 2(1), p. 28.

Kreidberg, J.A. (2003) 'Podocyte differentiation and glomerulogenesis', *Journal of the American Society of Nephrology*, 14(3), pp. 806-814.

Kugler, A. (1998) 'Matrix metalloproteinases and their inhibitors', *Anticancer research*, 19(2C), pp. 1589-1592.

Kunugi, S., Shimizu, A., Kuwahara, N., Du, X., Takahashi, M., Terasaki, Y., Fujita, E., Mii, A., Nagasaka, S. and Akimoto, T. (2011) 'Inhibition of matrix metalloproteinases reduces ischemia-reperfusion acute kidney injury', *Laboratory Investigation*, 91(2), pp. 170-180.

Kurian, G.A. and Pemaih, B. (2014) 'Standardization of in vitro cell-based model for renal ischemia and reperfusion injury', *Indian journal of pharmaceutical sciences*, 76(4), p. 348.

Kusakabe, M., Cheong, P.L., Nikfar, R., McLennan, I.S. and Koishi, K. (2008) 'The structure of the TGF-β latency associated peptide region determines the ability of the proprotein convertase furin to cleave TGF-βs', *Journal of cellular biochemistry*, 103(1), pp. 311-320.

Lafrance, J.-P. and Miller, D.R. (2010) 'Acute kidney injury associates with increased long-term mortality', *Journal of the American Society of Nephrology*, 21(2), pp. 345-352.

Lan, H.Y. (2003) 'Tubular epithelial-myofibroblast transdifferentiation mechanisms in proximal tubule cells', *Current opinion in nephrology and hypertension*, 12(1), pp. 25-29.

Lan, H.Y. (2011) 'Diverse roles of TGF-beta/Smads in renal fibrosis and inflammation', *Int J Biol Sci*, 7(7), pp. 1056-1067.

Lan, H.Y., Mu, W., Tomita, N., Huang, X.R., Li, J.H., Zhu, H.-J., Morishita, R. and Johnson, R.J. (2003) 'Inhibition of renal fibrosis by gene transfer of inducible Smad7 using ultrasound-microbubble system in rat UUO model', *Journal of the American Society of Nephrology*, 14(6), pp. 1535-1548.

Lawler, J. (2002) 'Thrombospondin-1 as an endogenous inhibitor of angiogenesis and tumor growth', *Journal of cellular and molecular medicine*, 6(1), pp. 1-12.

Lee, K.E., Kim, E.Y., Kim, C.S., Choi, J.S., Bae, E.H., Ma, S.K., Park, J.S., Do Jung, Y., Kim, S.H. and Lee, J.U. (2013) 'Macrophage-stimulating protein attenuates hydrogen peroxide-induced apoptosis in human renal HK-2 cells', *European journal of pharmacology*, 715(1), pp. 304-311.

Leonard, M.O., Cottell, D.C., Godson, C., Brady, H.R. and Taylor, C.T. (2003) 'The role of HIF-1α in transcriptional regulation of the proximal tubular epithelial cell response to hypoxia', *Journal of Biological Chemistry*, 278(41), pp. 40296-40304.

Levey, A.S., Eckardt, K.-U., Tsukamoto, Y., Levin, A., Coresh, J., Rossert, J., Zeeuw, D.D.E., Hostetter, T.H., Lameire, N. and Eknoyan, G. (2005) 'Definition and classification of chronic kidney disease: a position statement from Kidney Disease: Improving Global Outcomes (KDIGO)', *Kidney international*, 67(6), pp. 2089-2100.

Li, H., Sekine, M., Seng, S., Avraham, S. and Avraham, H.K. (2009) 'BRCA1 Interacts with Smad3 and Regulates Smad3-Mediated TGF-β Signaling during Oxidative Stress Responses', *PloS one*, 4(9), p. e7091.

Li, R.X., Yiu, W.H. and Tang, S.C.W. (2015) 'Role of bone morphogenetic protein-7 in renal fibrosis', *Frontiers in physiology*, 6.

Lièvre, V., Becuwe, P., Bianchi, A., Koziel, V., Franck, P., Schroeder, H., Nabet, P., Dauça, M. and Daval, J.-L. (2000) 'Free radical production and changes in superoxide dismutases associated with hypoxia/reoxygenation-induced apoptosis of embryonic rat forebrain neurons in culture', *Free Radical Biology and Medicine*, 29(12), pp. 1291-1301.

Liu, A., Dardik, A. and Ballermann, B.J. (1999) 'Neutralizing TGF-β1 antibody infusion in neonatal rat delays in vivo glomerular capillary formation', *Kidney international*, 56(4), pp. 1334-1348.

Liu, Y. (2010) 'New insights into epithelial-mesenchymal transition in kidney fibrosis', *Journal of the American Society of Nephrology*, 21(2), pp. 212-222.

Lo, R.S. and Massagué, J. (1999) 'Ubiquitin-dependent degradation of TGF-&bgr;-activated Smad2', *Nature Cell Biology*, 1(8), pp. 472-478.

Lowell, C.A. and Mayadas, T.N. (2012) 'Overview: studying integrins in vivo', *Integrin and Cell Adhesion Molecules: Methods and Protocols*, pp. 369-397.

Luo, D., Guan, Q., Wang, K., Nguan, C.Y.C. and Du, C. (2017) 'TGF-β1 stimulates movement of renal proximal tubular epithelial cells in a three-dimensional cell culture via an autocrine TGF-β2 production', *Experimental Cell Research*, 350(1), pp. 132-139.

M Teoh, C., Sl Tan, S. and Tran, T. (2015) 'Integrins as Therapeutic Targets for Respiratory Diseases', *Current molecular medicine*, 15(8), pp. 714-734.

Ma, C. and Chegini, N. (1999) 'Regulation of matrix metalloproteinases (MMPs) and their tissue inhibitors in human myometrial smooth muscle cells by TGF-β1', *Molecular human reproduction*, 5(10), pp. 950-954.

Ma, L.-J., Yang, H., Gaspert, A., Carlesso, G., Barty, M.M., Davidson, J.M., Sheppard, D. and Fogo, A.B. (2003) 'Transforming growth factor-β-dependent and-independent pathways of induction of tubulointerstitial fibrosis in β6−/− mice', *The American journal of pathology*, 163(4), pp. 1261-1273.

Mahmood, T. and Yang, P.-C. (2012) 'Western blot: technique, theory, and trouble shooting', *North American journal of medical sciences*, 4(9), p. 429.

Malek, M. and Nematbakhsh, M. (2015) 'Renal ischemia/reperfusion injury; from pathophysiology to treatment', *Journal of renal injury prevention*, 4(2), p. 20.

Marthandan, S., Menzel, U., Priebe, S., Groth, M., Guthke, R., Platzer, M., Hemmerich, P., Kaether, C. and Diekmann, S. (2016) 'Conserved genes and pathways in primary human fibroblast strains undergoing replicative and radiation induced senescence', *Biological research*, 49(1), p. 34.

Marthandan, S., Priebe, S., Baumgart, M., Groth, M., Cellerino, A., Guthke, R., Hemmerich, P. and Diekmann, S. (2015) 'Similarities in gene expression profiles during in vitro aging of primary human embryonic lung and foreskin fibroblasts', *BioMed research international*, 2015.

Mathieu, J., Zhou, W., Xing, Y., Sperber, H., Ferreccio, A., Agoston, Z., Kuppusamy, K.T., Moon, R.T. and Ruohola-Baker, H. (2014) 'Hypoxia-inducible factors have distinct and stage-specific roles during reprogramming of human cells to pluripotency', *Cell stem cell*, 14(5), pp. 592-605.

McCarty, M.F. (2006) 'Adjuvant strategies for prevention of glomerulosclerosis', *Medical hypotheses*, 67(6), pp. 1277-1296.

McClintock, D.S., Santore, M.T., Lee, V.Y., Brunelle, J., Budinger, G.R.S., Zong, W.-X., Thompson, C.B., Hay, N. and Chandel, N.S. (2002) 'Bcl-2 family members and functional electron transport chain regulate oxygen deprivation-induced cell death', *Molecular and cellular biology*, 22(1), pp. 94-104.

Meng, X.-M., Chung, A.C.K. and Lan, H.Y. (2013) 'Role of the TGF-β/BMP-7/Smad pathways in renal diseases', *Clinical science*, 124(4), pp. 243-254.

Midwood, K.S., Williams, L.V. and Schwarzbauer, J.E. (2004) 'Tissue repair and the dynamics of the extracellular matrix', *The international journal of biochemistry & cell biology*, 36(6), pp. 1031-1037.

Molitoris, B.A., Levin, A., Warnock, D.G., Joannidis, M., Mehta, R.L., Kellum, J.A., Ronco, C. and Shah, S.V. (2007) 'Improving outcomes of acute kidney injury: report of an initiative', *Nature clinical practice Nephrology*, 3(8), pp. 439-442.

Moll, S., Ebeling, M., Weibel, F., Farina, A., Del Rosario, A.A., Hoflack, J.C., Pomposiello, S. and Prunotto, M. (2013) 'Epithelial cells as active player in fibrosis: findings from an in vitro model', *PloS one*, 8(2), p. e56575.

Moore, K.M., Thomas, G.J., Duffy, S.W., Warwick, J., Gabe, R., Chou, P., Ellis, I.O., Green, A.R., Haider, S. and Brouilette, K. (2014) 'Therapeutic targeting of integrin αvβ6 in breast cancer', *Journal of the National Cancer Institute*, 106(8), p. dju169.

Morrisey, K., Evans, R.A., Wakefield, L. and Phillips, A.O. (2001) 'Translational regulation of renal proximal tubular epithelial cell transforming growth factor-β1 generation by insulin', *The American journal of pathology*, 159(5), pp. 1905-1915.

Moustakas, A. and Heldin, P. (2014) 'TGFβ and matrix-regulated epithelial to mesenchymal transition', *Biochimica et Biophysica Acta (BBA)-General Subjects*, 1840(8), pp. 2621-2634.

Moustakas, A., Souchelnytskyi, S. and Heldin, C.-H. (2001) 'Smad regulation in TGF-β signal transduction', *Journal of cell science*, 114(24), pp. 4359-4369.

Mune, M., Otani, H. and Yukawa, S. (2002) 'Effects of antioxidants on kidney disease', *Mechanisms of ageing and development*, 123(8), pp. 1041-1046.

Munger, J.S., Huang, X., Kawakatsu, H., Griffiths, M.J.D., Dalton, S.L., Wu, J., Pittet, J.-F., Kaminski, N., Garat, C. and Matthay, M.A. (1999) 'A Mechanism for Regulating Pulmonary Inflammation and Fibrosis: The Integrin αvβ6 Binds and Activates Latent TGF β1', *Cell*, 96(3), pp. 319-328.

Munshi, R., Hsu, C. and Himmelfarb, J. (2011) 'Advances in understanding ischemic acute kidney injury', *BMC medicine*, 9(1), p. 11.

Murugan, R. and Kellum, J.A. (2011) 'Acute kidney injury: what's the prognosis?', *Nature Reviews Nephrology*, 7(4), pp. 209-217.

Nakamura, J., Purvis, E.R. and Swenberg, J.A. (2003) 'Micromolar concentrations of hydrogen peroxide induce oxidative DNA lesions more efficiently than millimolar concentrations in mammalian cells', *Nucleic acids research*, 31(6), pp. 1790-1795.

Nakao, A. (2006) 'Inhibitory Smads: Mechanisms of Action and Roles in Human Diseases', in *Smad Signal Transduction*. Springer, pp. 379-395.

Nakao, A., Fujii, M., Matsumura, R., Kumano, K., Saito, Y., Miyazono, K. and Iwamoto, I. (1999) 'Transient gene transfer and expression of Smad7 prevents bleomycin-induced lung fibrosis in mice', *The Journal of clinical investigation*, 104(1), pp. 5-11.

Niu, W., Liu, X., Zhang, Z., Xu, K., Chen, R., Liu, E., Wang, J., Peng, C. and Niu, J. (2010) 'Effects of αvβ6 gene silencing by RNA interference in PANC-1 pancreatic carcinoma cells', *Anticancer research*, 30(1), pp. 135-142.

Nocera, M. and CHU, T. (1995) 'Characterization of Latent Transforming Growth Factor-β From Human Seminal Plasma', *American Journal of Reproductive Immunology*, 33(4), pp. 282-291.

Nony, P.A. and Schnellmann, R.G. (2003) 'Mechanisms of renal cell repair and regeneration after acute renal failure', *Journal of Pharmacology and Experimental Therapeutics*, 304(3), pp. 905-912.

Norman, J.T., Clark, I.M. and Garcia, P.L. (2000) 'Hypoxia promotes fibrogenesis in human renal fibroblasts', *Kidney international*, 58(6), pp. 2351-2366.

Okada, H. and Kalluri, R. (2005) 'Cellular and molecular pathways that lead to progression and regression of renal fibrogenesis', *Current molecular medicine*, 5(5), pp. 467-474.

Ostermann, M. and Joannidis, M. (2016) 'Acute kidney injury 2016: diagnosis and diagnostic workup', *Critical Care*, 20(1), p. 299.

Oxburgh, L. and de Caestecker, M.P. (2012) 'Ischemia–Reperfusion Injury of the Mouse Kidney', *Kidney Development: Methods and Protocols*, pp. 363-379.

Padanilam, B.J. (2003) 'Cell death induced by acute renal injury: a perspective on the contributions of apoptosis and necrosis', *American Journal of Physiology-Renal Physiology*, 284(4), pp. F608-F627.

Pasqualini, R., Bodorova, J., Ye, S. and Hemler, M.E. (1993) 'A study of the structure, function and distribution of beta 5 integrins using novel anti-beta 5 monoclonal antibodies', *Journal of Cell Science*, 105(1), pp. 101-111.

Pelton, R.W., Saxena, B., Jones, M., Moses, H.L. and Gold, L.I. (1991) 'Immunohistochemical localization of TGF beta 1, TGF beta 2, and TGF beta 3 in the mouse embryo: expression patterns suggest multiple roles during embryonic development', *The Journal of cell biology*, 115(4), pp. 1091-1105.

Phanish, M.K., Wahab, N.A., Colville-Nash, P., Hendry, B.M. and Dockrell, M.E.C. (2006) 'The differential role of Smad2 and Smad3 in the regulation of pro-fibrotic TGFβ1 responses in human proximal-tubule epithelial cells', *Biochemical Journal*, 393(2), pp. 601-607.

Pozzi, A. and Zent, R. (2011) 'TGF-β Sequestration by Mesangial Cell Integrin αvβ8', *The American journal of pathology*, 178(2), pp. 485-489.

Prunotto, M., Ghiggeri, G., Bruschi, M., Gabbiani, G., Lescuyer, P., Hocher, B., Chaykovska, L., Berrera, M. and Moll, S. (2011) 'Renal fibrosis and proteomics: current knowledge and still

key open questions for proteomic investigation', *Journal of proteomics*, 74(10), pp. 1855-1870.

Racusen, L.C., Monteil, C., Sgrignoli, A., Lucskay, M., Marouillat, S., Rhim, J.G. and Morin, J.-p. (1997) 'Cell lines with extended in vitro growth potential from human renal proximal tubule: characterization, response to inducers, and comparison with established cell lines', *Journal of Laboratory and Clinical Medicine*, 129(3), pp. 318-329.

Raghnaill, M.N., Bramini, M., Ye, D., Couraud, P.-O., Romero, I.A., Weksler, B., Åberg, C., Salvati, A., Lynch, I. and Dawson, K.A. (2014) 'Paracrine signalling of inflammatory cytokines from an in vitro blood brain barrier model upon exposure to polymeric nanoparticles', *Analyst*, 139(5), pp. 923-930.

Rahman, M., Shad, F. and Smith, M.C. (2012) 'Acute kidney injury: a guide to diagnosis and management', *American family physician*, 86(7).

Rakesh, S.U., Patil, P.R. and Mane, S.R. (2010) 'Use of natural antioxidants to scavenge free radicals: A major cause of diseases', *Int. J. Pharm. Tech. Res*, 2, pp. 1074-1081.

Ramamoorthy, P. and Shi, H. (2014) 'Ischemia induces different levels of hypoxia inducible factor-1α protein expression in interneurons and pyramidal neurons', *Acta neuropathologica communications*, 2(1), p. 51.

Rashid, M. and Schwartz, G.J. (2012) 'Overview, structure and function of the nephron', in *Pediatric Critical Care Study Guide*. Springer, pp. 133-168.

Rayner, H., Thomas, M. and Milford, D. (2016) 'Kidney Anatomy and Physiology', in *Understanding Kidney Diseases*. Springer, pp. 1-10.

Reiser, J. and Sever, S. (2013) 'Podocyte biology and pathogenesis of kidney disease', *Annual review of medicine*, 64, p. 357.

Renal, A. (2014) 'UK Renal Registry 14 th Annual Report', *UK Renal Registry*.

Rhyu, D.Y., Yang, Y., Ha, H., Lee, G.T., Song, J.S., Uh, S.-t. and Lee, H.B. (2005) 'Role of reactive oxygen species in TGF-β1-induced mitogen-activated protein kinase activation and epithelial-mesenchymal transition in renal tubular epithelial cells', *Journal of the American Society of Nephrology*, 16(3), pp. 667-675.

Rizzo, D.C. (2015) *Fundamentals of anatomy and physiology*. Cengage Learning.

Romeo, S., Sannino, A., Scarfì, M.R., Massa, R., d'Angelo, R. and Zeni, O. (2016) 'Lack of effects on key cellular parameters of MRC-5 human lung fibroblasts exposed to 370 mT static magnetic field', *Scientific reports*, 6, p. 19398.

Rosenberger, C., Mandriota, S., Jürgensen, J.S., Wiesener, M.S., Hörstrup, J.H., Frei, U., Ratcliffe, P.J., Maxwell, P.H., Bachmann, S. and Eckardt, K.-U. (2002) 'Expression of hypoxia-inducible factor-1α and-2α in hypoxic and ischemic rat kidneys', *Journal of the American Society of Nephrology*, 13(7), pp. 1721-1732.

Ruoslahti, E. (1991) 'Integrins', *Journal of Clinical Investigation*, 87(1), p. 1.

Russ, A.L., Haberstroh, K.M. and Rundell, A.E. (2007) 'Experimental strategies to improve in vitro models of renal ischemia', *Experimental and molecular pathology*, 83(2), pp. 143-159.

Ruthenborg, R.J., Ban, J.-J., Wazir, A., Takeda, N. and Kim, J.-w. (2014) 'Regulation of wound healing and fibrosis by hypoxia and hypoxia-inducible factor-1', *Molecules and cells*, 37(9), pp. 637-643.

Ryan, M.J., Johnson, G., Kirk, J., Fuerstenberg, S.M., Zager, R.A. and Torok-Storb, B. (1994) 'HK-2: an immortalized proximal tubule epithelial cell line from normal adult human kidney', *Kidney international*, 45(1), pp. 48-57.

Sánchez-Elsner, T., Ramírez, J.R., Rodriguez-Sanz, F., Varela, E., Bernabéu, C. and Botella, L.M. (2004) 'A cross-talk between hypoxia and TGF-β orchestrates erythropoietin gene regulation through SP1 and Smads', *Journal of molecular biology*, 336(1), pp. 9-24.

Saxena, S., Shukla, D. and Bansal, A. (2012) 'Augmentation of aerobic respiration and mitochondrial biogenesis in skeletal muscle by hypoxia preconditioning with cobalt chloride', *Toxicology and applied pharmacology*, 264(3), pp. 324-334.

Schiffer, M., Bitzer, M., Roberts, I.S., Kopp, J.B., ten Dijke, P., Mundel, P. and Böttinger, E.P. (2001) 'Apoptosis in podocytes induced by TGF-β and Smad7', *The Journal of clinical investigation*, 108(6), pp. 807-816.

Schrier, R.W., Wang, W., Poole, B. and Mitra, A. (2004) 'Acute renal failure: definitions, diagnosis, pathogenesis, and therapy', *The Journal of clinical investigation*, 114(1), pp. 5-14.

Semenza, G.L. (2000) 'HIF-1: mediator of physiological and pathophysiological responses to hypoxia', *Journal of applied physiology*, 88(4), pp. 1474-1480.

Semenza, G.L. (2001) 'HIF-1 and mechanisms of hypoxia sensing', *Current opinion in cell biology*, 13(2), pp. 167-171.

Semenza, G.L. (2003) 'Targeting HIF-1 for cancer therapy', *Nature reviews cancer*, 3(10), pp. 721-732.

Semenza, G.L. (2004) 'Hydroxylation of HIF-1: oxygen sensing at the molecular level', *Physiology*, 19(4), pp. 176-182.

Semenza, G.L., Agani, F., Booth, G., Forsythe, J., Iyer, N., Jiang, B.-H., Leung, S., Roe, R., Wiener, C. and Yu, A. (1997) 'Structural and functional analysis of hypoxia-inducible factor 1', *Kidney international*, 51(2), pp. 553-555.

Shah, Y.M. and Xie, L. (2014) 'Hypoxia-inducible factors link iron homeostasis and erythropoiesis', *Gastroenterology*, 146(3), pp. 630-642.

Shen, Y., Miao, N.-j., Xu, J.-l., Gan, X.-x., Xu, D., Zhou, L., Xue, H., Zhang, W. and Lu, L.-m. (2016) 'N-acetylcysteine alleviates angiotensin II-mediated renal fibrosis in mouse obstructed kidneys', *Acta Pharmacologica Sinica*.

Shimizu, T., Kuroda, T., Hata, S., Fukagawa, M., Margolin, S.B. and Kurokawa, K. (1998) 'Pirfenidone improves renal function and fibrosis in the post-obstructed kidney', *Kidney international*, 54(1), pp. 99-109.

Singer, E., Elger, A., Elitok, S., Kettritz, R., Nickolas, T.L., Barasch, J., Luft, F.C. and Schmidt-Ott, K.M. (2011) 'Urinary neutrophil gelatinase-associated lipocalin distinguishes pre-renal from intrinsic renal failure and predicts outcomes', *Kidney international*, 80(4), pp. 405-414.

Sirard, C., Kim, S., Mirtsos, C., Tadich, P., Hoodless, P.A., Itié, A., Maxson, R., Wrana, J.L. and Mak, T.W. (2000) 'Targeted disruption in murine cells reveals variable requirement for Smad4 in transforming growth factor β-related signaling', *Journal of Biological Chemistry*, 275(3), pp. 2063-2070.

Sitte, N., Merker, K. and Grune, T. (1998) 'Proteasome-dependent degradation of oxidized proteins in MRC-5 fibroblasts', *FEBS letters*, 440(3), pp. 399-402.

Song, K.-H., Cho, S.-J. and Song, J.-Y. (2016) 'αvβ1 integrin as a novel therapeutic target for tissue fibrosis', *Annals of translational medicine*, 4(20).

Sporn, M.B. and Roberts, A.B. (1992) 'Transforming growth factor-beta: recent progress and new challenges', *The Journal of cell biology*, 119(5), pp. 1017-1021.

Springer, T.A. and Wang, J.-H. (2004) 'The three-dimensional structure of integrins and their ligands, and conformational regulation of cell adhesion', *Advances in protein chemistry*, 68, pp. 29-63.

Stevens, P.E., de Lusignan, S., Farmer, C.K.T. and Tomson, C.R.V. (2012) 'Engaging primary care in CKD initiatives: the UK experience', *Nephrology Dialysis Transplantation*, 27(suppl 3), pp. iii5-iii11.

Sutton, T.A. (2009) 'Alteration of microvascular permeability in acute kidney injury', *Microvascular research*, 77(1), pp. 4-7.

Sutton, T.A., Fisher, C.J. and Molitoris, B.A. (2002) 'Microvascular endothelial injury and dysfunction during ischemic acute renal failure', *Kidney international*, 62(5), pp. 1539-1549.

Szeto, H.H., Liu, S., Soong, Y., Wu, D., Darrah, S.F., Cheng, F.-Y., Zhao, Z., Ganger, M., Tow, C.Y. and Seshan, S.V. (2011) 'Mitochondria-targeted peptide accelerates ATP recovery and reduces ischemic kidney injury', *Journal of the American Society of Nephrology*, 22(6), pp. 1041-1052.

Tan, X., Li, Y. and Liu, Y. (2007) 'Therapeutic role and potential mechanisms of active Vitamin D in renal interstitial fibrosis', *The Journal of steroid biochemistry and molecular biology*, 103(3), pp. 491-496.

Tatler, A.L., Saini, G., Goodwin, A., Gbolohan, O., Clifford, R.L., Al'Hourani, M., Porte, J., Violette, S., Weinreb, P. and Knox, A. (2012) 'S69 transcriptional mechanisms regulating expression of the Avb6 integrin in IPF', *Thorax*, 67(Suppl 2), pp. A34-A35.

Teramoto, S., Tomita, T., Matsui, H., Ohga, E., Matsuse, T. and Ouchi, Y. (2001) 'Hydrogen peroxide-induced apoptosis and necrosis in human lung fibroblasts: protective roles of glutathione', *The Japanese Journal of Pharmacology*, 79(1), pp. 33-40.

Thomas, M., Davies, A. and Dawnay, A. (2013) 'Acute kidney injury prevention, detection and management of acute kidney injury up to the point of renal replacement therapy', *NICE Clinical Guidelines.(August)*.

Tian, Y.-C., Fraser, D., Attisano, L. and Phillips, A.O. (2003) 'TGF-β1-mediated alterations of renal proximal tubular epithelial cell phenotype', *American Journal of Physiology-Renal Physiology*, 285(1), pp. F130-F142.

Tian, Y.-C. and Phillips, A.O. (2003) 'TGF-β1–Mediated Inhibition of HK-2 Cell Migration', *Journal of the American Society of Nephrology*, 14(3), pp. 631-640.

Trevillian, P., Paul, H., Millar, E., Hibberd, A. and Agrez, M.V. (2004) 'α v β 6 Integrin expression in diseased and transplanted kidneys', *Kidney international*, 66(4), pp. 1423-1433.

Turman, M.A. and Bates, C.M. (1997) 'Susceptibility of human proximal tubular cells to hypoxia: effect of hypoxic preconditioning and comparison to glomerular cells', *Renal failure*, 19(1), pp. 47-60.

Ucero, A.C., Benito-Martin, A., Fuentes-Calvo, I., Santamaria, B., Blanco, J., Lopez-Novoa, J.M., Ruiz-Ortega, M., Egido, J., Burkly, L.C. and Martinez-Salgado, C. (2013) 'TNF-related weak inducer of apoptosis (TWEAK) promotes kidney fibrosis and Ras-dependent

proliferation of cultured renal fibroblast', *Biochimica et Biophysica Acta (BBA)-Molecular Basis of Disease*, 1832(10), pp. 1744-1755.

Uchida, K., Nitta, K., Kobayashi, H., Kawachi, H., Shimizu, F., Yumura, W. and Nihei, H. (2000) 'Localization of Smad6 and Smad7 in the rat kidney and their regulated expression in the anti-Thy-1 nephritis', *Molecular Cell Biology Research Communications*, 4(2), pp. 98-105.

Veerasamy, M., Nguyen, T.Q., Motazed, R., Pearson, A.L., Goldschmeding, R. and Dockrell, M.E. (2009) 'Differential regulation of E-cadherin and α-smooth muscle actin by BMP 7 in human renal proximal tubule epithelial cells and its implication in renal fibrosis', *American Journal of Physiology-Renal Physiology*, 297(5), pp. F1238-F1248.

Vengellur, A. and LaPres, J.J. (2004) 'The role of hypoxia inducible factor 1α in cobalt chloride induced cell death in mouse embryonic fibroblasts', *Toxicological Sciences*, 82(2), pp. 638-646.

Venkatachalam, M.A., Griffin, K.A., Lan, R., Geng, H., Saikumar, P. and Bidani, A.K. (2010) 'Acute kidney injury: a springboard for progression in chronic kidney disease', *American Journal of Physiology-Renal Physiology*, 298(5), pp. F1078-F1094.

Verrecchia, F. and Mauviel, A. (2002) 'Transforming growth factor-β signaling through the Smad pathway: role in extracellular matrix gene expression and regulation', *Journal of Investigative Dermatology*, 118(2), pp. 211-215.

Waikar, S.S., Curhan, G.C., Wald, R., McCarthy, E.P. and Chertow, G.M. (2006) 'Declining mortality in patients with acute renal failure, 1988 to 2002', *Journal of the American Society of Nephrology*, 17(4), pp. 1143-1150.

Wang, B., Dolinski, B.M., Kikuchi, N., Leone, D.R., Peters, M.G., Weinreb, P.H., Violette, S.M. and Bissell, D.M. (2007) 'Role of αvβ6 integrin in acute biliary fibrosis', *Hepatology*, 46(5), pp. 1404-1412.

Wang, F., Yu, G., Liu, S.-Y., Li, J.-B., Wang, J.-F., Bo, L.-L., Qian, L.-R., Sun, X.-J. and Deng, X.-M. (2011) 'Hydrogen-rich saline protects against renal ischemia/reperfusion injury in rats', *Journal of Surgical Research*, 167(2), pp. e339-e344.

Wei, Q., Dong, G., Franklin, J. and Dong, Z. (2007) 'The pathological role of Bax in cisplatin nephrotoxicity', *Kidney international*, 72(1), pp. 53-62.

Weidemann, A., Bernhardt, W.M., Klanke, B., Daniel, C., Buchholz, B., Câmpean, V., Amann, K., Warnecke, C., Wiesener, M.S. and Eckardt, K.-U. (2008) 'HIF activation protects from acute kidney injury', *Journal of the American Society of Nephrology*, 19(3), pp. 486-494.

Weidemann, A. and Johnson, R.S. (2008) 'Biology of HIF-1α', *Cell Death & Differentiation*, 15(4), pp. 621-627.

Weight, S.C., Bell, P.R.F. and Nicholson, M.L. (1996) 'Renal ischaemia-reperfusion injury', *British Journal of Surgery*, 83(2), pp. 162-170.

Williams, Ç.H., Kajander, T., Hyypiä, T., Jackson, T., Sheppard, D. and Stanway, G. (2004) 'Integrin αvβ6 is an RGD-dependent receptor for coxsackievirus A9', *Journal of virology*, 78(13), pp. 6967-6973.

Williams, P., Lopez, H., Britt, D., Chan, C., Ezrin, A. and Hottendorf, R. (1997) 'Characterization of renal ischemia-reperfusion injury in rats', *Journal of pharmacological and toxicological methods*, 37(1), pp. 1-7.

Wipff, P.-J., Rifkin, D.B., Meister, J.-J. and Hinz, B. (2007) 'Myofibroblast contraction activates latent TGF-β1 from the extracellular matrix', *The Journal of cell biology*, 179(6), pp. 1311-1323.

Wrana, J.L., Attisano, L., Cárcamo, J., Zentella, A., Doody, J., Laiho, M., Wang, X.-F. and Massague, J. (1992) 'TGFβ signals through a heteromeric protein kinase receptor complex', *Cell*, 71(6), pp. 1003-1014.

Wrana, J.L., Attisano, L., Wieser, R., Ventura, F. and Massague, J. (1994) 'Mechanism of activation of the TGF-b receptor', *Nature*, 370(6488), pp. 341-346.

Wu, D., Potluri, N., Lu, J., Kim, Y. and Rastinejad, F. (2015) 'Structural integration in hypoxia-inducible factors', *Nature*, 524(7565), pp. 303-308.

Wu, D. and Yotnda, P. (2011) 'Induction and testing of hypoxia in cell culture', *Journal of visualized experiments: JoVE*, (54).

Xiong, J.P., Goodman, S.L. and Arnaout, M.A. (2007) 'Purification, analysis, and crystal structure of integrins', *Methods in enzymology*, 426, pp. 307-336.

Xu, F., Liu, C., Zhou, D. and Zhang, L. (2016) 'TGF-β/SMAD pathway and its regulation in hepatic fibrosis', *Journal of Histochemistry & Cytochemistry*, 64(3), pp. 157-167.

Xu, Q., Norman, J.T., Shrivastav, S., Lucio-Cazana, J. and Kopp, J.B. (2007) 'In vitro models of TGF-β-induced fibrosis suitable for high-throughput screening of antifibrotic agents', *American Journal of Physiology-Renal Physiology*, 293(2), pp. F631-F640.

Xu, X., Chua, K.-W., Chua, C.C., Liu, C.-F., Hamdy, R.C. and Chua, B.H.L. (2010) 'Synergistic protective effects of humanin and necrostatin-1 on hypoxia and ischemia/reperfusion injury', *Brain research*, 1355, pp. 189-194.

Xu, X., Tan, X., Tampe, B., Sanchez, E., Zeisberg, M. and Zeisberg, E.M. (2015) 'Snail is a direct target of HIF1α in hypoxia-induced endothelial to mesenchymal transition of human coronary endothelial cells', *Journal of Biological Chemistry*, p. jbc. M115. 636944.

Yanagita, M. (2012) 'Inhibitors/antagonists of TGF-β system in kidney fibrosis', *Nephrology Dialysis Transplantation*, 27(10), pp. 3686-3691.

Yang, C., Kaushal, V., Haun, R.S., Seth, R., Shah, S.V. and Kaushal, G.P. (2008) 'Transcriptional activation of caspase-6 and-7 genes by cisplatin-induced p53 and its functional significance in cisplatin nephrotoxicity', *Cell Death & Differentiation*, 15(3), pp. 530-544.

Yang, H.-C., Zuo, Y. and Fogo, A.B. (2010a) 'Models of chronic kidney disease', *Drug Discovery Today: Disease Models*, 7(1), pp. 13-19.

Yang, J. and Liu, Y. (2001) 'Dissection of key events in tubular epithelial to myofibroblast transition and its implications in renal interstitial fibrosis', *The American journal of pathology*, 159(4), pp. 1465-1475.

Yang, L., Besschetnova, T.Y., Brooks, C.R., Shah, J.V. and Bonventre, J.V. (2010b) 'Epithelial cell cycle arrest in G2/M mediates kidney fibrosis after injury', *Nature medicine*, 16(5), pp. 535-543.

Yin, X., Tian, W., Wang, L., Wang, J., Zhang, S., Cao, J. and Yang, H. (2015) 'Radiation quality-dependence of bystander effect in unirradiated fibroblasts is associated with TGF-β1-Smad2 pathway and miR-21 in irradiated keratinocytes', *Scientific reports*, 5.

Yu, L., Border, W.A., Huang, Y. and Noble, N.A. (2003) 'TGF-β isoforms in renal fibrogenesis', *Kidney international*, 64(3), pp. 844-856.

Yu, L., Hébert, M.C. and Zhang, Y.E. (2002) 'TGF-β receptor-activated p38 MAP kinase mediates Smad-independent TGF-β responses', *The EMBO journal*, 21(14), pp. 3749-3759.

Yuan, Y., Hilliard, G., Ferguson, T. and Millhorn, D.E. (2003) 'Cobalt inhibits the interaction between hypoxia-inducible factor-α and von Hippel-Lindau protein by direct binding to hypoxia-inducible factor-α', *Journal of Biological Chemistry*, 278(18), pp. 15911-15916.

Yurchenco, P.D. (2011) 'Basement membranes: cell scaffoldings and signaling platforms', *Cold Spring Harbor perspectives in biology*, 3(2), p. a004911.

Zeisberg, M. (2006) 'Bone morphogenic protein-7 and the kidney: current concepts and open questions', *Nephrology Dialysis Transplantation*, 21(3), pp. 568-573.

Zhang, N., Hong, B., Zhou, C., Du, X., Chen, S., Deng, X., Duoerkun, S., Li, Q., Yang, Y. and Gong, K. (2017) 'Cobalt Chloride-induced Hypoxia Induces Epithelial-mesenchymal Transition in Renal Carcinoma Cell Lines', *Annals of Clinical & Laboratory Science*, 47(1), pp. 40-46.

Zhang, Y.-B., Wang, X., Meister, E.A., Gong, K.-R., Yan, S.-C., Lu, G.-W., Ji, X.-M. and Shao, G. (2014) 'The effects of CoCl2 on HIF-1α protein under experimental conditions of autoprogressive hypoxia using mouse models', *International journal of molecular sciences*, 15(6), pp. 10999-11012.

Ziello, J.E., Jovin, I.S. and Huang, Y. (2007) 'Hypoxia-Inducible Factor (HIF)-1 regulatory pathway and its potential for therapeutic intervention in malignancy and ischemia', *Yale J Biol Med*, 80(2), pp. 51-60.

Zoccali, C., Kramer, A. and Jager, K.J. (2010) 'Chronic kidney disease and end-stage renal disease—a review produced to contribute to the report 'the status of health in the European union: towards a healthier Europe'', *NDT plus*, 3(3), pp. 213-224.

Conference presentations

International

1. ERA-EDTA, Vienna Austria, 2016
2. American Transplant Congress, Boston USA, 2016. Best poster award
3. European Congress of Immunology Conference, Vienna Austria, 2015

National

1. North East Postgraduate Conference, Newcastle UK, 2015
2. 3rd North East Renal Research Mini-symposium, 2015. Oral presentation
3. Poster Evening Event, Institute of Cellular Medicine, Newcastle University, 2015
4. British Society of Immunology Annual Congress, Brighton UK, 2014 Institute
5. Research Student Seminar, 2014. Oral presentation

Conference publications

1. Kapoor, R., Kirby, J., Logan, I. and Sheerin, N., 2016. MP178ISCHEMIA REPERFUSION INJURY INDUCES A PRO-FIBROTIC PHENOTYPE IN HUMAN PROXIMAL TUBULAR EPITHELIAL CELLS. Nephrology Dialysis Transplantation, 31(suppl 1), pp.i400-i401.

2. Kapoor R, Sheerin N, Kirby J. Role of TGF-β in Ischemia and Reperfusion Injury Induced Renal Fibrosis in Human Proximal Tubular Epithelial Cells. [abstract]. Am J Transplant. 2016; 16 (suppl 3). http://www.atcmeetingabstracts.com/abstract/role-of-tgf-in-ischemia-and-reperfusion-injury-induced-renal-fibrosis-in-human-proximal-tubular-epithelial-cells/.

3. Kapoor R. Hot topics from the Assemblies. In: Breathe Sep 2015, 11 (3) 229-230; DOI: 10.1183/20734735.113115

4. Kapoor RA, Kirby J, Sheerin N. The effect of injury on renal tubular cell phenotype. In: British Society for Immunology Annual Congress. 2014, Brighton, UK: Wiley-Blackwell Publishing.

Awards and Grants

1. Biolegend Travel award (£ 300), 2016
2. Best poster award at American Transplant Congress, Boston USA, 2016
3. Newcastle University travel award (£700), 2016
4. Overseas research scholarship (ORS, £15000/ year), 2013-2016
5. BSI-ECI 2015 Travel award (£440), 2015